Investigation of Solid Materials and their Transformation Processes by X-ray and Complementary Analytical Techniques

By

Manal Aboubakker M. Khoj

Thesis Submitted for

DOCTOR OF PHILOSOPHY IN CHEMISTRY

SCHOOL OF CHEMISTRY

CARDIFF UNIVERSITY

August 2016

Declaration

This work has not been submitted in substance for any other degree or award at this or any other university or place of learning, nor is being submitted concurrently in candidature for any degree or other award.

Signed ………………………………………… (candidate)   Date…………………………

STATEMENT 1

This thesis is being submitted in partial fulfillment of the requirements for the degree of …………………………(insert MCh, MD, MPhil, PhD etc, as appropriate)

Signed ………………………………………… (candidate)   Date …………………………

STATEMENT 2

This thesis is the result of my own independent work/investigation, except where otherwise stated.

Other sources are acknowledged by explicit references. The views expressed are my own.

Signed ………………………………………… (candidate)   Date …………………………

STATEMENT 3

I hereby give consent for my thesis, if accepted, to be available online in the University's Open Access repository and for inter-library loan, and for the title and summary to be made available to outside organisations.

Signed ………………………………………… (candidate)   Date …………………………

Abstract

The work presented in this thesis concerns the investigation of a family of cinnamic acid derivatives. A combination of complementary analytical techniques is used to explore detailed structural aspects, and subsequently, chemical and physical properties of some of the materials. The crystal structures of the materials have been determined by single crystal X-ray diffraction techniques.

Chapter 1 reviews the relevant background knowledge including crystal engineering aspects and supramolecular chemistry, intermolecular interaction, polymorphism in crystalline materials, solid state processes such as phase transformation and solid state photoreaction, cocrystallization, and the mechanogrinding approach.

Chapter 2 provides background information relating to the main experimental techniques employed in this work. These include single crystal X-ray diffraction, powder X-ray diffraction, thermal analysis (deferential scanning calorimetry) and high performance liquid chromatography.

Chapter 3 explores the polymorphism of *meta*-substituted-cinnamic acids and phase transformation between related polymorphs, resulting in the discovery of two rare cases of transformation of cinnamic acids, in which the two forms of the same polymorphic classification.

Chapter 4 investigates the feasibility of the cocrystallization of binary systems that contain the different cinnamic acids studied in Chapter 3, resulting in the discovery and characterization of several crystal structures of different binary systems. The binary systems investigated by a combination of thermal analysis and PXRD, revealing information on the effect of the components on the obtained structure.

Chapter 5 investigates the structural aspects of K^+ and NH^+ salts of the different cinnamic acids investigated in Chapter 3. The study extended to explore the feasibility of cocrystallization of different binary salts systems (bi-anion or bi-cation salts), resulting in the design of materials that undergo photodimerization reaction. The study also

provides considerable information on the effect of the substituents and the cations on the structure obtained.

Chapter 6 gives evidence of the occurrence of the photodimerization process in several solid systems (investigated in previous chapters) in which the structures showed optimal arrangement of the double bond. The work also includes the reaction occurring in some binary solid solution systems, revealing a random molecular distribution of molecules throughout the reactant crystalline materials. The study also investigates the photoreaction in systems exhibiting a criss-cross arrangement of the double bonds, providing information on the dimerization and oligomerization of the materials.

Chapter 7 reports interesting insights into the green chemistry approach of mechanogrinding and solvent drop grinding of a system contains 3-BrCA and 3-ClCA. Cocrystallization and the phase control is achieved via the process.

Chapter 8 gives an overview on the future work.

Acknowledgement

I am deeply thankful to many people that have supported and helped me throughout my PhD years. To begin with, I owe my deepest gratitude to my supervisor Dr. Benson M. Kariuki for his continuous encouragement, guidance, support and patience. I appreciate all his contributions of time and ideas. I feel privileged to have been given the opportunity to work on this exciting project supervised by him.

I thank Professor K. D. M. Harris for his help in allowing me to access the lab facilities. I am also thankful to Dr. Colan Hughes for training me on how to use the PXRD and DSC. In addition, I also appreciate his kindness for looking over the theoretical calculations of solid-state NMR.

Furthermore, I am indebted to Dr. Rob Jenkins and Dr. Ana Belenguer (at Cambridge University) who offered advice and training in using HPLC. The same appreciation applies to Dr. Niklaas Buurma and Dr. Hiwa Ahmad for allowing me to use their HPLC. Thank you to Dr. David Morgan for his help with XPS analysis. My thanks also go to Analytical Services team at Cardiff University for their help with Mass spectrometry analysis. I would like to convey my thanks to Dr. Andrew Williams and Dr. Dilruba Meah for checking through chapters of my thesis.

Undertaking this PhD would not have been possible to do without the support and encouragement that I received from my family and friends. They have played a crucial part during my research years in making me feel confident at all the times. Firstly, heartfelt thanks go to my parents for always believing in me keeping me going and giving me infinite amount of love. Similarly, I would like to give a special thanks to my brothers and sisters, despite the fact that they were thousands of miles away, it felt like they were always beside me whenever I needed help and support. Thank you to my sensible children, Omair, Azari, Layan, Sohaib and my baby Retal for making my years enjoyable and giving me the reason to continue. Finally, I give my deepest gratitude and biggest thanks to my husband, Ibrahim Bantan for making me feel that everything impossible was

possible, and for providing a true support and understanding all the way through. Thank you.

Table of content

Chapter 1: Introduction

Chapter 2: Fundamentals of techniques and experimental

Chapter 3: Investigation of *meta-trans*-cinnamic acids: structural characterization, polymorphism and temperature induced phase transformation

Chapter 4: Investigation of binary systems of *meta*-cinnamic acids: co-crystallization, phase characterization and transformation

Chapter 5: Investigation of cinnamates: phase characterization, the role of cations and anions, supramolecular assembly and cocrystallization of mixed cation and anions

Chapter 6: Investigation of solid-state photochemistry of cinnamates and acids

Chapter 7: Mechanogrinding: a green chemistry approach in controlling phase transformation and cocrystallization

Chapter 1: Introduction

1.1. Supramolecular chemistry, crystal engineering and intermolecular interaction

In molecular compounds, looking at the molecules as independent components was changed, more than sixty years ago, when H. M. Powell[1] brought to attention the idea of looking at organic crystal structures as a network. Considering the crystalline solid as the whole entity lead to enormous progress in fields such as crystal engineering and supramolecular chemistry. The idea behind supramolecular chemistry[2] is defined by Lehn in "*The chemistry of intermolecular bond*". Thus, with a comparison to the organic molecule, where atoms are connected to each other by covalent bonds, the molecules in crystalline materials are self-organized via non-covalent interactions (intermolecular interactions) to produce the whole building block (crystal). These interactions (e.g. hydrogen bonds, halogen-halogen interactions, π-π stacking, Van der Waals, electrostatic interactions, etc.) are considered as the "glue" that is responsible for holding together the molecules, in a long range periodic arrangement through the crystal entity.[3,4]

Intermolecular interactions, therefore, are a highly important and fundamental aspect in the understanding of molecular crystals. A good understanding of the influence of such interactions on the self-assembly of molecules in the crystalline lattice, particularly with regard to a family of related crystalline materials, is a vital in crystal engineering (the designing strategy of crystal architecture); to produce crystalline materials with desirable chemical and physical properties. For example, a variety of intermolecular interactions may arise as different functional groups are manipulated in their structure by, for instance, changing the substituent groups and, thus, different organization of the molecules in the crystals is expected which, in turn, may influence the properties of the crystalline materials.[5] Due to the significance of the intermolecular interactions in determining the three dimensional architecture, which subsequently influences the physical and chemical properties of the crystals, they have been of interest for different research aspects.[6–8]

Three properties are usually considered in relation to intermolecular interactions; strength, directionality and distance dependence.[3,4] In terms of strength, in comparison with the intramolecular interaction (the covalent interaction) responsible for the formation of the classical organic molecule, intermolecular interactions (non-covalent interactions) are regarded generally as weak. At ambient conditions, the majority of such interactions have a strength in the range 0.5-15 kcal mol^{-1} and, because the crystal structure is the result of a combination of different kinds of intermolecular interactions, the sum of all interactions are considered in the course of determining the stability of the crystal. Secondly, these interactions have either directional (anisotropic) or non-directional (isotropic) properties. The later depends on dispersion-repulsion forces. This kind of interaction can occur between non-polar components. Van der Waals interaction is an example of such interaction, for example (C$\cdots$C or H$\cdots$H). However, directional interactions depend on the distribution of electron density around the interacting components and they, because of their directionality property, have some influence in steering the molecules in a certain orientations. Such interactions are thus considered broadly when designing molecular assemblies (hydrogen bonds, for example). The third property usually considered for intermolecular interactions is a distance dependence. This is the fall-off of interaction between two sites on increasing the distance between them. For example, for an interaction that has an electrostatic nature, the interaction falls-off gradually. A brief outline on some intermolecular interactions, such as hydrogen bonds, halogen-halogen interaction and π-π interactions is presented in this chapter, as they are relevant to the work discussed in this thesis.

1.1.1. Hydrogen bonds

The hydrogen bond is a very widely explored interaction and has been key in the understanding of many crystalline materials. A hydrogen bond is a non-covalent attractive interaction that is induced between a hydrogen donor (X–H) and a hydrogen acceptor (Y–Z) and is represented as X-H$\cdots$Y-Z. In strong hydrogen bonds, the distance between X$\cdots$Y is less than the sum of Van der Waals radii of X and Y, and the angle of X-H$\cdots$Y (θ) is also an important feature in such an interaction. For many hydrogen bonds this angle tends to be almost linear (180°), although this is not always achievable in all systems.[9,10]

The strength and length of the hydrogen bonds depends on the nature of both X and Y and, accordingly, the bond can be regarded as a strong or weak hydrogen bond.[11] Table 1.1 shows distances and angles for selected hydrogen bonding systems. The stronger hydrogen bonds display more directional functionality in the crystals, as indicated by X-H···Y angles close to 180°, whereas very low directionality is exhibited by the weaker hydrogen bonds and the bond angle may be as low as 110°, as observed in some C-H···O systems. The directionality of hydrogen bonds has been frequently exploited in supramolecular crystal engineering and many design strategies are based on utilizing such directionality.[12]

Table 1.1. *Selected bond distance and angles observed for different strength hydrogen bonds*[4].

Hydrogen bonds, X—H···Y—Z				
Strength	**Examples**	**X-Y** $(D, \text{Å})$	**H···Y** $(d, \text{Å})$	**X-H···Y** $(\theta, °)$
Very strong $X\text{-}H \sim H\cdots Y$	$[F\text{-}H\text{-}F]^-$	2.2-2.5	1.2-1.5	175-180
Strong $X\text{-}H < H\cdots Y$	O-H···O-H	2.6-3.0	1.6-2.2	145-180
	O-H···N-H	2.6-3.0	1.7-2.3	140-180
	N-H···O=C	2.8-3.0	1.8-2.3	150-180
	N-H···O-H	2.7-3.1	1.9-2.3	150-180
	N-H···N-H	2.8-3.1	2.0-2.5	135-180
Weak $X\text{-}H \ll H\cdots Y$	C-H···O	3.0-4.0	2.0-3.0	110-180

Hydrogen bonds between the carboxylic acid groups in the crystalline material often adopt a dimeric synthon. However, a catemer synthon is also observed in some crystalline materials, such as in acetic acid, but this is rare. Figure 1.1 shows both synthons. Sanphui et al.[13] reported that "*among 6612 carboxylic acid structures archived in the CSD, 35.9% (2377 hits) are dimer and only 3.2% (210 hits) are catemer*".
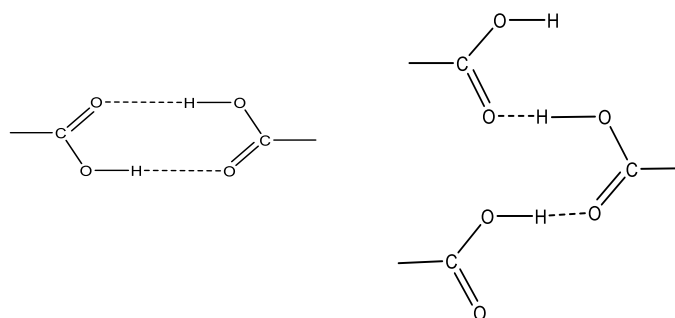
Figure 1.1. *The dimer (left) and catemer (right) synthons, showing hydrogen bonds as dashed lines.*

1.1.2. Halogen-halogen interactions

Halogen bonds exhibit both importance and applicability in several areas, ranging from biological to supramolecular chemistry,[14–17] despite being less common than hydrogen bonds.

The halogen bonds are generally attractive interactions that result from the anisotropic distribution of the electron density around the halogen atoms.[18,19] Thus, in the C-X system, for example, where the X is a halogen atom that is covalently bonded to C, a region of X along the C-X bond is positively charged, whereas the perpendicular region of X in relation to C-X is charged negatively (Figure 1.2a). This polarization allows the positively charged region to approach any electron donors (e.g. N, O or another halogen), resulting in electrostatically favourable interactions.

Halogen-halogen contacts ($R-X_1 \cdots X_2-R$) in the crystalline material can be classified according to their preferred geometries (their positions relative to each other) into two types (Figure 1.2 b and c). In Type i, the angle of $R-X_1 \cdots X_2$ (θ_1) and $X_1 \cdots X_2-R$ (θ_2) are equal, whereas in Type ii, $R-X_1 \cdots X_2$ and $X_1 \cdots X_2-R$ angles are $\theta_1 \approx 180°$, $\theta_2 \approx 90°$, respectively.[20–22] These interactions are also characterized by the inter-halogen distance. Thus when the inter-halogen distance is less than the sum of the Van der Waals radii of the corresponding halogen atoms, it is considered as a halogen–halogen interaction.[22]
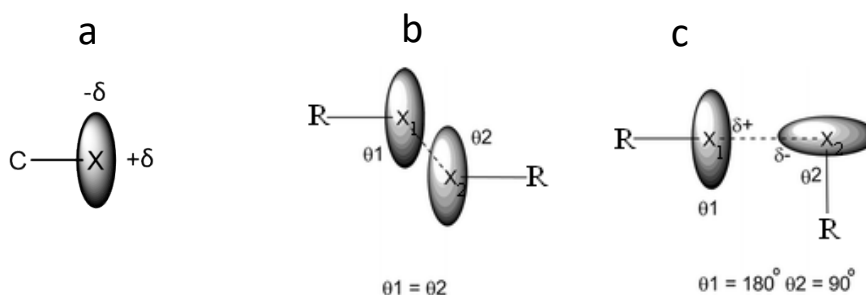
Figure 1.2. *(a) Charge distribution around X atom in C-X. (b) and (c) are the two geometries observed for halogen-halogen contacts, Type i and Type ii, respectively.*

The strength of the inter-halogen interactions is reported to increase, in the order $Cl \cdots Cl < Br \cdots Br < I \cdots I$, whereas the increase in the inter-halogen interaction distance exhibits reverse order on increasing the temperature.[23] On the other hand, due to the high electronegativity of the F atom, as well as the high polarity of C−F bond, it is expected

that the C-F⋯F-C interaction[20] will be weak. However, studies of F⋯F intermolecular interactions using experimental charge density and X-ray structural analysis have shown significant detectable F⋯F contacts that could influence the structural packing.[24–27]

Although halogen bonds show some directionality, they are generally considered to be weak in comparison with hydrogen bonds.[4] Examining the structures of the related family that differ only in their substituents can, for example, facilitate better understanding of the importance and functionality of these group on the crystal packing[20,28] which, in turn, can provide a useful tool for the crystal engineering field. This is part of the investigation reported in this thesis

1.1.3. π- π interactions

The π interaction is considered as weak and occurs between adjacent systems which have delocalized π electrons (such as aromatic rings). These interactions have been highly studied in biological supramolecular stabilization[29]. In the crystalline solid they have been considered widely, specifically for aspects such as crystal engineering, self-assembly and controlling crystal packing.[30,31]

Many classifications of interactions that comprise at least one part π-electrons are considered. Face-to-face and edge-to-face π interactions are types that are observed in many molecular crystals. When the two π-aromatic systems stack on top of each other as a sandwich, it is called a face-to-face stack (Figure 1.3a). However, if one of the π-aromatics shows a relative displacement with regard to the other π-aromatic, it is called an offset face-to-face (Figure 1.3b). Another type of edge to face π interaction is illustrated by the common example of C-H⋯π interactions (Figure 1.3c), and can be considered as a weak hydrogen bond. It occurs between the face of the π system of an aromatic ring and the hydrogen atom of another π-aromatic ring.[32]
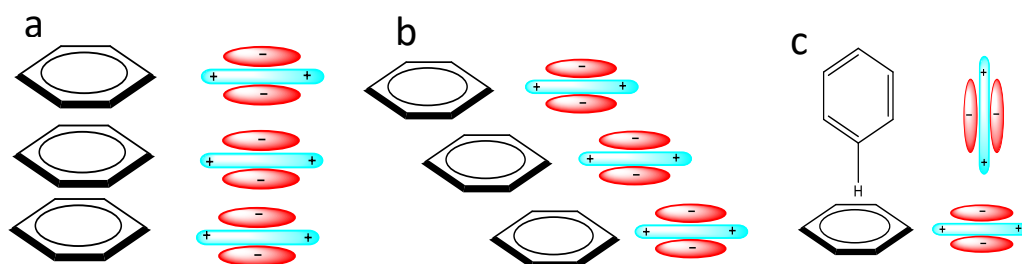
Figure 1.3. *Visualisation of the π interaction in benzene rings (a) face-to-face, (b) offset face-to-face and (c) edge-to-face.*

1.1.4. Other interactions

Another electrostatic interaction relevant to this work is the ion-dipole interaction. However, this interaction is not strictly defined as intermolecular interaction. It occurs in the structure when an electro negative atom, such as oxygen, coordinates to a positively charged ion such as an alkali metal cation. The oxygen lone pairs interact with the cation positive charge. Such an interaction has a highly directional influence on the crystal packing and can be advantageous for some aspects of crystal engineering.[4]

1.2. Polymorphism in crystalline solids

Polymorphism is a phenomenon that was discovered a long time ago, yet it continues, to be of a highly relevant topic of investigation. The term polymorphism refers to different crystalline forms (different crystal structures) that comprise identical chemical compounds. In other words, the same molecule adopts distinct arrangements to produce at least two different crystal structures. Figure 1.4 illustrates the different crystal structures of the same chemical component. Despite the same chemical composition, these distinctions in the crystalline state frequently lead to markedly different physical and chemical properties, such as, solubility, thermal stability, melting temperature, chemical reactivity etc.[33]
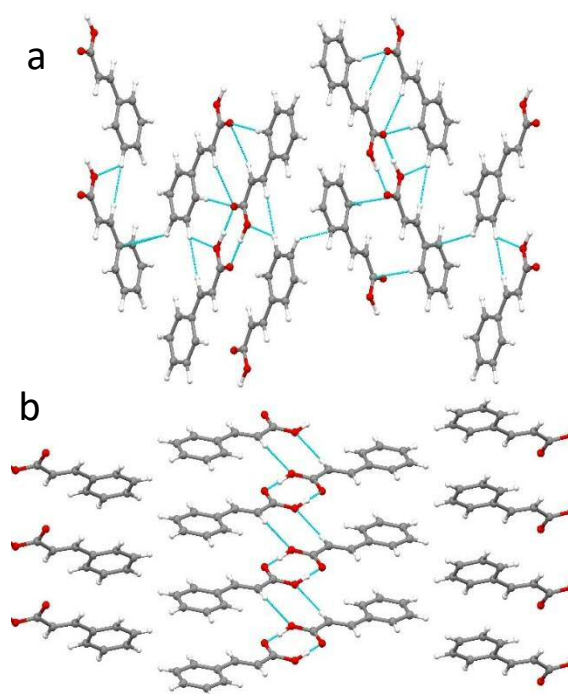
Figure 1.4. *The crystal structure of different polymorphs of trans-cinnamic acid (a) α form[34] and (b) β form[35]. Carbon atoms are shown in grey, hydrogen atoms in white and oxygen atoms in red. Some intermolecular interactions are represented by blue dashed lines.*

Polymorphism is a frequent phenomenon in organic crystalline materials. Many crystalline materials yield two or more polymorphic forms, although the presence of more than three polymorphs is not common. A recent study[36] found a new polymorphic form of aripiprazole; an eighth crystal structure (VIII) of this material. 5-methyl-2-[(2-nitrophenyl)amino]-3-thiophenecarbonitrile (ROY), is a famous example of the rare crystalline materials that crystallize in ten different polymorphic forms[37–39], where the crystal structures of seven polymorphs have been solved by SC-XRD. However, there are other cases, for instant urea and benzoic acid where, at ambient pressure, they exhibit only one crystalline form, despite numerous crystallization attempts[4]. The famous quotation by McCorne[40] highlighted the frequency of polymorphism and it stated that *"every compound has different polymorphic forms and that, in general, the number of forms known for a given compound is proportional to the time and energy spent in research on that compound"*. Accordingly, the expectation is that all crystalline materials exhibit polymorphism. A recent review[41] revealed the tendency for formation of polymorphs; 50% of crystalline solids display polymorphism whenever the polymorphs are screened. Therefore, effort during the crystallization stage may lead to different modifications of crystalline materials. Despite this, there is no guarantee of finding polymorphism for a given crystalline material.

The advancement of the analytical techniques, in particular X-ray single crystal structure determination (SC-XRD) and powder X-ray diffraction (PXRD), has a high impact on the identification and characterization of distinct polymorphs. Using SC-XRD, the 3D structure of different polymorphs can be easily visualized, whereas PXRD can be used as a fingerprint approach to characterize the bulk materials. Both techniques should be used in the characterization of different polymorphic forms, where accessible. The result obtained from SC-XRD reveals structural information, specifically for the single crystal, but the result is not necessarily representative for the bulk materials since concomitant crystallization of different polymorphs can happen (crystallization batches that result in more than one crystallized form). Thus the calculated PXRD pattern from single crystal structure determination should be compared with experimental data in order to identify any additional phases. Concomitant polymorphs[42] is a common phenomenon governed by thermodynamic and kinetic factors.

Concomitant crystallization is useful as an indication of the existence of additional polymorphic phases and, in the case of screening, of the possible polymorphs of the material but it is undesirable where only the specific pure polymorphic form is required for a particular application. In this regard, many studies[43] have been carried out in order to control specific polymorphic forms. Thus, different crystallization approaches with a variety of conditions have been employed, such as, seeding crystallization, variety solvent system crystallization, mill-grinding, etc. Despite this, it is not always easy to achieve control of specific polymorphs. There are many cases where it is rather difficult to even reproduce specifically an already known polymorphic form although no much effort was require when it is first produced. This phenomenon is known as the disappearing of polymorphism.[44]

1.2.1. Transition between polymorphs

The existence of two or more distinct polymorphic forms in a system raises questions with respect to stability and phase transformation. Two factors are considered in such a discussion; thermodynamics and kinetics.[33] The former provides information regarding the stability of the different polymorphs, the ability of conversion between the polymorphic forms and the conditions associated with transformation. The latter factor, however, concerns the time duration that is required for one polymorph to transform to another.

Thus, in a bi-polymorphic system, at a defined temperature and pressure, the form with lower free energy (G) is the most stable. Therefore, transformation may potentially occur from the less stable form (*meta*-stable) to the thermodynamically stable form (discussed later). However, as transformation is influenced by the kinetics factor, which is dependent on the energy barrier of transformation, a low energy barrier system results in a rapid transformation. In contrast, if the energy barrier of transformation is high, more time is required for the transformation to be observed; hence, infinite time has been proposed in some cases of polymorphic phase transition. The well-known example is the diamond/graphite system[45]; under ambient conditions diamond is a *meta*-stable form and it is anticipated that it would transform to the stable form, graphite. However, due to the effect of the kinetics factor, the transformation of diamond to graphite is infinitely slow and thus this transformation cannot be observed in ambient conditions.

Introducing an external influence, such as temperature or pressure often lowers the activation energy and, subsequently, transformation occurs.

From the thermodynamics viewpoint, the relation between the polymorphic forms, in respect of their stability, is classified as either monotropic or enantiotropic[46]. If the melting temperature of the two polymorphic forms is lower than the transition temperature, then the two polymorphic forms are monotropically related. An irreversible transformation is therefore expected to occur from the less stable to the thermodynamically stable form.

This is illustrated in Figure 1.5a, in which the free energy curves of the monotropically related polymorphs versus temperature for the two forms do not intersect before the melting points (the intersection of the curves for the two forms is at the transition temperature, T_t). In contrast, for the enantiotropically related forms, the transition temperature is below the melting temperatures and, opposite relative stability of the two forms is observed below and above this temperature. Consequently, reversible transformations are expected below and above the transition temperature. This relationship is illustrated in Figure 1.5b, where the two curves of A and B intersect at T_t before A and B melt; at Tt, $G_A=G_B$ and therefore A and B co-exist in equilibrium. However, below this point $G_A < G_B$ and thus, B can undergo transformation to A, while A can undergo phase transformation to B above T_t where $G_B < G_A$.

The transition that is induced in the crystalline materials, therefore, may help in understanding the relative stability. The thermal analysis by, for example, differential scanning calorimetry (DSC), is crucial in the investigation of the thermal behavior of polymorphic materials.
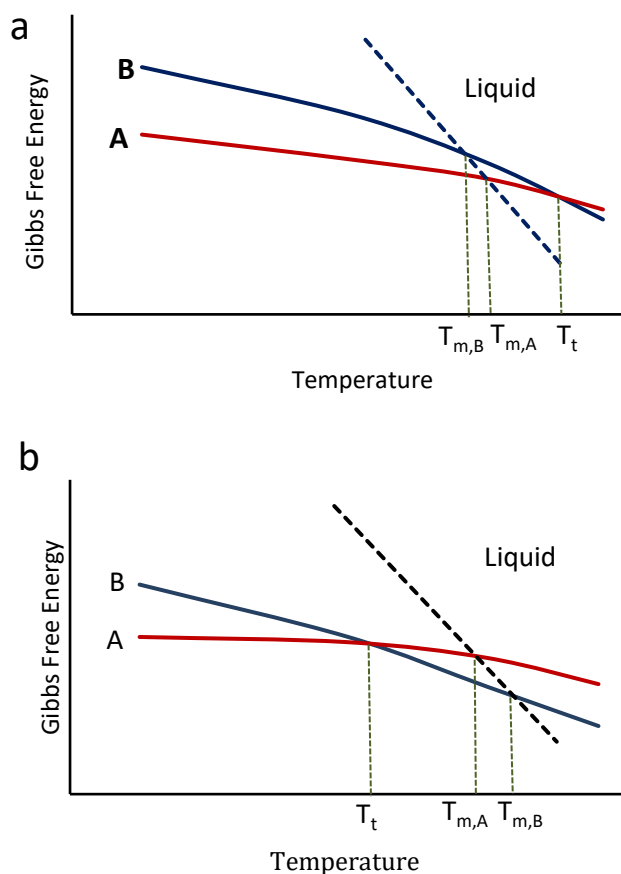
Figure 1.5. *The relation between Gibbs free energy and the temperature of the two related polymorphs; (a) monotropy and (b) enantiotropy.*

1.2.2. The importance of studying polymorphism

Polymorphism is a wide topic that has been investigated in many distinct disciplines associated with the molecular crystal; from academic research laboratories to the pharmaceutical industry.[47–50] This is because of the variety of properties displayed by different polymorphs which subsequently affect their applications,[51,52] as the properties of the crystalline solid are directly connected with its crystal structure.

Analyzing the structures of diverse polymorphs and relating them to intermolecular interactions, crystal packing and phase conversion is a valuable way of rationalizing the relationship between crystal construction and the associated properties. In this regard, the chemical properties (photoreaction for example) of organic crystals are often governed by the entire crystal environment (crystal packing) and subsequently, polymorphism may potentially influence this property.[53] Thus, the arrangement of the molecules in the crystal, which bring the reactive functional groups into an appropriate arrangement (distance and geometry) to satisfy the reaction criteria, is vitally important

for a solid-state reaction. Moreover, the variation of the crystal structure may also affect the reaction rate and stereochemistry of the products obtained.

The relationship between polymorphism and photo-reactivity has been investigated over the past fifty years. Cinnamic acid is a classic well-known example in this regard.[54,55] Three different polymorphic phases (α, β and γ) in relation to the photochemical reaction have been identified for this crystalline material (discussed later in Section 1.5). In the α form, neighbouring molecules are related by an inversion centre and the reactive double bonds are parallel in respect to each other, with a separation distance less than 4.2Å. The resultant molecule is a centrosymmetric dimer that reflects the molecular arrangement of the reactant (head-to-tail). In contrast, molecules in the β form are related by translation, by less than 4.2Å, resulting again in a parallel orientation of the reactive double bonds throughout the stacking. In this form, the dimeric product is mirror-symmetric, consistent with the arrangement of the reacting molecules (head-to-head). However, no reaction takes place when the γ form is exposed to UV irradiation, as the double bonds through the stack show longer contact distances than that required for the photo reaction.

In a recent study by M. Mishra and co-workers[56] the two different polymorphic forms of 3,4-dimethoxycinnamic acid (I and II) showed different initial photoreaction rates; being higher for polymorphic form I than II. However, a higher product yield was observed for II. This distinct behavior of the different polymorphic forms is correlated with differences in the crystal structure. Investigation of the correlation between the crystal structure and the photoreaction is an integral part of the present study.

1.3. Isostructures

The phenomenon in which different molecules (normally compounds of a related family) assemble to adopt similar crystal packing (with fundamentally the same relative molecular orientations throughout the structure), is termed as isostructurality[57]. In this case the space group and the unit cell parameters are not necessarily identical. This phenomenon is almost the opposite of polymorphism, in which the identical chemical compound adopts different crystal packing modes. Many structures of different materials exhibit isostructurality. For example, both 2,4,6-triiodoresorcinol (TIR) and 2,4,6-triiodophloroglucinol (TIG) showed two polymorphs, orthorhombic (TIR-O and

TIG-O) and monoclinic (TIR-M and TIG-M); the two orthorhombic forms are isostructural to each other and, similarly, the monoclinic structures are also isostructural in respect to each other.[58] In another example, substitution of functional groups of sulfonylhydrazone molecules by halogen and methyl, in the following pairs, Cl–Me, Br–Me, Cl–Br and Cl–F, showed isostructurality.[59]

1.4. Cocrystallization

One of the most intense modern studies of crystalline solids is the design of structures to produce functional materials. In this context, chemists apply an intelligent strategy of controlling the internal structure by introducing additional components within a single crystal entity to alter the crystal properties. Such research has become an important discipline of interest, particularly in areas such as crystal engineering, material science and pharmaceutical applications.[60–64]

The term "cocrystals" has been used generally to refer to these multicomponent systems of a crystalline solid that comprise more than one component. However, the nomenclature has been a subject of debate in solid state chemistry until recently. Many definitions have been proposed for the term "cocrystal". Desiraju[65] proposed using the previously used expression "molecular complex" to describe a crystal that is composed of different components in the same crystalline body and he suggested that this term should replace the "cocrystal" terminology. However, Dunitz[66] in his letter, argued the broad sense of the term "molecular complex" which has not solely been used for crystalline solids, and from his point of view "*cocrystal is the preferred term to describe a crystal containing more than a single component*". Such a broad definition was also descried by Stahly, whose work suggested that,[67,68] "*cocrystals encompass two or more components that produce a unique crystalline material having unique properties*". However, such a definition may include many systems such as molecular complexes, inclusion compounds, salts, solvate, solid solutions and possibly other multicomponent crystals; in other words, cocrystal is a term that can replace multicomponent crystal.[69] Therefore, other definitions reported in the literature are much more restricted in that they describe only a certain subset of the multicomponent crystal system. As an example, for the purpose of excluding all solvates and hydrates, cocrystals are defined as the crystalline materials that comprise more than one component and are all solids under ambient conditions.[70,71,4]

In this debate, many expressions have appeared in the literature to describe crystalline multicomponent materials according to focus of interest but, in the end, all probably remain as a subset of cocrystal, as exemplified by structural mimicry[72,73], mixed crystals[74,75], solid solution[76] and organic alloys[77].

In this regard, a "solid solution", which was considered extensively by Kitaigorodsky,[78,79] is a subset of "cocrystal" whereby the materials involved in the crystal are usually of a similar shape and size. Accordingly, they are either distributed randomly throughout the crystal to occupy the crystal sites in a substitution mode (molecules of different materials replace one another within the crystal) or they form domains which are also distributed randomly throughout the crystal. Therefore, nonstoichiometric bulk compositions of the involved materials in the crystals may be present. In this thesis, the term "solid solution" is used to describe a multicomponent crystalline system, comprising of more than one component which are all solid under ambient conditions and either randomly distributed or forming domains throughout the crystal. The term "cocrystallization" is used to describe the process used for producing these multi-component systems.

Formation of solid solution crystals was first investigated for inorganic materials[80] and widely utilized due to the ease of mixing the spherical atoms and ions. On the other hand, in molecular crystals, formation of such solid solutions has received much less attention despite considerable guidance in this field being provided by Kitaigorodsky[78,79] more than three decades ago. Thus, the similarity of molecular structures (size and shape), for example, is important in the formation of organic solid solutions. The investigation of such systems is expected to grow in coming years.[81–84]

This interest in solid solutions is partly driven by the advantage of continuously altering the properties by changing the composition (solubility, melting points, reactivity are examples of such properties). In this regard, many studies have reported a variety of reasons forming solid solution.[77,85–90] For example, cyclopentanone derivatives have been cocrystallized in a solid solution with the purpose of driving the molecules to pack into specific reactive arrangements[72]. In another example,[91] the interchangeability of Me/Cl in 2-benzyl-5-benzylidenecyclopentanone has been used as a means for engineering the photo-stable crystal into a photo-reactive crystal via cocrystallization as a solid solution.

1.4.1. Polymorphism in a cocrystalline material

Similarly to the mono-component materials, the crystalline solid of the multi component material (cocrystal) can also be crystallized with different molecular arrangements to produce polymorphic crystals. However, clear definition regarding the composition should be considered. Thus, for example, in a binary system comprising molecules A and B to form cocrystal A/B, the stoichiometry of A:B should be identical for all different crystal structures and, the distribution of the components should also be identical for true polymorphs. Many systems of multicomponent crystals exhibit polymorphic behavior.[92]

The term *pseudopolymorphism* has also been used as an acceptable term to describe multicomponent systems (the solvate system is a common known type) that not only have their molecules arranged differently but also have a slightly different molecular composition[33]. However, this term has been the subject of debate in the literature; Seddon[93] and Bernstein[94] argued that the term is incorrect and should not be used. On the other hand, Desiraju[95] pointed out "*This term brings to attention the fact that certain related multicomponent crystals, with slightly different chemical compositions or stoichiometries, have slightly different crystal structures in a manner reminiscent of polymorphism*". Nangia[96]emphasised that this term can be clearly understood and it may be adapted in other newly discovered systems.

In this regard, to avoid the confusion of naming the multicomponent system in which identical molecules of a binary system adopt different crystal structures (regardless of their bulk composition or their distribution in the crystal), the term "semi-polymorphism" will be used in this study. Figure 1.6 illustrates the difference between polymorphism and semi-polymorphism.
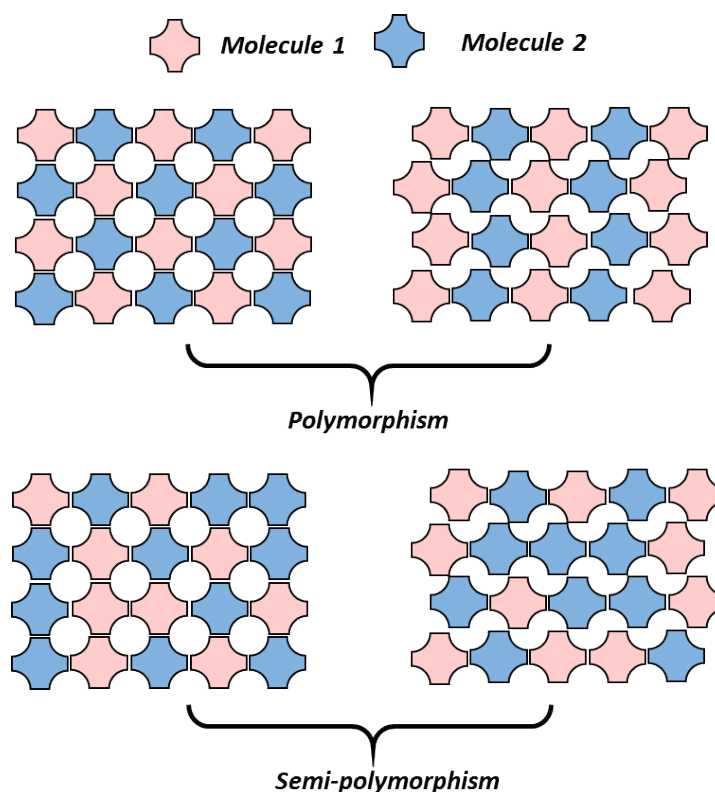
Figure 1.6: *Projection to illustrate the difference between polymorphism and semi-polymorphism.*

1.5. Solid-state photodimerization reaction

Organic solid-state reaction has the major advantage of being a green (solvent free) approach to organic synthesis[97–99]. Hence, generally, for this reaction to take place, appropriate solid crystalline material needs only to be exposed to, for example, appropriate energy radiation such as ultraviolet light (UV). Moreover, due to the constrained and regular molecular environment present in the crystalline material, photoreaction occurs with virtually no side reactions, to yield an almost pure stereo-selective chemical product. This is in contrast to the reaction that occurs in the conventional solution state, where by-products and variant stereo-selective products are more likely due to the free movement of the molecules, which allows the reactant functional groups to adopt several different orientations.[100] Therefore, great attention has been paid to solid-state reactions by the researchers.[53,101,102]

The [2+2] photocycloaddition is one of the most well-known reactions in organic solid-state photochemistry[100]. Historically, the solid [2+2] photodimerization reaction of cinnamic acids and its derivatives is particularly important. A great understanding of the direct relationship between the crystal structure and photo-reactivity has been achieved

through its rationalization,[54,55,103–110] leading to the development of the topochemical principle for solid-state reactivity.

Cinnamic acid and its derivatives were observed[54,103] to crystallize into three different polymorphs (denoted γ, α, and β). This classification was based on the relationship between the packing mode of the molecules and their behavior in [2+2] photodimerization reactions. Thus, under UV light, the γ form showed photo-inactive behaviour. However, α and β forms reacted to produce distinct dimeric products; a centrosymmetric (α-truxillic acid) dimer was produced by the α form crystals whereas the β form produced a mirror-symmetric (β-truxinic acid) dimer.

The 3D investigation of cinnamic acids' structures, using SC-XRD,[55] demonstrated the correlation between crystal structure and photo-reactivity. Thus, in these materials, each form (γ, α or β) has its characteristic unique packing mode. A general observation from the studies was that, in the α form, the molecules are aligned in head-to-tail orientation, whereas, the molecules showed a head-to-head alignment, in respect to each other, in the β form. However, a comparison of these forms (α and β) with the γ form showed a difference in the distance between the centres of the C=C bonds of potentially reactive monomer molecules; they are separated by less than *ca.* 4.2 Å in the α and β forms whereas the corresponding distance in the photo-stable γ form is greater than *ca.* 4.7 Å. Figure 1.7 illustrates the relationship between the monomer alignment and the corresponding photo chemical behaviour.

Thus, on the basis of these well-defined structure-reactivity relationships, the solid-state photodimerization reactions of trans-cinnamic acid and its derivatives represent a classic illustration of the topochemical principle.[54,55,104–108] A consequence of this principle is that the 3D crystal structure of the material provides information to enable prediction of whether or not the reaction can proceed and, the molecular structure of the product, if the reaction takes place. This is possible because the reaction involves the nearest functional reactive groups and proceeds with the minimal atomic and molecular displacements. With regard to the solid state [2+2] photodimerization reaction, Schmidt[55] determined that the reactive groups should be separated by less than 4.2Å and show parallel alignments with respect to each other.

However, although these criteria apply to most crystalline materials that undergo photodimerization, some reactivity is observed when the double bonds deviate to some extent from parallelism and therefore movement of the molecules prior to the reaction plays a role[111,112].
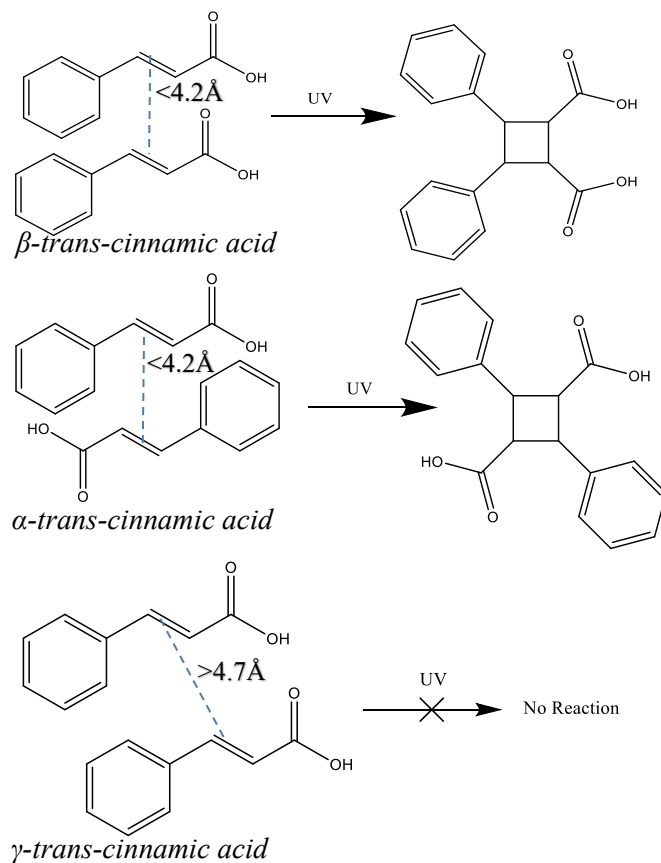
Figure 1.7. *The diagram illustrates the relationship between the arrangement of the monomer and the photodimerization reaction.*

Utilization of this knowledge in crystal engineering enables the design of materials that undergo solid-state photodimerization by organizing the molecular packing in the structure[113]. Various organization strategies has been successfully utilized for such purposes.[114–120] Introducing external additives into the crystal, for example, could effectively steer the molecules in a controllable manner from formation of photo-stable crystals, by bringing the reactive groups into appropriate geometry for the reaction. As previously mentioned in Section 1.4, cocrystallization is a frequently employed means for engineering the crystal functionality toward a photodimerization reaction.[121–123] Another method for templating the structure for a photodimerization reaction is salt formation.[124,125]

1.6. Mechanogrinding

Solid state mechanogrinding is a simple technique where, typically, the solids are ground in a pestle and mortar or a ball mill, to drive the transformation (i.e. chemical reaction, phase transformation and cocrystal formation). Such transformation is induced by the mechanical energy that is produced via grinding[126]. Mechanogrinding is a long established method in chemistry as, according to Takacs[127,128] "*Faraday induced the mechanochemical reduction of AgCl with Zn, Sn, Fe and Cu in 1820, using trituration in a mortar*". Since then, intensive progress in mechanogrinding has been driven by researchers in many areas from inorganic minerals to academic research and the pharmaceutical industry.[129–133]

Many examples have been reported in the literature, illustrating the effect of solid grinding, or solvent drop grinding, in inducing variant solid transformations. For example, crystalline materials have been transformed to amorphous[134], amorphous materials transformed to crystalline[135] and, additionally, the transformation between different polymorphic forms has also has been reported to be induced by grinding.[136] On the other hand, solid grinding has also been employed as a tool for cocrystallization.[137]

This technique is increasing in importance and is expected to continue growing, especially because it offers the option of solvent-free or solvent minimum media, which is a very attractive way of preforming environmentally friendly (green) processes[138].

However, the mechanism associated with the grinding process has been poorly understood and is still under study.[139,140] In this regard many postulates have been proposed in the literature; for example, in a study on picric acid complexes, vapour diffusion was suggested by Rastogi et al[141], as a mass transfer mechanism during solid state grinding. Another postulate was based on the work of co-grinding of racemic-bis-*β*-naphthol and benzoquinone, by Kuroda et al.[142] who proposed the molecular diffusion process and shearing the crystal during the solid grinding; in this work co-grinding of these solids generated a different structure to that observed during solution cocrystallization. Rothenberg[143] showed evidence suggesting that, to facilitate intermolecular contacts and mass transfer in solids, the formation of a liquid phase in the binary phase diagram is essential. Another postulate was suggested by Chadwick et al.,[144] based on the work done on the cocrystallization of benzophenone and

diphenylamine via grinding. They proposed that a melt is formed between the solid phases and thus *"with the shear induced by the grinding and the contact between the liquid and the residual solid surfaces induces the nucleation and growth of the co-crystal from the liquid phase, much in the same way as a synthetic chemist might scratch the wall of a reaction vessel to induce crystallization of a reaction product"*. On the other hand, solvent drop grinding was suggested, by Shan et al[145], to play a role in the enhancement of molecular collisions and formation of tiny cocrystal seeds. This explanation was based on the additional degrees of freedom generated by the solvent.

1.7. Aims of this project

Since the properties of crystalline materials depend on their structural packing, for the purpose of engineering crystal properties (photo-reactivity for example), exploring ways to tune the molecular building blocks to achieve specific packing that exhibits the required property of the materials, becomes very important. The methodology that is usually followed is the systematic study of a series of crystalline materials of related molecules. This may help in the rationalization of structures and, subsequently, may reveal an accessible route to the desired crystal packing, which may possess the property of interest.

Accordingly, the research carried out in this thesis was aimed at investigation of a series of solid state organic materials, namely cinnamic acid and its derivatives. Screening for new crystal forms of the same molecules or aggregates of the same molecules with other molecules was preformed, in order to gain information on the structural relationships and properties of the materials. This was achieved by subjecting these materials to systematic studies using a multi-technique approach, such as X-ray diffraction (SC-XRD and PXRD) and complementary analytical techniques.

The aims were as follows:
Firstly, exploration of different polymorphs of Cl, Br, F, methyl and tri-fluoromethyl meta-substitutions cinnamic acids, the transformation that may be induced between these systems and the feasibility of cocrystallization of these system, with the aim of providing information on the role of substituent groups in directing the structures.

Secondly, systematically investigate NH_4^+ and K^+ salts of those materials and the feasibility of mixed anions and mixed cations salts, with the aim of further understanding the effect of both substituent groups and the cation in order to provide information for designing materials of interest.

Thirdly, carry out the photodimerization reaction on the materials that showed appropriate geometry, with the goal of following the process first and then to gaining information to help in understanding the materials (for example, the distribution of the molecules throughout the solid solution).

Lastly, apply mechanogrinding as a green chemistry approach with the aim of cocrystallization of the materials that undergo the photodimerization reaction for a potential application of synthesis of asymmetric molecules. Controlling phases via mechanogrinding also integrates with the overall aim.

1.8. References

1   H. M. Powell, *J. Chem. Soc.*, 1948, 61–73.

2   J. Lehn, *Supramolecular Chemistry: Concepts and Perspectives*, VCH Verlagsgesellschaft mbH D-69451, Weinheim, 1995.

3   G. R. Desiraju, *Nature*, 2001, **412**, 397–400.

4   G. R. Desiraju, J. J. Vittal and A. Ramanan, *Crystal Engineering: A Textbook*, World Scientific Publishing Co. Pte. Ltd., Singapore, 2011.

5   S. Ebenezer, P. T. Muthiah and R. J. Butcher, *Cryst. Growth Des.*, 2011, **11**, 3579–3592.

6   B. K. Saha, A. Nangia and M. Jaskólski, *CrystEngComm*, 2005, **7**, 355–358.

7   C. B. Aakeröy, N. Schultheiss, A. Rajbanshi, J. Desper and C. Moore, *Cryst Growth Des.*, 2009, **9**, 432–411.

8   F. F. Awwadi, D. Taher, S. F. Haddad and M. M. Turnbull, *Cryst. Growth Des.*, 2014, **14**, 1961–1971.

9   G. Gilli and P. Gilli, *The Nature of the Hydrogen Bond: Outline of a Comprehensive Hydrogen Bond Theory*, Oxford University Press Inc., New York, 2009.

10   S. J. Grabowski, *Hydrogen Bonding: New Insights*, Springer, Dordrecht, 2006.

11   G. R. Desiraju and T. Steiner, *The Weak Hydrogen Bond In Structural Chemistry*

and Biology, Oxford University Press, Oxford, 2001.

12 M. Khan, V. Enkelmann and G. Brunklaus, *Cryst. Growth Des.*, 2009, **9**, 2354–2362.

13 P. Sanphui, G. Bolla, U. Das, A. K. Mukherjee and A. Nangia, *CrystEngComm*, 2013, **15**, 34–38.

14 P. Auffinger, F. A. Hays, E. Westhof and P. S. Ho, *Proc. Natl. Acad. Sci. U. S. A.*, 2004, **101**, 16789–16794.

15 P. Politzer, J. S. Murray and T. Clark, *Phys. Chem. Chem. Phys.*, 2010, **12**, 7748–7757.

16 F. Meyer and P. Dubois, *CrystEngComm*, 2013, **15**, 3058–3071.

17 P. Metrangolo, F. Meyer, T. Pilati, G. Resnati and G. Terraneo, *Angew. Chem. Int. Ed. Engl.*, 2008, **47**, 6114–6127.

18 B. Bankiewicz and M. Palusiak, *Struct. Chem.*, 2012, **24**, 1297–1306.

19 M. Palusiak, *J. Mol. Struct. THEOCHEM*, 2010, **945**, 89–92.

20 G. R. Desiraju and R. Parthasarathy, *J. Am. Chem. Soc.*, 1989, **111**, 8725–8726.

21 T. T. T. Bui, S. Dahaoui, C. Lecomte, G. R. Desiraju and E. Espinosa, *Angew. Chemie - Int. Ed.*, 2009, **48**, 3838–3841.

22 F. F. Awwadi, R. D. Willett, K. A. Peterson and B. Twamley, *Chem. Eur. J.*, 2006, **12**, 8952–8960.

23 V. G. Saraswatula and B. K. Saha, *New J. Chem.*, 2014, **38**, 897–901.

24 D. Chopra, T. S. Cameron, J. D. Ferrara and T. N. Guru Row, *J. Phys. Chem. A*, 2006, **110**, 10465–10477.

25 A. R. Choudhury and T. N. G. Row, *CrystEngComm*, 2006, **8**, 265–274.

26 R. B. K. Siram, D. P. Karothu, T. N. G. Row and S. Patil, *Cryst. Growth Des.*, 2013, **13**, 1045−1049.

27 A. Bach, D. Lentz and P. Luger, *J. Phys. Chem. A*, 2001, **105**, 7405–7412.

28 F. C. Pigge, V. R. Vangala and D. C. Swenson, *Chem. Commun.*, 2006, 2123–2125.

29 M. Egli, V. Tereshko, G. N. Mushudov, R. Sanishvili, X. Liu and F. D. Lewis, *J. Am. Chem. Soc.*, 2003, **125**, 10842–10849.

30 A. K. Tewari and R. Dubey, *Bioorg. Med. Chem.*, 2008, **16**, 126–143.

31 G. W. Coates, A. R. Dunn, L. M. Henling, J. W. Ziller, E. B. Lobkovsky and R. H. Grubbs, *J. Am. Chem. Soc.*, 1998, **120**, 3641–3649.

32 E. R. T. Tiekink and J. Zukerman-Schpector, *The Importance of Pi-Interactions*

in Crystal Engineering: Frontiers in Crystal Engineering, John Wiley & Sons, Ltd, Chichester, 2012.

33   J. Bernstein, *Polymorphism in Moleculer Solid*, Oxford University Press, Oxford, 2002.

34   J. A. K. Howard, M. F. Mahon, P. R. Raithby and H. A. Sparkes, *Acta Crystallogr. Sect. B*, 2009, **65**, 230–237.

35   I. Abdelmoty, V. Buchholz, L. Di, C. Guo, K. Kowitz, V. Enkelmann, G. Wegner and B. M. Foxman, *Cryst. Growth Des.*, 2005, **5**, 2210–2217.

36   S. P. Delaney, T. M. Smith, D. Pan, S. X. Yin and T. M. Korter, *Cryst. Growth Des.*, 2014, **14**, 5004–5010.

37   L. Yu, G. A. Stephenson, C. A. Mitchell, C. A. Bunnell, S. V. Snorek, J. J. Bowyer, T. B. Borchardt, J. G. Stowell and S. R. Byrn, *J. Am. Chem. Soc.*, 2000, **122**, 585–591.

38   S. Chen, I. A. Guzei and L. Yu, *J. Am. Chem. Soc.*, 2005, **127**, 9881–9885.

39   L. Yu, *Acc. Chem. Res.*, 2010, **43**, 1257–1266.

40   W. C. McCrone, *Polymorphism, In Physics and Chemistry of the Organic Solid State*, Interscience, New York, 1965.

41   A. J. Cruz-Cabeza, S. M. Reutzel-Edens and J. Bernstein, *Chem. Soc. Rev.*, 2015, **44**, 8619–8635.

42   J. Bernstein, R. J. Davey and J. O. Henck, *Angew. Chemie - Int. Ed.*, 1999, **38**, 3440–3461.

43   A. Llinàs and J. M. Goodman, *Drug Discov. Today*, 2008, **13**, 198–210.

44   D.-K. Bučar, R. W. Lancaster and J. Bernstein, *Angew. Chemie Int. Ed.*, 2015, **54**, 6972–6993.

45   A. Findlay, A. N. Campbell and N. O. Smith, *The Phase Rule and Its Applications*, Dover, New York, 9th ed., 1951.

46   R. Hilfiker, *Polymorphism: in the Pharmaceutical Industry*, Wiley-VCH Verlag GmbH & Co. KGaA, Weinheim, 2006.

47   A. Y. Lee, D. Erdemir and A. S. Myerson, *Annu. Rev. Chem. Biomol. Eng.*, 2011, **2**, 259–280.

48   J. Bauer, S. Spanton, R. Henry, J. Quick, W. Dziki, W. Porter and J. Morris, *Pharm. Res.*, 2001, **18**, 859–866.

49   S. Long, P. Zhou, S. R. Parkin and T. Li, *CrystEngComm*, 2015, **17**, 2389–2397.

50   G. Bolla, S. Mittapalli and A. Nangia, *Cryst. Growth Des.*, 2014, **14**, 5260–5274.

51   M. Sen Yuan, D. E. Wang, P. Xue, W. Wang, J. C. Wang, Q. Tu, Z. Liu, Y. Liu, Y. Zhang and J. Wang, *Chem. Mater.*, 2014, **26**, 2467–2477.

52   G. M. de Oliveira, A. P. B. Ribeiro, A. O. dos Santos, L. P. Cardoso and T. G. Kieckbusch, *LWT - Food Sci. Technol.*, 2015, **63**, 1163–1170.

53   V. Ramamurthy and K. Venkatesan, *Chem. Rev.*, 1987, **87**, 433–481.

54   M. D. Cohen, G. M. J. Schmidt and F. I. Songtag, *J. Chem. Soc.*, 1964, 2000–2013.

55   G. M. J. Schmidt, *J. Chem. Soc.*, 1964, 2014–2021.

56   M. K. Mishra, A. Mukherjee, U. Ramamurty and G. R. Desiraju, *IUCrJ*, 2015, **2**, 653–660.

57   L. Fábián and A. Kálmán, *Acta Crystallogr. Sect. B*, 1999, **55**, 1099–1108.

58   N. K. Nath, B. K. Saha and A. Nangia, *New J. Chem.*, 2008, **32**, 1693–1701.

59   R. Thakuria, N. K. Nath, S. Roy and A. Nangia, *CrystEngComm.*, 2014, **16**, 4681–4690.

60   Ö. Almarsson and M. J. Zaworotko, *Chem. Commun.*, 2004, 1889–1896.

61   K. Chadwick, G. Sadiq, R. J. Davey, C. C. Seaton, R. G. Pritchard and A. Parkin, *Cryst. Growth Des.*, 2009, **9**, 1278–1279.

62   N. K. Duggirala, M. L. Perry, Ö. Almarsson and M. J. Zaworotko, *Chem. Commun.*, 2016, **52**, 640–655.

63   K. Tsaggeos, N. Masiera, A. Niwicka, V. Dokorou, M. G. Siskos, S. Skoulika and A. Michaelides, *Cryst. Growth Des.*, 2012, **12**, 2187–2194.

64   M. J. Zaworotko, *ARS Pharm.*, 2009, **50**, 99–117.

65   G. R. Desiraju, *CrystEngComm.*, 2003, **5**, 466–467.

66   J. D. Dunitz, *CrystEngComm*, 2003, **5**, 506–506.

67   G. P. Stahly, *Cryst. Growth Des.*, 2007, **7**, 1007–1026.

68   G. P. Stahly, *Cryst. Growth Des.*, 2009, **9**, 4212–4229.

69   A. D. Bond, *CrystEngComm*, 2007, **9**, 833–834.

70   C. B. Aakeröy and D. J. Salmon, *CrystEngComm*, 2005, **7**, 439–448.

71   J. A. Bis, P. Vishweshwar, R. A. Middleton and M. J. Zaworotko, *Cryst. Growth Des.*, 2006, **6**, 1048–1053.

72   W. Jones, C. R. Theocharis, J. M. Thomas and G. R. Desiraju, *J. Chem. Soc., Chem. Commun.*, 1983, 1443–1444.

73   A. Bajpai, P. Natarajan, P. Venugopalan and J. N. Moorthy, *J. Org. Chem.*, 2012, **77**, 7858–7865.

74   J. C. MacDonald, P. C. Dorrestein, M. M. Pilley, M. M. Foote, J. L. Lundburg, R. W. Henning, A. J. Schultz and J. L. Manson, *J. Am. Chem. Soc.*, 2000, **122**, 11692–11702.

75   J. A. R. P. Sarma and G. R. Desiraju, *J. Am. Chem. Soc*, 1986, **108**, 2791–2793.

76   J. C. Noveron, M. S. Lah, R. E. Del Sesto, A. M. Arif, J. S. Miller and P. J. Stang, *J. Am. Chem. Soc.*, 2002, **124**, 6613–6625.

77   E. M. Engler, B. A. Scott, S. Etemad, T. Penney and V. V. Patel, *J. Am. Chem. Soc.*, 1977, **99**, 5909–5916.

78   A. I. Kitaigorodsky, *Mixed Crystals*, Springer-Verlag, Berlin Heidelberg, 1984.

79   A. I. Kitaigorodsky, *Physical Chemistry: Molecular Crystals and Molecules*, Academic Press, New York and London, 1973.

80   W. Pfeiler, *Alloy Physics: A Comprehensive Reference*, Wiley-VCH, Weinheim, 1947.

81   L. Bayés-García, T. Calvet, M. À. Cuevas-Diarte, S. Ueno and K. Sato, *J. Phys. Chem. B*, 2015, **119**, 4417–4427.

82   E. Schur, E. Nauha, M. Lusi and J. Bernstein, *Chem. Eur. J.*, 2015, **21**, 1735–1742.

83   M. Lusi, I. J. Vitorica-Yrezabal and M. J. Zaworotko, *Cryst. Growth Des.*, 2015, **15**, 4098−4103.

84   M. K. Mishra, U. Ramamurty and G. R. Desiraju, *J. Am. Chem. Soc.*, 2015, **137**, 1794−1797.

85   R. M. Myasnikova, *Acta Chim. Hungarica-Models Chem.*, 1993, **130**, 363–375.

86   H. Oonk, P. van der Linde, Y. Haget, L. Bonpunt, N. Chanh and M. Cuevas-Diarte, 1991, **88**, 329–341.

87   G. Madhurambal and M. Mariappan, *Indian J. Pure Appl. Phys.*, 2010, **48**, 264–270.

88   C. Vithana, H. Uekusa, A. Sekine and Y. Ohashi, *Acta Crystallogr. Sect. B*, 2002, **58**, 227–232.

89   F. Giordano, R. Bettini, C. Donini, A. Gazzaniga, M. R. Caira, G. G. Z. Zhang and D. J. W. Grant, *J. Pharm. Sci.*, 1999, **88**, 1210–1216.

90   D. Braga, F. Grepioni, L. Maini, M. Polito, K. Rubini, M. R. Chierotti and R. Gobetto, *Chem. Eur. J.*, 2009, **15**, 1508–1515.

91   C. R. Theocharis, G. R. Desiraju and W. Jones, *J. Am. Chem. Soc.*, 1984, **106**, 3606–3609.

92   S. Aitipamula, P. S. Chow and R. B. H. Tan, *CrystEngComm*, 2014, **16**, 3451–3465.

93   K. R. Seddon, *Cryst. Growth Des.*, 2004, **4**, 1087–1087.

94   J. Bernstein, *Cryst. Growth Des.*, 2005, **5**, 1661–1662.

95   G. R. Desiraju, *Cryst. Growth Des.*, 2004, **4**, 1089–1090.

96   A. Nangia, *Cryst. Growth Des.*, 2006, **6**, 2–4.

97   A. Albini and M. Fagnoni, *Green Chem.*, 2004, **6**, 1–6.

98   K. Tanaka and F. Toda, *Chem. Rev.*, 2000, **100**, 1025–1074.

99   G. W. Cave, C. L. Raston and J. L. Scott, *Chem. Commun.*, 2001, 2159–2169.

100   Y. Ohashi., *Reactivity in Molecular Crystals*, Kodansha Ltd., Tokyo (Japan), VCH Verlagsgesellschaft mbH, Weinheim (FRG) and VCH Publishers Inc., New York, NY (USA), 1993.

101   I. Turowska-Tyrk, *J. Phys. Org. Chem.*, 2004, **17**, 837–847.

102   A. K. Galwey, *React. Kinet. Mech. Catal.*, 2015, **114**, 1–29.

103   A. Mustafa, *Chem. Rev.*, 1952, **51**, 1–21.

104   M. D. Cohen, *Pure Appl. Chem.*, 1964, **9**, 567–574.

105   M. D. Cohen and G. M. J. Schmidt, *J. Chem. Soc.*, 1964, 1996–2000.

106   G. M. J. Schmidt, *Pure Appl. Chem.*, 1971, **27**, 647–678.

107   J. M. Thomas, *Pure Appl. Chem.*, 1979, **51**, 1065—1082.

108   M. Hasegawa, *Pure Appl. Chem.*, 1986, **58**, 1179–1188.

109   V. Enkelmann, G. Wegner, K. Novak and K. B. Wagener, *J. Am. Chem. Soc.*, 1993, **115**, 10390–10391.

110   H. Nakanishi, W. Jones and J. M. Thomas, *J. Phys. Org. Chem.. Chem*, 1981, **85**, 3636–3642.

111   F. H. Allen, M. F. Mahon, P. R. Raithby, G. P. Shields and H. A. Sparkes, *New J. Chem .*, 2005, **29**, 182–187.

112   A. Natarajan, J. T. Mague, K. Venkatesan and V. Ramamurthy, *Org. Lett.*, 2005, **7**, 1895–1898.

113   G. R. Desiraju, *Proc. Indian natn. Sci. Acad.*, 1986, **52**, 379–399.

114   S. Karthikeyan and V. Ramamurthy, *J. Org. Chem.*, 2007, **72**, 452–458.

115   M. Nagarathinam, A. M. P. Peedikakkal and J. J. Vittal, *Chem. Commun.*, 2008, 5277–5288.

116   K. Biradha and R. Santra, *Chem. Soc. Rev.*, 2013, **42**, 950–967.

117   L. R. MacGillivray and G. S. Papaefstathiou, *Encycl. Supramol. Chem.*, 2004,

1316–1321.

118   T. Friscic and L. R. MacGillivray, *Z. Krist.*, 2005, **220**, 351–363.

119   V. Ramamurthy and J. Sivaguru, *Chem. Rev.*, 2016, **116**, 9914–9993.

120   N. Nguyen, A. R. Clements and M. Pattabiraman, *New J. Chem.*, 2016, **40**, 2433–2443.

121   D.-K. Bučar, A. Sen, S. V. S. Mariappan and L. R. MacGillivray, *Chem. Commun.*, 2012, **48**, 1790–1792.

122   Y. Maekawa, S. Kato and M. Hasegawa, *J. Am. Chem. Soc.*, 1991, **113**, 3867–3872.

123   C. Vithana, H. Uekusa, A. Sekine and Y. Ohashi, *Cryst. Growth Des.*, 2005, **5**, 1755–1760.

124   Y. Ito, T. Kitada and M. Horiguchi, *Tetrahedron*, 2003, **59**, 7323–7329.

125   G. K. Kole, G. K. Tan and J. J. Vittal, *CrystEngComm*, 2012, **14**, 7438–7443.

126   S. L. James, C. J. Adams, C. Bolm, D. Braga, P. Collier, T. Friščić, F. Grepioni, K. D. M. Harris, G. Hyett, W. Jones, A. Krebs, J. Mack, L. Maini, A. G. Orpen, I. P. Parkin, W. C. Shearouse, J. W. Steed and D. C. Waddell, *Chem. Soc. Rev.*, 2012, **41**, 413–447.

127   L. Takacs, *J. Therm. Anal. Calorim.*, 2007, **90**, 81–84.

128   L. Takacs, *Jom-Journal Miner. Met. Mater. Soc.*, 2000, **52**, 12–13.

129   P. Baláž, M. Baláž and Z. Bujňáková, *Chem. Eng. Technol.*, 2014, **37**, 747–756.

130   A. Nasser and U. Mingelgrin, *Appl. Clay Sci.*, 2012, **67-68**, 141–150.

131   D. R. Weyna, T. Shattock, P. Vishweshwar and M. J. Zaworotko, *Cryst. Growth Des.*, 2009, **9**, 1106–1123.

132   E. Boldyreva, *Chem. Soc. Rev.*, 2013, **42**, 7719–7738.

133   W. Jones and M. D. Eddleston, *Faraday Discuss.*, 2014, **170**, 9–34.

134   K. J. Crowley and G. Zografi, *J. Pharm. Sci.*, 2002, **91**, 492–507.

135   M. R. Caira, Y. Robbertse, J. J. Bergh, M. Song and M. M. De Villiers, *J. Pharm. Sci.*, 2003, **92**, 2519–2533.

136   S.-Y. Lin, *Pharm. Res.*, 2014, **31**, 1619–1631.

137   S. R. Bysouth, J. A. Bis and D. Igo, *Int. J. Pharm.*, 2011, **411**, 169–171.

138   N. Shan and W. Jones, *Green Chem.*, 2003, **5**, 728–730.

139   K. D. M. Harris, *Nat. Chem.*, 2012, **5**, 12–14.

140   T. Friščič and W. Jones, *Cryst. Growth Des.*, 2009, **9**, 1621–1637.

141   R. P. Rastogi and N. B. Singh, *J. Phys. Chem.*, 1966, **70**, 3315–3324.

142   R. Kuroda, Y. Imai and N. Tajima, *Chem. Commun.*, 2002, 2848–2849.

143   G. Rothenberg, A. P. Downie, C. L. Raston and J. L. Scott, *J. Am. Chem. Soc.*, 2001, **123**, 8701–8708.

144   K. Chadwick, R. Davey and W. Cross, *CrystEngComm*, 2007, **9**, 732–734.

145   N. Shan, F. Toda and W. Jones, *Chem. Commun.*, 2002, 2372–2373.

Chapter 2: Fundamentals of techniques and experimental

2.1. Crystallography

X-ray crystallography is an analytical technique which is based on diffraction of X-ray radiation by a crystalline solid material to give a visual image of how the atoms, molecules or ions are arranged in three dimensional space. The science of crystallography began more than a century ago, when the first diffraction pattern was observed by Laue. A year later, Bragg and son used X-rays to determine the first crystal structure. Since then, the science of crystallography has grown significantly and its progress, which is related to computational advancement, has made a significant contribution to the development and understanding of crystalline solids. This is mainly due to its role in facilitating the determination of the relative position of atoms or ions in the structure, which, in turn, enables the researcher to identify the geometrical relationship, between the atoms in terms of bond length and angles, non-bonded distance and molecular conformational.[1,2]

The basic requirements for this technique are; a radiation source, a sample and detector. For single crystal diffraction, the sample has to be a single crystal. An outline on the principle of X-ray crystallography is given in the following sections.[3–9]

2.1.1. X-ray background

X-ray radiation was first discovered by Rontgen in 1895. It is an electromagnetic radiation of high energy and short wave-length (between 0.1-100Å).This wave-length is of similar order to the molecular bond distance (between 0.8-3.0Å), which enables the X-ray to be diffracted by the crystal and hence, useful information about the atomic arrangement in the crystalline solids can be obtained.

X-rays used in a diffraction experiment can be generated in different ways. In the X-ray tube often used as a laboratory source, a high speed accelerating electron beam (emitted from a heated filament cathode) which bombards the target metal anode (stationary or rotating solid anode). Among other effects, this leads to the inner-shell electrons (*K* shell) of the metal being ejected (ionized), leaving vacancies in the inner-shell. The outer-shell electrons (*L* or *M* shells) thereafter fill in this hole with an emission of energy as X-ray photons (Figure 2.1). Molybdenum and copper are the most common metal tar-

gets used in the laboratory to generate X-rays with characteristic wave-lengths of 0.71073Å and 1.54184Å, respectively. The shorter wave-length of the molybdenum X-rays source helps to collect data with a lower absorption. In contrast, copper radiation is more suitable for crystals with larger unit cell dimensions, since the diffraction pattern tends to spread out further due to the longer wavelength.
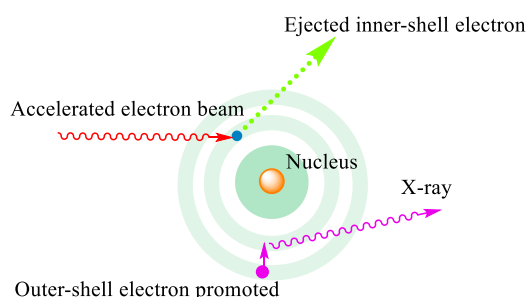
Figure 2.1: X-ray generation

High intensity X-ray sources have been developed. The synchrotron[3,7] is an example of an intense source in which electrons are accelerated around a ring of hundreds of metres in diameter, at a speed of approximately the same order as the speed of light. The electron beam is bent by bending magnets, causing the generation of electromagnetic radiation from IR to X-ray. The advantage is that any single wave-length of X-ray can be selected through the use of a monochromator. Additionally, the beam is very intense and enables the determination of weakly diffracted crystals.

2.1.2. Crystalline solids

A typical crystalline solid consists of molecules, ions or atoms arranged in a specific way to form units which are precisely repeated in a well-defined long range order, through three dimensional space to give a highly ordered structure. Thus, by knowing the contents of the repeating unit (unit cell) and the way in which this unit is repeated (by translation symmetry), the crystal structure can be determined.

If each motif was described using a single point, by applying the symmetry operations, a regular infinite repeating array of points in all 3 directions would be produced; this is called the **crystal lattice**. All lattice points in the crystal have an identical environment.

By joining up lattice points in three dimensions, a box shape is generated (unit cell). The **unit cell** can be defined accordingly, as the smallest repeated unit in the crystal that displays the highest possible degree of symmetry. The unit cell dimensions can be

described by six parameters; three vectors a, b and c (describing the translation of the unit in space along *x, y and z* directions, respectively) and the angles between each pair of vectors, angle α between b and c axes, angle β between a and c axes and angle γ between a and b axes (Figure 2.2).
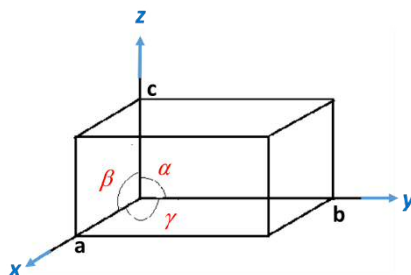
Figure 2.2: *Unit cell definition showing the unit cell parameters a, b, c, α, β and γ.*

Although it seems that infinite box shapes can be generated by joining the lattice points, in reality, by consideration of the possible symmetry implications on the lattice, there are only seven possible basic unit cell geometries that can be generated (shown in Table 2.1). These are called crystal systems. When the lattice points lie only at the corners of the unit cell, the lattice is primitive (P). However, additional lattice points are possible. An example is C which corresponds to a centred lattice where the other lattice points sit on face C. Similarly A and B refer to a centred lattice where additional lattice points sit on face A or B, respectively. F has additional lattice points on all the faces. I represents body centring where the additional lattice point is at the centre of the cell.

Table 2.1. *The seven crystal system and possible Bravais lattices.*

Crystal system	Cell parameters	Possible lattice type
Cubic	$a = b = c$, $\alpha = \beta = \gamma = 90°$	P, I, F
Tetragonal	$a = b \neq c$, $\alpha = \beta = \gamma = 90°$	P, I
Orthorhombic	$a \neq b \neq c$, $\alpha = \beta = \gamma = 90°$	P,C(A), I, F
Hexagonal	$a = b \neq c$, $\alpha = \beta = 90°$; $\gamma = 120°$	P
Trigonal	$a = b \neq c$, $\alpha = \beta = 90°$; $\gamma = 120°$	P
Monoclinic	$a \neq b \neq c$, $\beta \neq 90°$; $\alpha, \gamma = 90°$	P, C
Triclinic	$a \neq b \neq c$, $\alpha, \beta, \gamma \neq 90°$	P

The unit cell usually comprises one or more molecules. If the unit cell involves more than one molecule (most of crystalline materials do), these molecules are usually related to each other by symmetry operations. As mentioned previously, the unit cell contains

the maximum possible symmetry. Thus, the smallest repeated unit required to reproduce the unit cell by applying the symmetry operations is called the **asymmetric unit**.

The symmetry applied to the asymmetric unit within the unit cell is described by one of the 230 unique **space groups**. In the crystalline solid, two types of symmetry can be observed; non-translation symmetry (such as inversion, reflection, rotation and rotation-inversion). However, the addition of translation leads to other kinds of symmetry. For such example, the combination of a mirror plane with a translation of half a unit cell length generates a glide plane. Similarly, combining a rotation with a translation operation gives a screw axis. Full descriptions of these space groups are presented in the International Tables for Crystallography Volume A[10]. The symbol of the space group illustrates the symmetry in the unit cell. For example, a capital letter P in space group $P2_1/a$ for a monoclinic crystal system shows that it is a primitive unit cell, while the 2_1 symbol represents the screw axis along the b-axis, and "a" represents the glide plane along the a-axis, perpendicular to the b-axis.

When the diffraction pattern is collected, the space group can be determined from the distribution of reflection intensities. Some reflections at certain points may be missing (producing zero intensity for sets of Bragg reflections) and this is called **systematic absence**. Systematic absence is the result of destructive wave interference and can be useful in assigning possible space groups, as it depends on the presence of certain space symmetry; glide planes or screw axes, for example.

2.1.3. Theory of X-ray diffraction

In the case of the X-ray diffraction experiment, the incident X-rays interact with the electron cloud of the atoms in the crystal and, subsequently, scattering of X-rays occurs in all directions. The theory behind the interaction between the X-rays and the crystal lattice can be explained by Bragg's law.

The crystal lattice (described earlier in Section 2.1.2) consists of an array of lattice points. The family of lattice points in the same plane form a "lattice plane". Each set of parallel planes are known as Miller planes and can be identified by integers represented by values of h,k,l (Miller indices). A set of Miller planes are equally spaced and the separation distance expressed as d_{hkl} (Figure 2.3). The X-ray beam is considered to be reflected from the set of Miller planes, giving rise to diffraction spots and patterns. How-

ever, as the scattering of X-rays occur in all directions, the diffracted X-rays undergo constructive and destructive interference. For X-rays to interfere constructively (to produce diffraction spots and patterns) Bragg's law (Equation 2.1) should be satisfied.[5]

$$2.1$$

For a given wave-length (λ) of incident X-rays, and inter-plane spacing d_{hkl} with a diffraction angle of θ_{hkl}, the satisfaction of this equation requires that the path difference between the two parallel beams to be an multiple integer (1, 2, 3,…) of the wavelength.
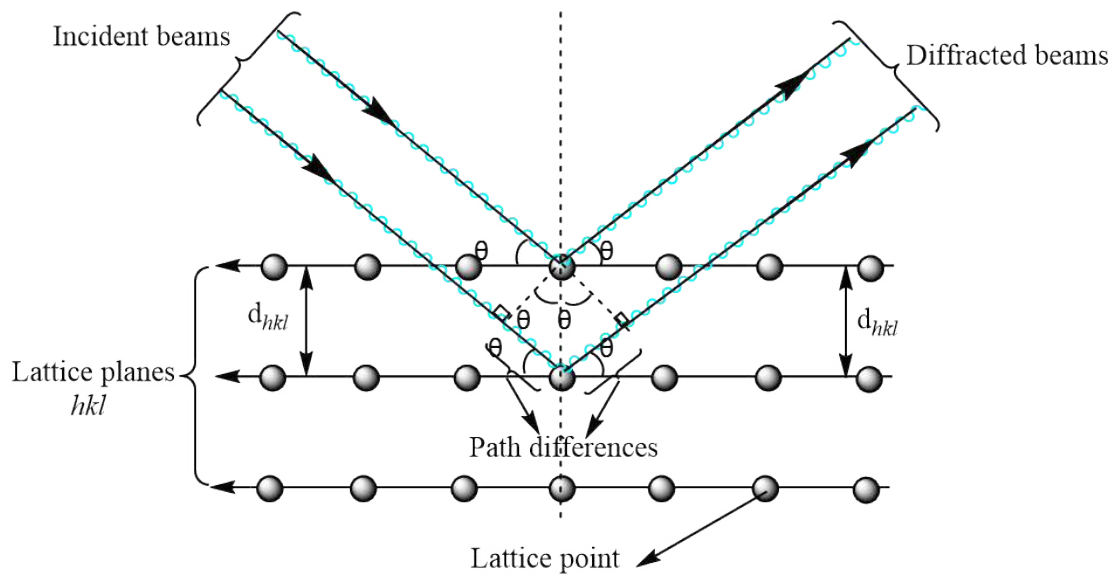
Figure 2.3. *2D view of the crystal lattice showing the X-rays diffraction by the lattice planes and it relation to Bragg's law.*

2.1.4. Reciprocal lattice and the Ewald sphere

As seen in Section 2.1.3, each diffraction spot resulted from the constructive interference from a set of Miller planes and, it can, therefore, be identified by the corresponding value of *hkl*. Each set of diffraction spots give a frame of data. Combining all frames of diffraction produces the reciprocal lattice. The **reciprocal lattice** is the lattice in diffraction space that corresponds to the lattice of the crystal in real space. Each Bragg reflection is associated with a vector, whose direction is perpendicular to the set of planes (*hkl*). The end points of these vectors produce periodic points known as reciprocal lattice points and the collection of these points forms the reciprocal lattice. Thus, each set of lattice planes in the crystal (*hkl*) has a corresponding single point in the reciprocal lattice.

The reciprocal lattice can be therefore defined by the three vectors, a^*, b^* and c^* and the relationship between them and the crystal lattice a, b, c in such the way that a^* is perpendicular to the "a" plane (100), b^* is perpendicular to the "b" plane (010) and c^* is perpendicular to the "c" plane. The magnitude of the vector is $1/d_{hkl}$. This can be understood by recalling Bragg's equation and rearranging it (equation 2.2).

$$\text{—} \quad \text{–} \qquad\qquad\qquad 2.2$$

This shows that sin θ and d spacing are inversely related and, therefore, if the crystal lattice has a large d value, the diffraction pattern will be compressed. In other words, the dimensions of the reciprocal lattice are inversely related to the dimensions of the crystal lattice.

The reciprocal lattice is very useful in understanding the practical applications of a diffraction experiment. In this regard, the concept of the Ewald sphere[9,6] is important to comprehend. Representing the Ewald sphere in 2D, as shown in Figure 2.4, a circle is drawn with its centre at the crystal origin (0) with the radius of $1/\lambda$ (where λ is the wavelength of the radiation used). Bragg's law is satisfied when the reciprocal lattice point touches the circle and, thus, the reflection (*hkl*) can be represented by the vector from the crystal origin to the reciprocal lattice point. However, if the end of the diffracted vector (or a reciprocal lattice point) does not lie on the circle, Bragg's law is not satisfied and a reflection will not be observed.
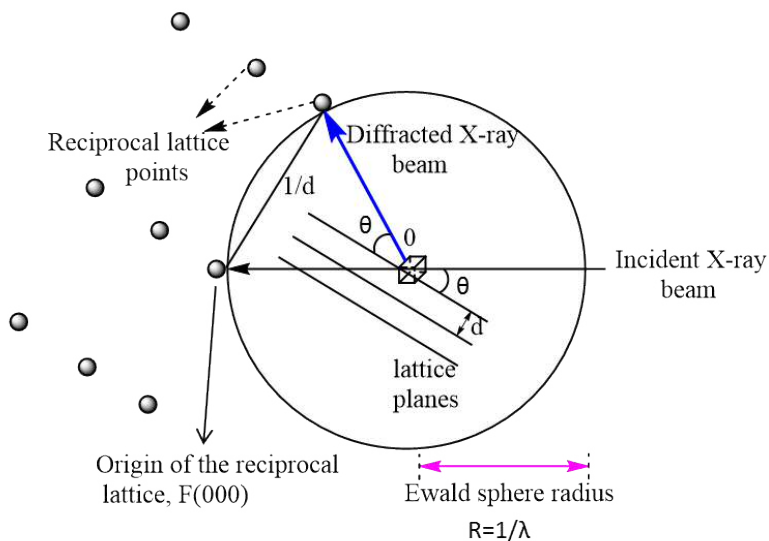
Figure 2.4: The Ewald Sphere.

2.1.5. Obtaining a crystal structure

In practice, there are four basic steps involved in obtaining the crystal structure, by a single crystal X-ray experiment. These steps are simplified by the flowchart in Figure 2.5 and are; grow a high quality single crystal, collect the data, solve the structure and refine the structure.[5,3] These steps are explained later in more detail.
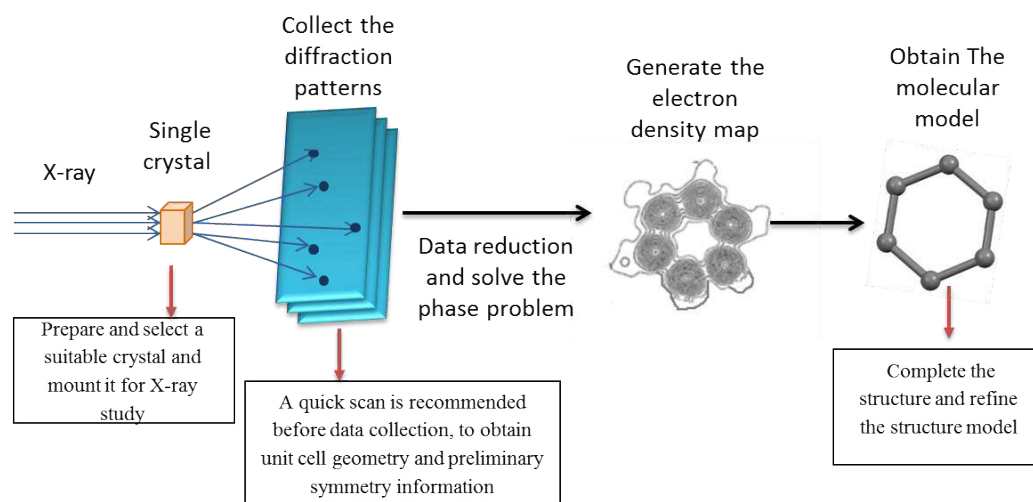
Figure 2.5: *Summary of the steps involved in a crystal structure determination.*

2.1.5.a. Growing a suitable single crystal

For a single crystal X-ray diffraction technique, the crystal obtained should be of high quality, as this determines the final quality of the structure. The regularity of the external shape of the crystal is not important but the periodicity and regularity in the internal arrangements of the molecules, with all unit cells identical and aligned in the same orientation, is the aim. In terms of the crystal size, as the diffraction intensity is proportional to the crystal size, a few tenths of a millimeter is typically acceptable and ideally about 0.1-0.3 mm in each dimension being preferred.

The growing of crystals[5] can be regarded as an art. Sometimes the initial experiment of sample preparation produces suitable single crystals whereas in some cases, recrystallization is required. The ability to precisely control the process of molecular assembly from the solution, for example, is crucial for obtaining a suitable single crystal. Thus, slowing down the crystallization process, allows the molecules to pack efficiently. There are several techniques used for growing suitable crystals. Solution methods are by far the most widely used. Examples include; solvent evaporation, anti-solvent vapour diffusion and seeding. These are now discussed.

Solvent evaporation

A solution of the sample in an appropriate solvent is prepared and placed in a vial. The vial then sealed, with a few holes, and left to let the solvent evaporate slowly. As the solvent evaporates, the concentration of the solution will rise until the crystalline solid appears in the solution. This technique has been used for crystallizations in this study.

Vapour diffusion

In this technique, two liquids (A and B) are required. The first can dissolve the sample to form a solution (A) and B, which cannot dissolve the sample is the anti-solvent. B is usually chosen to be more volatile than solvent A and both A and B are miscible. A solution of the sample in solvent A is placed into a small vial, while solvent B is placed in a larger container. The smaller vial is placed into the larger vial (Figure 2.6) which is then sealed. As the solvent B evaporates, it will diffuse into the inner solution and, this process will decrease the solubility of the compound in solvent A and thus the crystals will form slowly.
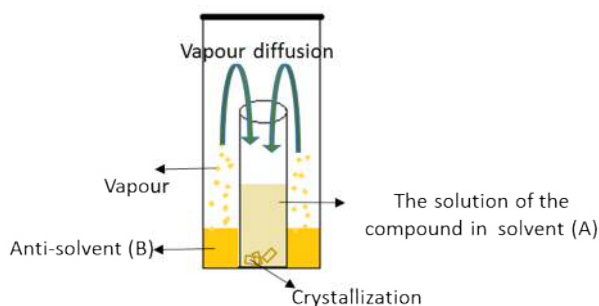
Figure 2.6: Diagram of crystal growing by the vapour diffusion technique.

Seeding crystallization

Seeding is a process in which a nucleation point is introduced into a vial containing the sample solution in order to provide a starting point for the crystal to grow. This technique is usually used to obtain a larger single crystal or to control the phase. Thus, the seed (crystals of the desired substance) is placed into a saturated solution of the compound and evaporation is allowed to generate the required crystal.

Solvents used for crystallization in this study

All crystallization solvents used in this study were commercially available and no further purification was done; ethanol (Aldrich, >99.8%), methanol (Fisher, >99.5%), acetone (Fisher, >99%), acetonitrile (Fisher, >99.99%), dimethylformamide (Alfa Aesar

>99%), dichloromethane (Fisher, >99%), glacial acetic acid (Fisher, >99%), isopropanol (Fisher, >99%) and di-ethyl ether (Fisher, >99%).

2.1.5.b. Data collection

Once a suitable single crystal for an X-ray experiment is obtained, the next step is to expose it to the X-ray beam and collect the data using a diffractometer. Figure 2.7 shows a typical diffractometer.
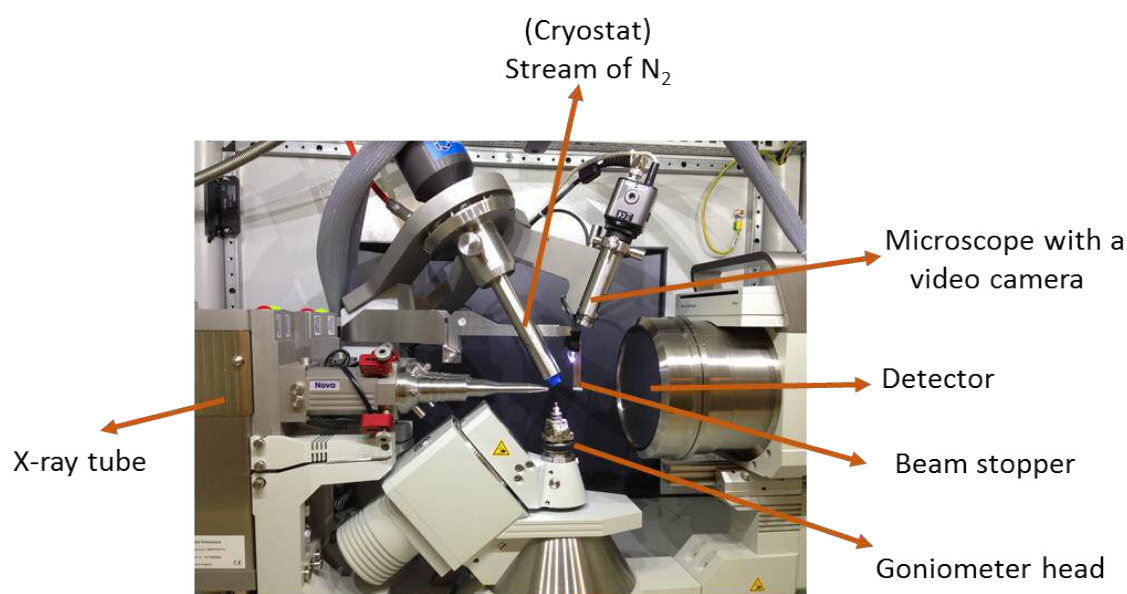
Figure 2.7: *A typical diffractometer.*

Single Crystal Diffractometers

During the experiment, the monochromatic X-ray radiation (generated from the X-ray source, for example, X-ray tube) is focused on the crystal positioned on a goniometer head. The crystal is usually mounted on a plastic loop or glass fibre, which is attached to the goniometer head, and because of the requirement to rotate the crystal during the data collection, an amorphous sticky oil is usually used to stick the crystal onto the loop or the glass fibre. In order to facilitate centring of the crystal in the X-ray beam, a microscope with a video camera is used to magnify the crystal. The location and intensity of the diffracted X-ray beams is recorded by the detector. Photographic film was used in the past but, in a modern instrument, a charge-coupled device (CCD) or an image plate (IP) detector is used. Between the crystal and the detector, a beam stop is placed to prevent non-diffracted X-rays from directly hitting the detector. In the case of measuring

the data at lower temperatures (for example, when lowering thermal vibrations of the atoms is required, or to stabilize air sensitive crystals) a stream of cooled N_2 is used.

Obtaining the unit cell

Before the full data collection, a quick scan is advised. This enables the quality of the crystal to be assessed and the unit cell dimensions to be determined. By indexing these diffraction frames (by assigning of *hkl* indices to each measured reflection) unit cell dimensions, the crystal system and Bravai's lattice can be calculated. The Laue class and space group can also be determined by analysis of the distribution of reflection intensities. Accordingly, a data collection strategy is then calculated using the diffractometer software. In practice, around 1000 to 5000 reflections are usually measured, by rotating the crystal relative to the incident X-ray beam. Because of existence of the symmetry (a diffraction pattern, for example, always has inversion symmetry), only a maximum of hemisphere of the reflection data usually needs to be measured. A crystal that displays higher symmetry requires less data than a crystal of lower symmetry.

It is worth noting that, although some information about the crystal can be determined after collecting a few images, it is necessary to measure full data in order to calculate accurate atom positions.

2.1.5.c. Structure factor and data reduction

The electrons in the structure interact with incident X-rays and scatter them. The measured amplitude of the scattered X-ray from the atom is known as the atomic scattering factor (f_j). The atomic scattering factor is influenced by the electron density of the atom (atomic number) and the Bragg angle of diffraction.

Each reflection results from the contribution of the scattering of all atoms in the unit cell and it depends on the atomic position in the unit cell and the atom type. Thus, for a specific reflection (*hkl*), the resultant scattering can be described by the structure factor *F*(*hkl*). Each reflection is associated with two numerical values; amplitude   and phase   of the diffracted wave. The amplitude represents the magnitude of the wave while the phase represents the horizontal shift of the original wave (Figure 2.8a). It is also useful to represent this diffracted wave using a vector (Figure 2.8b), with the length of the arrow representing the amplitude while the direction is the phase.[3,11]
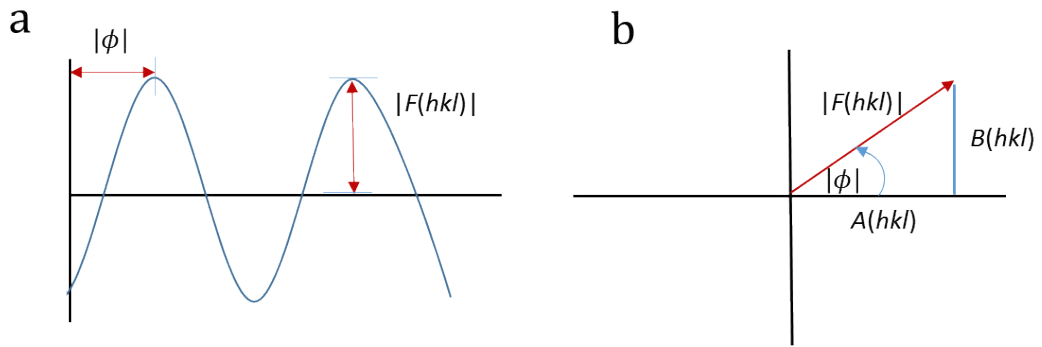
Figure 2.8: *Depiction of how waves can be converted into Cartesian coordinates (a) represented in wave form, (b) represented in a vector form.*

The scattered wave can be described by a complex quantity which is linked to the scattering. The structure factor $F(hkl)$ of a specific Miller index $(h\ k\ l)$ for a crystal comprising N atoms can be obtained from the following expression:

$$2.3$$

Where j is the atom labelled as $j= 1, 2, 3…N$, $(x_j,\ y_j,\ z_j)$ are the fractional atom coordinates in the unit cell while f_j denote the atomic scarring factor for the atom type j.

From Figure 2.8b, the amplitude of the structure factor can be expressed as:

$$2.4$$

where the phase angle $\hspace{3cm}$ 2.5

The intensity generated in a diffraction experiment, $I(hkl)$, is related to the square of the amplitude of the structure factor. Various factors affect the measured intensity and, corrections such as Lorentz, polarization and absorption correction need to be applied. The outcome of this process is a file listing the Miller indices *(hkl)* and their corresponding intensities I and the standard deviation $\hspace{1cm}$ of the intensity. From this information the structure amplitude $|F_{h,k,l}|$ and its $\hspace{0.5cm} F_{(h,k,l)}$ can be obtained directly. The process of converting the raw measured intensities $I(hkl)$ to the structure factor amplitude after the application of corrections is known as data reduction.

2.1.5.d. Fourier transform and the phase problem

After processing of the data, computational work is carried out in order to solve the structure[7,8] by generating an electron density map (i.e. the location of the atoms in the determined unit cell).

The crystal structure is related to the X-ray diffraction pattern by a mathematical process known as Fourier transform. Similarly, the electron density distribution within the unit cell is related to the amplitude of the structure factor and the X-ray phase by the Fourier transform and this can be expressed by the following equation:

$$\qquad\qquad - \qquad\qquad\qquad\qquad\qquad\qquad 2.6$$

is the electron density for every point (*x, y, z*) in the unit cell, V is the volume of the unit cell,   is the structure factor amplitude and   is the phase. If both the amplitude and phase could be measured directly from the X-ray experiment, the electron density of each position (*x, y, z*) within the unit cell can be calculated using equation 2.6 and, hence, the structure can be easily determined. However, the experimental diffraction data only provides information of the magnitude of the structure factor, i.e. only the amplitudes are known but, unfortunately, the phase information is lost. This is known as the "phase problem". To overcome this problem, methods have been developed; direct methods, Patterson method and superflip are examples. The process of solving the phase problem is known in crystallography as structure solution. In this study, direct methods were the main approach used to solve the phase problem.

Direct methods

These methods are used most frequently for small molecules (100-200 atoms) that comprise atoms of similar atomic number. They are a mathematical approach that enables the estimation of possible phase information using the diffraction intensities. It is essentially a trial and error method and is based on two concepts. One is that the electron density can only have a positive or zero value and cannot be negative. The other concept is that the electron density is concentrated at the atom positions. These concepts aid in the determination of the relationships of the diffraction phases,

particularly for those of the most intense diffraction (as they contribute most to the diffraction pattern).

Thus, in the methods, a set of the three strongest reflections (known as a triplet set) is chosen and then the probable relationships between their phases worked out. Many trial sets are used (often several hundred) to provide some information on the most probable phases. Based on this information, other reflections are used to see how well the probabilities are satisfied, and then Fourier transform performed, using the best probable phases and their corresponding amplitude to generate the electron density map. If this map contains recognizable fragments then structure solution has been obtained. However, new trial sets should be attempted in cases where the generated fragment is unrecognizable. After the structure is solved, it is then subject to the refinement process.

2.1.5.e. Structure refinement

The process of refinement can be regarded as part of structure solution, as the structure can be completed. In order to obtain the best molecular model after the structure solution, the process of refinement is vitally important. This process will hopefully enhance the molecular model to fit better against the experimental diffraction data (i.e. to bring the molecular model closer to the actual molecular structure). This can be done by subjecting the molecular model through cycles of refinement by adjusting some parameters, for example, adding or deleting atoms, moving the atoms (positional coordinates) and generating the atomic displacement parameters that represent the vibration of the atom (thermal ellipsoids). Thermal ellipsoids for asymmetric units of some structures determined in this work are presented in the appendix.

A diffraction pattern can be calculated after each cycle of refinement via Fourier transformation, using the new set of phases generated after each cycle of refinement. As the refinement progresses, the differences between the calculated diffraction pattern and the experimental is hopefully minimized, allowing better a molecular model to be obtained.

R-factor

In order to assess the agreement between the calculated model and the experimental data, an analytical statistical method is used. This provides a numerical value, called the

residual factor, or *R*-factor, that can be used to monitor the refinement process. The mathematical definition of this value is shown in equation 2.7.

$$\underline{\hspace{4cm}} \hspace{4cm} 2.7$$

The *R*-factor gives the average relative deviation between the observed, ____ and calculated, ____ . Thus lower *R*-factor values indicate better molecular models, and vice versa. A typical R-factor for complete crystal structure is around 0.02-0.07.

Disorder

Disorder occurs in the crystal when the same atom adopts two or more sites in the structure. This type is known as positional disorder and usually occurs in a molecule (or even part of it) that is able to take on a different orientation or different conformation. It can also occur when two different atoms occupy the same site in different unit cells. This type is known as substitutional disorder and is usually found on the cocrystallization of different substituents to form solid solution.

Disorder can be identified in the structure during the refinement process by unusually elongated anisotropic displacement ellipsoids or by the appearance of a residual electron density in the electron map after the structure has been assigned. It can also affect the R-factor of the structure and thus dealing with this behaviour correctly may contribute to lowering the R-factor. To model the disorder, the amount of each component is determined according to the distribution of the electron density map, considering that the total occupancy of the different components should be unity.

2.1.5.f. The experimental method used for single crystal structure determination

Single-crystal X-ray diffraction (SC-XRD) data were recorded at either 150K or ambient temperature using either a Nonius Kappa CCD diffractometer (graphite monochromated Mo-Kα radiation; $\lambda = 0.71073$ Å) or an Agilent SuperNova Dual Atlas diffractometer with mirror monochromator and either MoKα ($\lambda = 0.71073$ Å) or CuKα ($\lambda = 1.54180$ Å) radiation. The temperature was controlled using an Oxford Cryosystem cooling apparatus. Crystal structures were solved using direct methods in the program Shelxs-2013[12] and refined using Shelxl-2014[12]. Non-hydrogen atoms were refined with anisotropic displacement parameters. Hydrogen atoms were inserted in idealized

positions and refined using a riding model with U_{iso} equal to 1.2 or 1.5 times the value of U_{eq} for the atom to which it is bonded. In some structures, the hydrogen atom of the carboxylic acid group is disordered, and modelled with a total occupancy of unity.

2.2. X-ray powder diffraction

The majority of the crystal structures are determined using the single crystal X-ray diffraction technique but the information provided is about the measured single crystal. However, in order to characterize the bulk material, powder X-ray diffraction (PXRD) is used. It can be used as a fingerprint technique and to determine whether the sample is pure or a mixture of phases and it is vital in identifying polymorphism in a material. This is the main purpose of using PXRD in this study.

The theoretical aspects of powder X-ray diffraction are similar to those discussed for single crystal diffraction (Sections 2.1.1 to 2.1.4) although there are significant differences in the experimental aspect regarding the sample preparation, data collection and the data analysis.[13]

Sample preparation and powder diffraction experiments

In comparison with SC-XRD, where a single crystal is required, the PXRD experiment uses a polycrystalline powder sample of randomly oriented particles in which ideally there is no preferred crystallite orientation. This sample is then placed in a sealed glass capillary or sandwiched flat between two pieces of tape and exposed to X-rays.

During the experiment, an incident X-ray beam is diffracted by the crystalline particles, with each particle behaving as a single crystal giving rise its own diffraction pattern. However, because the sample exists as randomly oriented crystalline particles there will be, for each set of the planes, at least some of the crystalline particles in the correct orientation to diffract X-rays. Thus, each accessible lattice plane at the 2θ angle defined by Bragg's law produces a cone of diffraction (Figure 2.9). The 3D of diffraction data is, as a consequence, compressed into 1D to produce a PXRD pattern. This causes overlaps of diffraction peaks in the PXRD pattern. This leads to difficulties in extracting information for structural determination, when compared with a SC-XRD determination.[4,13]

A typical recorded PXRD pattern is shown in Figure 2.10. It comprises reflection intensities as a function of the diffraction angle (2θ). The peak positions provide information regarding the Miller indices and, therefore, the unit cell parameters, whereas information relating to the unit cell contents can be extracted from the peak intensities.
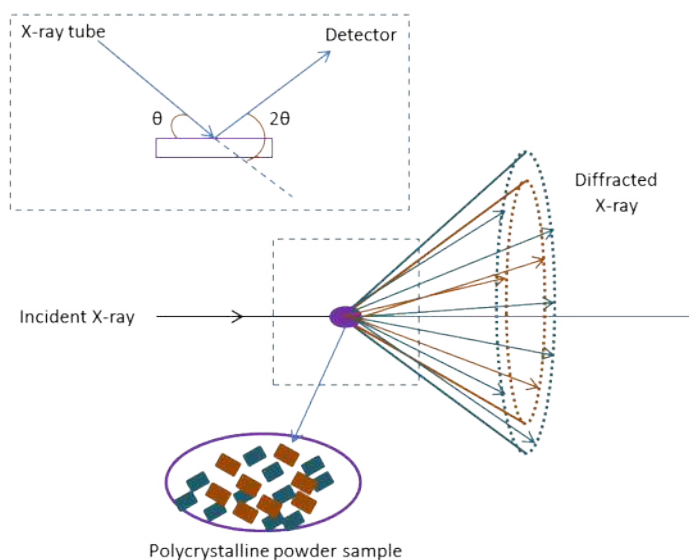
Figure 2.9: *Projection of PXRD experiment. Cones of diffraction produced from a polycrystalline powdered sample (simplification shows only two orientations, blue and brown, and each set of crystals has one set of diffracting plane). θ is the angle between the incident beam and the plane, whereas 2θ is the angle between the incident and diffracted beams.*
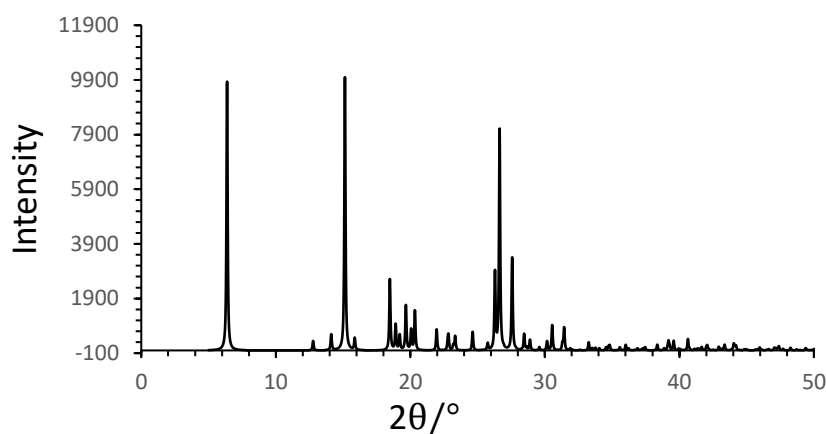
Figure 2.10: *A typical PXRD pattern.*

2.2.1. The experimental method used for PXRD

Powder XRD has been used in this study for the identification of the crystallization products. It was carried out at ambient temperature using a Bruker D8 instrument operating in transmission mode (CuKα1 radiation, germanium monochromated). A

typical scan was from 5-35° in 2θ and the exposure time in the range of 2-16 seconds per step (depending on the sample) the step size was around 0.02°.

2.3. Differential scanning calorimetry

Differential scanning calorimetry[14,15] (DSC) is a simple, and frequently used analysis technique for the investigation of the thermal properties of materials. It provides information on the energy absorbed or released on heating or cooling the sample.

For the experiment, a few milligrams of the sample is accurately weighted and placed in a sealed aluminum pan. Both sample and the reference (empty pan) are subjected to the same heat program. During the experiment, the difference of the heat flow between the sample and the reference (the flow of energy into or out of the sample) is recorded as a function of temperature. This provides qualitative and quantitative information of any physical and chemical process (endothermic or exothermic), such as, polymorphic phase transformation, melting or crystallization. For example, when the sample undergoes an endothermic event (e.g. melting), heat energy is absorbed by the sample and, hence, energy flows into the sample, enabling it to maintain the same heating rate as the reference. This is reflected by an endothermic peak in the DSC thermogram. Figure 2.11 shows an example of a thermogram. Thus, DSC is a useful technique in many studies, such as investigations of multi-components systems and also the study of polymorph phase transformation.
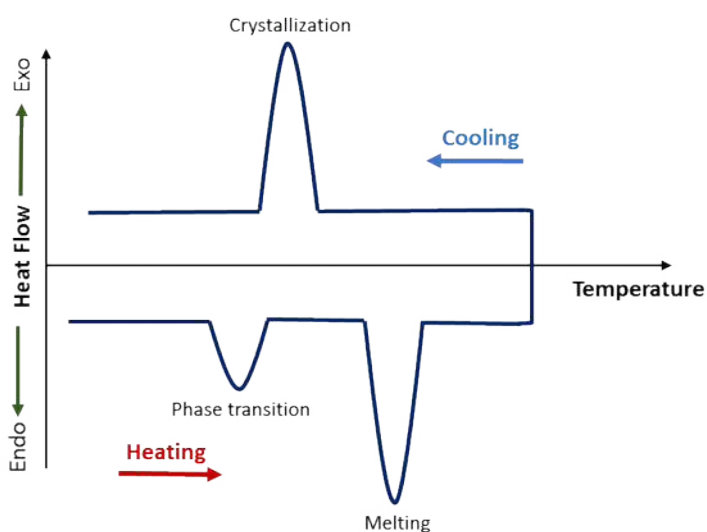
Figure 2.11: *Schematic illustration showing different DSC thermal events that may be observed using DSC.*

2.3.1. The experimental method used for DSC

For the thermal analysis, Differential Scanning Calorimetry (DSC) was carried out using a TA Instruments DSC Q100. About 2-5 mg of a sample was placed in a covered hermetic aluminium pan. Heating/cooling rates within the range 10-20 °C min^{-1} were used, with an equilibration time of 1 min between heating and cooling cycles.

2.4. HPLC

High performance liquid chromatography (HPLC) is a widely used analytical technique for separation, identification and quantification of species of different materials (for example organic, inorganic and biological samples).[16]

The principle of this technique[16,17] depends on the differences in the interaction between the stationary phase and the analytes. This leads to the separation of the components as they flow through the stationary phase, as each component presents has a different elution time. The stationary phase is fixed in a column while the mobile phase is moved through the column carrying the analyte.

The difference between HPLC and ordinary liquid chromatography (LC) is the use of high pumping pressures in HPLC that force the mobile phase to elute through the stationary phase, instead of eluting the mobile phase through the column by gravity.

There are many types of HPLC. Normal and reversed-phase (Rf) are widely used types, in which the separation is based on the relative polarities of the mobile and stationary phases. In normal-phase HPLC, the stationary phase is polar and the mobile phase is non-polar. However, a non-polar stationary phase (often hydrocarbon) and the polar mobile phase are used in Rf-HPLC. For separation experiments in this study, Rf-HPLC is used.

In this case, the analytes distribute between the polar mobile phase (such as acetonitrile) and the non-polar stationary phase (hydrocarbon chains attached to the silica) according to their relative polarity. Thus, the most polar molecule elutes first as there is more attraction between the polar molecules (analyte) and the mobile phase (it will move with the mobile phase and pass out of the column first). However, the less polar molecule will display the opposite behaviour and is attracted more by the non-polar stationary phase and is, therefore, slowed down.

The analytes then pass through a detector and the signals will translate into a chromatogram (graphical display of the peaks generated as the separated components pass through the detector versus time).

2.5. NMR Spectroscopy

Nuclear magnetic resonance spectroscopy (NMR)[18] is an analytical technique that is frequently used to characterize organic materials. It provides information on the chemical and physical properties of atoms or molecules, such as structure, dynamics, reaction state, and chemical environment of atoms in the molecule. These can be derived by exploiting the magnetically distinct nucleus of certain atoms being studied; hydrogen and carbon, for example, are commonly used nuclei.

The nuclei are electronically charged and many have spin. When a strong magnetic field is applied, different nuclei change their spin orientation leading to energy differences between the two states involved. This small energy difference (ΔE) is usually given as a frequency. The NMR spectrum is a plot of the frequencies of the absorption peaks versus intensities of the NMR signals.

2.6. CASTEP

CASTEP[19,20,21] is a software package that is based on density functional theory (DFT). It allows simulation and calculation of a variety of properties of a material. A complete NMR simulation can be produced using CASTEP.

2.7. References

1   K. Hasegawa, *Rigaku J.*, 2012, **28**, 14–18.

2   S. Galli, *J. Chem. Educ.*, 2014, **91**, 2009–2012.

3   W. Clegg, *Crystal Structure Determination*, Oxford University Press, Oxford, New York, 1998.

4   C. Hammond, *The Basics of Crystallography and Diffraction*, Oxford University Press, Oxford, New York, 2nd ed., 2001.

5   A. J. Clegg, B. William, J. M. Cole, J. S. O. Evans, P. Main, S. Parsons and D. J. Watkin, *Crystal Structure Analysis: Principles and Practice*, Oxford University Press, Oxford, 2nd ed., 2009.

6   J. P. Glusker and K. N. Trueblood, *Crystal Structure Analysis: A Primer*, Oxford

University Press, Oxford, 3rd ed., 2010.

7   L.-L. Ooi, *Principle of X-ray Crystallography*, Oxford University Press Inc., New York, 2010.

8   W. Clegg, *X-ray Crystallography*, Oxford University Press, Oxford, 2nd ed., 2015.

9   *The 15th BAC/CCG Intinsive Teaching School in X-ray Structure Analysis*, University of Durham, 2015.

10   J. A. Ibers and W. C. Hamilton, *International Tables for X-ray Crystallography. Vol. 4, Revised and Supplementary Tables to Volumes 2 and 3*, Kynoch Press, Birmingham, 1974.

11   M. F. C. Ladd and R. A. Palmer, *Structure Determination by X-ray Crystallography*, Plenum Press, New York, 3rd ed., 1994.

12   G. M. Sheldrick, *Acta Crystallogr. A*, 2008, **64**, 112–122.

13   R. Guinebretiere, *X-ray Diffraction by Polycrystalline Materials*, Wiley InterScience (Online Service), London, 2007.

14   P. Gabbott, *Principles and Applications of Thermal Analysis*, Blackwell Pub, Oxford, Ames, Iowa, 2008.

15   M. E. Brown, *Introduction to Thermal Analysis: Techniques and Applications*, Chapman and Hall, London, 1988.

16   G. D. Christian, *Analytical Chemistry*, N.J. : Wiley, Hoboken, 6th ed., 2004.

17   D. A. Skoog, D. M. West, F. J. Holler and S. R. Crouch, *Fundamentals of Analytical Chemistry*, Brooks/Cole CENGAGE Learning, Australia, 9th ed., 2014.

18   D. L. Pavia, G. M. Lampman, G. S. Kriz and J. R. Vyvyan, *Introduction to Spectroscopy*, Brooks,Cole, Cengage Learning, USA, 4th ed., 2009.

19   S. J. Clark, M. D. Segall, C. J. Pickard, P. J. Hasnip, M. J. Probert, K. Refson and M. C. Payne, *Zeitschrift fuer Krist.*, 2005, 567–570.

20   C. J. Pickard and F. Mauri, *Phys. Rev. B Condens. Matter Mater. Phys.*, 2001, **63**, 245101/1–245101/13.

21   J. R. Yates, C. J. Pickard and F. Mauri, *Phys. Rev. B Condens. Matter Mater. Phys.*, 2007, **76**, 024401/1–024401/11.

Chapter 3: Investigation of *meta-trans*-cinnamic acids: structural characterization, polymorphism and temperature induced phase transformation

3.1. Introduction

Cinnamic acid (3-phenyl-propenoic acid) is a natural simple organic substance. Its importance has been shown by wide-spread applications of its derivatives in a variety of scientific fields. From a medical perspective, for example, cinnamic acid and its derivatives display biological activities as antioxidants, insect repellents, and have antidiabetic and antifungal properties, in addition to their anticancer efficacy.[1-5] In chemistry, the importance of cinnamic acid originates from its three main reactive sites; the phenyl ring where the substitution reaction can be induced, the α,β-unsaturation site where the addition reaction can occur and the carboxylic acid group. In organic solid state chemistry, cinnamic acid has been a model compound since the pioneering work of Schmidt and co-workers.[6-8] Since then, cinnamic acid derivatives have been continuously of interest in solid state chemistry.[9-11]

As discussed previously in the Chapter 1, polymorphs have different thermodynamic stabilities and therefore transition may be expected from one polymorph to another, i.e. from one crystal structure to another, in response to a relatively small disruption in environmental conditions such as temperature or pressure.[12-14] Thus, analysis of the structures of related polymorphs provides the means of exploring the delicate balance between the interactions that feature in crystalline solids and, may help in understanding the mechanism behind the transformation. The observation that polymorphic phase transitions may occur in *trans*-cinnamic acids arose from the seminal work of Schmidt and co-workers,[8] although this issue received little attention until relatively recently.[15-17]

A study of polymorphic phase transformation of the 3-bromo-*trans*-cinnamic acid system showed[15] that β and γ polymorphs can coexist at ambient temperatures. At higher temperatures ($\approx$ above than 100 °C), however, the γ structure transforms irreversibly to the β structure. The transformation of β *trans*-cinnamic acid to the α form of the acid has also been reported.[8,16]

Transformations between two members of the same polymorphic classification (i.e. α, β or γ) are of particular relevance to the work in this chapter; examples are the transformation of the triclinic α polymorph of 2-ethoxy-*trans*-cinnamic acid to a second triclinic form on heating above 333 K[18], transformation of the triclinic β polymorph of 4-trifluoromethyl-*trans*-cinnamic acid to a second triclinic form on cooling below 132 K[19], and transformation of the monoclinic β polymorph of 4-bromo-*trans*-cinnamic acid to a second monoclinic form on cooling below *ca.* 250–260 K[17]. In all cases, the transformations are reported to be reversible. However, to the best of our knowledge, the co-existence (as stable and *meta*-stable polymorphs) of two members of the same polymorphic classification (α, β or γ) for a simple *trans*-cinnamic acid has not been reported previously.

Therefore, the exploration of polymorphic forms of *meta*-cinnamic acid derivatives and possible transformation was a prime aim of the study in this chapter. A systematic study on a set of different *meta*-cinnamic acids; 3-trifluoromethyl-*trans*-cinnamic acid (3-CF$_3$CA), 3-fluoro-*trans*-cinnamic acid (3-FCA), 3-methyl-*trans*-cinnamic acid (3-MeCA), 3-chloro-*trans*-cinnamic acid (3-ClCA) and 3-bromo-*trans*-cinnamic acid (3-BrCA), has been carried out (see Scheme 3.1). A series of crystallization experiments were performed in order to obtain different polymorphs and the characterization of the product was done using SC-XRD and PXRD techniques. Further investigation of possible phase transitions has been studied by thermal analysis (Differential Scanning Calorimetry). In addition, the possibility of single crystal-to-single crystal (SC-SC) transformation has also been investigated in this study using SC-XRD. The study explores the possible correlation between *meta*-substituents and the structures obtained, intermolecular interactions (hydrogen and halogen contacts), phase transition and the potential of the photo-chemical reaction of the structures.

It is worth noting that the naming of polymorphs in this study follows the classification of cinnamic acids by Schmidt. The first polymorphs of the acid discovered in this study are labelled α, γ, β. Where there are two polymorphs of the same classification, then the first is farther labelled 1 and the second labelled 2 (e.g. γ_1, γ_2). All labels previously reported have not been changed.
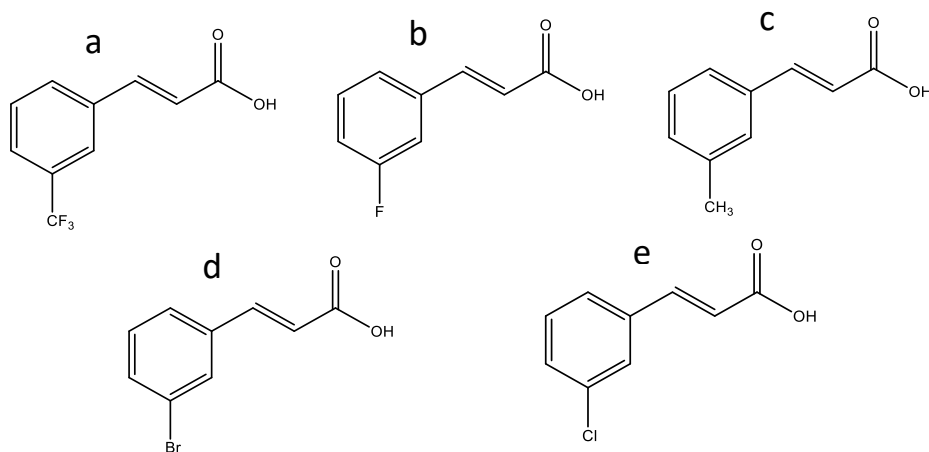
Scheme 3.1. *Molecular structure of (a) 3-CF₃CA, (b)3-FCA, (c)3-MeCA, (d) 3-BrCA and (e) 3-ClCA.*

3.2. Crystallization

Slow evaporation of the solvent at ambient temperature was used in this study as a general crystallization method. An appropriate amount of acid was dissolved in different solvents or mixture of solvents followed by agitation by stirring, sonic-bath or both, to accelerate dissolution. The solutions were then covered with perforated aluminium foil or para-film, and left to evaporate under ambient laboratory conditions until the crystals appeared, usually after several days. The results are summarized in Table 3.1.

3-CF₃CA was purchased from Aldrich (>98%). PXRD of the material revealed that it was a mono-phasic sample of the γ_1 polymorph. In attempts to obtain different polymorphs, slow evaporation of the solution in different solvents or ≈ 1:1 volume ratios of mixtures of the solvents at ambient temperature was done using methanol (MeOH), acetone (AC), acetonitrile (ACN), di-ethyl ether (DEE), glacial acetic acid (GAA), ethanol (EtOH), EtOH/MeOH, EtOH/AC, MeOH/AC, AC/ACN, MeOH/ACN and EtOH/ACN. All crystallizations except DEE, produced mono-phasic γ_1 (γ_1 and γ_2 mention below will be discussed in Section 3.3.1.a). Crystallization from DEE revealed, by PXRD, additional peaks to those observed for the γ_1 phase, indicating the existence of traces of another phase, but it could not be identified by crystal habit. Colourless plate single crystals of γ_1 suitable for crystal structure determination were obtained from crystallization from ethanol. The pure γ_2 phase of the acid was crystallized from the melt. An appropriate amount of the acid was transferred into a covered Petri dish and heated on a hotplate until the entire sample melted and the sample was then allowed to cool slowly. The obtained crystals were suitable for single crystal structure determination.

3-FCA was supplied by Alfa Easer (>98%). Different solvents were used for crystallization experiments (EtOH, MeOH, AC, ACN, dimethylformamide (DMF), dichloromethane (DCM), deuterated acetone (d.AC) and GAA. In addition, the following mixed solvent systems (~1:1volume ratios) were used: EtOH/MeOH, MeOH/AC, AC/ACN, MeOH/ACN and EtOH/ACN). The crystals obtained in all cases were colourless plates. Except crystallization from ACN and d.AC, all experiments gave the same monophasic product, which were designate as β_1 (β_1 and β_2 mentioned below will be discussed in Section 3.3.1.b). Crystallization from ACN and d.AC, on the other hand, produced β_1 together with smaller amounts of a second phase which were designated as β_2. Single crystals for the crystal structure determination were from ACN for β_1 and from d.AC for β_2. PXRD for the supplied acid showed that it is β_1, while pure β_2 was obtained from the crystallization of acid from the melt.

3-MeCA was obtained from Alfa Easer (>98%). The PXRD of the supplied sample indicated that it was the γ phase. Attempts were made to crystallize the acid using different solvents including EtOH, MeOH, AC, isopropanol (i-POH), ACN, GAA as well using $\approx$ 1:1 volume ratio mixtures of solvents, EtOH/MeOH, MeOH/H_2O, EtOH/H_2O, MeOH/AC, EtOH/AC, and AC/H_2O. The crystal for structure determination was obtained from EtOH.

3-BrCA, with purity >98%, was obtained from Alfa Easer. PXRD experiment on the sample from the supplied bottle showed a monophasic γ form. It was reported[8,15] that the γ form of the acid was produced by crystallization from EtOH and the β form from acetic acid (AA). However, our experiments showed that the crystallization of the acid from EtOH produced β crystals, while crystallization of the acid from GAA gave the β phase contaminated with γ. Initial attempts at crystallization of the acid from MeOH gave the pure γ phase, but repeating the same crystallization method subsequently produced a mixture of γ and β. Interestingly, later crystallization of the acid from MeOH gave just the β form. Crystallization of the acid from i-POH produced β together with a new polymorph designated as γ_2. However, repeating the same crystallization experiment from i-POH gave β contaminated with γ and, surprisingly, no γ_2. Crystallization of the acid from DEE produced a mixture of γ, γ_2 and β phases. Crystallization from AC and ACN produced mixtures of γ and β. The crystal for structure determination of γ_2 was obtained from i-POH.

3-ClCA was purchased from Alfa Easer (>98%) and PXRD of the original sample revealed that it was the γ phase. γ-3-ClCA was produced by Cohen et al.[8] from the crystallization of AA, while the β form was reported to be produced from EtOH. However, it was found[20] that crystallization of the acid from cooled EtOH (15 °C) produced the γ form. Crystallization from water diffusion into a solution in AA was reported to produce β form.[21] Our investigation revealed that crystallization of the acid from GAA gave the β phase with contamination by γ, while crystallization of the acid from MeOH gave the pure γ phase. Crystallization in different solvents such as EtOH, AC and ACN gave mixtures of γ and β. Crystallization of the acid from the melt produced pure β. Single crystals for structure determination were obtained from acetone for γ and from GAA for β.

Table 3.1. Summary of the crystallization solvents used in this chapter and the crystalline forms obtained.

		3-CF$_3$CA	3-FCA	3-MeCA	3-BrCA	3-ClCA
Solvents	**MeOH**	γ_1	β_1	γ	$(\gamma ,\gamma+ \beta, \beta)$	γ
	EtOH	γ_1	β_1	γ	β	$\gamma+ \beta$
	AC	γ_1	β_1	γ	$\gamma+ \beta$	$\gamma+ \beta$
	ACN	γ_1	$\beta_1+ \beta_2$	γ	$\gamma+ \beta$	$\gamma+ \beta$
	DEE	$\gamma_1+ \gamma_2$	-	-	$(\gamma+ \gamma_2+\beta)$	-
	GAA	γ_1	β_1	γ	$\gamma+ \beta$	$\gamma+ \beta$
	DMF	-	β_1	-	-	-
	DCM	-	β_1	-	-	-
	d.AC	-	$\beta_1+ \beta_2$	-	-	-
	i-POH	-	-	γ	$(\beta +\gamma_2 ,\gamma+\beta)$	-
	MeOH/ EtOH	γ_1	β_1	γ		-
	MeOH/AC	γ_1	β_1	γ	-	-
	MeOH/ACN	γ_1	β_1	-	-	-
	EtOH/ACN	γ_1	β_1	-	-	-
	EtOH/AC	γ_1	β_1	γ	-	-
	AC/ACN	γ_1	β_1	-	-	-
	MeOH/H$_2$O	-	-	γ	-	-
	EtOH/H$_2$O	-	-	γ	-	-
	AC/H$_2$O	-	-	γ	-	-

3.3. Results and Discussion

3.3.1. Novel polymorphs of cinnamic acids: discovery and structure determination

3.3.1.a. 3-Trifluoromethyl-*trans*-cinnamic acid (3-CF$_3$CA)

Searching the Cambridge structure data base (CSD) indicated that no crystal structure has been reported for 3-CF$_3$CA. The crystals from purchased acid samples were not suitable for single crystal diffraction technique. Thin, colourless, plate-like crystals, suitable for single crystal X-ray diffraction, were obtained from EtOH. The crystal structure determination revealed the acid to be a γ form and it was labelled 1 (i.e. γ_1) to differentiate it from another discovered γ phase of the acid as discussed in Section 3.1.

γ_1-3-CF$_3$CA

The crystal structure of the γ_1 polymorph of 3-CF$_3$CA is monoclinic (space group P2$_1$/a) with one molecule in the asymmetric unit (Figure 3.1a); crystallographic data are shown in Table 3.2. In the crystal structure the normal carboxylic acid dimer via hydrogen bonds is observed clearly linking two molecules across a centre of inversion. Looking along the a-axis it is clear that the dimeric units are stacked in two orientations, nearly perpendicular to each other (Figure 3.1b). The angle between the planes of the molecules in the two orientations is 87.01°. In each stack of dimers, the distance between the centres of the C=C bonds of neighbouring molecules is 4.904Å which is outside of the Schmidt criteria of photodimerization reaction. Viewing the structure along the b-axis (Figure 3.1c) revealed a structure with the bulky CF$_3$ groups forming a bi-layer. In this structure weak C-H···F hydrogen interactions are observed. The shortest distance between the F···F from different CF$_3$ groups is about 3.003Å, which is greater than the sum of the Van der Waals radii of fluorine atoms.[22] Weak C-H···F interactions are observed in the structure (Table 3.3). This observation is consistent with the Thalladi et al.[23] observation that the C-F group would prefer to form C-H···F interactions rather than F···F contacts, in contrast to heavier halogens. Hydrogen bond details are summarized in Table 3.3.
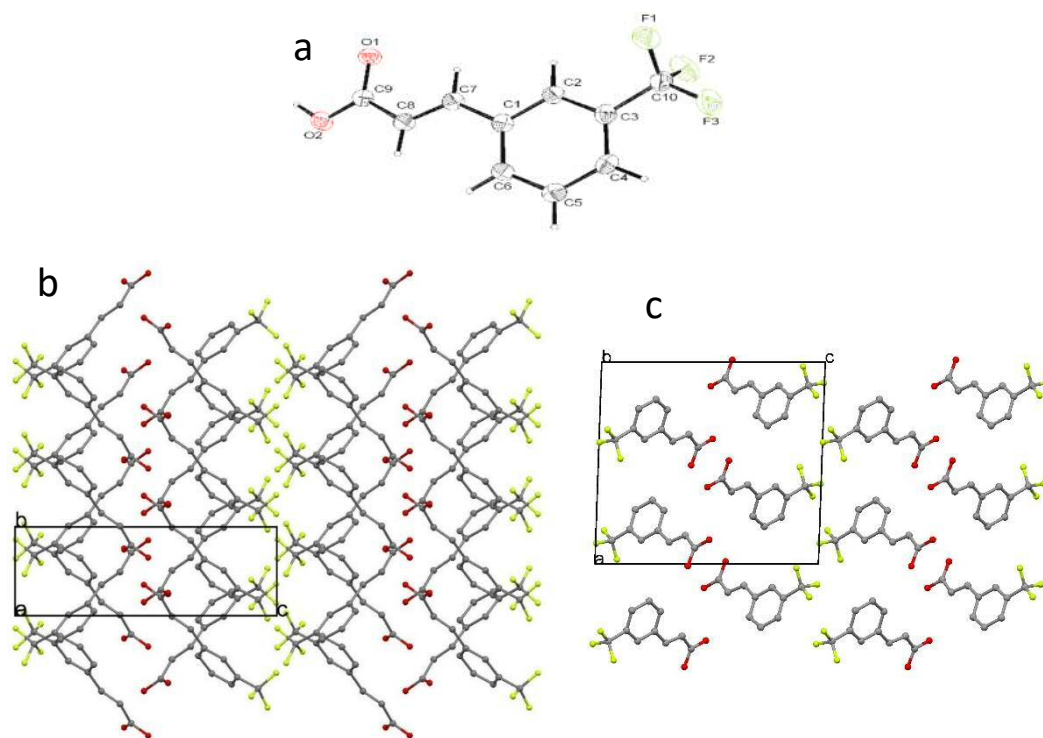
Figure 3.1. *(a) The asymmetric unit of the γ₁ polymorph of CF₃CA. The crystal structure of the γ₁ polymorph of CF₃CA viewed (b) along the a-axis, showing a criss-cross arrangement generated from the two orientations of molecular planes and (c) along the b-axis, showing a layered structure. For clarity, hydrogen atoms are omitted from (b) and (c).*

Table 3.2. *Crystallographic data for the crystal structure determination of γ₁-3-CF₃CA.*

Formula	$C_{10} H_7 F_3 O_2$	Z	4
Formula weight	216.16	Density (calculated), (Mg/m³)	1.565
Temperature, (K)	150(2)	Absorption coefficient, (mm⁻¹)	0.148
λ , Å	0.71073	F(000)	440
Crystal system	Monoclinic	Crystal size, (mm³)	0.02×0.14×0.5
Space group	P2₁/a	Reflections collected	3726
a, (Å)	12.9859(6)	Independent reflections	2104
b, (Å)	4.9043(3)	R(int)	0.0376
c, (Å)	14.4129(5)	Goodness-of-fit on F²	1.114
α, (°)	90	Final R₁ indices [*I*>2sigma(*I*)]	0.0478
β, (°)	91.951(3)	Final wR₂	0.1235
γ, (°)	90	R₁ indices (all data)	0.0684
Volume, (Å³)	917.38(8)	wR₂ (all data)	0.1466

Table 3.3. *Selected intermolecular interactions in the structure of γ₁-3-CF₃CA.*

A-B···D	A-D (Å)	A-B···D (°)
O_2-H···O_1	2.618	174.47
C_8-H_8···O_2	3.488	178.62
C_6-H_6···O_2	3.512	178.35
C_5-H_3···O_1	3.404	137.85
C_4-H_4···F_2	3.507	161.45

It is worth noting that, throughout the stack of the molecules, $\pi\cdots\pi$ interactions are observed between the C=Cπ system and π system of the benzene ring, with a distance between the centroid of C=C (CDB) and centroid of the benzene ring (CBR) of 3.402Å. However, the distance between the centroids of the two benzene rings throughout the stack is about 4.904Å (Figure 3.2).
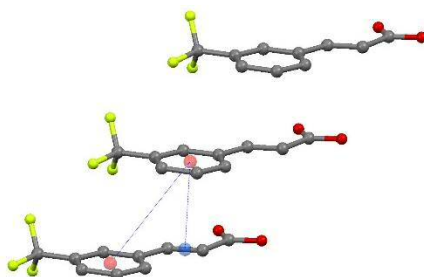
Figure 3.2: $\pi\cdots\pi$ in the γ_1-3-CF$_3$CA structure. The CBR is shown in red while the CDB is shown in blue.

γ_2-3-CF$_3$CA

As mentioned in Section 3.2, PXRD of the crystallization from DEE revealed the existence of γ_1 and another unknown polymorph. Unfortunately no difference in crystal morphology was observed between the crystals under the optical microscope. However, crystallization from the melt produced colourless, plate-like crystals of the new phase, suitable for single crystal determination. The crystal structure determined was a different γ phase from γ_1 (determined above) and has been designated as γ_2. The simulated PXRD of γ_2 crystal was identical to the additional peaks observed by PXRD for the crystals from DEE.

The crystal structure of γ_2 is triclinic (space group P$\bar{1}$), the asymmetric unit comprising of one molecule of 3-CF$_3$CA and showing disorder for the trifluoromethyl group; each fluorine atom is disordered over 3 positions (Figure 3.3a) with occupancies for the components of 0.574(12), 0.142(5) and 0.282(12). Notably, this disordered behaviour for the CF$_3$ group has not been detected in the case of γ_1. The crystallographic data of the γ_2 structure are summarized in Table 3.4.

Table 3.4. Crystallographic data for the crystal structure determination of γ₂-3-CF₃CA.

Formula	$C_{10} H_7 F_3 O_2$	Z	2
Formula weight	216.16	Density (calculated), (Mg/m³)	1.556
Temperature, (K)	150(2)	Absorption coefficient, (mm⁻¹)	1.303
λ , Å	1.54184	F(000)	220
Crystal system	Triclinic	Crystal size, (mm³)	0.26 x 0.22 x 0.07
Space group	P$\bar{1}$	Reflections collected	2755
a, (Å)	4.9458(3)	Independent reflections	1765
b, (Å)	6.5474(6)	R(int)	0.0359
c, (Å)	14.8620(13)	Goodness-of-fit on F²	1.040
α, (°)	83.545(7)	Final R₁ indices [*I*>2sigma(*I*)]	0.0518
β, (°)	84.754(6)	Final wR₂	0.1368
γ, (°)	75.188(7)	R₁ indices (all data)	0.0630
Volume, (Å³)	461.34(6)	wR₂ (all data)	0.1490

Similar to γ_1, the conventional centrosymmetric hydrogen bonded dimer units with carboxylic acid hydrogen bonds is also observed. As shown in Figure 3.3b, viewing along the [110] direction, the stacks of the dimer units are arranged in parallel layers (in which the planes of the molecules form 42.21° angles with the (100) plane. The dimer units are separated by bilayers of CF_3 groups. F···F contacts between disordered trifluoromethyl groups are observed, with distances ranging from 2.612 to 2.897Å, less than the sum of r(F)[22]. However considering the highest occupancy component of the disordered group of CF_3, the shortest F···F distance in this bi-layer is 2.712Å, showing a type i F··· F interaction (discussed in Chapter 1). Interestingly the weak hydrogen interaction between F and C-H is also observed, as shown in the summary of some hydrogen interactions in Table 3.5. Similarly to the γ_1 form, the π···π interaction is also observed with a slightly shorter distance between CDB and CBR of 3.373Å. However, the distance between CBR and CBR throughout the stack is 4.946Å; higher than the value in γ_1.

These observations suggest that fluorine atoms in this structure are involved in two types of interactions; halogen-halogen interactions between F atoms, as well as C-H···F weak hydrogen interactions (see Table 3.5). In the γ_1 structure, F atoms are only involved in the weak hydrogen interactions (C-H···F). The distance between the centres of the C=C bonds of neighbouring molecules along the stacks is 5.02Å. As in the γ_1 structure, the distance here also suggests photo-stability of this structure.
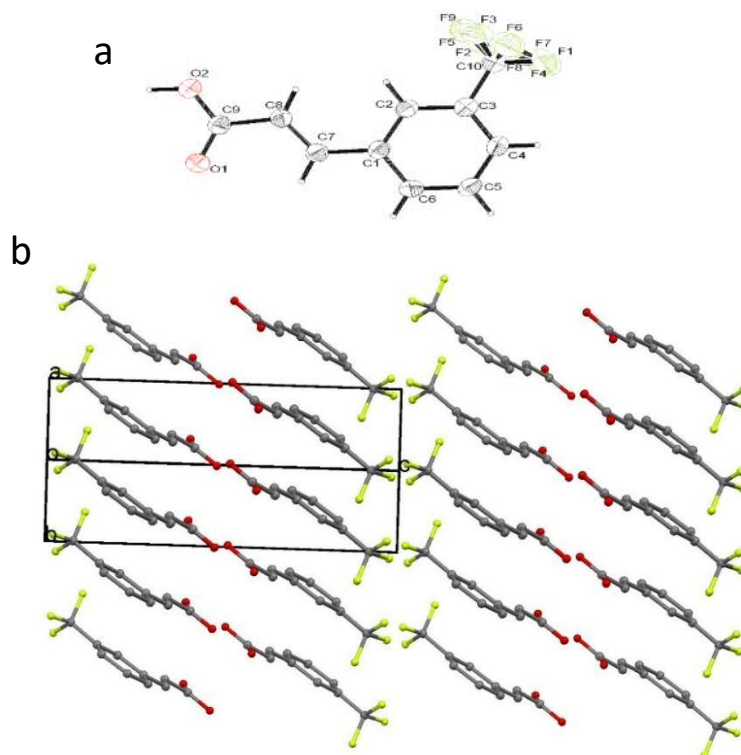
Figure 3.3. *(a) The asymmetric unit of the γ₂ polymorph of 3-CF₃CA, note the disordered 3-fluoromethyl group in γ₂. (b) The crystal structure of the γ₂ polymorph of CF₃CA viewed along [110] direction, showing parallel orientation of the planes of the molecules.*

Table 3.5. *Selected intermolecular interactions in the structure of γ₂-3-CF₃CA.*

A-B···D	A-D (Å)	A-B···D (°)	
O_2-H···O_1	2.613	172.10	
C_5-H_5···O_2	3.337	131.12	
C_4-H_4···F_1	3.534	161.29	
A-B···C-D	**B···C (Å)**	**A-B···C (°)**	**B···C-D (°)**
C_{10}-F_3···F_3-C_{10}	2.861	138.87	138.87
C_{10}-F_1···F_1-C_{10}	2.713	145.90	145.90

Comparison of the two polymorphs of 3-CF3CA (γ_1 and γ_2) revealed two categories of differences; (i) the conformation of the asymmetric unit and (ii) the crystal packing. The asymmetric units have different conformations, with the torsion angle C(8)-C(7)-C(1)-C(2) for the γ_1 form of 178.36°, while it is only 1.46° for γ_2. Therefore, as is seen in Figure 3.4, the two molecules from the different polymorphs (γ_1 in red and γ_2 in blue) can be superimposed, except for the 3-CF3-phenyl group, where a 180° rotation is observed. In terms of structure packing, the molecules in the layers are related to each other by a

criss-cross arrangement in γ_1 whereas, in the γ_2 form, the molecules are parallel for all layers.
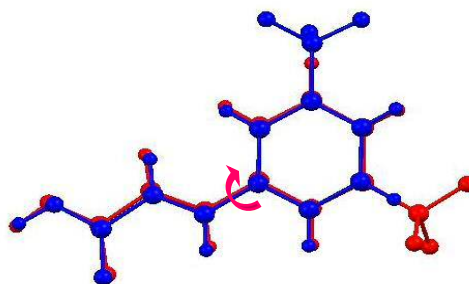
Figure 3.4. *An over lay of molecules of γ_1-CF$_3$CA (red) and γ_2-CF$_3$CA (blue). The pink arrow shows the required rotation to fit the two molecules. For γ_2-3-CF$_3$CA only fluorine atoms that correspond to the major disorder component are shown.*

3.3.1.b. 3-Flouro-*trans*-cinnamic acid (3-FCA)

Crystallization of 3-FCA revealed two distinct crystalline phases which were denoted as β_1 and β_2 (discussed later), consistent with the classification of *trans*-cinnamic acids. Crystallization from all solvents listed in the experimental section (followed by analysis of the crystallization products by PXRD) was found to favour the formation of the β_1 polymorph, yielding mono-phasic samples of β_1 in all cases, with the exception of ACN and d.AC, for which the β_2 polymorph was also present as a minor second phase. The two polymorphs were indistinguishable based on crystal morphology and initial structural characterization of β_2 was by a trial and error analysis of crystals from the mixed-phase sample.

β_1 3-FCA

The crystal structure of the β_1 polymorph of 3-FCA is triclinic (space group P$\bar{1}$). The asymmetric unit comprises of one molecule, with the 3-fluorophenyl group disordered between two orientations related by a 180° rotation about the C(phenyl)–C(vinyl) bond. The refined occupancies of the major and minor components are 0.927 (4) and 0.073 (4) (Figure 3.5a).

The crystal structure comprises pairs of planar molecules linked by hydrogen bonds, forming the dimeric motif commonly observed for carboxylic acids. The dimers are stacked parallel to the a-axis (Figure 3.5b) and the long axis of the molecule forms an angle of 107° with the stacking direction. Crystallographic data are shown in Table 3.6.
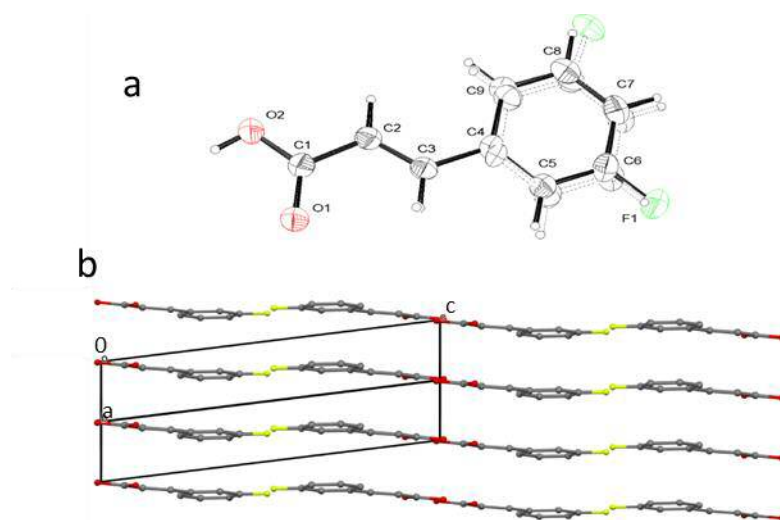
***Figure 3.5**. (a) The asymmetric unit in the β₁ polymorph of 3-FCA showing the disorder, and (b) the crystal structure viewed along the [1-10] direction, showing the parallel orientation of the planes of the molecules. Only the orientation of the fluorophenyl rings, corresponding to the major disorder component, is shown in the packing diagrams. For clarity, hydrogen atoms are omitted from the structure.*

Table 3.6. *Crystallographic data for the crystal structure determination of β₁-3-FCA.*

Formula	$C_9 H_7 F O_2$	Z	2
Formula weight	166.15	Density (calculated), (Mg/m³)	1.453
Temperature, (K)	150(2)	Absorption coefficient, (mm⁻¹)	1.011
λ , Å	1.54178	F(000)	172
Crystal system	Triclinic	Crystal size, (mm³)	0.48 × 0.19 × 0.06
Space group	P$\bar{1}$	Reflections collected	2238
a, (Å)	3.8430(3)	Independent reflections	1448
b, (Å)	6.2681(4)	R(int)	0.0139
c, (Å)	15.9607(12)	Goodness-of-fit on F²	1.060
α, (°)	93.547(5)	Final R₁ indices [*I*>2sigma(*I*)]	0.0556
β, (°)	96.858(6)	Final wR₂	0.1543
γ, (°)	94.011(5)	R₁ indices (all data)	0.0645
Volume, (Å³)	379.82(5)	wR₂ (all data)	0.1639

Considering the highest occupancy component of the acid, the arrangement of the 3-FCA molecules is such that the structure contains fluorine-rich layers parallel to the ab-plane. As seen in the γ₁ structure of 3-CF₃CA, fluorine atoms here are also involved in weak C-H⋯F interactions. On the other hand, the shortest F⋯F distance between the fluorine layers is 3.615 Å which is longer than the sum of r(F) atoms (2.94Å)[22]. Two weak hydrogen bonds (C-H⋯O) are also observed connecting pairs of molecules related by a head-to-tail orientation. Figure 3.6 shows the hydrogen bond interactions in the structure and Table 3.7 summarizes the geometry of hydrogen bonds. The planes of all molecules are parallel and the distance between the centres of the C=C bonds of neighbouring molecules, which are in a head-to-head alignment, along the a-axis is 3.843Å.
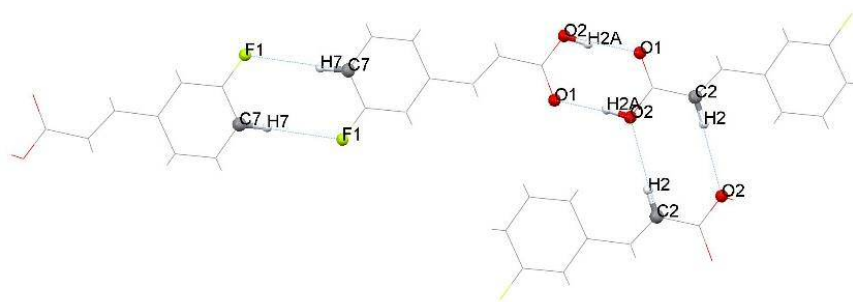
Figure 3.6. *Segment of the structure β₁-3-FCA, showing hydrogen bonds as blue dashed lines.*

Table 3.7. *Selected intermolecular interactions in the structure of β₁-3-FCA.*

A-B···D	A-D (Å)	A-B···D (°)
$O_2-H_{2A}···O_1$	2.623	171.8°
$C_2-H_2···O_2$	3.547	170.32
$C_7-H_7···F_1$	3.533	160.45

β₂ 3-FCA

The crystal structure of the *β₂* polymorph of 3-FCA (Figure 3.7) is monoclinic (space group P2₁/c) with one molecule in the asymmetric unit. The 3-fluorophenyl group is disordered between two orientations in a similar manner to *β₁*, with the two orientations related by a 180° rotation about the C(phenyl)–C(vinyl) bond. The refined occupancies for the major and minor components are 0.831(3) and 0.169(3). Crystallographic data are shown in Table 3.8.

Figure 3.7. *Crystal structure of the β₂ polymorph of 3-FCA viewed along the [110] direction, showing the two orientations of the molecular planes. Only the orientation of the fluorophenyl rings corresponding to the major disorder component, is shown in the packing diagram. For clarity, hydrogen atoms are omitted from the structure.*

Table 3.8. *Crystallographic data for the crystal structure determination of β₂-3-FCA.*

Formula	$C_9 H_7 F O_2$	Z	4
Formula weight	166.15	Density (calculated), (Mg/m³)	1.440
Temperature, (K)	150(2)	Absorption coefficient, (mm⁻¹)	1.002
λ , Å	1.5418	F(000)	344
Crystal system	Monoclinic	Crystal size, (mm³)	0.03× 0.12 × 0.20
Space group	P2₁/c	Reflections collected	2253
a, (Å)	6.5290(4)	Independent reflections	1462
b, (Å)	3.7750(2)	R(int)	0.0160
c, (Å)	31.1015(18)	Goodness-of-fit on F²	1.091
α, (°)	90	Final R₁ indices [*I*>2sigma(*I*)]	0.0512
β, (°)	91.250(4)	Final wR₂	0.1436
γ, (°)	90	R₁ indices (all data)	0.0597
Volume, (Å³)	766.38(8)	wR₂ (all data)	0.1512

As for the β₁ polymorph, the crystal structure of the β₂ polymorph contains hydrogen-bonded dimers. These dimers are stacked along the b-axis to form layers parallel to the ab-plane and separated by regions of high fluorine density. The distance between the centres of the C=C bonds of neighbouring molecules along the b-axis is 3.775 Å. In this structure, each molecule is connected to four other molecules via (C-H···F) weak hydrogen bond interactions. Similarly to the β₁ structure, weak C-H···O are also observed connecting two molecules in a head-to-tail alignment. In this structure, the shortest distance between the adjacent fluorine atoms within the fluorine layers, for the major component, is 3.209Å, which is greater than the sum of F-F radii[22]. The geometry of hydrogen bonds involved in the structure are summarized in Table 3.9, and depicted in Figure 3.8.
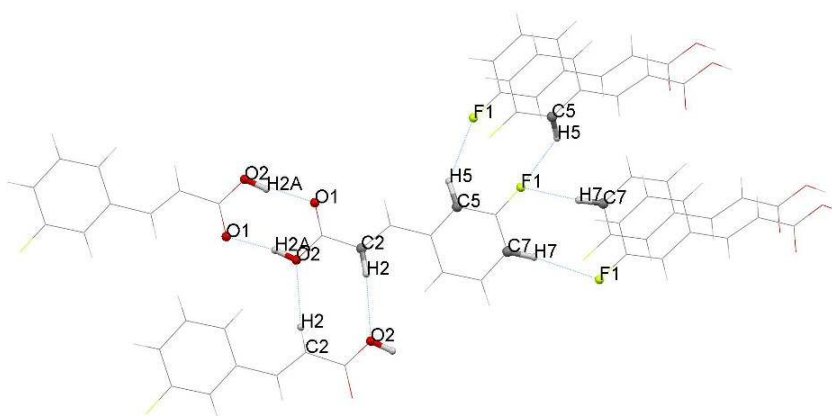
Figure 3.8. *Segment of the structure of β₂-3-FCA, the blue dashed lines showing hydrogen bonds.*

Table 3.9. *Selected intermolecular interactions in the structure of β_2-3-FCA*

A-B⋯D	A-D (Å)	A-B⋯D (°)
O_2-H⋯O_1	2.619	170.9°
C_2-H_2⋯O_2	3.5530	170.32
C_5-H_5⋯F_1	3.448	140.10
C_7-H_7⋯F_1	3.422	170.47

In both structures, β_1 and β_2, the double bond separation distances in the stack are in the range required for photo-dimerization, and this will be discussed in detail in Chapter 6. The main difference between the crystal structures of the β_1 and β_2 polymorphs concerns the structural relationship between neighbouring layers. In the β_2 polymorph the layers are related by c-glide symmetry and the planes of the molecules in adjacent layers are not parallel, with the angle between the planes of 59.5°. In contrast, in the β_1 polymorph structure, the planes of all molecules are parallel. The β_2 polymorph of 3-FCA is isostructural with the β polymorph of *trans*-cinnamic acid.[24]

3.3.1.c. 3-Methyl-*trans*-cinnamic acid (3-MeCA)

Crystallization of the acid using various solvents, which were mentioned in Section 3.2, and analysis of the product by PXRD showed monophasic samples, identified afterwards as the γ phase. Crystal structure determination revealed that the acid crystallized in the monoclinic crystal system (space group P2$_1$/a). Crystallographic data are summarized in Table 3.10. The asymmetric unit consists of one molecule of 3-MeCA. Both strong and weak hydrogen bonds are involved in stabilizing the structure. Pairs of molecules are related across a centre of inversion by a pair of hydrogen bonds (via carboxylic acid groups) to form a dimer. In the carboxylic acid group the bond distances are O(1)-C(9)=1.268(3) and for O(2)-C(9)=1.268(3); the similarity in the distances indicating the disordered hydrogen atoms for the group. As seen in Figure 3.9a, each molecule donates two weak hydrogen bonds (C-H⋯O) and accepts two C-H⋯O hydrogen bonds from a pair of molecules which are oriented perpendicular to its plane. The geometry of the hydrogen bonds involved is summarized in Table 3.11. As seen in the γ_1-3CF$_3$CA structure, π-π contacts are also observed. Thus the distance between CDB and BRC is only 3.434Å. On the other hand the BRCs throughout the stack are further apart, at 4.984Å (Figure 3.9b).

Table 3.10. *Crystallographic data for the crystal structure determination of γ-3-MeCA.*

Formula	$C_{10}H_{10}O_2$	Z	4
Formula weight	162.18	Density (calculated), (Mg/m^3)	1.243
Temperature, (K)	293(2)	Absorption coefficient, (mm^{-1})	0.086
λ, Å	0.71073	F(000)	344
Crystal system	Monoclinic	Crystal size, (mm^3)	0.04×0.06 ×0.39
Space group	P2$_1$/a	Reflections collected	3881
a, (Å)	12.5578(13)	Independent reflections	2074
b, (Å)	4.9836(5)	R(int)	0.0417
c, (Å)	13.8759(13)	Goodness-of-fit on F^2	1.092
α, (°)	90	Final R$_1$ indices [I>2sigma(I)]	0.0743
β, (°)	93.559(10)	Final wR$_2$	0.1758
γ, (°)	90	R$_1$ indices (all data)	0.1356
Volume, (Å^3)	866.72(15)	wR$_2$ (all data)	0.2144
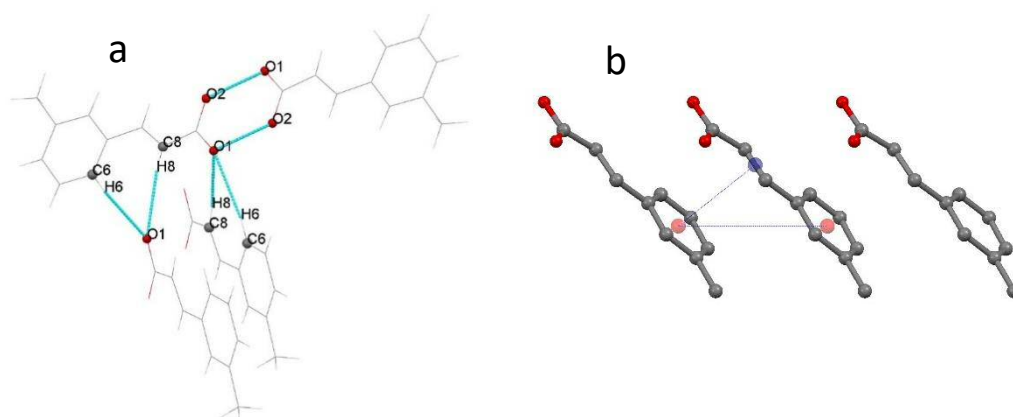
Figure 3.9. *A section of the structure showing: (left) Hydrogen bonds (the disordered hydrogen atom of the carboxylic group are omitted, and (right) π···π interaction, the CBR is shown in red while the CDB is in blue.*

Table 3.11. *Selected intermolecular interactions in the structure of 3-MeCA.*

A-B···D	A-D (Å)	A-B···D (°)
O$_2$-H···O$_1$	2.622	172.26
C$_8$-H$_8$···O$_1$	3.466	173.75
C$_6$-H$_6$···O$_1$	3.618	172.68

Figure 3.10 shows the structure packing, viewed along the a-axis. The molecules are packed in a criss-cross manner, where the two molecules in the criss-cross motif are approximately perpendicular to each other (86.47°). The molecules are arranged in stacks and the C=C double bonds in neighbouring molecules along the stacks are parallel and separated by 4.985Å, which is longer than that normally found in photo-reactive crystalline *trans*-cinnamic acids and therefore no reaction is expected for this material.
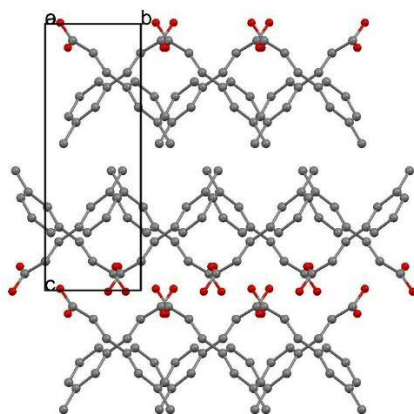
Figure 3.10. *The crystal structure of the 3-MeCA viewed along the a-axis, showing a criss-cross arrangement generated from the two orientations of molecular planes. Hydrogen atoms are omitted from the structure for clarity.*

3.3.1.d. 3-Bromo-*trans*-cinnamic acid (3-BrCA)

Prior to this work, the acid was reported to exist in two polymorphic forms, designated as γ and β.[6,14,20] Schmidt[6] reported the unit cell dimensions and space group information whereas the crystal structure of the γ form was determined by Ahn et al.[15] and that of the β form by Kanao et al.[21] In this study a new previously unknown polymorphic form of the acid was discovered and denoted as γ_2.

γ-3-BrCA

The crystal structure of γ-3-BrCA, as determined by Ahn et al.[15], is monoclinic (space group P2$_1$/a), the asymmetric unit comprising of one molecule of 3-BrCA. The structure is isostructural to both γ_1-3-CF$_3$CA and γ-3-MeCA (as discussed later in Section 3.3.3). In this structure the common dimer units formed by carboxylic acid groups via hydrogen bonds are observed. Viewing the structure along the b-axis, the dimeric units are arranged to form layers and these layers are separated by a bromine bi-layer. Between these bi-layers, bromine atoms are in contact with each other. The shortest Br$\cdots$Br distance is 3.571Å (shorter than the sum of Van der Waals radii of Br-Br atoms ≈ 3.7[22]) and the arrangement is type i, as discussed in Section 1.1.2 , forming an angle of θ=149.12°.

Moreover, weak hydrogen bonds are also observed in the structure in a manner similar to that in the 3-MeCA structure (Section 3.3.1.c), where the two molecules are related perpendicularly and one of them is the C-H$\cdots$O donor and the other is the accepter (Figure 3.11). The geometry of hydrogen bonds and halogen-halogen interactions involved in this structure are summarized in Table 3.12. Similarly to both γ_1-3CF$_3$CA and γ-3-MeCA, the

$\pi\cdots\pi$ interaction is also observed here, with a distance between the centroid of C=C (CDB) and the centroid of benzene ring (CBR) of 3.432°. However, the distance between the centroids of the two benzene ring throughout the stack is about 4.933Å (Figure 3.11).
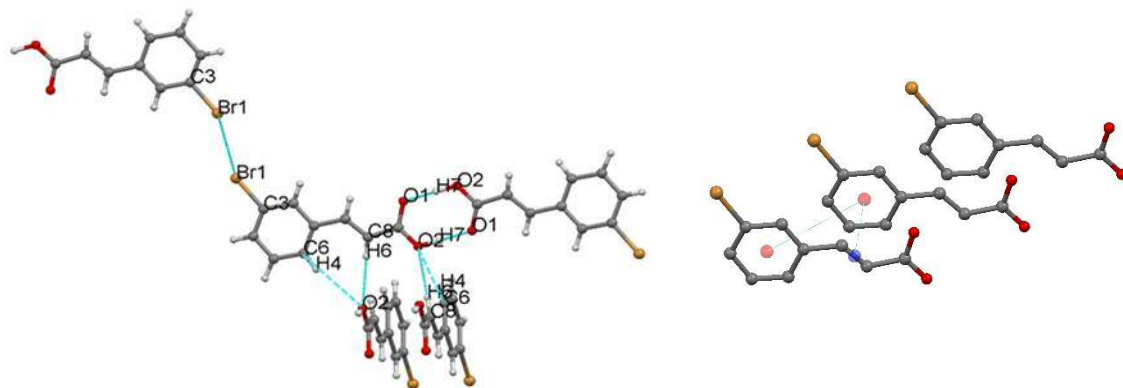
Figure 3.11: *Part of the γ-3-BrCA structure, showing intermolecular interaction: (Left) the hydrogen bonds and Br⋯Br contact. (Right) The π⋯π interaction, with the CBR shown in red and the CDB in blue.*

Table 3.12. *Selected intermolecular interactions in the structure of γ-3-BrCA*

A-B⋯D	A-D (Å)	A-B⋯D (°)	
O_2-H_9⋯O_1	2.613	177.18	
C_8-H_6⋯O_2	3.430	178.48	
C_6-H_4⋯O_2	3.658	166.73	
A-B⋯C-D	B⋯C (Å)	A-B⋯C (°)	B⋯C-D (°)
C_3- Br_1⋯Br_1-C_3	3.571	149.12	149.12

γ₂-3-BrCA

Crystals of γ_2 were obtained by crystallization of the acid in i-POH. The γ_2 form is monoclinic with space group $P2_1/n$ and one molecule in the asymmetric unit (see the crystallographic data in Table 3.13). Six hydrogen bonds are involved in connecting each molecule to other molecules; two of these bonds form the dimer normally seen for the carboxylic acid groups. The other four bonds are weak C-H⋯O interactions (Figure 3.12 and Table 3.14). The shortest Br⋯Br distance is 4.054Å, which is longer than the range of distance d(Br⋯Br) associated with Br–Br bonding (3.38-3.68 Å)[25], suggesting a less important role for this interaction. However, as seen in Figure 3.12, Br atoms are involved in Br⋯π interactions and the distance between the Br atoms and the nearest C of the ring (Br⋯Cπ) is 3.521Å, forming an angle between C(3)-Br(1)⋯C(4)π of 160.44°. This type

of interaction can be classified as a halogen$\cdots\pi$ interaction[26] and can be present in a system containing a halogen atom and a nucleophilic site (π).[27]

Table 3.13. *Crystallographic data for the crystal structure determination of γ_2-3-BrCA.*

Formula	$C_9 H_7 Br O_2$	Z	4
Formula weight	227.06	Density (calculated), (Mg/m³)	1.739
Temperature, (K)	293(2)	Absorption coefficient, (mm⁻¹)	4.691
λ, Å	0.71073	F(000)	448
Crystal system	Monoclinic	Crystal size, (mm³)	$0.04 \times 0.08 \times 0.43$
Space group	$P2_1/n$	Reflections collected	3068
a, (Å)	4.9666(9)	Independent reflections	1840
b, (Å)	28.396(6)	R(int)	0.0723
c, (Å)	6.1511(14)	Goodness-of-fit on F^2	1.136
α, (°)	90	Final R_1 indices [I>2sigma(I)]	0.0779
β, (°)	91.08(2)	Final wR_2	0.2343
γ, (°)	90	R_1 indices (all data)	0.1319
Volume, (Å³)	867.3(3)	wR_2 (all data)	0.2838
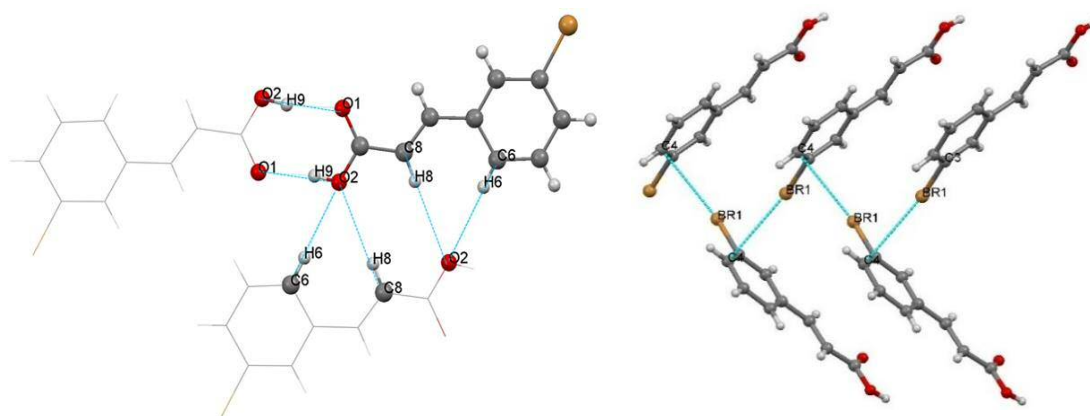
Figure 3.12. *Segments of the structure of γ_2-3-BrCA showing: (left) hydrogen bonds, (right) Br$\cdots\pi$ interactions.*

Table 3.14. *Selected intermolecular interactions in the structure of γ_2-3-BrCA*

A-B$\cdots$D	A-D (Å)	A-B$\cdots$D (°)
O_2-$H_9\cdots O_1$	2.634	169.92
C_8-$H_8\cdots O_2$	3.662	160.99
C_6-$H_6\cdots O_2$	3.474	155.12

β-3-BrCA

The crystal structure of 3-BrCA was reported by Kanao et al.[21] and showed that the acid crystallized in a monoclinic crystal system, with a space group of C2/c and one 3-BrCA molecule as the asymmetric unit. In this structure, pairs molecules are connected via two hydrogen bonds (O-H$\cdots$O) from carboxylic acid groups to form the commonly observed dimeric unit, as seen in the previously discussed forms of the acid (γ and γ_2). A striking

66

feature of this structure is seen in Figure 3.13, in which the structure extends along the b-axis via a C-Br⋯O interaction with a distance of Br⋯O of 3.339Å (shorter than the sum of Van der Waals radii of r(Br) 1.85Å and r(O) 1.52Å).[22] The chain is formed by a zig-zag arrangement of the molecules. Such intermolecular interactions between halogen (Cl, Br, and I) atoms and electronegative atoms (such as O) has been described[28] to be highly directional, attractive and originating mainly from electrostatic effects. This is due to the anisotropic electron distribution around the halogen atom leading to an attractive electrostatic interaction with the electronegative atom.
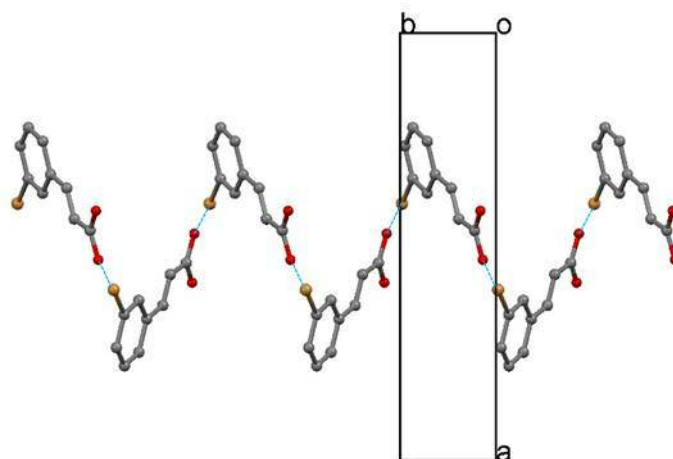
Figure 3.13. Part of the β-3-BrCA structure, showing C-Br⋯O interactions (blue lines) along the b-axis.

Viewing the structure of γ_2 down the c-axis (Figure 3.14b) revealed a herringbone pattern of packing of the dimeric units, resulting from the two approximate perpendicular orientations (79.28°) of the planes of molecules relative to each other. In contrast, as shown in Figure 3.14c, viewing the structure along the a-axis, the molecules in the β form pack in a smooth wavy shape, while the criss-cross arrangement of packing is clearly visible for the γ structure, Figure 3.14a. A common feature of all structures (γ, γ_2 and β) is that, the molecules show a head-to-head alignment. However, the distances between the parallel double bonds vary. The β form has appropriate geometry to undergo the photo-dimerization reaction to produce 3,3`di-bromotruxinic acid[29]. However, γ and γ_2 structures should both be photostable, as the distance between the two double bonds of the nearest neighbouring molecules are greater than the Schmidt criteria for the photo-dimerization reaction.

It is worth noting that, Br atoms are engaged in different halogen interactions with each polymorphic form containing one type; the γ form has C-Br···Br-C, the γ_1 form showed C-Br···π while C-Br···O was observed in the β form. Thus, optimization of the conditions for a certain interaction, can increase the possibility of forming different polymorphs. In this regard, C–Br···Br and C-Br···π interactions have been reported to be important in determining crystal packing.[30] Zhang et al.[31] reported two different polymorphic forms of {2-[1-(2,6-diisopropylphenylimino)ethyl]-pyridyl}palladium dibromide and both C-Br···π and C–H···Br intermolecular interactions contributed to the differences of the structure packing of the two polymorphic forms.
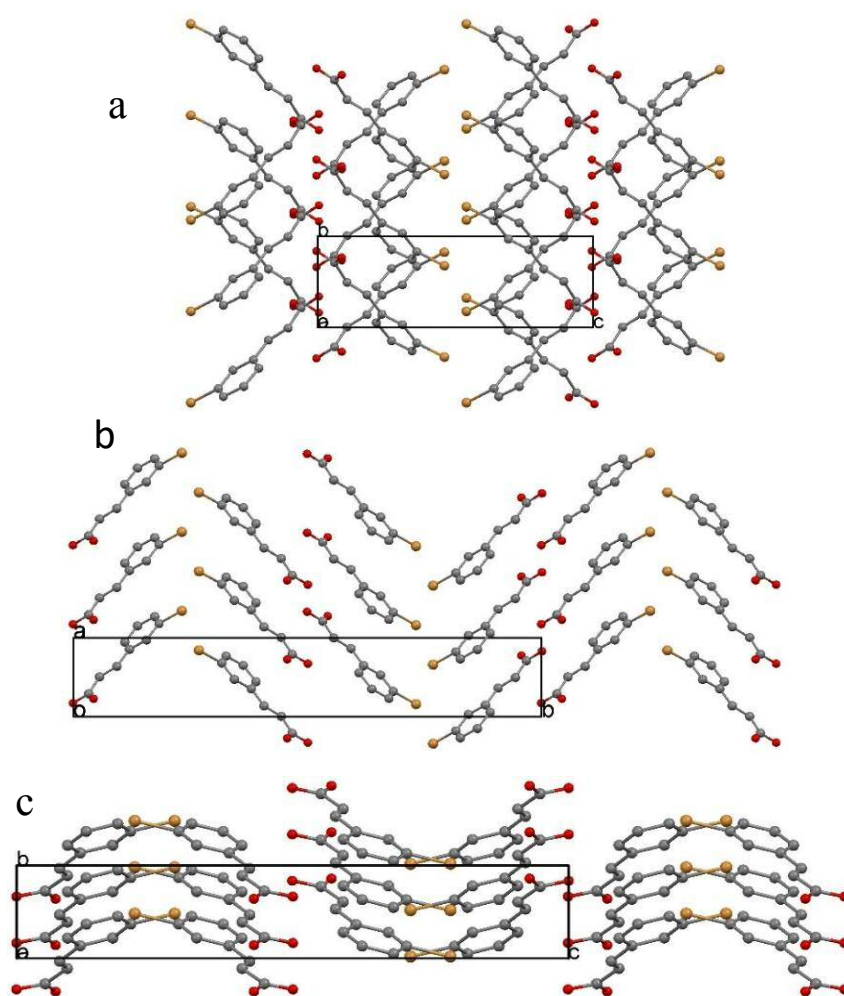
Figure 3.14. *Packing mode of (a), (b) and (c) are γ, γ_2 and β polymorphs of 3-BrCA.*

3.3.1.e. 3-Chloro-*trans*-cinnamic acid (3-ClCA)

Two phases of 3-ClCA have been reported in the Cambridge structure data base, CSD, (γ and β), but no coordinates of the structure have been reported for the γ form (just the unit cell dimension and space group information[6] (a =12.5Å, b= 4.93Å, c =14.1Å, α= 90°,

$\beta=94.0°$ and $\gamma=90°$, space group P2$_1$/a). For the β structure, the unit cell information was reported by Schmidt in 1964[6] (a =13.0Å, b= 8.6Å, c =3.9Å, α= 94.5°, β=90° and γ=117.5°, space group P$\overline{1}$) but, as in γ structure, no coordinates of the structure were reported by this study. In another study of β-3-ClCA, published by S. Kanao et al.[21] in 1990, the crystal structure information (a =8.618(4)Å, b=13.627(5)Å, c =3.909(1)Å, α= 96.26°(3), β=90° and γ=75.71°(3), space group P$\overline{1}$), including the coordinates was reported. However, the calculated powder pattern of the determined structure did not fit the experimental PXRD pattern of the β form satisfactorily, so the crystal structure of β-3-ClCA has been re-determined in this study and the calculated powder pattern for the re-determined structure fits the experimental one (see Figure 3.15). Comparing the published and re-determined structures (Figure 3.16) shows high similarity, suggesting that they are not different polymorphs. However, the differences in the PXRD patterns may be due to the differences in the crystal structure determination conditions, such as temperature. As reported by S. Kanao et al.[21], the structure was determined in temperature range of 283-303K, where in our case the structure was determined at about 293K.
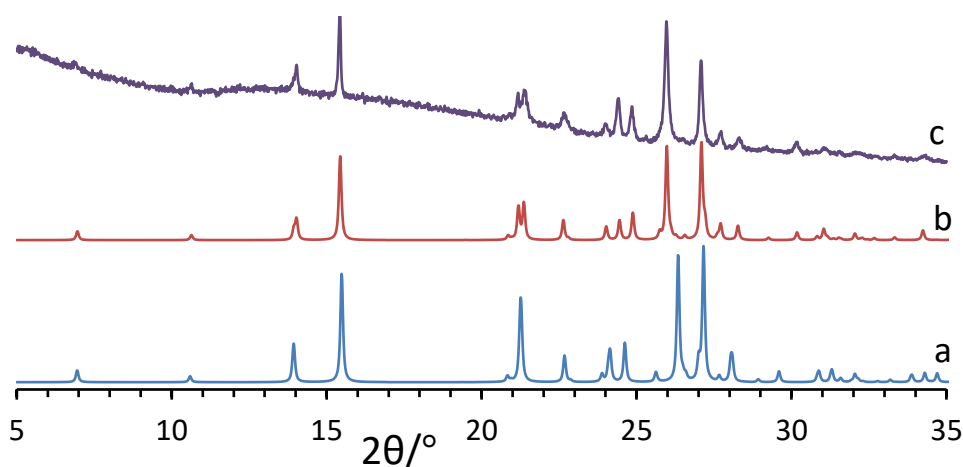
Figure 3.15. *The calculated PXRD pattern of the crystal structure determination of β-3-ClCA (a) previously reported by S. Kanao et al[21], (b) determined in this study. (c) The experimental PXRD of β-3-ClCA.*
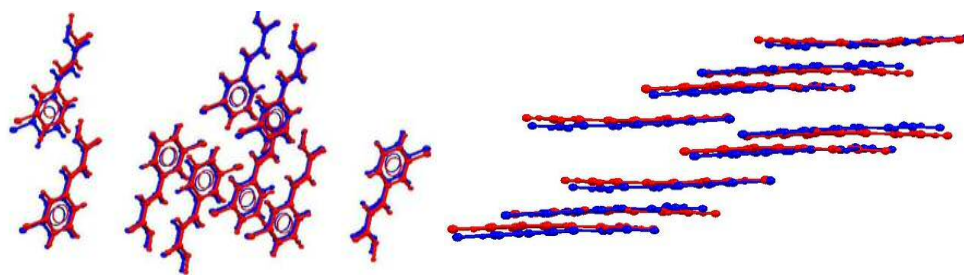
Figure 3.16. *An overlay of part of the β-3-ClCA structures; where red represents the structure reported by by S. Kanao et al[21], and blue represents the structure determined in this study.*

γ-3-ClCA

The crystal structure of the **γ** polymorph of 3-ClCA is monoclinic (space group P2$_1$/a) with one molecule in the asymmetric unit (see crystallographic data in Table 3.15). The crystal structure comprises pairs of acid units linked by hydrogen bonds, to form a dimeric motif. Viewing the structure along the c-axis, these dimers are arranged in a criss-cross fashion, forming a bilayer of Cl atoms (Figure 3.17). The Cl atoms are in contact between these bilayers with the distance of 3.444Å (shorter than the sum of Cl-Cl radii ≈3.5Å)[22], and showing type i halogen-halogen interactions, discussed in Chapter 1 (see Table 3.16). Weak hydrogen interactions (C-H···O) are also observed in the structure (Table 3.16). The distance between the parallel C=C of head-to-head aligned molecules is 4.953Å, indicating a solid state photo-stable material. It is worth noting that the structure shows π···π interactions similar to those observed in the structures of γ$_1$-3CF$_3$CA, γ-3-MeCA and γ-3-BrCA (Sections 3.3.1.a, 3.3.1.c and 3.3.1.d, respectively). The distance between the centroid of C=C and the centroid of the benzene ring is 3.436° but, in contrast, a greater distance is observed between the BRCs throughout the stack (4.953Å).

Table 3.15. *Crystallographic data for the crystal structure determination of γ-3-ClCA.*

Formula	C$_9$ H$_7$ Cl O$_2$	Z	4
Formula weight	182.60	Density (calculated), (Mg/m^3)	1.423
Temperature, (K)	293(2)K	Absorption coefficient, (mm^{-1})	3.595
λ, Å	1.54180	F(000)	376
Crystal system	Monoclinic	Crystal size, (mm^3)	0.035 x 0.066 x 0.295
Space group	P 2$_1$/a	Reflections collected	2706
a, (Å)	12.3739(5)	Independent reflections	1664
b, (Å)	4.9534(2)	R(int)	0.0191
c, (Å)	13.9481(5)	Goodness-of-fit on F^2	1.042
α, (°)	90	Final R$_1$ indices [*I*>2sigma(*I*)]	0.0396
β, (°)	94.326(4)	Final wR$_2$	0.1037
γ, (°)	90	R$_1$ indices (all data)	0.0482
Volume, (Å^3)	852.48(6)	wR$_2$ (all data)	0.1115
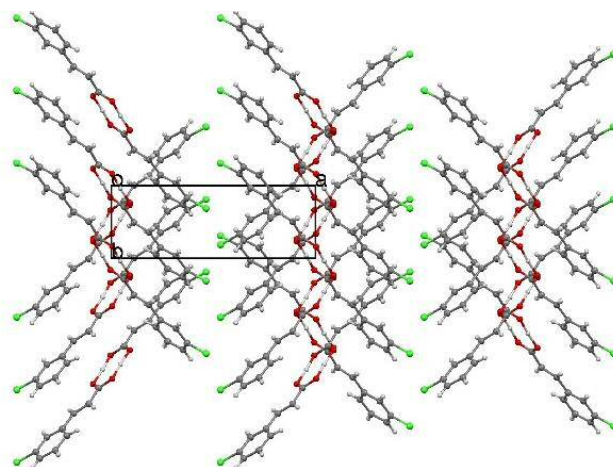
Figure 3.17. *The crystal structure of the γ-3-ClCA viewed along the c-axis, showing a criss-cross arrangement.*

Table 3.16. *Selected intermolecular interactions in the structure of γ-3-ClCA.*

A-B···D	A-D (Å)	A-B···D (°)	
O_2-H···O_1	2.619	175.96	
C_8-H_8···O_1	3.435	172.84	
C_6-H_6···O_1	3.651	172.61	
A-B···C-D	**B···C (Å)**	**A-B···C (°)**	**B···C-D (°)**
C_3-Cl_1···Cl_1-C_3	3.444	147.93	147.93

β-3-ClCA

The *β* form of 3-ClCA has a triclinic crystal system with space group (P$\overline{1}$) and one molecule in the asymmetric unit. The crystallographic data for the *β* structure determined in this study are shown in Table 3.17. The acid units are aligned in a head-to-head orientation, with pairs of acids held together by hydrogen bonding via two carboxylic groups (see Table 3.18). Viewing the structure along the c-axis (Figure 3.18), the Cl atoms form layers parallel to the ac plane and the shortest Cl···Cl distance is 4.227Å, which is longer than the sum of the radii of two Cl atoms ≈ 3.5.[22] The molecules stack along the c-axis, leading to a spacing between the C=C bonds of about 3.908Å, showing an optimum geometry for [2+2] solid-state photodimerization reaction[29]. As seen in Figure 3.18 and Table 3.18, the structure is further stabilized by weak hydrogen bonds (C-H···O) connecting pairs of molecules.

71

Table 3.17. *Crystallographic data for the crystal structure determination of β-3-ClCA.*

Formula	$C_9 H_7 Cl O_2$	Z	2
Formula weight	182.60	Density (calculated), (Mg/m³)	1.430
Temperature, (K)	293(2)K	Absorption coefficient, (mm⁻¹)	3.613
λ , Å	1.54180	F(000)	188
Crystal system	Triclinic	Crystal size, (mm³)	0.12 x 0.13 x 0.19
Space group	P$\bar{1}$	Reflections collected	2525
a, (Å)	8.5737(6)	Independent reflections	1628
b, (Å)	13.0598(8)	R(int)	0.0104
c, (Å)	3.9079(3)	Goodness-of-fit on F²	1.059
α, (°)	90.225(5)	Final R_1 indices [I>2sigma(I)]	0.0337
β, (°)	94.263(5)	Final wR_2	0.0958
γ, (°)	103.521(5)	R_1 indices (all data)	0.0353
Volume, (Å³)	424.16(5)	wR_2 (all data)	0.0978
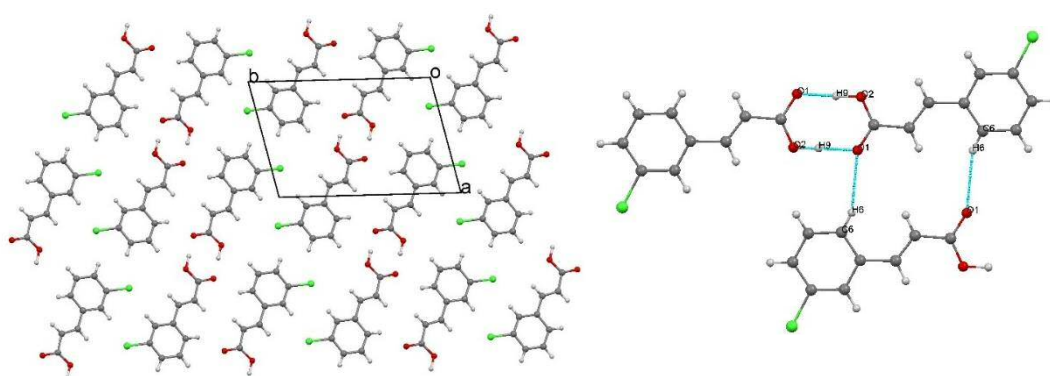
Figure 3.18. *The crystal structure of β-3-ClCA viewed along the c-axis, showing a layer arrangement of the molecules (left). (Right) Part of the structure showing hydrogen bonds represented by light blue dashed lines.*

Table 3.18. *Selected intermolecular interactions in the structure of β-3-ClCA.*

A-B⋯D	A-D (Å)	A-B⋯D (°)
O_2-H_9⋯O_1	2.845	175.58
C_6-H_6⋯O_1	3.468	146.22

3.3.2. Thermal properties: investigation of phase transition by DSC

3.3.2.a. 3-CF₃CA system

Thermal properties were investigated by DSC analysis. On heating the γ_1 polymorph, of 3-CF₃CA, from ambient temperature to 145 °C, two endodermic events were clearly observed with onset temperatures of 119.15 °C and 134.37 °C (Figure 3.19a). The second endotherm, at 134.37 °C, is consistent with the melting temperature of the acid. Interestingly, after melting the sample and cooling it at 20 °C/min, PXRD showed that the sample was not the original form. Instead, it was the γ_2 form, proving that the

crystallization of the sample from the melt produced γ_2. Heating the sample to 130 °C (below the endothermic peak corresponding to melting point of the acid) followed by cooling at 20 °C/min to room temperature, revealed thermal event at *ca.* 119 °C in the heating cycle, whereas no thermal event was observed in the cooling cycle (Figure 3.19b). Subsequent PXRD analysis of the sample recovered from the DSC pan showed that the result was the γ_2 polymorph (Figure 3.20), indicating that the endotherm observed in the heating cycle is attributed to a solid-state irreversible phase transition from the γ_1 polymorph to the γ_2 polymorph.

With this knowledge, it was possible to produce a larger amount of γ_2 by placing γ_1 on a hotplate in a covered Petri dish and letting it melt and then cooling it to ambient temperature.

Such transformation represents a novel system in cinnamic acid derivatives. Thus, the enantiotropically related polymorphs γ_1 and γ_2 are from the same class γ (the classification designed by Schmidt in respect the photodimerization reaction) and the transformation is irreversible. Therefore, two polymorphic phases that are enantiotropically related co-exist. The phase transition studies reported previously for the cinnamic acids can be classified into two categories.

(i) Transformation between enantiotropically related polymorphs from different classes. For example, γ and β polymorphs of 3-BrCA, where the γ form transformed irreversibly to β on heating.[15] The β polymorph of *trans*-cinnamic acid also showed[8] transformation to the α form above 45 °C but the transformation was found to proceed for over 6 months for a sample stored at the room temperature.[16]

(ii) Another category concerns transformation that was induced between enantiotropically related polymorphs of the same class (γ, β or α) but, the transition proceeds reversibly, preventing the co-existence of these polymorphs. For example, the α form of 2-ethoxy-*trans*-cinnamic acid transformed reversibly to another α form in the temperature range of 333 to 393K.[18] A recent study on 4-Br-*trans*-CA revealed the reversible phase transition of the acid at 252K/256K (cooling/heating) from one β form to another β form.[17]

Thus, the transformation discussed in this study is a third category of the transition in the cinnamic acids family, as it involved irreversible transformation between members of the same classification (α, β or γ).
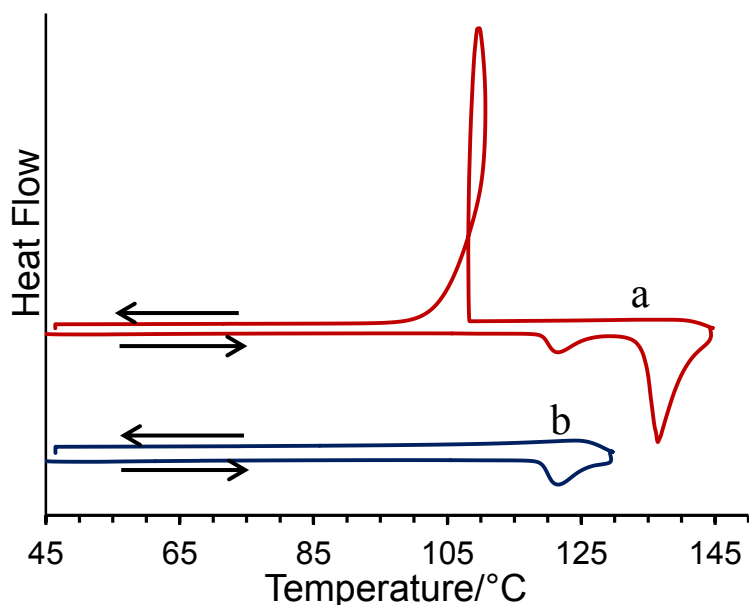
Figure 3.19*: Thermal analysis investigation of the γ_1 phase of 3-CF$_3$CA. (a) Two endothermic events in the heating cycle, namely transformation and melting. (b) The irreversible transformation event.*
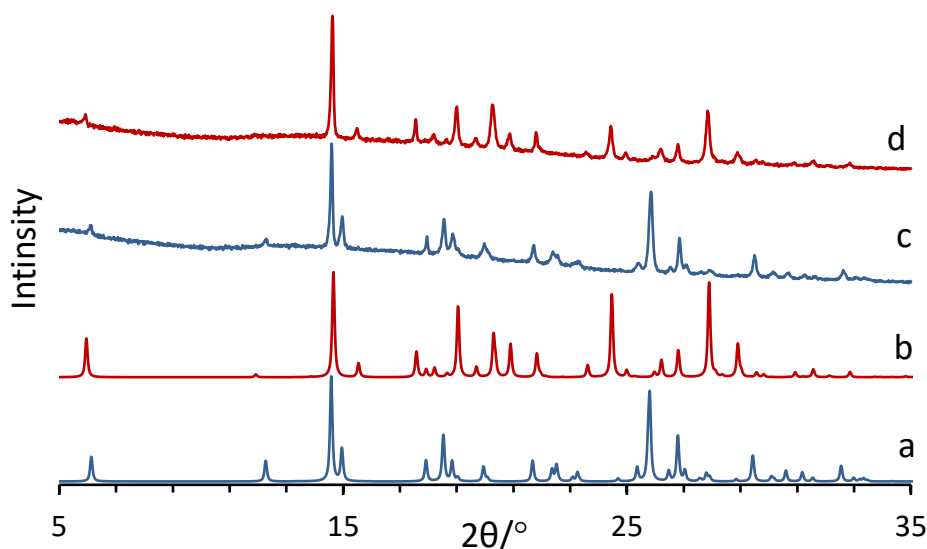
Figure 3.20*. The calculated PXRD pattern of the crystal structure determination of (a) γ_1-3-CF$_3$CA, (b) γ_2-3-CF$_3$CA, and the experimental PXRD pattern of (c) γ_1-3-CF$_3$CA, (d) the γ_1 form of acid after the DSC cycle below the m.p. showing the transformation to γ_2-3-CF$_3$CA.*

Examining the 3-CF$_3$CA structures before and after the transformation indicates that a lot of movements are required to transform γ_1 to γ_2. A key observation is the change of the molecular conformation, as discussed Section 3.3.1.a, where the phenyl substituted ring

in the γ_1 structure rotates by 180° compared to γ_2 structure. The molecules also rearrange themselves with changes in their intermolecular interactions. The dimeric motif of the hydrogen bonded carboxylic group motif is present in both structures (see Figure 3.21).

The material was observed to undergo sublimation at high temperatures. In spite of this, the possibility of SC-SC transformation was investigated. The crystal of γ_1 was examined using SC-XRD and then placed on a slide and coated with perfluoropolyether oil in order to reduce sublimation. It was heated on a hotplate (approximately 125 °C) for 10 seconds. Observation of the crystal under the optical microscope showed a clear reduction in the crystal size. Nevertheless, determination of the crystal structure was possible and it revealed that, despite large structural differences between the two structures (γ_1 and γ_2), a SC-SC transition occurred and, surprisingly, without loss of crystallinity.

Further investigation was carried out by cooling both γ_1 and γ_2 from 40 to -150 °C and then reheating to ambient temperature. No thermal event was observed to occur during this cycle, indicating that no further phase transition occurred upon cooling. In contrast, a single fully reversible phase transition has been reported for 4-CF$_3$CA at low temperatures around 132-131K.[19]
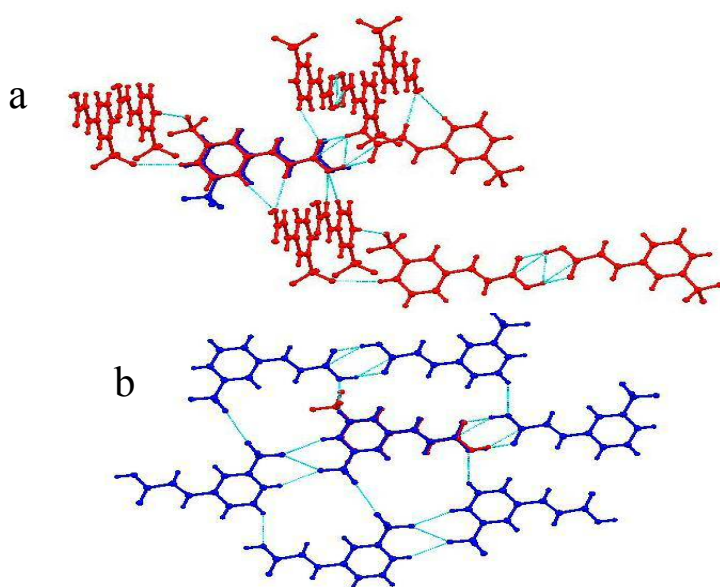
Figure 3.21: *Polymorphs of 3-CF$_3$CA: γ_1 in red and γ_2 in blue, showing the overlay of the two molecules from different polymorphs in the middle, surrounding by the other molecules in (a) the γ_1 structure, and (b) the γ_2 structure, blue lines show intermolecular interactions.*

3.3.2.b. 3-FCA system

On heating the *β$_1$* polymorph of 3-FCA from ambient temperature to 175 °C, DSC revealed two endothermic processes with onset temperatures of 119 °C and 167 °C (Figure 3.22a). The second endotherm is consistent with the melting temperature.

When heated the sample below the melting point (Figure 3.22b), endothermic event was observed at *ca*. 119 °C on the heating cycle. Subsequent cooling of the sample showed no thermal event, indicating that this phase transition was irreversible. PXRD on the sample after DSC confirmed that the sample was the *β$_2$* polymorph, Figure 3.23. The results indicated that thermal event observed at *ca*. 119 °C on the heating cycle is attributed to a solid-state irreversible phase transition from the *β$_1$* polymorph to the *β$_2$* polymorph. Visual examination of this sample showed that it contained crystals suitable for SC-XRD. However, direct observation of the phase transition by SC-XRD was difficult because of significant sublimation of the crystal as the temperature was increased towards the phase transition temperature. However, for a crystal of the *β$_1$* polymorph, "protected" in a drop of perfluoropolyether oil (to reduce the rate of sublimation), SC-XRD studies confirmed that the phase transition at *ca*. 119 °C occurred with retention of single crystal integrity.

It is noteworthy that, the transformation is another example of the novel irreversible transformation between cinnamic acid polymorphs with the same class, as designated by Schmidt (α, *β* or *γ*) and previously discussed for *γ* forms of 3-CF$_3$CA (Section 3.3.2.a). However, the transformation here occurred between the *β* forms of enantiotropically related polymorphs.

In further DSC studies to explore the behaviour of the *β$_1$* and the *β$_2$* polymorphs at low temperature, no thermal events were observed for either polymorph on cooling from ambient temperature to -150 °C and then heating to room temperature.

Although the process of transformation from *β$_1$* polymorph to *β$_2$* did not involve conformational modification of the molecules, as previously observed in the 3-CF$_3$CA system, significant changes in the molecular arrangement were observed. Thus, as seen in Figure 3.24, the transformation can be described by two hypothetical steps; the first step involves rotation of the molecules in one layer of hydrogen-bonded dimers by *ca*.

60° about the C-F bond (red arrows in Figure 3.24a) without disrupting the hydrogen bonding. The second step involves readjustment of the unit cell, including doubling of the c-axis, as required to obtain the monoclinic β_2 structure from the triclinic β_1 structure.
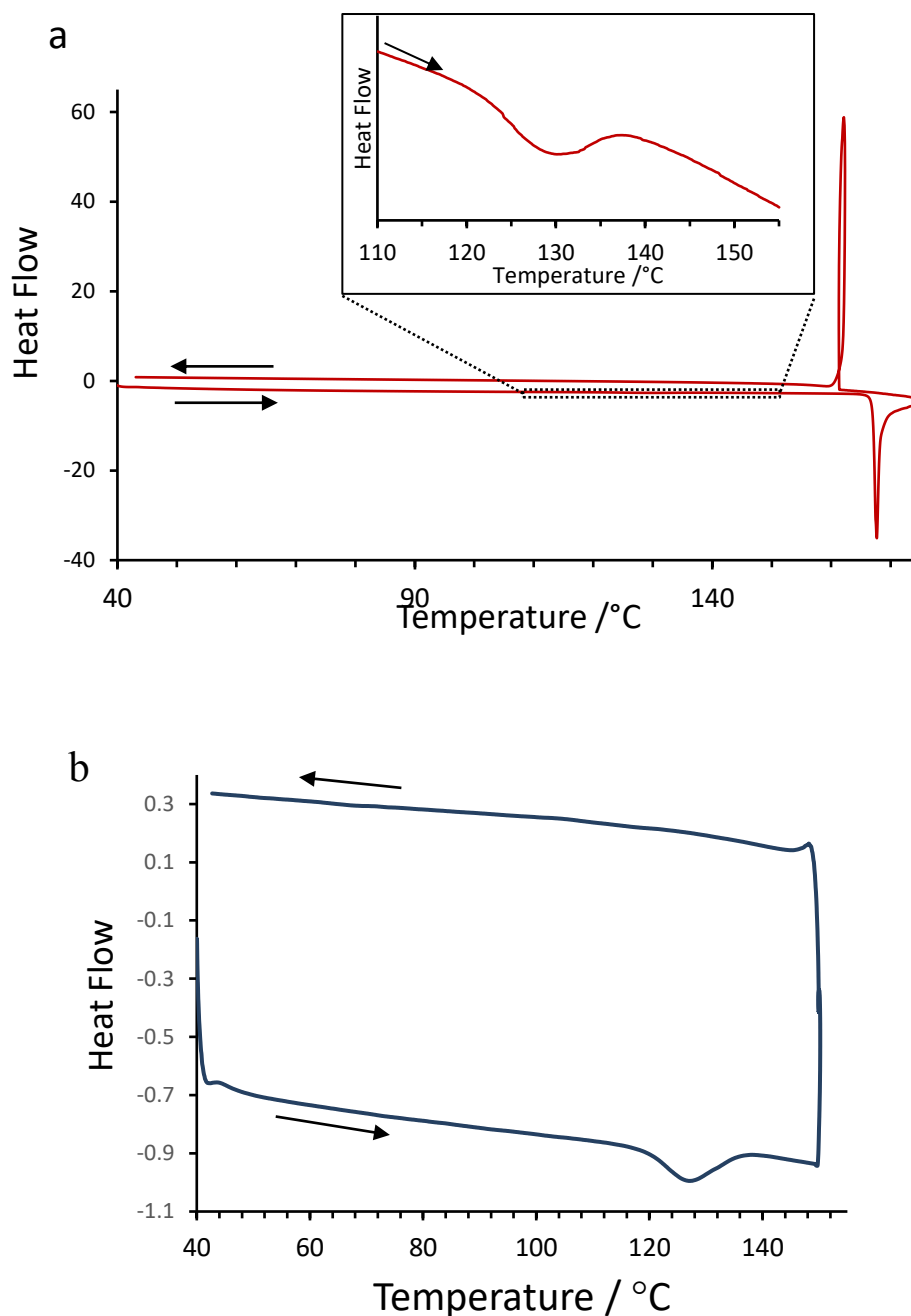
Figure 3.22. *DSC experiment starting from a sample of the β_1 polymorph: (a) heated to 175 °C followed by cooling (the inset shows the endotherm due to the polymorphic phase transition from β_1 to β_2), and (b) heated to 150 °C followed by cooling (note that the reverse phase transition from β_2 to β_1 does not occur on cooling).*
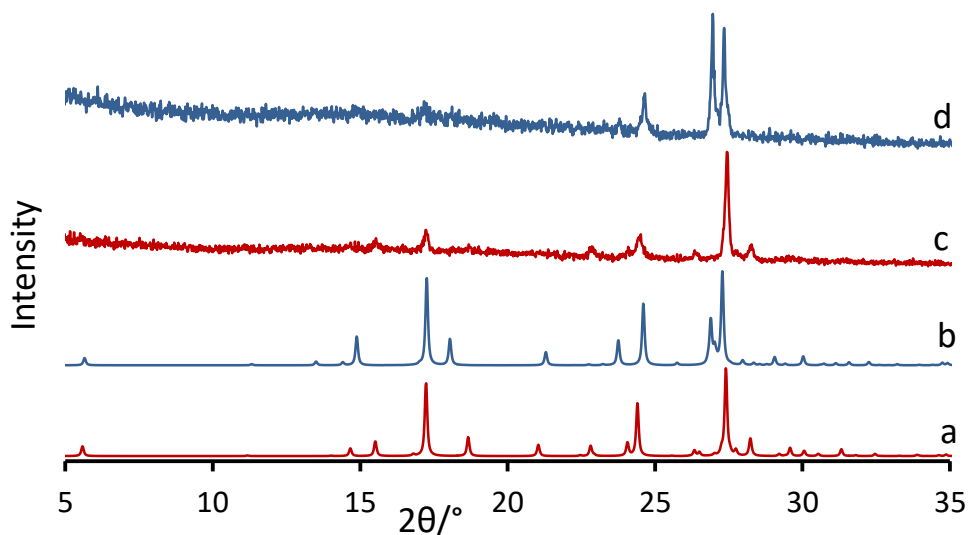
Figure 3.23. *The calculated PXRD pattern of the crystal structure determination of (a) β₁-3-FCA, (b) β₂-3-FCA, and the experimental PXRD pattern of (c) β₁-3-FCA (b) the β₁ form of acid after the DSC cycle below the m.p. showing the transformation to β₂-3-FCA.*
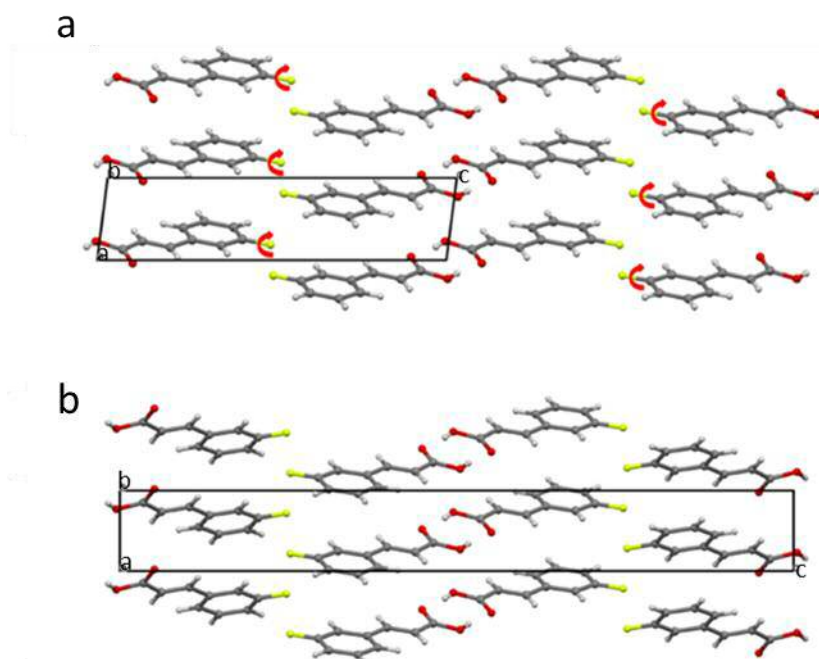
Figure 3.24. *(a) Crystal structure of the β₁ polymorph of 3-FCA viewed along the b-axis with red arrows indicating the rotation about the C–F bonds that would lead to the structure of the β₂ polymorph. (b) Crystal structure of the β₂ polymorph of 3-FCA viewed along the a-axis. Only the major component is shown.*

3.3.2.c. 3-MeCA system

Subjecting the acid to thermal analysis (DSC) by heating the sample, from room temperature to 125 °C, revealed one endothermic event, due to melting at 121.93 °C and consequently only an exothermic crystallization peak was observe in the cooling cycle (see Figure 3.25). As illustrated in Figure 3.26, PXRD analysis of the sample recovered after the DSC cycle revealed an identical pattern to the one before the DSC experiment, with a slight peak broadening, possibly resulting from poor crystallinity of the acid. For further investigation, a larger amount of acid was melted on the hotplate and then allowed to crystallize by cooling down. This method produced poor single crystals, although the crystal structure could been determined (with high R factor of 15%). Comparing the crystal structures from solution and from melt shows no difference, indicating that there is no phase transformation upon heating the sample. Similarly, no thermal event was observed on cooling the sample from room temperature to -150 °C and reheating to room temperature.
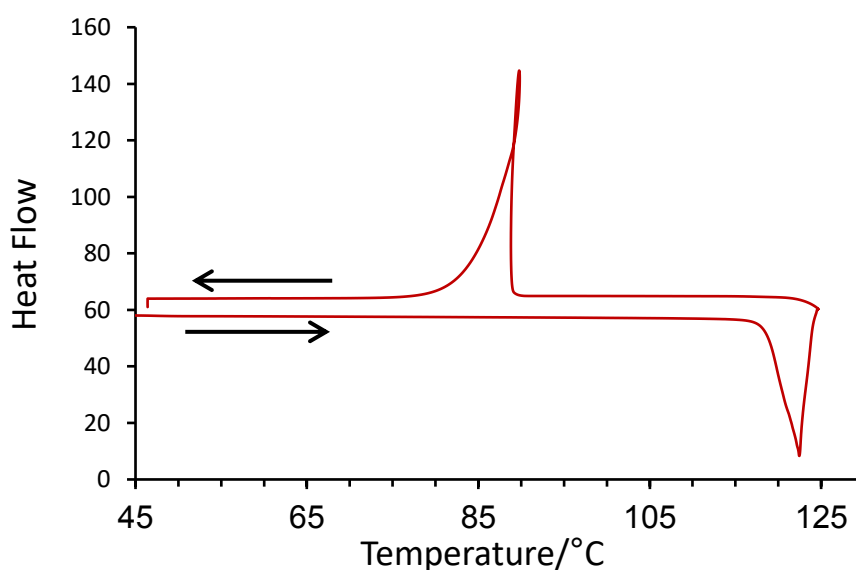
Figure 3.25. *Thermal analysis investigation of the γ phase of 3-MeCA, showing no thermal event apart from melting and recrystallizing.*
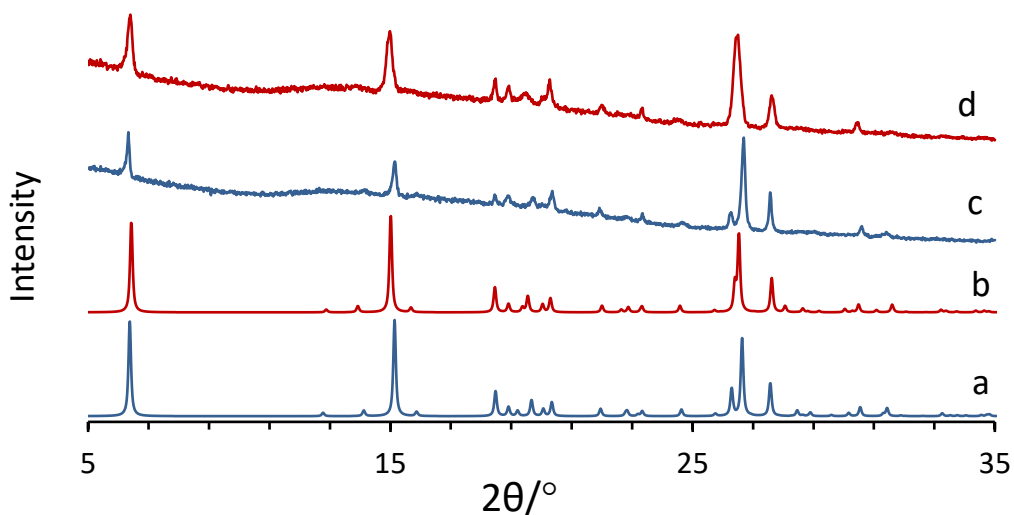
Figure 3.26. *The calculated PXRD pattern of the crystal structure determination of γ-3-MeCA crystallized (a) from solution, (b) from melt, and the experimental PXRD pattern of γ-3-MeCA (a) from solution and (b) from melt.*

3.3.2.d. 3-ClCA system

It was reported[15] that a preliminary check of the thermal behaviour of γ-3-ClCA revealed no phase transformation. However, in this study, similar thermal behaviour was observed for γ-3-ClCA, as has been seen in DSC experiments for both 3-CF$_3$CA and 3-FCA and in one reported for γ-3-BrCA.[15] In the heating cycle, from 40 to 200 °C at 20 °C/min, two endotherms were observed, with onset temperatures of about 143 °C and 163 °C (Figure 3.27a) with the second (higher temperature) event being attributed to melting. In order to characterize the first event, a fresh sample was heated from 40 to 155 °C (i.e. below the melting point) and cooled (Figure 3.27b). No exothermic event was observed in the cooling cycle, indicating that the endothermic process was irreversible. The PXRD pattern recorded for the sample recovered after cooling (Figure 3.28) showed that it was β-3-ClCA and the first thermal event was therefore attributed to a solid-state irreversible polymorphic phase transformation from γ-3-ClCA to β-3-ClCA. Similar behaviour to both 3-CF$_3$CA and 3-FCA was observed for 3-ClCA, regarding SC-SC transformation. Thus a single crystal of the γ of 3-ClCA converted to a single crystal of the β the form upon heating, without losing its integrity. Further investigation was carried out by cooling both phases of the acid from 40 to -150 °C and heating again to room temperature. The thermogram showed no thermal events, indicating no transformation upon cooling both phases of the acids.
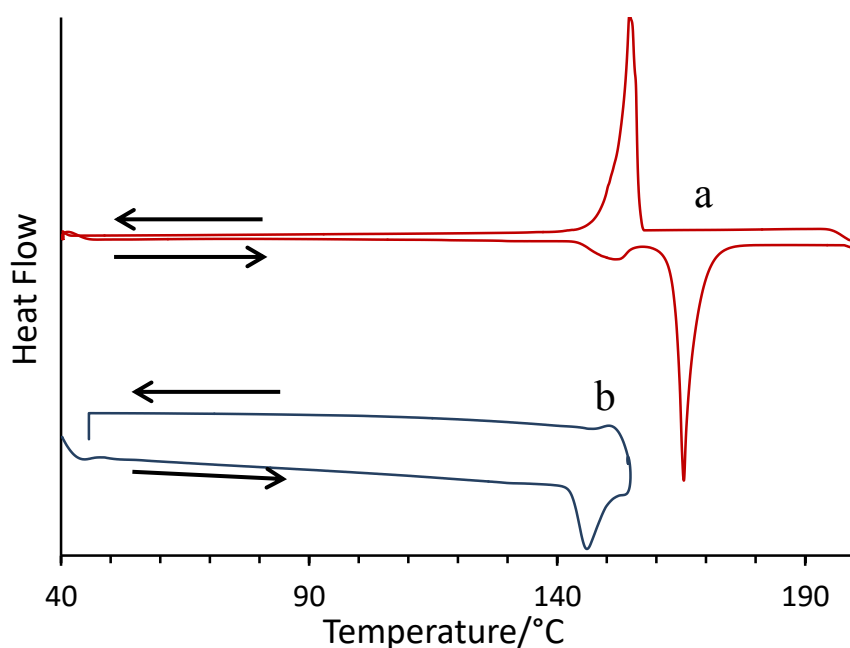
Figure 3.27. *Thermal analysis (DSC) investigation of the γ phase of γ-3-ClCA, (a) heated to 200 °C and then cooled to room temperature exhibits two endothermic events showing the transformation and melt, (b) heated to 155 °C followed by cooling (note that the reverse phase transition from γ to β does not occur on cooling).*
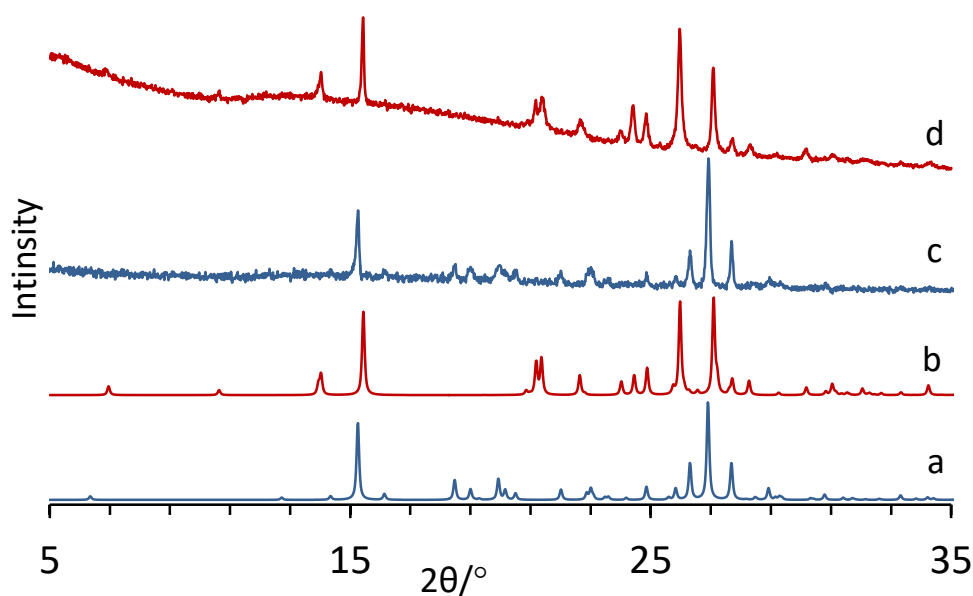
Figure 3.28. *The calculated PXRD pattern of the crystal structure determination of (a) γ-3-ClCA, (b) β-3-ClCA, and the experimental PXRD patterns of (c) γ-3-ClCA and (d) the γ form of acid after the DSC cycle without melting, showing the transformation to β-3-ClCA.*

In γ-3-ClCA, hydrogen-bonded carboxylic acid dimers form stacks parallel to the b-axis. A herringbone arrangement between stacks (along [100]) forms layers in the structure (the layers are displayed as red and blue molecules in Figure 3.29a). In the phase transformation from γ-3-ClCA to β-3-ClCA, the structure changes from monoclinic

(P2₁/c), to triclinic (P$\overline{1}$) and hence, as seen in Figure 3.29b, phase transformation must involve substantial molecular reorientation, although the conformation of the molecules remains unchanged, similarly to that previously observed in the thermal behaviour of 3-FCA.
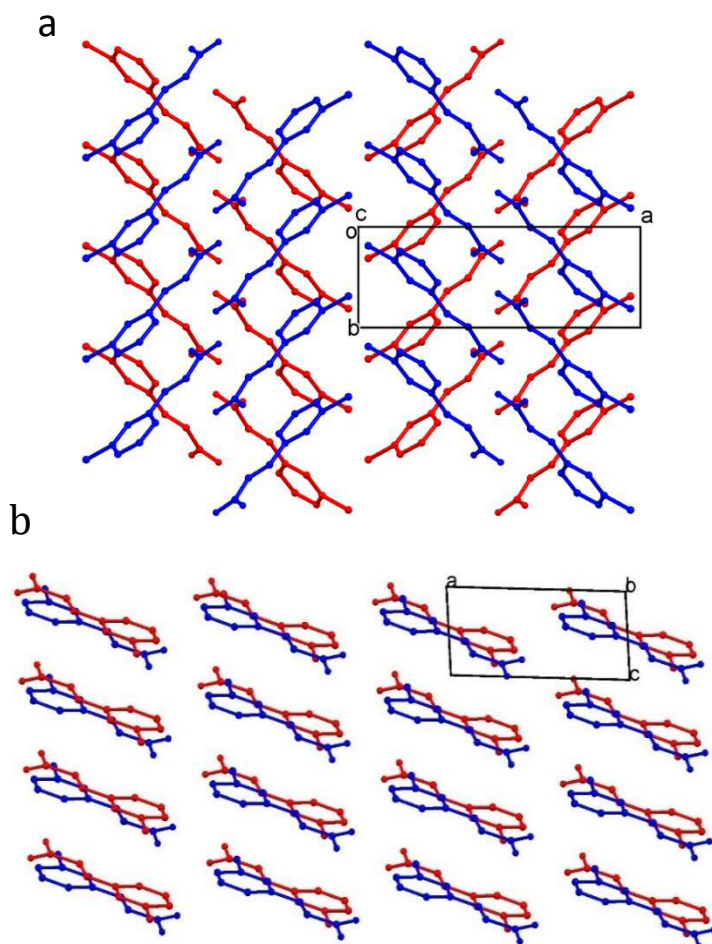
Figure 3.29. *The crystal structures of (a) γ-3-ClCA and (b) β-3-ClCA.*

3.3.2.e. 3-BrCA system

The bromo-analogue, γ-3-BrCA has also been reported to undergo a transformation to β-3-BrCA.[15] However, in this case, the transformation involves a change from one monoclinic form (P2₁/a) to another (C2/c). Repetition of the DSC experiment for γ-3-BrCA under the same conditions as γ-3-ClCA showed a slightly higher onset temperature at about 145 °C. Examining the structures of 3-BrCA before and after the phase transition indicates that the transformation involved a conformational change of the molecules in addition to a spatial rearrangement. To confirm the nature of the transformation the structure of γ-3-BrCA was determined and then the crystal was heated to approximately 145 °C. Redetermination of the crystal structure using the same crystal was possible. This

indicated that the process was SC-SC. Both γ and β were subjected to cooling from 40 to -150 °C and heated again to room temperature. Similar results to 3-ClCA were obtained, indicating that there was no phase transition.

It should be noted that due to a concomitant crystallization of γ_2-3-BrCA with γ-3-BrCA and β-3-BrCA, although several crystallizations were attempted, further investigation of the thermal behaviour of the acid was impossible.

3.3.3. Effect of the different *meta*-substituents on structure and transformation

With the information discussed so far in this chapter regarding crystal structures and the phase transition of the set of the five different *meta*-cinnamic acid derivatives, 3-CF₃CA, 3-FCA, 3-MeCA, 3-ClCA and 3-BrCA, comments can be made about the effect of changing the substituents on the structural and transformational behaviour.

The first observation relates to the γ structures of 3-CF3CA, 3-MeCA, 3-BrCA and 3-ClCA. They are isostructural to each other, as seen by examining their unit cell dimensions, space groups, and crystal packing (Figure 3.30). All structures have similar O-H$\cdots$O and C-H$\cdots$O interactions, as seen in Figure 3.31, and the π-π interactions of the type C=C$\pi\cdots\pi$(benzene) are also observed in these isostructural sets. However, both 3-BrCA and 3-ClCA showed halogen-halogen interactions whereas, C-H$\cdots$F contacts were observed in the 3-CF₃CA structure. The 3-MeCA also adopted isostructural packing, indicating less importance of the additional interactions, such as halogen-halogen (in γ-3-BrCA and γ-3-ClCA) and CH$\cdots$F (in γ_1-3-CF₃CA), in the role of steering the molecules towards different packing arrangements. It was reported that halo-methyl replacement is expected to provide information on the assumption of the strength of the halogen$\cdots$halogen contact.[32,33] So, the other interactions such as hydrogen bonds and π-π interactions that are present in the isostructural set (3-CF₃CA, 3-MeCA, 3-BrCA and 3-ClCA) are more likely to dominate the structural packing.
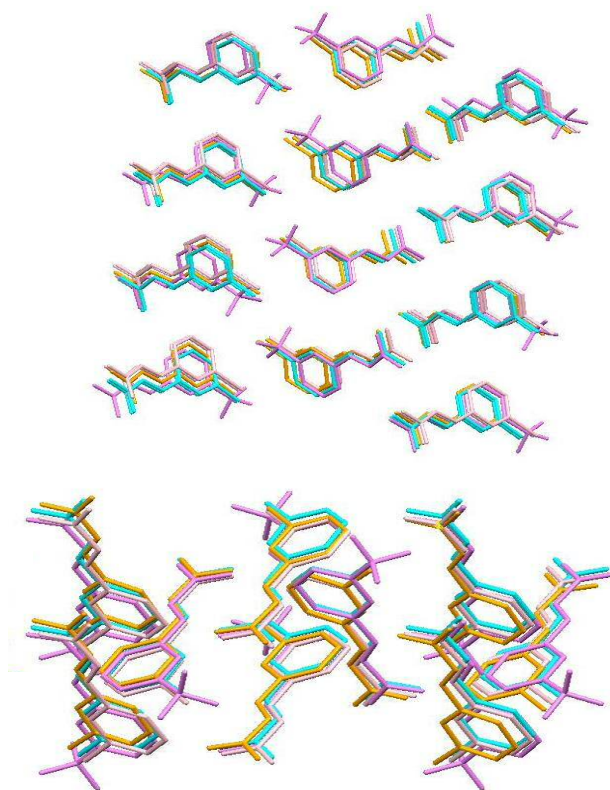
Figure 3.30. *An overlay of γ forms of the structures of; pink=3-BrCA, cyan=3MeCA, violet=3CF₃CA and orange=3-ClCA, from two different views.*
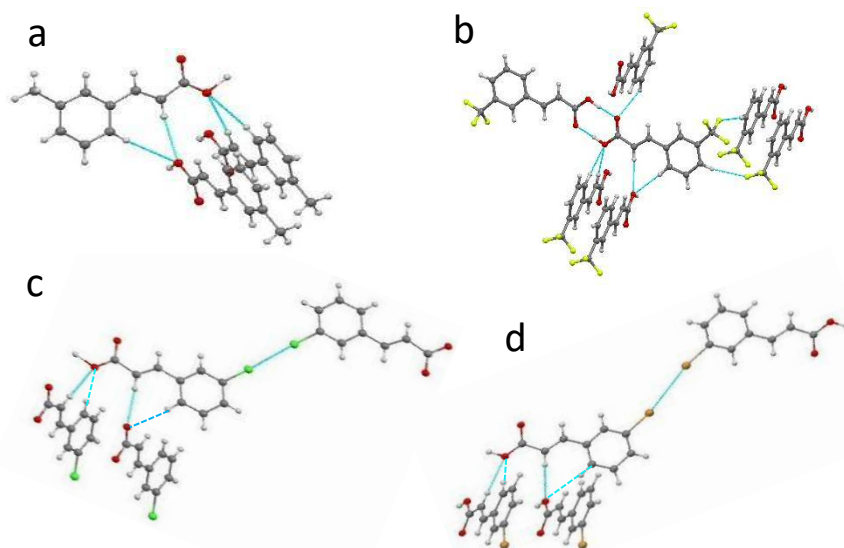
Figure 3.31*. γ phases of the acids showing the additional intermolecular interactions that arise from replacing the methyl group in (a) with CF₃ (b) with Cl (c) and with Br (d).*

On the other hand, β_1 and β_2 structures of 3-FCA adopted different structures from the above set of isostructural structures. Thus, the question arises as to why. A possible explanation is that the size of F is too small, compared with others groups (CF₃, Me, C-

Cl and Br) to fill the same space as the larger groups. A recent study[34] on a system of N-benzylideneanilines revealed that replacing the fluorinated substituent molecules with heavier halogen analogues (Cl or Br) leads to different crystal packing features, particularly when interacting fluorine atoms were replaced. Consistently, both polymorphic forms of 3-FCA showed the involvement of fluorine atoms in the intermolecular interactions of the type (C-H$\cdots$F)[23]. Such interactions were observed to play an important role in the supramolecular structure.[35] In contrast, in the γ form of 3-BrCA and 3-ClCA, Br and Cl preferred to participate in a halogen$\cdots$halogen interaction (Sections 3.3.1.d and 3.3.1.e). So, the differentiation of intermolecular interactions generated by different substituents (F, Cl and Br) is bound to play a role in influencing the crystal packing.

Upon heating γ phases of the isostructural acids, similar behaviour might be expected, leading to similar structures on transformation. However, surprisingly, each structure behaved distinctly from others upon heating. Thus, no phase transition was observed in the case of γ-3-MeCA. However, γ_1-3-CF$_3$CA, γ-3-BrCA, γ-3-ClCA produced different distinct polymorphs. This different behaviour leads to questions about the cause of the differences and whether the substituent groups play any role. To better understand their behaviour the relationship between some acids will be discussed.

Firstly, considering the γ forms of 3-CF$_3$CA (γ_1) and 3-MeCA, it is notable that applying heat induced a phase transition in 3-CF$_3$CA but not in 3-MeCA. It has been reported that the replacement of H by F has a dramatic influence on the crystal structure and, subsequently, on chemical and physical properties of various small organic molecules[36]. However, in the present work, replacing the hydrogen atoms in the 3-methyl group by F atoms in the structure of γ-3-MeCA has led to the isostructural crystal, although an increase of intermolecular interaction complexity around the 3-CF$_3$ was observed, the C-H$\cdots$F interaction, for example. In both structures, the hydrogen bonds associated with the carboxylic acid and C-H$\cdots$O weak hydrogen bonds are also observed. However, as discussed in Section 3.3.1.a, in the γ_2 form of the acid (the form obtained from transformation of γ_1-3-CF$_3$CA) the CF$_3$ is involved in a number of significant intermolecular interactions. Thus, in addition to the C-H$\cdots$F interaction, fluorine atoms are also involved in the C-F$\cdots$F-C interaction (Figure 3.32). In contrast, such interactions cannot be obtained if the fluorine atoms are replaced by hydrogen atoms. This might

indicate why 3-MeCA did not transform to a structure similar to γ_2-3-CF$_3$CA on the one hand and emphasizes the importance of the C-F⋯F-C interaction on the other hand.
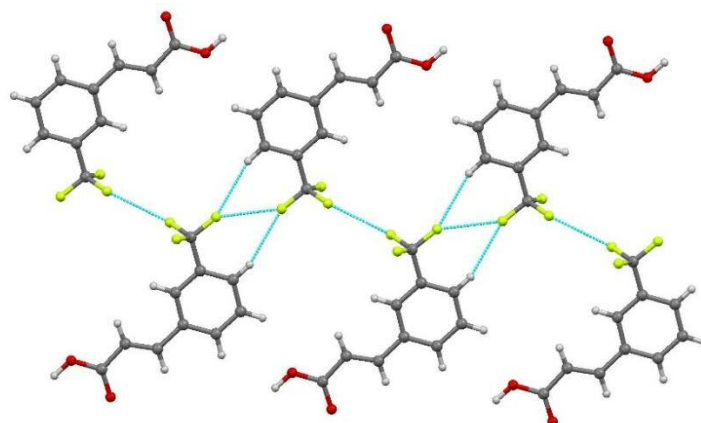
Figure 3.32. *Part of the structure of γ_2-3-CF$_3$CA showing the intermolecular interactions that involve CF$_3$ groups.*

Secondly, in the case of the replacement of the Me group by either Cl or Br, it has been suggested that such interchanging of groups of similar size may not lead to significant change in the structure. Examples are presented in the literature of materials where a methyl substituent is isostructural with those of corresponding substituted Cl or Br compounds[37,38]. The γ forms of 3-MeCA of 3-ClCA and 3BrCA are isostructural, as discussed previously, despite the halogen-halogen interactions (C-Cl⋯Cl-C and C-Br⋯Br-C) observed as a result of replacing the methyl group with Cl and Br. Thus, it might be expected that γ-3-MeCA may exhibit similar thermal properties, regarding the transformation to β structures, to 3-ClCA, but it does not. To explain the difference, both β structures of 3-ClCA and 3-BrCA are re-examined in terms of the intermolecular interaction involved with Cl and Br.

As discussed previously in Section 3.3.1.d (Figure 3.13), in the β form of 3-BrCA, Br atoms are involved in C-Br⋯O interactions and this influences the extension of the structure along b-axis. However, replacing this group with a methyl group would influence the structure as the three hydrogen atoms would form C-H⋯O interactions; this might explain why γ-3-MeCA would be unlikely to transform to a structure similar to β-3-BrCA.

In the case where the Me group is replaced by Cl in the β form of 3-ClCA, despite the lack of obvious interactions that can significantly influence the structure, the γ-3-MeCA did not transform to the structure of β-3-ClCA. A noticeable feature is that, as is seen in

Figure 3.33, the stack distance between Cl atoms from one molecule to another is only 3.908Å and that might be less appropriate for the Me group. In this regards, analysis of the CDS of phenyl-X group (X= Cl and Me) separation distances between 3.5-4Å(X···X) shows 1,042 hits for Cl···Cl and only 374 hits for CH_3···CH_3. This is in line with the suggestion that stacking of Cl atoms with a distance Cl···Cl 3.5-4Å is more favourable than the stacking of CH_3···CH_3 with these distances.

However, in the γ form of 3-MeCA, through the stacking of molecules, CH_3···CH_3 is present with a distance of more than 4.5Å, suggests that γ form is probably a preferred form for 3-MeCA. This might be a reason for dissimilar behavior of the γ forms of 3-ClCA and 3-MeCA with respect to thermo-transformation.
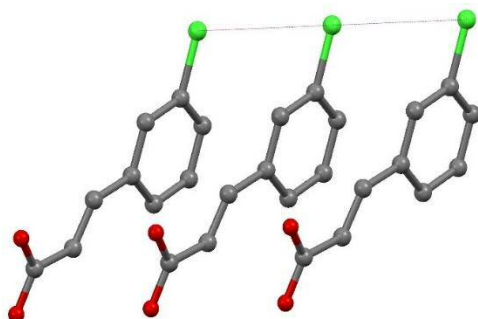
Figure 3.33. *Part of the β-3-ClCA structure representing the relationship between Cl atoms in the stack.*

Finally, as shown in Sections 3.3.1(a and d), in spite of the observation that the molecules in γ_1-3-CF$_3$CA and γ-3-BrCA undergo a conformational change on transition, different packing modes are observed after transformation. In fact, after the phase transition, β-3-BrCA is monoclinic whereas γ_2-3-CF$_3$CA is triclinic. The structure of γ_2-3-CF$_3$CA has parallel layers and hydrogens bonds (O-H···O, C-H···O, and C-H···F) and F···F contacts are involved in stabilizing the structure. In contrast in β-3-BrCA, the molecules assume two orientations and both hydrogens bonds (O-H···O) and Br···O interactions are observed. The differentiation in the intermolecular interactions that accompany a change in substituent groups suggests the role of the identity of these substituents.

It is worth noting that, unlike isostructural γ_1-3-CF$_3$CA and γ-3-BrCA, the transformation of 3-ClCA from γ to β does not require a change in the molecular conformational and only a rearrangement of the packing is observed, and hence they are transformed to different structures.

These comments highlight the important role played by the identity of the substituents in generating the different crystal structures observed for *meta*-cinnamic acid derivatives, as well their role in the generation of different crystal structures on transformation of the isostructural set.

3.4. Conclusion

The study reported reveals a number of interesting observations about cinnamic acids derivatives. Thus, two β-type polymorphs of 3-FCA (β_1 and β_2), two γ-type polymorphs of 3-CF$_3$CA (γ_1 and γ_2) in addition to one γ-type polymorph of 3-BrCA (γ_2) have been discovered and structurally characterized. This represents rare cases in derivatives of *trans*-cinnamic acid, in which two distinct polymorphs co-exist at ambient conditions within the same structural classification (β-type in the case of 3-FCA and γ-type for 3-CF$_3$CA). The β_1 polymorph of 3-FCA transforms irreversibly to the β_2 polymorph on heating above 119 °C, with further heating leading to melting at 167 °C. Similarly, the γ_1 polymorph of 3-CF$_3$CA undergoes irreversible transition on heating above *ca.* 119 °C to produce γ_2 and, with further heating, melts at around 134 °C. The γ_1-3-BrCA was not obtained in pure form.

The structure characterization of γ-3-MeCA has also been carried out in this study. No transformation was observed upon heating. Thermal investigation of γ-3-ClCA demonstrated a transformation upon heating to produce β-3-ClCA.

An extended study indicated that all phase transitions reported in this study occurred in a SC-SC manner, although considerable change is required for transformation in some structures. For example, both 3-CF$_3$CA and 3-BrCA changed their molecular conformational during thermal transformation.

The results of this study have also revealed that, apart from 3-FCA, all other acids reported in this study crystallized as γ forms and they are isostructural to each other. Thus, the size of the substituents was shown to be of greater importance than the intermolecular interactions involved. This, accordingly, lead to the possibility of replacing the substituent groups (Cl, Br and CF$_3$) with Me, hence, 3-MeCA adopts a similar packing motif.

On heating the γ isostructural derivatives, each acid behaved distinctly. For example, 3-MeCA remains in its γ form whereas the other acids transformed into different forms. Therefore, the identity of the substituted groups clearly influences the thermal properties of the materials and hence, plays an importance role in the determination of the final product structures, particularly when they are involved in different intermolecular interactions.

3.5. References

1   K. Patra, S. Bose, S. Sarkar, J. Rakshit, S. Jana, A. Mukherjee, A. Roy, D. P. Mandal and S. Bhattacharjee, *Chem. Biol. Interact.*, 2012, **195**, 231–239.

2   P. Sharma, *J. Chem. Pharm. Res.*, 2011, **3**, 403–423.

3   R. B. Kasetti, S. A. Nabi, S. Swapna and C. Apparao, *Food Chem. Toxicol.*, 2012, **50**, 1425–1431.

4   B. Korošec, M. Sova, S. Turk, N. Kraševec, M. Novak, L. Lah, J. Stojan, B. Podobnik, S. Berne, N. Zupanec, M. Bunc, S. Gobec and R. Komel, *J. Appl. Microbiol.*, 2013, **116**, 955–966.

5   P. De, M. Baltas and F. Bedos-Belval, *Curr. Med. Chem.*, 2011, **18**, 1672–1703.

6   G. M. J. Schmidt, *J. Chem. Soc.*, 1964, 2014–2021.

7   B. M. D. Cohen and G. M. J. Schmidt, *J. Chem. Soc.*, 1964, 1996–2000.

8   M. D. Cohen, G. M. J. Schmidt and F. I. Sonntag, *J. Chem. Soc.*, 1964, 2000–2013.

9   M. A. Fernandes, D. C. Levendis and C. B. de Koning, *Cryst. Eng.*, 2001, **4**, 215–231.

10   R. F. Bryan and D. P. Freyberg, *J. Chem. Soc. Perkin II*, 1975, 1835–1840.

11   C. Generate, *J. Chem. Soc. Perkin II*, 1975, 68–74.

12   W. Xiong, S. Zhang, C. Ji, L. Li, Z. Sun and C. Song, *Inorg. Chem. Commun.*, 2014, **41**, 79–83.

13   E. V. Boldyreva, H. Sowa, H. Ahsbahs, S. V. Goryainov, V. V. Chernyshev, V. P. Dmitriev, Y. V. Seryotkin, E. N. Kolesnik, T. P. Shakhtshneider, S. N. Ivashevskaya and T. N. Drebushchak, *J. Phys. Conf. Ser.*, 2008, **121**, 1–11.

14   M. Bujak and R. J. Angel, *J. Phys. Chem. B*, 2006, **110**, 10322–10331.

15   S. Ahn, K. D. M. Harris, B. M. Kariuki and D. M. S. Zin, *J. Solid State Chem.*, 2001, **156**, 10–15.

16   I. Fonseca, S. E. Hayes, B. Blümich and M. Bertmer, *Phys. Chem. Chem. Phys.*, 2008, **10**, 5898–5907.

17   J. L. R. Yates and H. A. Sparkes, *CrystEngComm*, 2013, **15**, 3547–3553.

18   M. A. Fernandes, D. C. Levendis and F. R. L. Schoening, *Acta Crystallogr. Sect. B*, 2004, **60**, 300–314.

19   J. A. K. Howard and H. A. Sparkes, *CrystEngComm*, 2008, **10**, 502–506.

20   B. M. Kariuki, D. M. S. Zin, M. Tremayne and K. D. M. Harris, *Chem. Mater.*, 1996, **8**, 565–569.

21   S. Kanao, S. Kashino and M. Haisa, *Acta Crystallogr. Sect. C*, 1990, **46**, 2436–2438.

22   A. Bondi, *J. Phys. Chem.*, 1964, **68**, 441–451.

23   V. R. Thalladi, H.-C. Weiss, D. Bläser, R. Boese, A. Nangia and G. R. Desiraju, *J. Am. Chem. Soc.*, 1998, **120**, 8702–8710.

24   I. Abdelmoty, V. Buchholz, L. Di, C. Guo, K. Kowitz, V. Enkelmann, G. Wegner and B. M. Foxman, *Cryst. Growth Des.*, 2005, **5**, 2210–2217.

25   G. L. Liu, C. M. Liu and H. Li, *J. Solid State Chem.*, 2011, **184**, 481–487.

26   E. R. T. Tiekink and J. Zukerman-Schpector, *The Importance of Pi-Interactions in Crystal Engineering: Frontiers in Crystal Engineering*, John Wiley & Sons, Ltd, Chichester, 2012.

27   A. Forni, S. Pieraccini, S. Rendine, F. Gabas and M. Sironi, *ChemPhysChem*, 2012, **13**, 4224–4234.

28   J. P. M. Lommerse, A. J. Stone, R. Taylor and F. H. Allen, *J. Am. Chem. Soc.*, 1996, **118**, 3108–3116.

29   S. Kanao, S. Kashino and M. Haisa, *Acta Crystallogr. Sect. C*, 1990, **46**, 2439–2442.

30   M. Mazik, A. C. Buthe and P. G. Jones, *Tetrahedron*, 2010, **66**, 385–389.

31   W. Zhang, X. Tang, H. Ma, W.-H. Sun and C. Janiak, *Eur. J. Inorg. Chem.*, 2008, 2830–2836.

32   C. Capacci-Daniel, S. Dehghan, V. M. Wurster, J. A. Basile, R. Hiremath, A. A. Sarjeant and J. A. Swift, *CrystEngComm*, 2008, **10**, 1875–1880.

33   B. Omondi, M. A. Fernandes, M. Layh, D. C. Levendis, J. L. Look and T. S. P. Mkwizu, *CrystEngComm*, 2005, **7**, 690–700.

34   G. Kaur and A. R. Choudhury, *Cryst. Growth Des.*, 2014, **14**, 1600–1616.

35   P. Mocilac, I. A. Osman and J. F. Gallagher, *CrystEngComm*, 2016, **18**, 5764–5776.

36   M. Barceló-Oliver, C. Estarellas, A. García-Raso, A. Terrón, A. Frontera, D.

Quiñonero, I. Mata, E. Molins and P. M. Deyà, *CrystEngComm*, 2010, **12**, 3758–3767.

37   R. Thakuria, N. K. Nath, S. Roy and A. Nangia, *CrystEngComm*, 2014, **16**, 4681–4690.

38   M. R. Edwards, W. Jones, W. D. S. Motherwell and G. P. Shields, *Mol. Cryst. Liq. Cryst. Sci. Technol. Sect. A.*, 2001, **356**, 337–353.

Chapter 4: Investigation of binary systems of *meta*-cinnamic acids: cocrystallization, phase characterization and transformation

4.1. Introduction

Cocrystallization of molecular organic solids has the potential to have a high impact on engineering strategies for crystal design by enabling the functional groups to be precisely tuned to generate materials with desirable functional properties.[1–4]

Systematic investigation of the parent materials and their cocrystals, in particular focusing on studies of multicomponent system that form solid solutions, is valuable in opening up new avenues that may help in understanding structure-property relationships. This could then enhance the tailoring of molecular structure by varying the composition of crystals with subsequent changes to the crystalline properties.[5–10] In this regard the photo-stable derivatives of cinnamic acids, cinnamamides, and trans-stilbenes have been engineered to adopt photoreactive crystal structures as a result of mixing of two binary systems in the form of solid solution.[11,12] Therefore, the general objective of the work in this chapter was focused primarily on screening for the feasibility of cocrystallization (forming solid solutions) of binary systems of *meta*-cinnamic acid derivatives, based on the structural characterizations explored in Chapter 3. The influence of different substituents on the structural construction of the solid solutions was investigated, with the aim of engineering crystals that exhibit the photodimerization reaction. The specific reasoning for selecting the binary systems can be summarized as follows:

1) γ-3-ClCA and γ-3-BrCA are isostructural (discussed in Chapter 3) and so would be expected to form a solid solution. It is not surprising that they both underwent phase transformations on heating, but it is noteworthy that they showed transformation to different crystal structures. This presented an opportunity to investigate the effect of cocrystallization on the crystal forms obtained and the phase transformation process (see Section 4.3.1).

2) The transformation in 3-BrCA, from γ to β, has been reported previously[13], and as discussed in Chapter 3, 3-FCA underwent phase transition from β_1 (triclinic) to β_2 (monoclinic) on heating. These materials are not isostructural. Furthermore, the difference between the volumes of C-Br (40.8Å³) and C-F (27.9Å³) is significant (C-Br and for C-F volumes were calculated using VEGA[14] program), and so in addition to whether these acids cocrystallize, the next question is which crystal structure the solid solution would adopt. These issues will be discussed in Section 4.3.2.

3) Recalling the results from Chapter 3, both acids 3-CF$_3$CA and 3-MeCA, showed isostructural packing for the γ phase. In addition, γ_1-3-CF$_3$CA showed transformation to another γ phase (γ_2) whereas 3-MeCA showed no transformation. Thus, exploring the CF$_3$/CH$_3$ interchangeability, inspired by the Cl-CH$_3$ rule[15] and due to their relatively similar volumes, an investigation of the cocrystallization of 3-CF$_3$CA and 3-MeCA may aid understanding of the behaviour of 3-MeCA. Details will discuss in Section 4.3.3.

4) The β forms of cinnamic acids can undergo photodimerzation reactions upon exposure to UV light.[16] The results discussed in Chapter 3 showed that both 3-BrCA and 3-ClCA crystallized mainly in the β form from a solution of glacial acetic acid. In contrast, both 3-MeCA and 3-CF$_3$CA generated only the γ forms and no β structure of the acids has been discovered. Thus, in Section 4.3.4 the investigation was carried out by cocrystallizing (3-ClCA/3-MeCA), (3-ClCA/3-CF$_3$CA), (3-BrCA/3-MeCA) and (3-BrCA/3-CF$_3$CA) with the aim of generating the β form of the solid solution.

4.2. Experimental Methods

4.2.1. Cocrystallization from solution

The normal method of crystallization was by dissolving the materials of a binary system in the appropriate solvent and leaving the solution at room temperature to allow slow evaporation of the solvent. For all binary systems studied in this chapter, a 1:1 molar ratio of 3-ClCA:3-BrCA, 3-BrCA:3-FCA, 3-CF$_3$CA:3-MeCA, 3-ClCA:3-MeCA, 3-ClCA:3-CF$_3$CA, 3-BrCA:3-MeCA and 3-BrCA:3-CF$_3$CA was crystallized from methanol (MeOH) or glacial acetic acid (GAA) and, the products were characterized by PXRD and SC-XRD when possible. The results are discussed in Section 4.3. Specific conditions are summarized in Section 4.2.1.a, 4.2.1.b and 4.2.1.c and discussed in section 4.3.1, 4.3.2 and 4.3.3.

4.2.1.a. 3-ClCA and 3-BrCA

For cocrystallization from solution, a mixture of 3-ClCA and 3-BrCA was used. A 1:1 molar ratio of 3-ClCA:3-BrCA dissolved in MeOH gave colourless blocks with a powder diffraction pattern isostructural to γ phases of 3-ClCA and 3-BrCA and hence the product was designated γ-3-ClCA/3-BrCA. Crystallization in a similar manner, using acetone (AC) as the solvent, produced a mixture of two types of crystals; colourless thick plate and a small amount of thin needle crystals. PXRD showed the existence of two phases: γ-3-ClCA/3-BrCA (the same as from MeOH) and a second phase isostructural to γ_2-3-BrCA (denoted γ_2-3-ClCA/3-BrCA). Using GAA as the solvent for a 1:1 molar ratio of 3-ClCA and 3-BrCA produced long colourless plate-like crystals with a PXRD pattern similar to that of β-3-BrCA and so the material is referred to as β-3-ClCA/3-BrCA. 1:2 and 2:1 molar ratios of 3-ClCA:3-BrCA were also crystallized in GAA. Details are discussed in Section 4.3.1.

4.2.1.b. 3-BrCA and 3-FCA

For cocrystallization from solution, mixtures with different molar ratios (1:1, 4:1 and 9:1) of 3-BrCA:3-FCA were dissolved in MeOH. Crystallization of the 1:1 sample gave colourless plate-like crystals with a PXRD pattern that indicated a mixture of two phases. One was similar to the β phase of 3-BrCA and the other to the β_1 phase of 3-FCA and hence the products were designated as β-3-BrCA/3-FCA and β_1-3-BrCA/3-FCA, respectively. The results were reproducible. Crystallization in the same solvent using 4:1 3-BrCA:3-FCA produced colourless plate-like crystals with a PXRD pattern different from the previous crystallization attempts and the product was designated as γ_2-3-BrCA/3-FCA since the structure determination was similar to γ_2-3-BrCA (discussed previously in Chapter 3). The generation of this phase (γ_2-3-BrCA/3-FCA) was unreliable, as crystals with a PXRD similar to β_1-3-BrCA/3-FCA in addition to γ-3-BrCA/3-FCA (similar to γ-3-BrCA) and β-3-BrCA/3-FCA were also produced. Crystallization in the same manner using 9:1 3-BrCA:3-FCA produced mainly β-3-BrCA/3-FCA contaminated with β_1-3-BrCA/3-FCA. Crystallization of 1:1 (3-BrCA:3-FCA) from GAA and MeOH showed no difference in the crystal habit and PXRD pattern. Details will be discussed in Section 4.3.2.

4.2.1.c. 3-MeCA and 3-CF$_3$CA

A mixture of 1:1 γ-3-MeCA:γ_1-3-CF$_3$CA was crystallized from MeOH produced fragile long plate crystals with a PXRD pattern similar to γ_1-3-CF$_3$CA. Similarly, 1:4 and 4:1 mixtures of 3-MeCA:3-CF$_3$CA, also crystallized in MeOH gave the same crystal habit, but PXRD showed a similar pattern to γ-3-MeCA for the 1:4 starting ratio and similar to γ_1-3-CF$_3$CA for the 4:1 ratio. Details of the structure will discussed in Section 4.3.3.

4.2.2. Preparation of physical mixtures of acids prior to DSC study

To investigate the thermal behaviour of different binary systems, appropriate amounts of the acids were accurately weighted and ground lightly to ensure uniform mixing, with care being taken to avoid the formation a solid solution (monitored by PXRD). The following physical mixtures were produced: 5:1, 4:1, 3:1, 2:1, 1:1, 1:2, 1:3 and 1:5 ratios of γ-3-ClCA:γ-3-BrCA, 2:1, 1:1, 1:2, 1:4, 1:6, 1:8 and 1:9 ratios of β_1-3-FCA: γ-3-BrCA, 1:4 and 4:1 ratios of γ-3-MeCA:γ_1-3-CF$_3$CA, and 1:1 ratios of γ-3-ClCA:γ-3-MeCA, γ-3-ClCA:γ_1-3-CF$_3$CA, γ-3-BrCA:γ-3-MeCA and γ-3-BrCA/γ_1-3-CF$_3$CA. The reason for the selection these ratios of different binary systems are discussed in the Result and Discussion section.

4.2.3. Crystallization from sublimation

3-ClCA, 3-BrCA and a 1:1 physical mixture of 3-ClCA:3-BrCA were put in vials, placed on the hot plate and heated to about 190°C, above melting point of the acids. The materials that crystallized from the vapour onto the side of the vials were collected and characterized.

4.2.4. X-ray photoelectron spectroscopy (XPS)

A Kratos Axis Ultra DLD system was used to collect XPS spectra using a monochromatic Al $K\alpha$ X-ray source operating at 120W. Data was collected with pass energies of 160 eV for survey spectra, and 40 eV for the high resolution scans. The system was operated in the Hybrid mode, using a combination of magnetic immersion and electrostatic lenses and acquired over an area approximately 300×700 μm^2. A magnetically confined charge compensation system was used to minimize charging of the sample surface, and all spectra were taken with a 90° take off angle. A base pressure of $\sim 1 \times 10^{-9}$ Torr was maintained during collection of the spectra.

4.2.5. Solid-state ^{13}C NMR

^{13}C NMR experiments were performed on a Varian VNMRS spectrometer *(EPSRC UK National Solid-state NMR Service at Durham)* with frequencies of 100.562 MHz.

CASTEP software[17,18] was used to calculate the NMR theoretical chemical shifts of the carbon atoms. For the calculation, the atomic coordinates were taken from the SC-XRD structure for γ-3-BrCA[13], β-3-BrCA[19] and β-3-ClCA/3-BrCA. The theoretical structure of β-3-ClCA (isostructural to β-3-BrCA) was simulated first, as it has not been obtained experimentally. Thus, the simulation involved replacing Br with Cl followed by energy minimization.

4.2.6. Molecular fragment volumes

The program used to calculate volumes of C-Cl, C-Br, C-F, C-CH$_3$ and C-CF$_3$ groups was VEGA.[14]

4.3. Results and Discussion

4.3.1. Investigation of a binary system of 3-ClCA/3-BrCA

Since both Br and Cl are electronically similar and they occupy approximately similar volumes (40.8 and 36.8Å^3 for C-Br and C-Cl respectively, calculated using VEGA)[14], their derivatives can be expected to crystallize isostructurally.[20] For example, as discussed in Chapter 3, γ-3-ClCA and γ-3-BrCA are isostructural and both undergo phase transformations on heating. This behaviour is not surprising but the observation that they transform to different structures is noteworthy. Thus the properties of a binary system composed of 3-ClCA and 3-BrCA was investigated.

4.3.1.a. Thermal investigation of cocrystallization
A 1:1 physical mixture

Thermal analysis techniques, such as DSC, are an effective rapid tool for screening cocrystals.[21,22] Thus, to investigate the feasibility of forming cocrystals, a DSC experiment was carried out first using a physical mixture, with a 1:1 ratio of γ-3-ClCA and γ-3-BrCA. An endothermic peak due to the phase transformation was observed at about 155 ºC on heating (Figure 4.1a) but there was no clear distinction for the two components due to the small difference between their peak temperatures, which are around 146 ºC and 153 ºC for γ-3-ClCA and γ-3-BrCA respectively. The peaks

associated with melting also merged into a broad asymmetric feature at about 172 ºC and crystallization was observed as an exothermic event at around 152 ºC on cooling.

The same sample was then taken through a second cycle of heating and cooling (Figure 4.1b). The phase transition peak was not observed and, additionally, the peak due to melting was more symmetrical in the second cycle, a result consistent with the existence of just a single phase. This is in agreement with the results of Lin and co-workers,[23] in which multiple peaks were observed on heating in the first cycle of physical mixtures of indomethacin and saccharin. However, re-heating the same sample showed only one endothermic peak, indicating the formation of cocrystalline material.

The PXRD pattern recorded for the sample obtained following the heating/cooling cycle is similar to that of β-3-BrCA, but with peak shifts to slightly higher values of 2θ, as shown in Figure 4.2. This observation is consistent with the formation of a solid solution of β-3-BrCA together with a molecule (i.e., 3-ClCA) with slightly lower molecular volume (giving rise to slightly contracted unit cells compared to pure β-3-BrCA) in accordance with Vegard's Law[24].
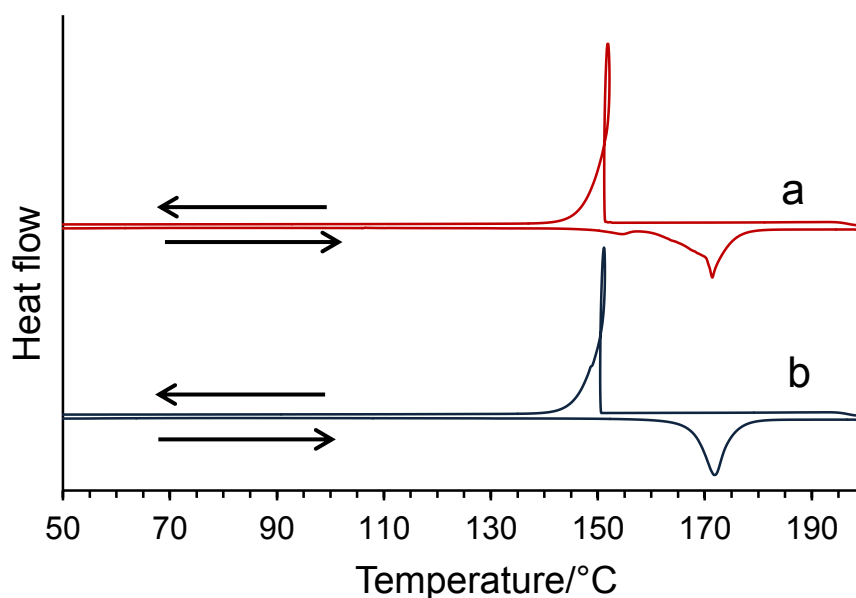
Figure 4.1. *DSC plot for a 1:1 mixture of γ-3-ClCA:γ-3-BrCA showing (a) the first cycle and (b) the second cycle of the DSC experiment.*
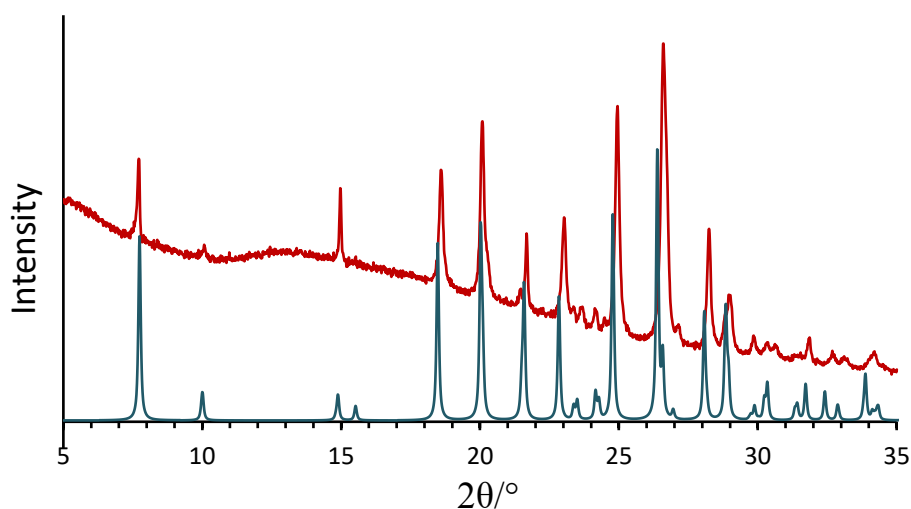
Figure 4.2. *An experimental PXRD pattern of a 1:1 mixture of γ-3-ClCA:γ-3-BrCA after the second DSC cycle (red) and the calculated PXRD for β-3-BrCA (blue).*

Physical mixtures in other ratios

To confirm the formation of solid solution, additional physical mixtures were prepared with γ-3-ClCA:γ-3-BrCA in ratios of: 5:1, 4:1, 3:1, 2:1, 1:2, 1:3 and 1:5. The samples were subjected to two consecutive cycles of heating and cooling (referred to as *first* and *second* DSC cycles) from 40 to 200 °C and back to room temperature at 20 °C/min. The samples were then collected and analysed using PXRD (discussed below).

The DSC plots for all the physical mixtures showed generally similar behaviour to that observed for the 1:1 mixture, already discussed earlier in this section. The results in the temperature range 130-199 °C from the first and second heating cycles for all the physical mixtures along with γ-3-ClCA and γ-3-BrCA are illustrated in Figure 4.3 and 4.4, respectively. In the first cycle for all cases, a small endothermic peak due to γ to β phase transformation is observed at around 150-160 °C. The transformation from γ to β is consistent with the behaviour of the pure acids 3-ClCA and 3-BrCA which was discussed in Chapter 3. The transformation of the mixture of γ-3-ClCA and γ-3-BrCA will be discussed in Section 4.3.1.b. The melting peaks, at around 160-185°C, are asymmetric (Figure 4.3) as they are an overlay of the independent behaviour of β-3-ClCA and β-3-BrCA (the apparent shift in the melting temperature for β-3-BrCA with composition is attributed to the process being mediated by the molten β-3-ClCA). This shift in the melting temperature versus the composition is usually observed in a system that comprises a mixture of different components.[23,25]

The second DSC cycle showed just one endotherm associated with melting for all the samples. The peak is more symmetrical (Figure 4.4), a result consistent with the formation of a mainly monophasic sample on crystallization from the molten mixture of 3-ClCA and 3-BrCA. A break in the trend is observed at a 3-ClCA:3-BrCA ratio of 4:1. Starting with pure 3-BrCA, the gradual decrease in the onset temperature as the amount of 3-ClCA in the sample is increased up to a β-3-ClCA:β-3-BrCA ratio of 4:1 (Figure 4.4) indicates the formation of a solid solution. Broadening of the endothermic peaks, at a 3-ClCA:3-BrCA ratio of 4:1, is also observed (discussed below).

The PXRD patterns in the 2θ range (22-27.5°) for the samples obtained after the second DSC cycle are shown in Figure 4.5. The patterns for samples with 3-ClCA:3-BrCA ratios 1:5 to 2:1 (marked i) match β-3-BrCA with shifts in the peaks. On the other hand, a similar powder pattern to β-3-ClCA was observed for the solids with 3-ClCA:3-BrCA ratios 3:1 to 5:1, again with a slight shift in the peaks (see Figure 4.5 (ii). The shift in peak positions (for example, as seen in Figure 4.6) is indicative of the formation of solid solutions.[26,27]

The break in the trend in the DSC plot that was observed at a 3-ClCA:3-BrCA ratio of 3:1 to 4:1 is coincidentally close to the change in crystal structure, from the structure that is similar to β-3-BrCA to a structure similar to β-3-ClCA. Thus, two solid solutions with structures similar to either β-3-ClCA or β-3-BrCA are formed, depending on the composition. The critical composition is around a 3-ClCA:3-BrCA ratio of 3:1, where the PXRD showed the switch of phase from that similar to β-3-BrCA to a structure similar to β-3-ClCA. The structure similar to β-3-BrCA has 3-ClCA:3-BrCA ratios 1:5 to 2:1, in contrast, the structure similar to β-3-ClCA has 3-ClCA:3-BrCA ratios 3:1 to 5:1. Three decades ago it was proposed by Kitaigorodsky[28] that the formation of a continuous solid solution is determined by the isostructurality of the comprising crystalline materials. On the other hand, a more recent study by Schur et al.[5] showed that although acridine and phenazine are not isostructural in all of their polymorphs, their cocrystallization resulted in a continuous solid solution over a wide range of compositions. In contrast, our result suggested the formation of two continuous solid solutions of non-isostructural crystalline materials. A solid solution comprising of 3-ClCA and 3-BrCA switches from one structural type to another when the 3-ClCA content is approximately 70%. Despite the structural differences, the photo-chemical

properties of the crystal were maintained, as both forms exhibit a *β* structure type of cinnamic acid that undergoes a photoreaction to produce *β* truxinic acid dimeric products.

In addition, the broadening in the peak that was observed in the second DSC cycle at a 3-ClCA:3-BrCA ratio of 4:1 clearly suggests the occurrence of two events. This may be attributed to the existence of a mixture of a solid solution with the structure similar to *β*-3-ClCA with different ratios of 3-ClCA:3-BrCA, expected to be between 3:1 and 5:1. The other possibility for these events could be the existence of different 3-ClCA/3-BrCA solid solutions which are isostructural to *β*-3-ClCA and *β*-3-BrCA.

For clarity, in this study the 3-ClCA/3-BrCA solid solution that is isostructural to 3-BrCA is denoted as *β*-3-ClCA/3-BrCA, while the one that is isostructural to 3-ClCA is *β*$_1$-3-ClCA/3-BrCA.
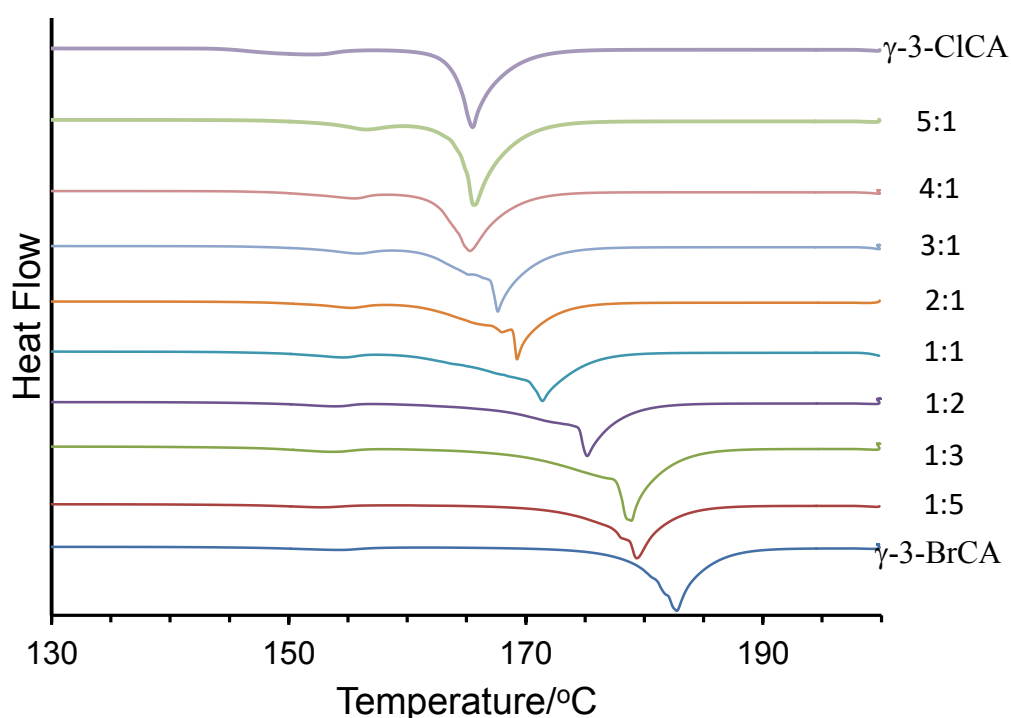
Figure 4.3. *Plots for different mixtures of γ-3-ClCA:γ-3-BrCA, γ-3-ClCA and γ-3-BrCA, showing the first DSC cycle.*
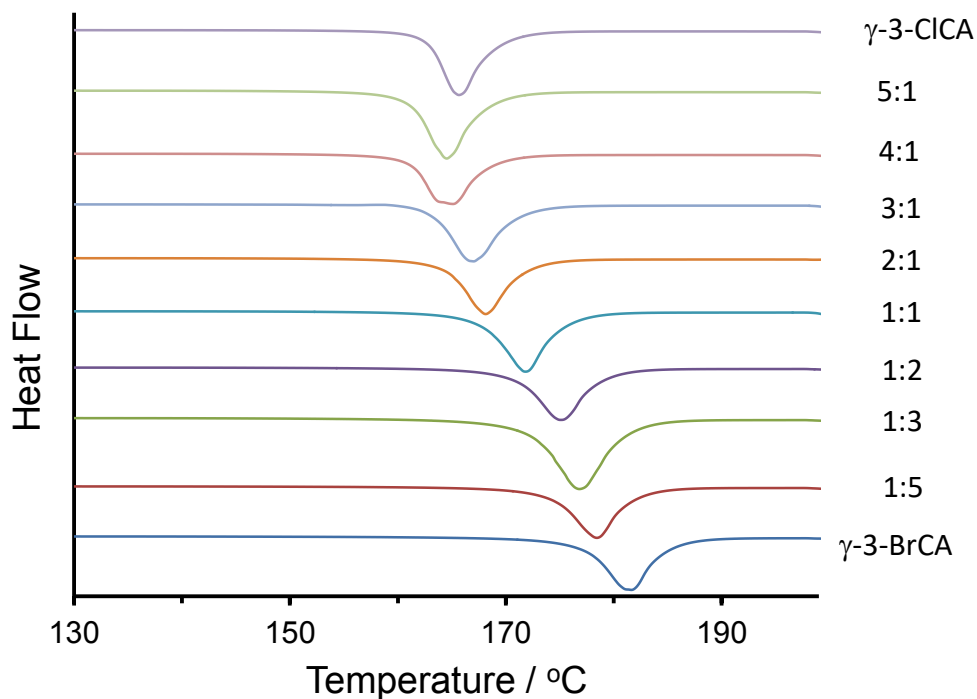
Figure 4.4. *Plots for different mixtures of γ-3-ClCA:γ-3-BrCA, γ-3-ClCA and γ-3-BrCA, showing the second DSC cycle.*
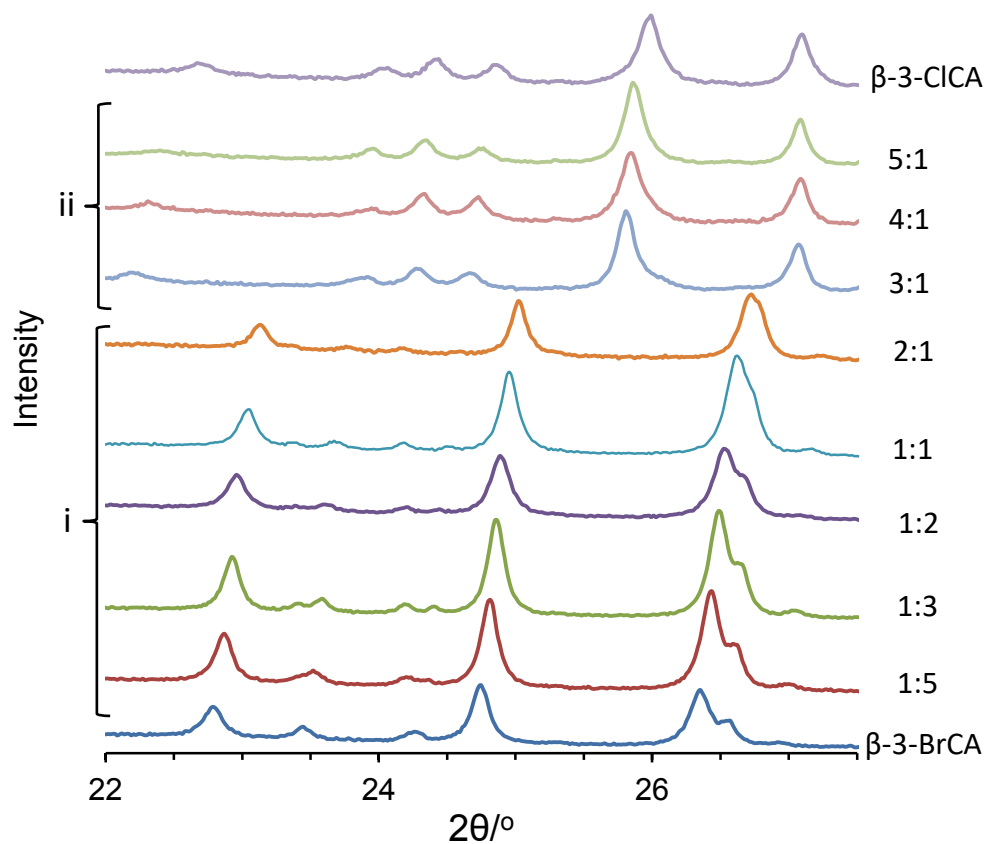
Figure 4.5. *The PXRD data for the recovered samples of different mixtures of γ-3-ClCA:γ-3-BrCA, pure γ-3-ClCA and γ-3-BrCA after the second DSC cycle illustrating two structures types similar to (i) β-3-ClCA and (ii) β-3-BrCA.*
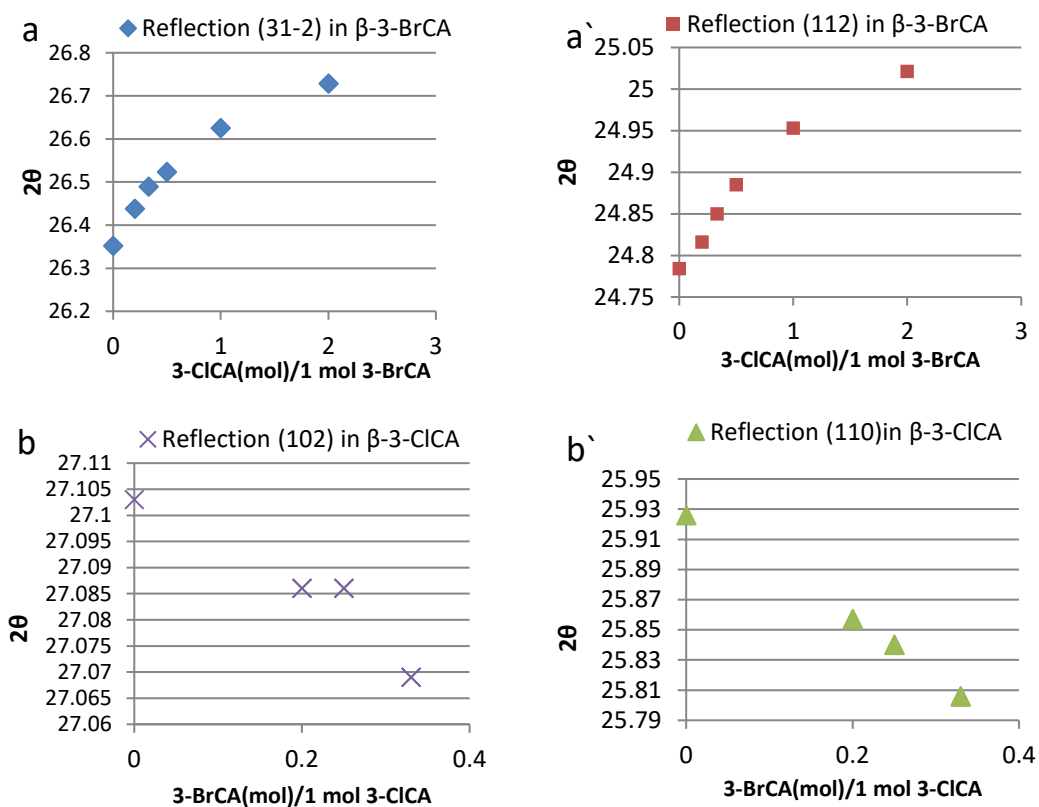
Figure 4.6. *The 2θ shift in some selected peaks of PXRD patterns, (a) and (a`) in the structures similar to β-3-BrCA, (b) and (b`) in the structures similar to β-3-ClCA.*

4.3.1.b. Thermal study of physical mixtures of *γ*-3-ClCA and *γ*-3-BrCA below the melting point and their cocrystallization from sublimation

As mentioned in Chapter 3, irreversible transformation of both acids (*γ*-3-ClCA and *γ*-3-BrCA) is observed when samples are heated below the melting point. The aim here was to investigate the effect of the phases on each other at high temperature. To explore this, DSC thermal analysis and PXRD were used for the phase characterization.

Thermal study of physical mixtures of *γ*-3-ClCA and *γ*-3-BrCA (cocrystallization below the m.p.)

Physical mixtures of *γ*-3-ClCA:*γ*-3-BrCA in ratios of 1:2 (a), 1:1 (b) and 2:1(c) were heated above the transition temperature but below the melting point and the products analysed. PXRD patterns recorded before the DSC experiment, indicated the existence of both components as separate phases. On heating the mixtures from 40 °C to 155 °C, one irreversible endothermic event was observed for each sample.

As seen in Figure 4.7, PXRD showed that both samples (a) and (b) produced β-3-BrCA and the solid solution of β-3-BrCA/3-ClCA. Similar results was shown for the product from sample (c), which comprised β-3-BrCA and the solid solution of β-3-ClCA. However, traces of β-3-ClCA were also observed for sample (c) (the peak indicated by the arrow in Figure 4.7 is corresponding to the β-3-ClCA structure). It is clearly noticed that a significant amount of the solid solution of β-3-BrCA/3-ClCA was produced from these samples and, a consistent shift of the reflections around 24.7 and 26.4° reflected the composition of solid solutions.

The pure β-3-BrCA and the solid solution were distinguished by the shift in the PXRD peak positions on formation of the solid solution. As expected from the DSC cycle, the result here indicated that, below the melting point for the physical mixture, the endothermic event observed in the DSC scans is due to phase transformation from γ to β with cocrystallization, probably resulting from a process involving sublimation (this will be discussed later).
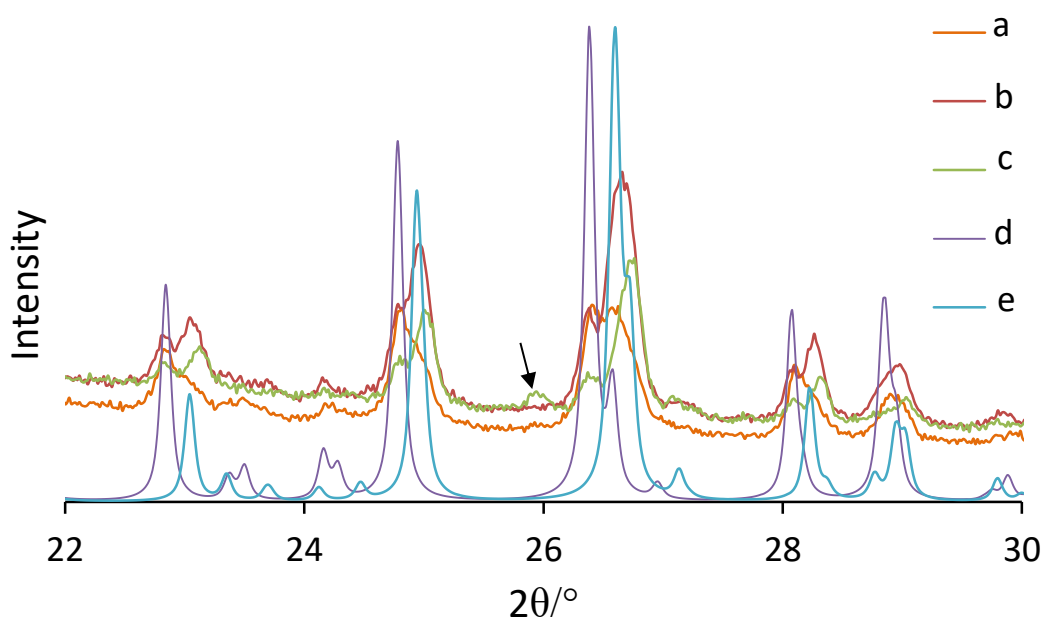
Figure 4.7. *Plot showing the overlay of PXRD patterns for the recovered samples after a DSC cycle of heating above the transformation temperature and below m.p then cooling to room temperature for γ-3-ClCA:γ-3-BrCA (a)1:2, (b)1:1 and (c)2:1. (d) and (e) are the calculated PXRD patterns of β-3-BrCA and a 1:1 β-3-BrCA/3-ClCA solid solution, respectively.*

Cocrystallization from sublimation

Both acids sublimed at high temperatures and two experiments were carried out to explore exploitation of this property for crystallization. Firstly, using the method in the experimental section, crystallization of pure 3-BrCA by sublimation produced β-3-BrCA crystals, while a mixture of γ and β forms were produced for 3-ClCA using the same method. Cocrystallization by sublimation of a 1:1 ratio of 3-BrCA:3-ClCA produced only the β-3-BrCA/3-ClCA solid solution, as shown by PXRD and confirmed by SC-XRD structure determination (discussed in Section 4.3.1.c).

Secondly, pure γ-3-ClCA and γ-3-BrCA, as well as, a 1:1 mixture were heated using DSC below the transformation temperature ~135°C and then PXRD was run on the recovered samples. For 3-ClCA, only the γ phase was detected (i.e. no change). Both γ and β phases were observed for 3-BrCA. Mixtures of phases including β-3-BrCA/3-ClCA solid solution, β-3-BrCA, γ-3-ClCA, and traces of γ-3-BrCA were observed for the 1:1 mixture. These results indicate that sublimation may play a major role in the formation of the solid solution prior to melting, particularly at higher temperatures.

4.3.1.c. Cocrystallization from solution and vapour: structural determination

For a further investigation of the structures and phase transformation (discussed in Sections 4.3.1.a and 4.3.1.b), cocrystallization of the acids from solution and vapour was carried out.

γ-3-ClCA/3-BrCA

The γ phase was obtained by crystallization using a 1:1 molar ratio of 3-ClCA:3-BrCA with MeOH as a solvent. The crystal structures of γ-3-ClCA and γ-3-BrCA are identical and so, unsurprisingly, the PXRD pattern of the cocrystal was similar but with a shift in the peak positions, indicative of a structure intermediate between the two pure materials. SC-XRD data were recorded in order to confirm the composition. The structure is monoclinic, P2₁/a and is identical to those of γ-3-ClCA and γ-3-BrCA. Crystallographic data are shown in Table 4.1 and the structure is depicted in Figure 4.8a. The asymmetric unit, as shown in Figure 4.8b, consists of one planar molecule of 3-halo-cinnamic acid, with a disordered *meta*-position of the benzene ring with refined Cl/Br occupancies of 0.556(4)/0.444(4). X-ray photoelectron spectroscopy (XPS) showed the presence of

both Cl and Br in a ratio (3.37% and 2.78%), in good agreement with the refined occupancies.
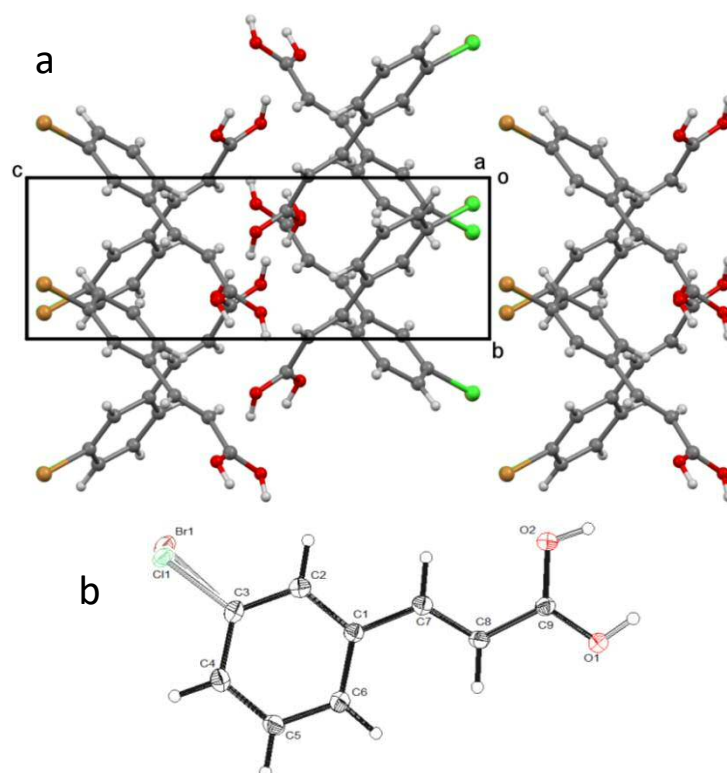
Figure 4.8. *(a) The crystal structure of γ-3-ClCA/3-BrCA. (b) The asymmetric unit in the γ-3-ClCA:3-BrCA solid solution, showing the disorder*.

γ₂-3-ClCA/3-BrCA

Crystallization of a 1:1 molar ratio of 3-ClCA:3-BrCA from AC gave a mixture of plate crystals of the γ phase, contaminated with needle crystals of a second phase, designated as γ₂. Similar to γ₂-3-BrCA (discussed in Chapter 3) the crystal structure of the γ₂-3-ClCA:3-BrCA solid solution is monoclinic, with the space group P2₁/n and one planar 3-halo-cinnamic acid molecule present in the asymmetric unit (Figure 4.9a). The substituent in the *meta*-position of the ring is disordered, with refined Cl/Br occupancies of 0.61(1)/0.39(1). Crystallographic data are shown in Table 4.1. The molecules exist as hydrogen bonded centrosymmetric pairs. The pairs are stacked parallel to the a-axis, with neighbouring screw-axis related stacks forming a herringbone structure. Molecular orientation does not change perpendicular to the stacking (i.e. parallel to the c-axis, see Figure 4.9b). In contrast to γ₂-3-ClCA:3-BrCA, neighbouring molecules in γ-3-ClCA:3-BrCA flip by *ca.* 90º on moving along the a-axis. It is noted that the Cl:Br ratios for the crystals examined were *ca.* 3:2 in both cases although the starting solutions were 1:1 mixtures.
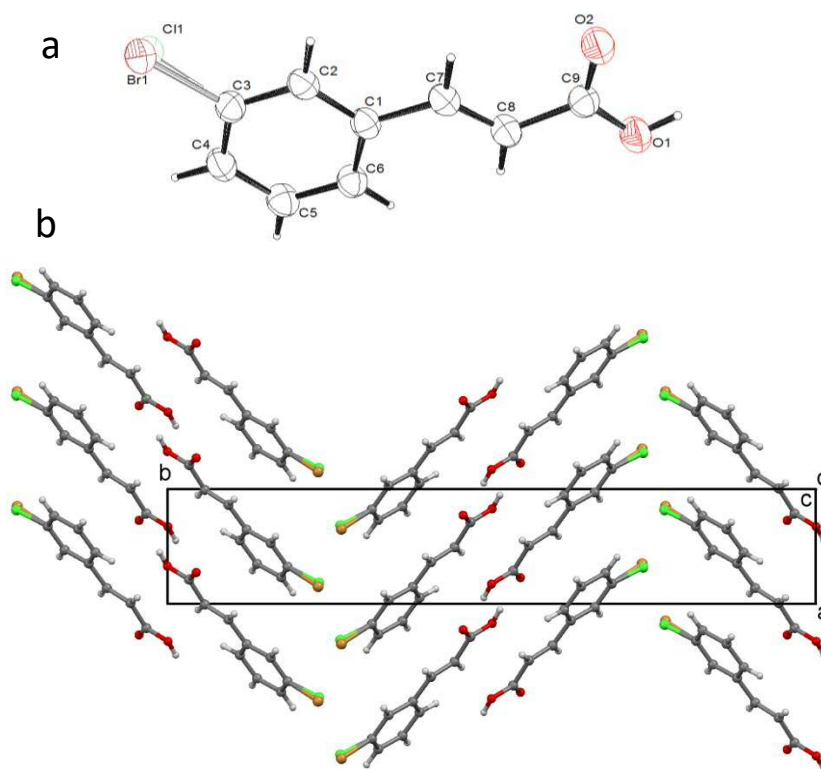
Figure 4.9. *(a) The asymmetric unit in the γ₂-3-ClCA/3-BrCA solid solution showing the disorder. (b) The crystal structure of γ₂-3-ClCA/3-BrCA solid solution.*

β-3-ClCA/3-BrCA

As mention previously, pure 3-ClCA gave the *β* form from GAA (with a trace amount of the *γ* phase) and *β*-3-BrCA was also obtained from the same solvent. Crystallization of the cocrystal was attempted using an equimolar solution of 3-ClCA and 3-BrCA in GAA. The PXRD pattern for the product was identical to that obtained from crystallization of a 1:1 melt.

The crystal structure of *β*-3-ClCA/3-BrCA (Figure 4.10) is monoclinic (C2/c space group), with a unit cell similar to *β*-3-BrCA rather than to *β*-3-ClCA. The similarity to *β*-3-BrCA has been shown earlier (Section 4.3.1.a) by comparison of PXRD patterns. The asymmetric unit is one molecule of 3-halo-cinnamic acid with a disordered Br and Cl location in the *meta*-position. The refined occupancies showed approximately equal amounts of Cl and Br (0.510(4) and 0.490(4), respectively), in agreement with XPS analysis (3.78% Br and 3.52% Cl). The molecules form the familiar carboxylic acid hydrogen bonded dimer. A significant feature is the arrangement of the adjacent C=C double bonds, suggesting the photodimerization capability (further discussed in Chapter 6). Crystallographic data are summarized in Table 4.1.

According to the discussion in Chapter 1, the crystals of (γ, γ_2 and β)-3-ClCA/3-BrCA solid solutions are an example of semi-polymorph materials.
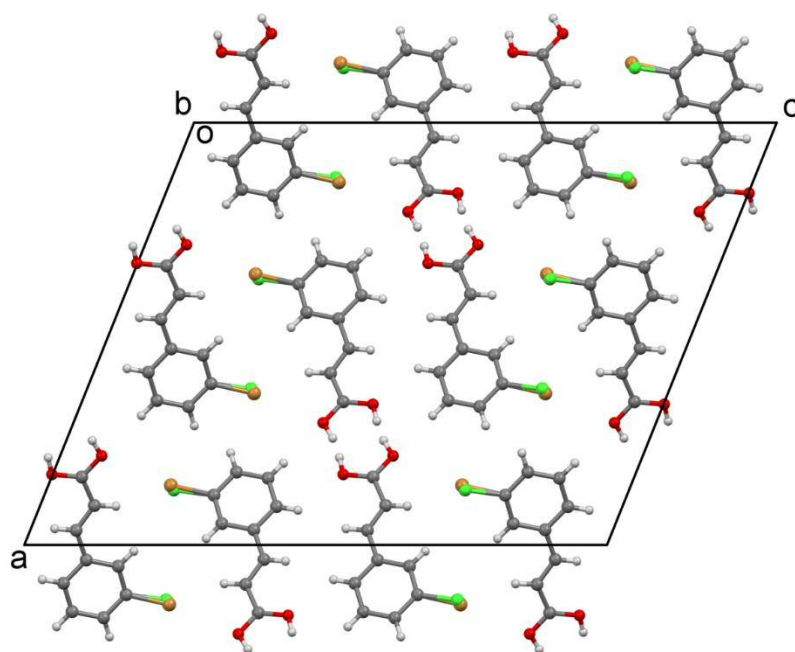
Figure 4.10. *The crystal structure of β-3-ClCA/3-BrCA solid solution.*

Table 4.1. *Crystallographic data for the crystal structure determination of the 3-ClCA/3-BrCA solid solutions.*

	γ-3-ClCA/3-BrCA	γ_2-3-ClCA/3-BrCA	β-3-ClCA/3-BrCA
Formula	$C_9 H_7 Br_{0.44} Cl_{0.56} O_2$	$C_9H_7Br_{0.39}Cl_{0.61}O_2$	$C_9 H_7 Br_{0.49} Cl_{0.51} O_2$
Formula weight	202.38	199.93	204.38
Temperature, (K)	150(2)	293(2)	150(2)
λ , Å	0.71073	1.54184	0.71073
Crystal system	Monoclinic	Monoclinic	Monoclinic
Space group	$P2_1/a$	$P2_1/n$	$C2/c$
a, (Å)	12.2786(9)	4.9671(5)	19.0797(10)
b, (Å)	4.9068(2)	28.125(3)	3.86490(10)
c, (Å)	14.1487(10)	6.1401(7)	24.4818(12)
α, (°)	90	90	90
β, (°)	95.242(2)	91.259(9)	111.944(2)
γ, (°)	90	90	90
Volume, (Å³)	848.87(9)	857.56(17)	1674.52(13)
Z	4	4	8
Density (calculated), (Mg/m³)	1.584	1.549	1.621
Absorption coefficient, (mm⁻¹)	2.356	4.585	2.589
F(000)	408	404	823
Crystal size, (mm³)	0.30 x 0.25 x 0.07	0.46 x 0.07 x 0.04	0.39 × 0.2 × 0.04
Reflections collected	3358	2909	4412
Independent reflections	1927	1649	1877
R(int)	0.0348	0.0372	0.0309
Goodness-of-fit on F^2	1.053	1.086	1.073
Final R_1 indices [I>2sigma(I)]	0.0407	0.0678	0.0285
Final wR_2	0.0818	0.1856	0.0648
R_1 indices (all data)	0.0617	0.0769	0.0334
wR_2 (all data)	0.0988	0.1924	0.0678

Other ratios preparation of 3-ClCA:3-BrCA

Further investigation of cocrystallization with initial ratios of 1:2 (batch a) and 2:1 (batch b) of 3-ClCA:3-BrCA was carried out. Single crystal structure determination of two crystals (a$_1$, a$_2$) from batch (a) and two crystals (b$_1$, b$_2$) from batch (b) was performed. All crystals have a similar structure to β-3-ClCA/3-BrCA solid solution. In these structures, Cl and Br are disordered, with 0.378(6):0.622(6) in crystal a$_1$ and 0.397(5):0.603(5) in Crystal a$_2$. In contrast, the Cl:Br disorder in b$_1$ and b$_2$ crystals were 0.720(3):0.280(3) and 0.781(3):0.219(3), respectively. Crystallographic data of all crystals are summarized in Table 4.2.

The calculated PXRD patterns of a$_1$, a$_2$, b$_1$, and b$_2$ crystals are similar and, interestingly, show the peak shifts consistent with the amount of Cl and Br present in the crystal structure (see Figure 4.11). Unfortunately, cocrystallization with an initial ratio of 4:1 and 1:4 of 3-ClCA:3-BrCA in GAA gave a mixture of γ and β solid solutions. Therefore, investigation of SC-XRD did not proceed further.
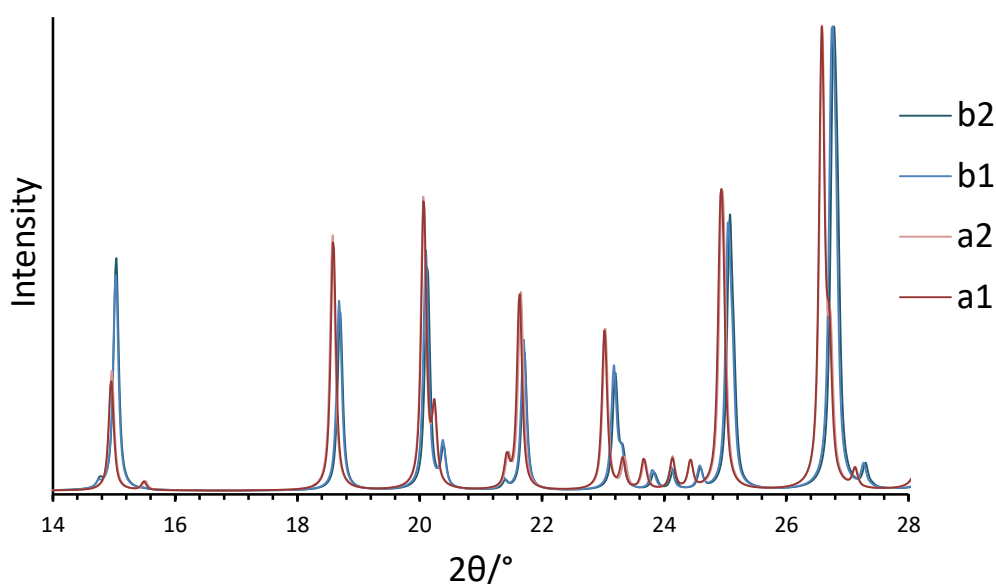
Figure 4.11. *The plot of the overlay of calculated PXRD patterns of the samples a$_1$, a$_2$, b$_1$ and b$_2$, illustrating the shifts in the peaks, consistent with the 3-ClCA:3-BrCA ratio in the crystal.*

Table 4.2. Crystallographic data for the crystal structure determination of the β-3-ClCA/3-BrCA solid solutions of different ratios.

	β-3-ClCA/3-BrCA (Cl:Br)(1:2) a_1	β-3-ClCA/3-BrCA (Cl:Br)(1:2) a_2	β-3-ClCA/3-BrCA (Cl:Br)(2:1) b_1	β-3-ClCA/3-BrCA (Cl:Br)(2:1) b_2
Formula	$C_9 H_7 Br_{0.62} Cl_{0.38} O_2$	$C_9 H_7 Br_{0.60} Cl_{0.40} O_2$	$C_9 H_7 Br_{0.28} Cl_{0.72} O_2$	$C_9 H_7 Br_{0.22} Cl_{0.78} O_2$
Formula weight	210.22	209.27	195.00	192.32
Temperature, (K)	293(2)	293(2)	293(2)	293(2)
λ, Å	1.54184	1.54184	1.54184	1.54184
Crystal system	Monoclinic	Monoclinic	Monoclinic	Monoclinic
Space group	C2/c	C2/c	C2/c	C2/c
a, (Å)	19.0798(8)	19.0922(8)	18.9851(9)	18.9679(5)
b, (Å)	3.95630(10)	3.95390(10)	3.9300(2)	3.92600(10)
c, (Å)	24.8852(11)	24.6441(10)	24.6092(11)	24.5946(8)
α, (°)	90	90	90	90
β, (°)	113.236(5)	112.089(5)	111.583(5)	111.631(4)
γ, (°)	90	90	90	90
Volume, (Å³)	1726.10(11)	1723.80(11)	1707.39(14)	1702.53(8)
Z	8	8	8	8
Density (calculated), (Mg/m³)	1.618	1.613	1.517	1.501
Absorption coefficient, (mm⁻¹)	5.152	5.104	4.316	4.172
F(000)	841	838	792	784
Crystal size, (mm³)	0.06 0.2 0.28	0.06 0.12 0.47	0.20 0.26 0.33	0.13 0.38 0.65
Reflections collected	4739	5224	2900	2718
Independent reflections	1652	1712	1660	1652
R(int)	0.0227	0.0254	0.0145	0.0106
Goodness-of-fit on F^2	1.085	1.087	1.128	1.121
Final R_1 indices [I>2sigma(I)]	0.0364	0.0348	0.0349	0.0325
Final wR_2	0.1021	0.0984	0.0946	0.0957
R_1 indices (all data)	0.0384	0.0392	0.0393	0.0337
wR_2 (all data)	0.1042	0.1012	0.0976	0.0969

Crystallization from sublimation

As discussed earlier in Section 4.3.1.b, PXRD showed the formation of β solid solutions of 3-ClCA/3-BrCA from vapour. In order to confirm the structure, SC-XRD was carried out on a single crystal that crystallized from the vapour of the 1:1 physical mixture of γ-3-ClCA:γ-3-BrCA. The crystal structure showed that a 3-ClCA/3-BrCA solid solution of the β-3-BrCA structure had been formed with disordered Br:Cl in the ratio *ca.* 0.43(1):0.57(1). The structure was determined with a R factor of 4%. Crystallographic data are shown in Table 4.3.

Table 4.3. Crystallographic data for the crystal structure determination of the β-3-ClCA/3-BrCA solid solution crystallized from vapour.

Formula	$C_9 H_7 Br_{0.43} Cl_{0.57} O_2$	Z	8
Formula weight	201.49	Density (calculated), (Mg/m³)	1.563
Temperature, (K)	293(2)	Absorption coefficient, (mm⁻¹)	2.248
λ, Å	0.71073	F(000)	813
Crystal system	Monoclinic	Crystal size, (mm³)	0.03 0.05 0.34
Space group	C2/c	Reflections collected	4055
a, (Å)	19.017(5)	Independent reflections	2038
b, (Å)	3.9408(7)	R(int)	0.0327
c, (Å)	24.915(6)	Goodness-of-fit on F^2	1.024
α, (°)	90	Final R_1 indices [I>2sigma(I)]	0.0446
β, (°)	113.45(3)	Final wR_2	0.0764
γ, (°)	90	R_1 indices (all data)	0.1048
Volume, (Å³)	1713.0(6)	wR_2 (all data)	0.0936

4.3.1.d. Characterization of *β* solid solutions using solid-state ^{13}C NMR

Solid-state NMR[29] (SS-NMR) is a powerful technique for the study of the chemical environment of a target nucleus in the crystal. Thus, full effects of anisotropic or orientation-dependent interactions are observed in the spectrum. In contrast, in solution NMR only an average of the anisotropic effects is observed, due to rapid random movements. In this study, solid-state ^{13}C NMR was firstly carried out to investigate the differences between the two polymorphs, *γ*-3-BrCA and *β*-3-BrCA, as it is a powerful complementary tool in the study of polymorphs[30,31]. Secondly, an attempt was made to differentiate between *β*-3-BrCA and the *β*-3-ClCA/3-BrCA solid solution, since they have similar crystal structures.

[13]C CPMAS spectra of *γ*-3-BrCA, *β*-3-BrCA and *β*-3-ClCA/3-BrCA are illustrated in Figure 4.12, and CASTEP[17,18] calculations were used for assigning the resonance peaks of carbons atoms (see Table 4.4). Additionally, due to *β*-3-BrCA and *β*-3-ClCA adopting different crystal structures, the structure of *β*-3-ClCA that is identical to *β*-3-BrCA[19] was first theoretically generated and then the theoretical SS-NMR resonance peaks of carbon atoms were calculated.

The three spectra, as seen in Figure 4.12, are quite similar. The spectra of *γ*-3-BrCA and *β*-3-BrCA displayed only small differences between them. The resonance peaks associated with the carbons of the benzene ring seem to show the largest differences, in particular for C(2) and C(6). This is because, in *γ* and *β* 3-BrCA the molecules have different conformations (see Figure 4.13). Accordingly, the resonance peak of C(2) is deshielded (shifted to higher δ(ppm)) in the *γ* structure relative to the *β* structure (136.535 and 127.4 ppm, respectively). In contrast, C(6) in the *γ* structure is more shielded (lower δ(ppm)) than it is for the *β* structure (124.786 and 130.709 ppm, respectively). In other words, the δ(ppm) values of the resonance peaks of C(2) and C(6) in the *γ* structure are swapped with the values for the *β* structure. This effect is consistent with the environment of C(2) and C(6) relative to the double bond. This result suggests that the double bond has a greater effect on the carbons C(2) and C(6) than the C(3) (the carbon that is bonded to bromine). These differences in the spectra are in agreement with the different molecular conformation in the crystal structures of the *γ* and *β* polymorphs.

In contrast, very similar spectra are observed in the spectra of β-3-BrCA and β-3-ClCA/3-BrCA, except for the peak at 137.954 ppm in the β-3-ClCA/3-BrCA spectrum which is not observed for β-3-BrCA. This peak was assigned to C(3), the carbon bonded to the Br or Cl atom. In the case of β-3-BrCA, the disappearance of the peak of the carbon attached to the Br atom, is expected due to the quadrupole coupling constant associated with the Br[79] and Br[81],[32–35] which leads to broadening for the atom that is directly bonded to it, making it difficult to detect. This effect is less for Cl than Br,[35] therefore, the resonance peak of C(3) in the solid solution, where both Br and Cl exist in the structure, is clearly observed (Figure 4.12c labelled *). The peak shows good agreement with the calculated data for C(3) for both β-3-BrCA and β-3-ClCA, as illustrated in Table 4.4 (highlighted in pink). Note that the resonance peak of C(2) in the solid solution material is more shielded (lower δ) than in β-3-BrCA (Figure 4.12c labelled *) and is consistent with the theoretical calculation in both β-3-BrCA and β-3-ClCA.
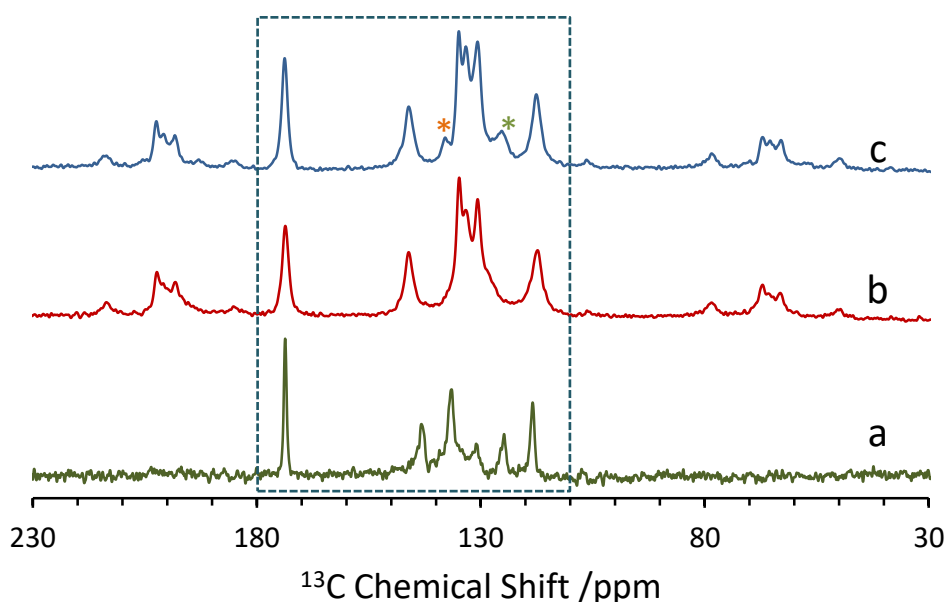
Figure 4.12. *Solid-state* ^{13}C *NMR spectra of (a) γ-3-BrCA, (b) β-3-BrCA and (c) β-3-ClCA/3-BrCA solid solution. The stars mark the additional peaks that are present in solid solution material compared to β-3-BrCA. Spinning side bands are outside the box.*
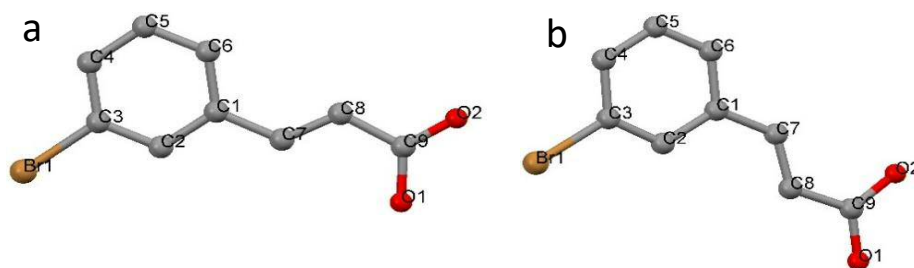
Figure 4.13. *Molecules of (a) γ and (b) β phase of 3-BrCA, showing different conformations.*

Table 4.4. *Resonance assignment for γ-3-BrCA, β-3-BrCA and β-3-ClCA/3-BrCA together with the values obtained from the theoretical calculations.(ND: not detected).*

	δ [ppm]					
	Theoretical			Experimental		
Assignment	γ-3-BrCA	β-3-BrCA	β-3-ClCA	γ-3-BrCA	β-3-BrCA	β-3-ClCA/3-BrCA
C_1	137.0644	134.9346	134.8883	136.535	133.353	133.304
C_2	137.157	128.52668	126.16538	136.535	127.4	125.324
C_3	143.2686	143.70382	140.12946	ND	ND	137.954
C_4	136.194	136.231	132.86036	136.535	134.821	134.870
C_5	132.277	134.91608	135.17536	131.003	133.353	133.304
C_6	126.683	133.61968	133.43448	124. 786	130.709	130.709
C_7	146.0466	149.07462	148.6857	143.241	146.080	146.080
C_8	120.0167	117.32208	117.97954	118.422	117.269	117.590
C_9	173.271	173.61362	173.8266	173.690	173.641	173.788

4.3.1.e. Transformation of γ-3-ClCA/3-BrCA solid solution to β solid solution

Phase transformation among organic cocrystalline materials and inorganic solid solution alloys has been reported in the literature.[36–39] Additionally, the phase transformation of the solid solution has also been reported[40] but, to our knowledge, not with regard to solid solution of cinnamic acid derivatives. The high temperature behaviour of γ-3-ClCA/3-BrCA was investigated in the knowledge that the pure acids, γ-3-ClCA and γ-3-BrCA,[13] underwent phase transformation at high temperatures (as discussed previously in Chapter 3) to give β forms with different structures. A DSC thermogram for a sample of γ-3-ClCA/3-BrCA is shown in Figure 4.14a. In a similar manner to the pure acids, one phase transition endotherm and a symmetrical endothermic melting event are observed in the heating cycle, consistent with the behaviour of one entity (i.e. a solid solution). A phase transition endotherm occurred at 140 ºC, as shown in Figure 4.14a, due to irreversible conversion to β-3-ClCA/3-BrCA (Figure 4.14b). That was confirmed by PXRD on the sample recovered after the DSC experiment and prior to the melting event, which showed a similar PXRD pattern to β-3-BrCA (see Figure 4.15). Thermal analysis (DSC) of β-3-ClCA/3-BrCA solid solution showed one symmetrical endothermic event in the heating cycle consistent with the melting of a solid solution.

DSC and PXRD results support the proposition that γ-3-ClCA/3-BrCA and β-3-ClCA/3-BrCA are solid solutions.

Unfortunately, γ₂-3-ClCA/3-BrCA was obtained only as a minor component in a mixture and so meaningful results of its thermal behaviour could not be obtained.
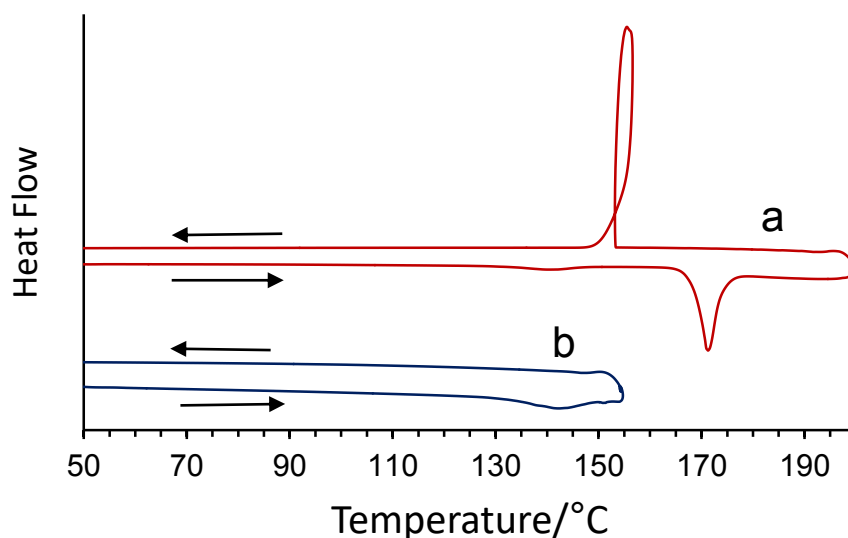
Figure 4.14. *Thermal analysis of γ-3-ClCA/3-BrCA solid solution. (a) Two endothermic events on heating showing the transformation and melting. (b) Showing the irreversible transformation event.*
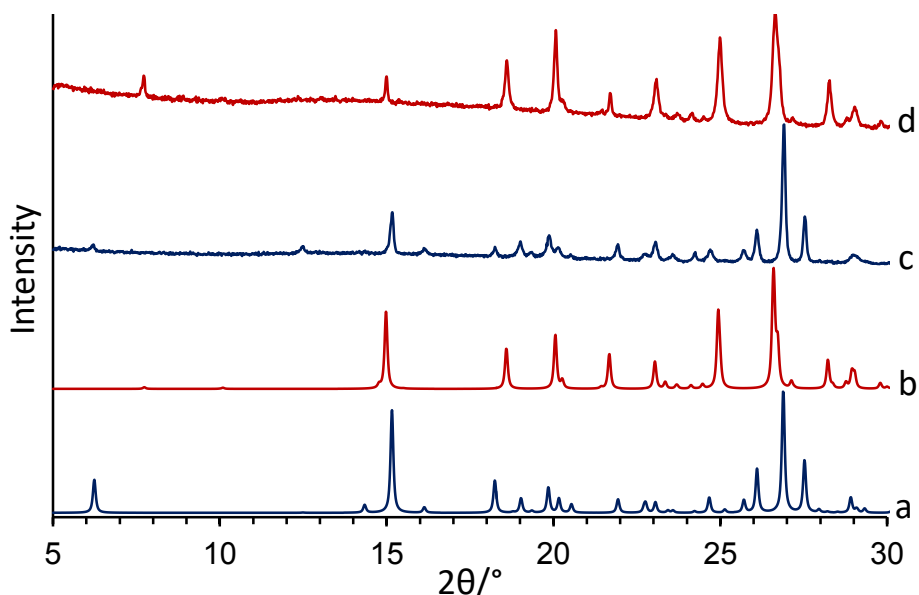
Figure 4.15. *The calculated PXRD pattern from the crystal structures of (a) γ-3-ClCA/3-BrCA (b) β-3-ClCA/3-BrCA, and the experimental PXRD pattern of (c) γ-3-ClCA/3-BrCA and (d) the result after the DSC cycle of heating the γ form of solid solution before the m.p showing the transformation to β-3-ClCA/3-BrCA.*

4.3.1.f. Single crystal to single crystal (SC-SC) phase transformation of *γ*-3-ClCA/3-BrCA solid solution to *β* solid solution

The results discussed in the previous section (4.3.1.e) indicate the occurrence of an irreversible transformation from *γ*-3-ClCA/3-BrCA to *β*-3-ClCA/3-BrCA solid solution. In addition to that, both *γ*-3-BrCA and *γ*-3-ClCA showed a SC-SC transformation (discussed in Chapter 3). This suggests that the transformation of *γ*-3-ClCA/3-BrCA solid solution might be a SC-SC transition as well. Therefore, to probe this, the study was extended to explore the behaviour of the single crystal. The structure of *γ*-3-ClCA/3-BrCA solid solution was first examined using SC-XRD. The crystal structure determination shows that Cl and Br are disordered on the *meta*-position of the benzene ring with occupancies of 0.573(5):0.427(5) and with the final R-factor of 4%. The same crystal was then placed on a glass slide and heated on a hotplate to about 145 ºC for *ca.* 1.5 min. The same crystal was mounted on the diffractometer and the crystal structure redetermined, showing that the crystal had undergone phase transition to produce the *β*-3-ClCA/3-BrCA solid solution. In the crystal structure both Cl and Br are disordered by 0.504(7):0.496(7), and surprisingly, the structure was refined to R-factor of 5%, a clear indication of SC-SC phase transition in this solid solution system. It is worth noting that, although the crystal had suffered some sublimation, the phase transition occurred retaining crystal integrity and without losing crystallinity. Figure 4.16 shows the crystal before and after heating and a summary of the crystallographic data for the crystal before and after transformation is shown in Table 4.5.
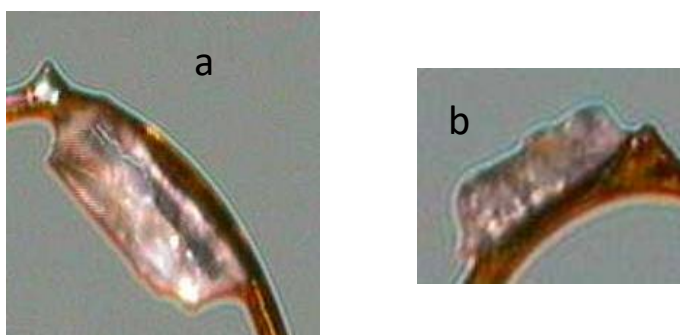
Figure 4.16. *Photographs of the single crystal γ-3-ClCA/3-BrCAsolid solution (a) before and (b) after heating.*

Table 4.5. *Crystallographic data for the crystal structure determination of the 3-ClCA/3-BrCA solid solution before and after SC-SC transformation.*

	γ-3-ClCA/3-BrCA (Before transformation)	β-3-ClCA/3-BrCA (After transformation)
Formula	$C_9 H_7 Br_{0.43} Cl_{0.57} O_2$	$C_9 H_7 Br_{0.50} Cl_{0.50} O_2$
Formula weight	201.49	204.56
Temperature, (K)	293(2)	293(2)
λ, Å	1.54184	1.54184
Crystal system	Monoclinic	Monoclinic
Space group	$P2_1/a$	$C2/c$
a, (Å)	12.3864(7)	19.053(5)
b, (Å)	4.9353(3)	3.9451(7)
c, (Å)	14.2105(8)	24.660(5)
α, (°)	90	90
β, (°)	94.822(5)	111.81(3)
γ, (°)	90	90
Volume, (Å^3)	865.62(9)	1720.9(6)
Z	4	8
Density (calculated), (Mg/m^3)	1.546	1.579
Absorption coefficient, (mm^{-1})	4.632	4.837
F(000)	407	823
Crystal size, (mm^3)	0.07 0.08 0.26	0.04 0.07 0.16
Reflections collected	2865	4998
Independent reflections	1670	1706
R(int)	0.0280	0.0512
Goodness-of-fit on F^2	1.064	1.060
Final R_1 indices [I>2sigma(I)]	0.0430	0.0516
Final wR_2	0.1112	0.1373
R_1 indices (all data)	0.0526	0.0785
wR_2 (all data)	0.1252	0.1576

4.3.2. Investigation of cocrystallization in a binary system of 3-FCA and 3-BrCA

The results from the previous section (4.3.1) showed the ability of forming solid solution material that comprises 3-BrCA and 3-ClCA, and that was expected due to the relatively similar sizes of Br and Cl atoms (26.0Å^3 and 19.9Å^3, respectively)[41]. However, exploring the ability of forming cocrystalline materials involving 3-FCA and 3-BrCA is more challenging, as F and Br atoms have significantly different volumes (9.6Å^3 and 26.0Å^3)[41] and, additionally, none of the known structures of 3-FCA and 3-BrCA are isostructural. This is in line with the observation by Kitaigorodsky[28], that the formation of mixed crystals (in the form of solid solution) is based on the similarity of the shape and the size of the mixed materials, with the consideration of electronic and structural similarity for a total miscibility. The question, thus, is whether cocrystallization of 3-FCA and 3-BrCA forms a stoichiometric cocrystal, as seen in the case of 3,4-dimethoxycinnamic acid/2,4-dinitrocinnamic acid[42], rather than forming a solid solution, as observed previously in the case of 3-ClCA/3-BrCA. Thus, investigation of this behaviour will be addressed in detailed.

4.3.2.a. Thermal investigation of binary systems of 3-FCA and 3-BrCA

Initially, physical mixtures that comprised 2:1, 1:1, 1:2, 1:4, 1:6, 1:8 and 1:9 (i, ii, iii, iv, v, vi and vii) molar ratios of β_1-3-FCA:γ-3-BrCA, were prepared and subjected to a DSC study followed by PXRD analysis. The study involved heating and cooling the samples at 20 °C/min from 40 to 190 °C then back to 40 °C (assigned as first DSC cycle), followed by another heating and cooling cycle (second cycle). The sample was then recovered and analysed using PXRD. Results from the first heating cycle (temperature range 100-190 °C) of DSC scans for the all physical mixtures along with β_1-3-FCA and γ-3-BrCA are illustrated in Figure 4.17.

The data in Figure 4.17 i and ii shows that, in the case of 2:1 and 1:1 physical mixtures, a broad endothermic event is observed at around 145 °C and 147 °C, respectively and this is expected to correspond to the melting of 3-FCA (as the pure 3-FCA melts at 167 °C). The shift in melting temperature is expected due to the existence of the acid with the 3-BrCA as a mixture (discussed in Section 4.3.1.a). In all other cases a small endothermic event was clearly observed at around 148-150°C, followed by small exothermic event at around 151-153 °C and then another endothermic event at around 156-180°C. The first endothermic event is believed to correspond to the melting of 3-FCA (it is worth noting that this peak is expected to overlap with the transformation peak of 3-BrCA from γ to β structure). Consequently, 3-BrCA dissolves in molten 3-FCA and then cocrystallization occurs, with an associated exotherm. This event is followed by a broad endothermic event corresponding to the melting of the solid solutions.
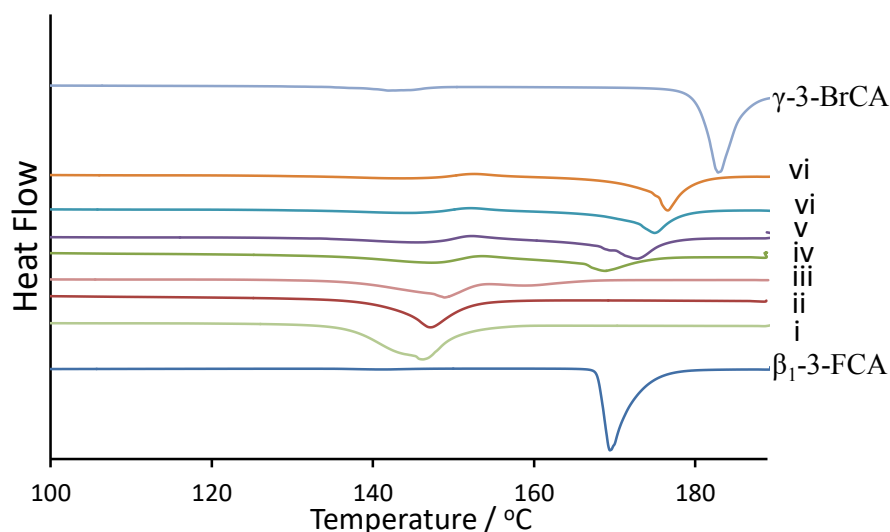
Figure 4.17. *Plots for different mixtures of β_1-3-FCA and γ-3-BrCA along with pure β_1-3-FCA and γ-3-BrCA, showing the first heating DSC cycle.*

Investigation of the exothermal events in the heating cycle

To investigate this behaviour further, physical mixtures of 1:4, 1:6, 1:8 and 1:9 of β_1-3-FCA:γ-3-BrCA (iv`, v`, vi`, vii`, respectively) were subjected to the same DSC cycle. However, the samples were heated only until 160 °C, just after the exothermic peak observed earlier (Figure 4.18). The samples were cooled and then recovered and characterized using PXRD. The heating DSC cycle for all samples showed the endothermic melting of the 3-FCA. This was then followed by an exothermic event (marked a) due to the crystallization of molten material. Surprisingly, another exothermic event was observed on cooling the sample (labelled b), shown in Figure 4.18. This exothermic peak is probably due to either; (i) cocrystallization of the materials that correspond to the structure similar to β_1-3-FCA (note that the area under the peaks increases as the amount of 3-FCA in the mixture increases) or (ii) the phase transformation of the crystalline materials from one to another. However, the discussion below will show that the former possibility (i) is the more likely option to consider.

PXRD of the samples (iv`, v`, vi`, vii`) after DSC shows a similar pattern to β-3-BrCA with shifts in the peaks, suggesting the formation of 3-BrCA/3-FCA solid solutions with a structure similar to β-3-BrCA (see Figure 4.19). However, peaks associated with the structure that is similar to β_1-3-FCA were not observed in the PXRD pattern (this will be discussed later in this section).
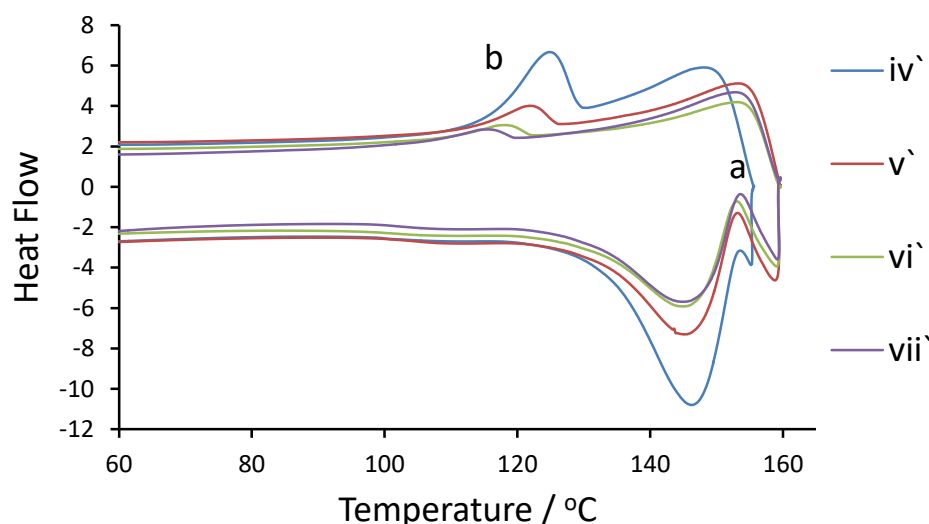
Figure 4.18. Plots for different mixtures of β_1-3-FCA and γ-3-BrCA showing the DSC cycle with heating to 160 °C and then cooling to room temperature, (a) marks the crystallization events observed in the heating cycle.
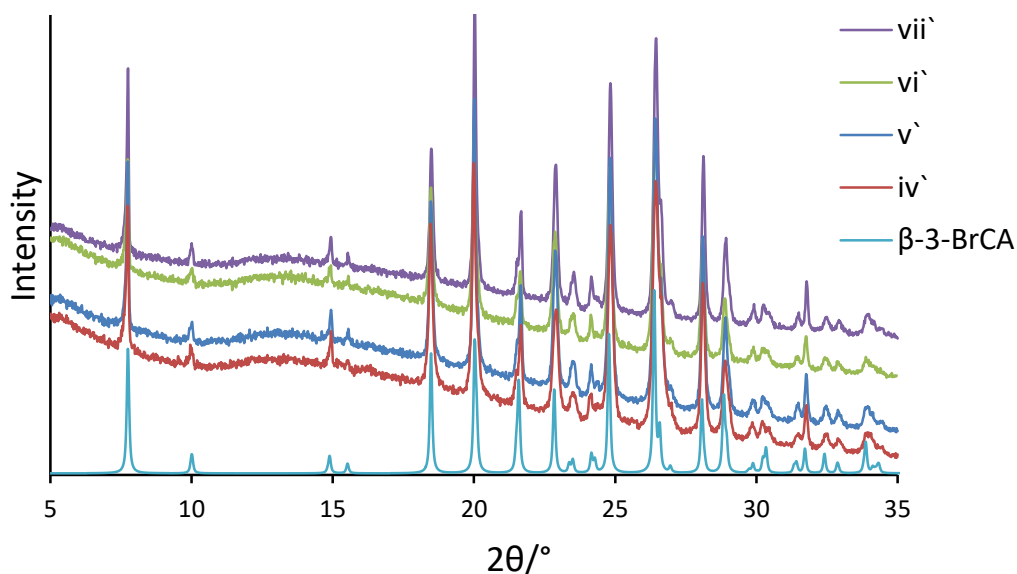
Figure 4.19. *The PXRD data for the recovered DSC samples after heating to 160 °C for different mixtures of β₁-3-FCA:γ-3-BrCA.*

Further investigation of the products from the first DCS cycle

The same samples (i, ii, iii, iv, v, vi and vii), from the first DSC cycle, illustrated in Figure 4.17, were then taken through a second DSC cycle followed by PXRD analysis. From the thermograms in Figure 4.20 of the second DSC cycle, two overlapped endothermic events were clearly observed in the case of i and ii. However, they separated more as the ratio of 3-FCA decreased, until mixture vi was reached, where only one endothermic peak was observed. The results suggest the likely existence of two distinct materials for the mixtures i, ii, iii, iv and v, but only one for samples vi and vii.

The samples recovered after DSC were characterized using PXRD (Figure 4.21) and the results revealed that, in the case of the physical mixture of i and ii, two distinct solid solutions are formed; one with the crystal structure that is similar to that of β-3-BrCA and, the other is similar to β_1-3-FCA (this is also supported by the appearance of the two endothermic events in the second DSC cycle in Figure 4.20, reflecting the two structures of a solid solution). In the PXRD, peak shifts from the corresponding pure acids were also observed, which are consistent with the formation of solid solutions. It is worth noting that, to identify the structure of the solid solution that is similar to β_1-3-FCA, the most intense peak in the pattern of the structure of β_1-3-FCA at ~ 27.45° was considered.

In the case of the mixture iii, the PXRD pattern shows, again, a similar pattern to β-3-BrCA, with broad peaks at ~ 27.17° that may correspond to the overlap of the two peaks; one is the most intense peak of the β_1-3-FCA structure and the other is from β-3-BrCA (present at ~ 27.00°). For the mixtures iv and v, the identification of these overlapped peaks becomes more difficult. This is because more overlapping occurs and, at the same time, the peak that is associated with the structure that is similar to β_1-3-FCA become less intense, due to the lower amount of this solid solution in the sample. Therefore, only the pattern of the structure similar to β-3-BrCA is observed in the PXRD pattern of iv and v. The second DSC cycles of iv and v were consistent with the result from i, ii and iii for which the two observed endothermic events suggest the existence of two distinct materials. PXRD and the second DSC cycle of vi and vii showed only solid solutions with a structure similar to β-3-BrCA.

Thus, the combination of thermal analysis (DSC) along with PXRD analysis indicated that 3-BrCA and 3-FCA form two types of substitutional β solid solutions, one with the crystal structure of β-3-BrCA and another with the crystal structure of β_1-3-FCA. The maximum amount of 3-FCA that can be introduced to form a single phase of a solid solution similar to a β-3-BrCA structure is about 1/8 of 3-BrCA.

The formation of a solid solution is supported by analysing PXRD peak positions. Considering the peak at around 2θ of 26.36 in β 3-BrCA, a slight shift to higher 2θ in the solid solutions 3-FCA/3-BrCA is observed as the amount of 3-FCA increases (Figure 4.21 and 4.22). This trend supports the formation of the solid solution because, as the quantity of 3-FCA in the solid solution increases, the general shift of the peaks to lower d spacing (higher 2θ) is consistent with the fact that the F atom is smaller than the Br atom and, consequently, a decrease in the unit cell volume is expected as the amount of the 3-FCA increases. Similarly, the peaks in the PXRD pattern of β_1-3-FCA, especially the intense peak around 27.45°, shows a slight shift to lower 2θ (high d spacing) for 2:1 and 1:1 samples of 3-FCA/3-BrCA; present at ~ 27.31° and 27.27° respectively. This is consistent with an increase expected as a result of adding 3-BrCA to the structure of 3-FCA and fits with what has been observed earlier in a binary system of 3-ClCA/3-BrCA (Section 4.3.1.a).

Surprisingly, the structure of β_1-3-FCA is observed for the solid solution instead of the β_2-3-FCA structure, although the latter structure was produced every time the acid (pure) was crystallized from melt. This indicates that the structure of β_1-3-FCA is probably more favourable, when some 3-BrCA molecules are introduced to form a solid solution, than the structure of β_2-3-FCA.

The results indicate that cocrystallization of 3-FCA and 3-BrCA from melt forms cocrystalline materials in the form of solid solutions, rather than forming a stoichiometric cocrystal, although there is a significant difference in the atom size of F and Br. To confirm the results, further investigation on cocrystallization of the acids from solution was carried out.
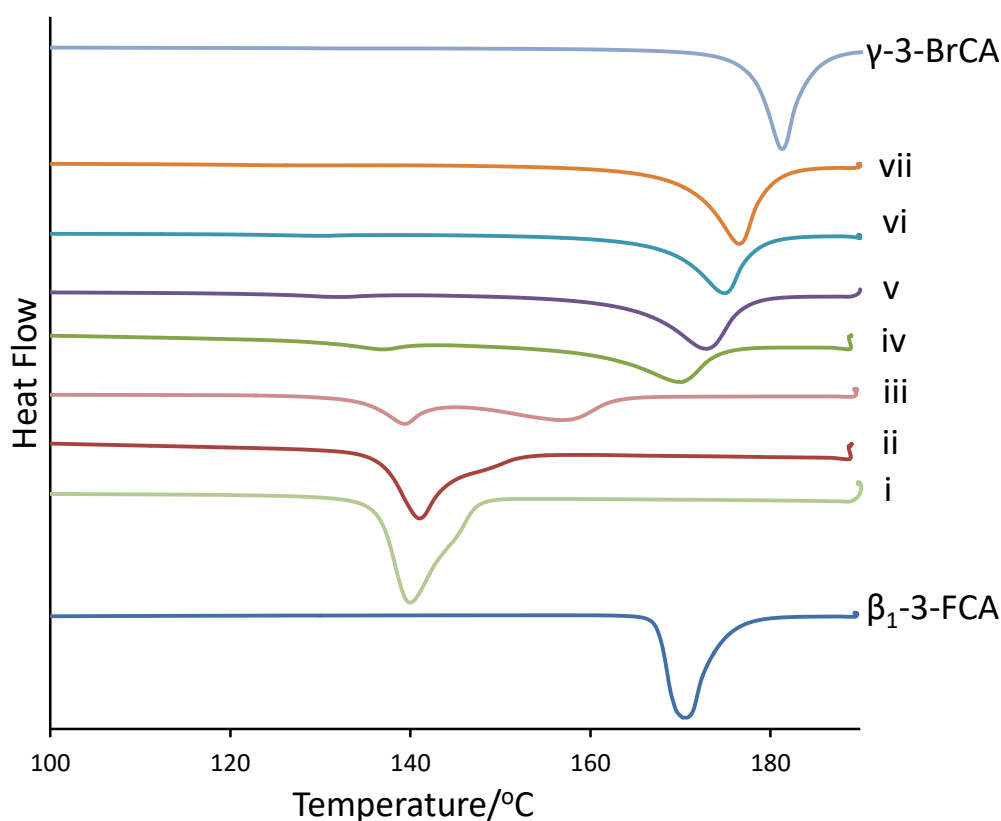
Figure 4.20. *Plots for different mixtures of β_1-3-FCA and γ-3-BrCA along with pure β_1-3-FCA and γ-3-BrCA, showing the second heating DSC cycle.*
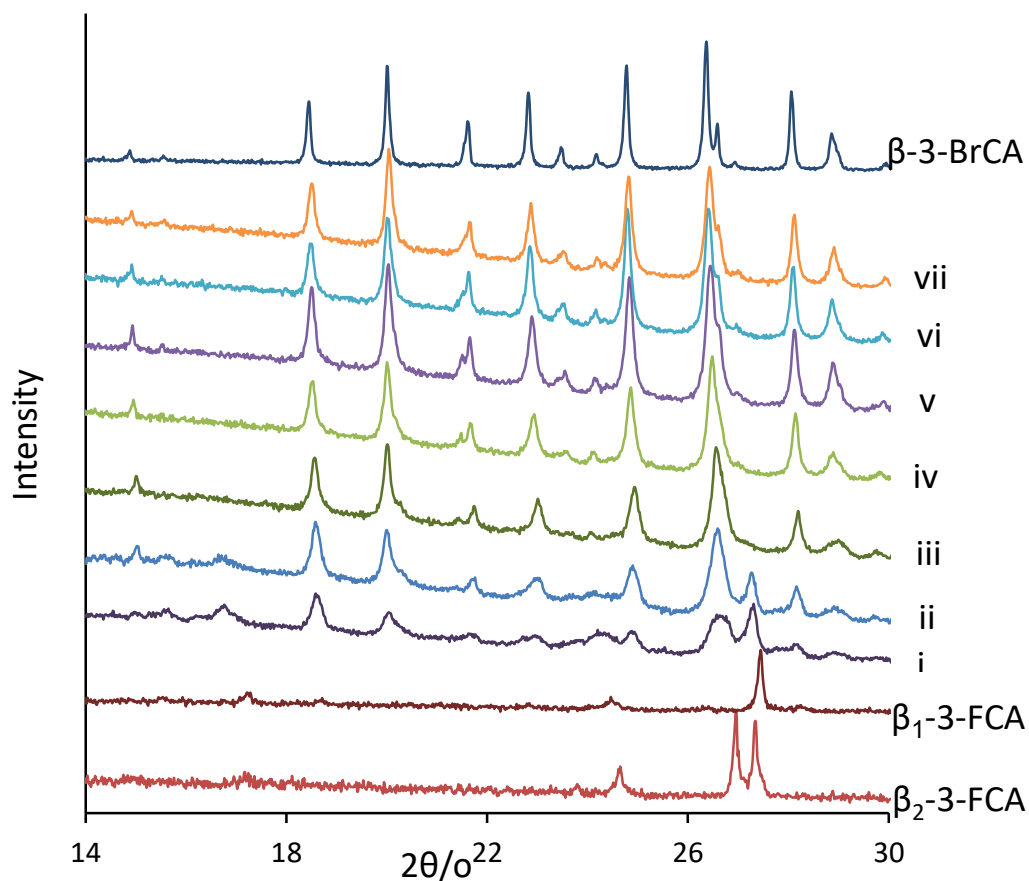
Figure 4.21. *The PXRD data for the recovered DSC samples of different mixtures of β₁-3-FCA and γ-3-BrCA, along with the experimental PXRD pattern of β₁-3-FCA, β₂-3-FCA and β-3-BrCA.*
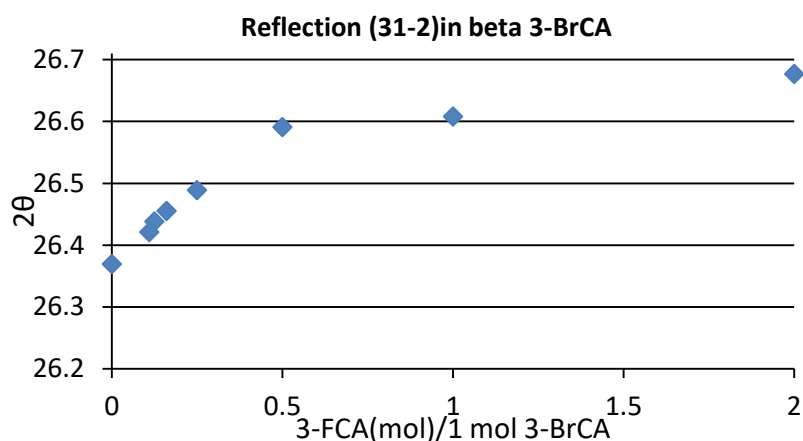
Figure 4.22. *The 2θ shift for samples with structures similar to β-3-BrCA.*

4.3.2.b. Cocrystallization of 3-FCA/3-BrCA from solution: phase characterization

For investigation of the structures, cocrystallization of the acids from solution was carried out. Crystallization of a 1:1 molar ratio of 3-BrCA:3-FCA from MeOH reveals only two distinct types of cocrystals in the form of solid solution; one with a structure similar to *β*-3-BrCA, designated in this study as *β*-3-BrCA/3-FCA (structure A) and the

other to β_1-3-FCA, designated here as β_1-3-BrCA/3-FCA (structure B). The crystal structures of both phases were determined using SC-XRD. PXRD analysis on the sample from different locations of the crystallization vial showed that the material from the bottom was mainly structure A, whereas the crystals collected from the side were predominately structure B. Repetition of the crystallization under the same conditions using MeOH and GAA gave the same results, as confirmed by PXRD.

However, crystallization with a 3-BrCA:3-FCA of 4:1 in MeOH gave two forms of 3-BrCA/3-FCA solid solutions; a structure that is similar to β_1-3-FCA (denoted as β_1-3-BrCA/3-FCA, structure B) and another phase with a PXRD pattern similar to γ_2-3-BrCA (labelled as structure C). The structure of C was confirmed by SC-XRD and denoted as γ_2-3-BrCA/3-FCA, and is discussed below.

Unfortunately, it was difficult to reproduce the crystallization of structure C and, instead, solid solutions with the structure similar to γ-3-BrCA, denoted as γ-3-BrCA/3-FCA (structure D) appeared along with structures A and B. The different solid solution structures are summarized in Table 4.6.

PXRD patterns from all crystallization batches discussed above revealed isostructural materials to (γ, γ_1 and β)-3-BrCA and β-3-FCA structures (That is there is no additional phases). The results illustrate the formation of cocrystalline materials in the form of solid solution, confirming the result discussed in Section 4.3.2.a, in the case of cocrystallization of 3-BrCA and 3-FCA from melt.

The crystal structures of A to D are semi-polymorphs (as discussed in Chapter 1) and they are discussed below.

Table 4.6. *Summary of the different solid solution structures comprising 3-BrCA/3-FCA.*

Label of the structure	The structure is similar to	Solid solution
A	β-3-BrCA	β-3-BrCA/3-FCA
B	β_1-3-FCA	β_1-3- BrCA/3-FCA
C	γ_2-3-BrCA	γ_2-3-BrCA/3-FCA
D	γ-3-BrCA	γ -3-BrCA/3-FCA

Structure A

The crystal structure of solid solution A (β-3-BrCA/3-FCA) is monoclinic (space group C2/c). The asymmetric unit comprises one molecule, with halogens (Br:F) disordered in the *meta*-position of the benzene ring, as shown in Figure 4.23, with refined occupancies of 0.882(4) for Br and 0.118 (4) for F. The crystal structure (Figure 4.24a) shows very similar packing to the one observed previously for β-3-BrCA, and this is also reflected by the similarity of their PXRD patterns (Section 4.3.2.a.). Molecules interact to form a carboxylic acid hydrogen bonded dimer and as seen in the case of the β-3-ClCA/3-BrCA solid solution, adjacent C=C double bonds are only 3.97Å apart, suggesting a capability of photodimerization.
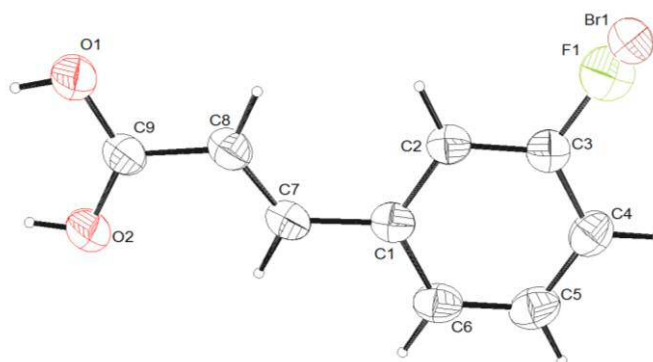
Figure 4.23. *The asymmetric unit in the β-3-BrCA/3-FCA solid solution showing the disordered halogens (Br/F) and OH group.*

Structure B

Similarly to β_1-3-FCA, the crystal structure of B (β_1-3-BrCA/3-FCA) solid solution is triclinic P$\overline{1}$ space group. One planar 3-halo-cinnamic acid molecule comprises the asymmetric unit. The substituent in the *meta*-position of the ring is disordered, with refined F:Br occupancies of 0.92(1):0.08(1). In the crystal structure the familiar carboxylic acid dimer pattern is clearly observed and the molecules are arranged similarly to the β_1-3-FCA structure (see Figure 4.24b)

Structure C and D

Structure C (γ_2-3-BrCA/3-FCA) is monoclinic (P2$_1$/n) (similar to γ_2-3-BrCA). Phase D (γ-3-BrCA/3-FCA) is also monoclinic P2$_1$/a, and is similar to γ-3-BrCA. In both structures, the asymmetric unit is one molecule of 3-halo-cinnamic acid with a disordered bromine and fluorine location in the *meta*-position. The refined occupancies are approximately similar to those already seen in structure A; Br and F of 0.91(1) and 0.09(1), respectively for structure D and of 0.88(1) and 0.12(1), respectively for

structure C. In both phases, pairs of molecules are related by a centre of inversion to form the normal hydrogen bonded dimer. Crystal structure and crystallographic data for all the above determined structures (A, B, C and D) are shown in Figure 4.24 and Table 4.7, respectively.
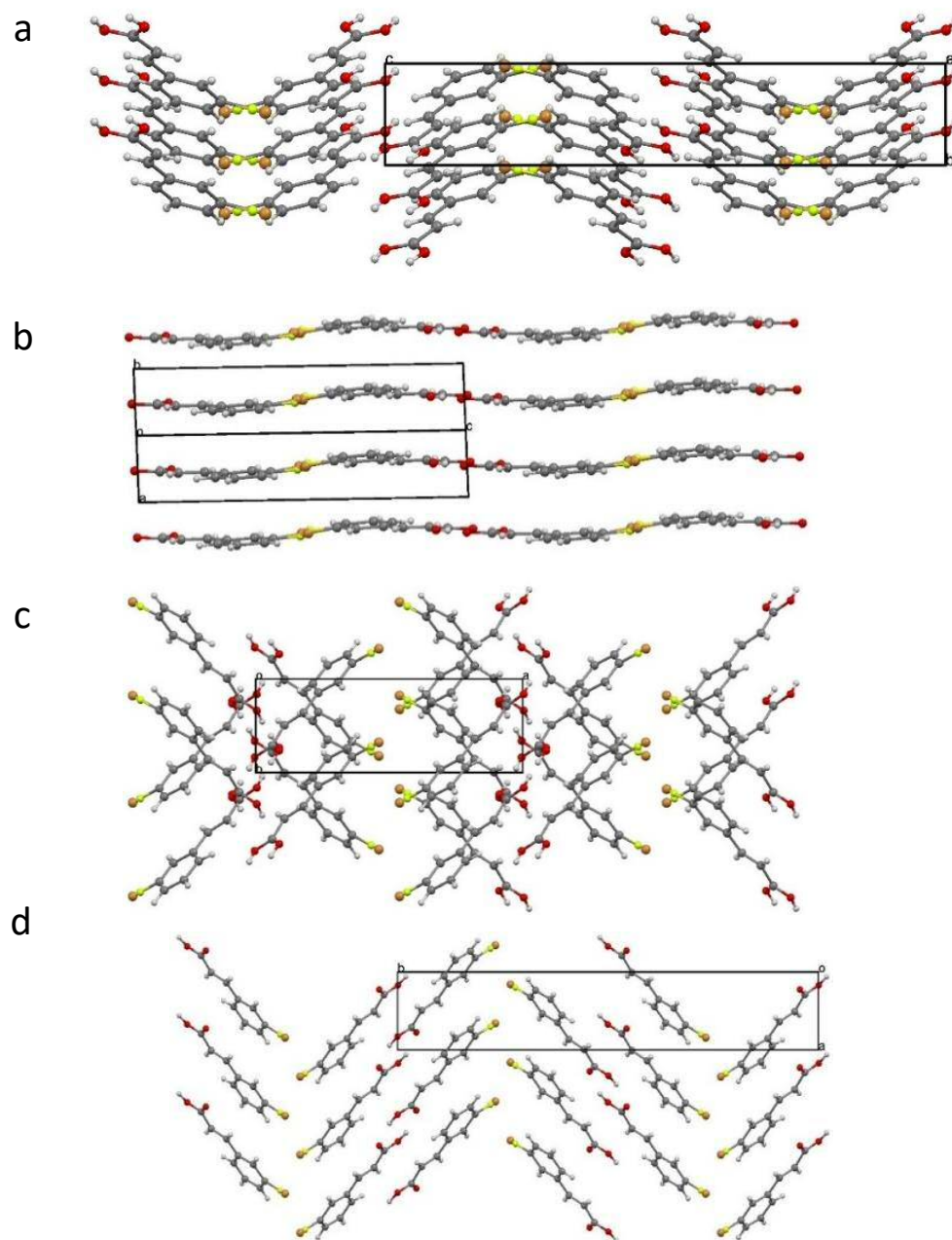
Figure 4.24. *The crystal structures of (a) β-3-BrCA/3-FCA, (b) β₁-3-BrCA/3-FCA, (c) γ-3-BrCA/3-FCA and (d) γ₂-3-BrCA/3-FCA.*

Table 4.7. *Crystallographic data for the crystal structure determination of the different phases of 3-BrCA/3-FCA solid solutions.*

	β-3-BrCA/3-FCA (A)	β_1-3-BrCA/ 3-FCA (B)	γ-3-BrCA/3-FCA (D)
Formula	$C_9 H_7 Br_{0.88} F_{0.12} O_2$	$C_9 H_7 Br_{0.08} F_{0.92} O_2$	$C_9 H_7 Br_{0.91} F_{0.09} O_2$
Formula weight	218.60	171.21	221.27
Temperature, (K)	293(2)	293(2)	293(2)
λ, Å	1.54184	0.71073	1.54184
Crystal system	Monoclinic	Triclinic	Monoclinic
Space group	C2/C	P$\bar{1}$	P2$_1$/c
a, (Å)	19.1722(17)	3.9247(6)	14.3905(16)
b, (Å)	3.9703(2)	6.3364(9)	4.9327(6)
c, (Å)	24.866(2)	16.295(3)	12.3836(14)
α, (°)	90	84.116(13)	90
β, (°)	113.318(4)	84.565(13)	95.058(11)
γ, (°)	90	87.165(12)	90
Volume, (Å³)	1738.2(2)	400.97(11)	875.61(17)
Z	8	2	4
Density (calculated), (Mg/m³)	1.671	1.418	1.678
Absorption coefficient, (mm⁻¹)	5.364	0.509	5.549
F(000)	867	176	438
Crystal size, (mm³)	0.23 x 0.07 x 0.02	0.21 x 0.11 x 0.03	0.25 x 0.05 x 0.03
Reflections collected	4975	2893	2712
Independent reflections	1700	1847	1680
R(int)	0.0335	0.0504	0.0188
Goodness-of-fit on F²	1.064	1.010	1.044
Final R$_1$ indices [I>2sigma(I)]	0.0389	0.1422	0.0490
Final wR$_2$	0.0951	0.3736	0.1261
R$_1$ indices (all data)	0.0430	0.3216	0.0634
wR$_2$ (all data)	0.0985	0.4851	0.1383

	γ_2-3-BrCA/ 3-FCA (C)		
Formula	$C_9 H_7 Br_{0.88} F_{0.12} O_2$	Z	4
Formula weight	219.90	Density (calculated), (Mg/m³)	1.686
Temperature, (K)	293(2)	Absorption coefficient, (mm⁻¹)	5.493
λ, Å	1.54184	F(000)	436
Crystal system	Monoclinic	Crystal size, (mm³)	0.25 x 0.07 x 0.02
Space group	P2$_1$/n	Reflections collected	2825
a, (Å)	4.9703(2)	Independent reflections	1655
b, (Å)	28.3495(11)	R(int)	0.0157
c, (Å)	6.1481(3)	Goodness-of-fit on F²	1.098
α, (°)	90	Final R$_1$ indices [I>2sigma(I)]	0.0422
β, (°)	91.186(4)	Final wR$_2$	0.1117
γ, (°)	90	R$_1$ indices (all data)	0.0448
Volume, (Å³)	866.12(6)	wR$_2$ (all data)	0.1142

Consistency of results

In structures A, C and D, Br and F are disordered with the major occupancy for Br while the minor component is F. In order to confirm these occupancies, single crystal diffraction data were recorded for 12 randomly collected single crystals. The results,

shown in Table 4.8, give an overall average of 88% for Br and 11% for F, proving the consistency of the results. This agrees with Section 4.3.2.a, where the thermal investigation of a binary system of 3-FCA/3-BrCA showed that, for every 8 molecules of 3-BrCA a maximum of only one molecule of 3-FCA can be introduced to form a single phase of a solid with a structure that is similar to 3-BrCA structures. These results showed a good agreement with the observation made by Omondi et al.[43], where the solid solution was produced by cocrystallization of 2,6-difluoro-N-phenylformamide(I) and 2,6-dichloro-N-phenylformamide(II). Structure determination of one crystal from the batch showed that Cl and F atoms are disordered in the structure, with occupancies of 0.728(4) for the Cl and 0.272(4) for the F. Thus, the difference in occupancies of the solid solution's components is proportional to the difference in the size of substituent groups.

Table 4.8. *The distribution of Br and F in different crystal structures, showing the average. The different colours indicate different crystallization vials.*

Start Prep. ratio Br:F	Solvent	In crystal structure		Average %	
		Br (%)	F (%)	Br (%)	F (%)
1:1	MeOH	89	11		
1:1	MeOH	90	10		
1:1	MeOH	89	11	89	11
1:1	MeOH	89	11		
1:1	MeOH	88	12		
1:1	MeOH	89	11		
1:1	MeOH	88	12	89	11
1:1	MeOH	90	10		
1:1	Acetic acid	84	15		
4:1	MeOH	88	12		
4:1	MeOH	88	12		
9:1	MeOH	94	06		
Average for all %		**88**	**11**		

4.3.3. Investigation of cocrystallization in a binary system of 3-CF₃CA/3-MeCA

Recalling the results from Chapter 3, γ_1-3-CF$_3$CA and γ-3-MeCA are isostructural. γ_1-3-CF$_3$CA transformed to another gamma phase (γ_2) whereas 3-MeCA showed no

transformation. Thus, investigation of the cocrystallization of the two acids may help in understanding of the feasibility of inducing transformation of 3-MeCA.

4.3.3.a. Cocrystallization from solution

1:1 3-CF₃CA:3-MeCA preparation

3-CF$_3$CA and 3-MeCA in a 1:1 starting molar ratio were cocrystallized from MeOH. SC-XRD revealed that the structure is monoclinic P2$_1$/a and, unsurprisingly, it is similar to those of γ_I-3-CF$_3$CA and γ-3-MeCA. The asymmetric unit consists of one molecule of 3-substituted-cinnamic acid, with disordered methyl and trifluoromethyl groups in the *meta*-position of the ring, with refined CF$_3$:Me occupancies of 0.577(4)/0.423(4) (Figure 4.25). Crystallographic data are shown in Table 4.9. The PXRD pattern is identical to that calculated from single crystal data.
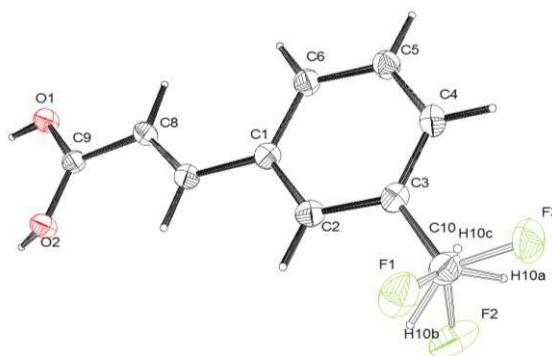
Figure 4.25. *The asymmetric unit in the 3-CF₃CA/3-MeCA solid solution showing disordered 3-Me group and 3-CF₃. The OH group is also disordered.*

4:1 and 1:4 3-CF₃CA:3-MeCA preparation

In further crystallization experiments, γ-CF$_3$CA:γ-3-MeCA starting molar ratios of 4:1 and 1:4 (E and F, respectively) were cocrystallized from MeOH, with the resultant crystals characterized by PXRD analysis and the structure confirmed by SC-XRD. E and F are both monoclinic P2$_1$/a. The asymmetric unit is one molecule of 3-substituted-cinnamic acid, with disordered methyl and trifluoromethyl groups in the *meta*-position of the ring. The refined occupancies of Me:CF$_3$ are different in both crystals; 0.78(1):0.21(1) in the crystal from sample E and 0.17(1):0.83(1) for the crystal from sample F. This shows consistency with the starting ratio. On the other hand, the crystallographic data shows that the unit cell volume of the CF$_3$CA/3-MeCA solid solution that contains more CF$_3$CA is bigger than the solid solution that contains more 3-MeCA. This is consistence with the volume size of CF$_3$ and Me groups (56.5 Å^3 for C-CF$_3$ and 40.2 Å^3 for C-CH$_3$ as calculated using VEGA[14] program). Thus as we

increased the amount of CF$_3$CA the volume of the solid solution unit cell increased. The crystallographic data are shown in Table 4.9.

As shown in Figure 4.26, the PXRD pattern of sample E is identical with the calculated PXRD pattern from single crystal data, and similar to the PXRD pattern of γ_1-3-CF$_3$CA. Similarly the calculated PXRD pattern of the solid solution from F is identical to the experimental pattern, which is similar to that of γ-3MeCA. This result suggests the formation of continuous solid solution.
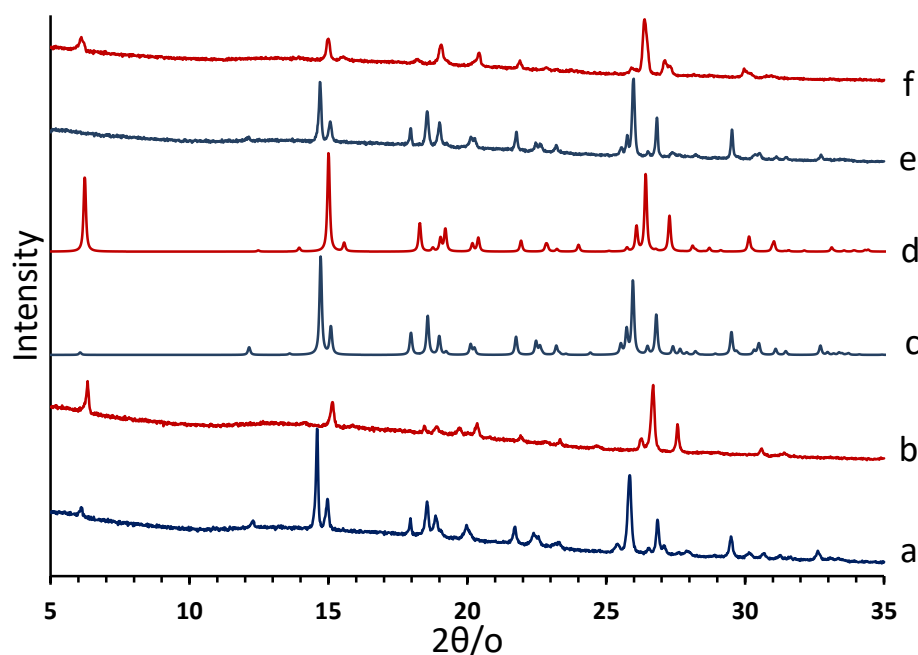
Figure 4.26. *The experimental PXRD pattern of (a) γ_1-3-CF$_3$CA, (b) γ-3-MeCA, (e) sample E and (f) sample F, and the calculated PXRD pattern for (c) sample E and (d) sample F. Similar patterns are displayed in a similar colour.*

Table 4.9. *Crystallographic data for the crystal structure determination of the γ-3-CF$_3$CA/3-MeCA solid solutions.*

	γ-3-CF$_3$CA/3-MeCA (1:1)prep	γ-3-CF$_3$CA/3-MeCA (4:1)prep	γ-3-CF$_3$CA/3-MeCA (1:4)prep
Formula	C$_{10}$ H$_{8.27}$ F$_{1.73}$ O$_2$	C$_{10}$ H$_{7.67}$ F$_{2.33}$ O$_2$	C$_{10}$ H$_{9.49}$ F$_{0.51}$ O$_2$
Formula weight	193.22	204.15	171.45
Temperature, (K)	150(2)	293(2)	293(2)
λ , Å	0.71073	1.54184	1.54184
Crystal system	Monoclinic	Monoclinic	Monoclinic
Space group	P2$_1$/a	P2$_1$/a	P2$_1$/a
a, (Å)	12.6693(14)	13.0141(16)	12.7017(14)
b, (Å)	4.8477(8)	4.9294(5)	4.9320(4)
c, (Å)	14.615(2)	14.5690(15)	14.1949(18)
α, (°)	90	90	90
β, (°)	92.155(9)	91.886(9)	92.803(12)
γ, (°)	90	90	90
Volume, (Å^3)	897.0(2)	934.12(18)	888.17(17)
Z	4	4	4
Density (calculated), (Mg/m^3)	1.431	1.452	1.282
Absorption coefficient, (mm^{-1})	0.122	1.145	0.797
F(000)	399	419	360
Crystal size, (mm^3)	0.25 x 0.07 x 0.04	0.26 x 0.08 x 0.06	0.34 x 0.05 x 0.03
Reflections collected	3184	2735	2664
Independent reflections	2034	1784	1640
R(int)	0.0461	0.0240	0.0202
Goodness-of-fit on F^2	1.096	1.105	1.203
Final R$_1$ indices [*I*>2sigma(*I*)]	0.0623	0.0834	0.0848
Final wR$_2$	0.1469	0.2617	0.2023
R$_1$ indices (all data)	0.1026	0.1007	0.1280
wR$_2$ (all data)	0.1765	0.2787	0.2256

4.3.3.b. Thermal analysis study of E, F and related physical mixtures

DSC experiments were carried out on both E and F solid solutions (obtained as discussed in Section 4.3.3.a). For comparison, physical mixtures comprising 4:1 and 1:4 ratios of γ-CF$_3$CA:γ-3-MeCA (G and H, respectively) were also investigated. The samples were heated from 40 to 155 °C and back to 40 °C at 20°C/min. All samples were labelled and this is summarized in Table 4.10.

Table 4.10. *Summary of labelling binary systems comprising CF$_3$CA:3-MeCA.*

label	Acids	Prep ratio	type
E	γ-3-CF$_3$CA:γ-3-MeCA	4:1	Solid solution
F	γ-3-CF$_3$CA:γ-3-MeCA	1:4	Solid solution
G	γ$_1$-3-CF$_3$CA:γ-3-MeCA	4:1	Physical mixture
G$_1$	γ$_1$-3-CF$_3$CA:γ-3-MeCA	4:1	Physical mixture
H	γ$_1$-3-CF$_3$CA:γ-3-MeCA	1:4	Physical mixture
I	γ$_1$-3-CF$_3$CA:γ-3-MeCA	8:1	Physical mixture
I$_1$	γ$_1$-3-CF$_3$CA:γ-3-MeCA	8:1	Physical mixture

Sample E (solid solution prepared by a 4:1 3-CF₃CA:3-MeCA starting ratio)

On heating sample E, a small endothermic peak was observed around 124 °C (Figure 4.27) which overlapped with other endothermic peaks. These peaks are probably due to the melting of the distinct materials (variety composition of solid solution), or may be due to phase transition and melt. However, one exothermic peak was observed in the cooling cycle. PXRD analysis of the recovered material after the DSC (Figure 4.29) showed an identical pattern to E, indicating of a re-cocrystallization of the material from the melt.
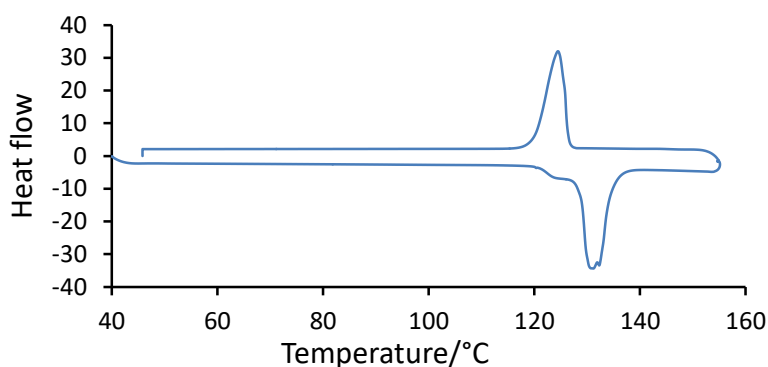
Figure 4.27. Thermal analysis of sample E with the DSC cycle from 40 to 155 °C and then to 40 °C.

Sample G (physical mixture of 4:1 γ_1-3-CF₃CA:γ-3-MeCA)

DSC analysis for G showed four endothermic events around 101, 116, 124 and 132°C (Figure 4.28). They can probably be attributable to the melting of the distinct components (this is discussed below). In the cooling cycle, similarly with sample E, one crystallization peak is observed. PXRD analysis of the recovered sample after DSC showed that it had cocrystallized from melt and, surprisingly with a crystal structure similar to γ_1-3-CF₃CA, rather than γ_2-3-CF₃CA, as illustrated in Figure 4.29, showing consistency with the result obtained for sample E.

This is surprising because, recalling the results from Chapter 3, γ_2-3-CF₃CA is the resultant product from crystallization of the acid from the melt. Therefore, a solid solution with γ_2-3-CF3CA structure would be expected rather than the γ_1-3-CF₃CA. This result indicates that, although the amount of 3-MeCA that was introduced in the mixture was a quarter of the amount of 3-CF₃CA, it plays a significant role in steering the structure of the mixed crystal towards packing with the structure of γ_1-3-CF₃CA which, in turn, is isostructural to γ-3-MeCA, rather than cocrystallization with the structure similar of γ_2-3-CF₃CA (this will investigate further in the flowing section).

Sample I (physical mixture of 8:1 γ₁-3-CF₃CA:γ-3-MeCA)

Further investigation with a smaller amount of 3-MeCA in the mixture was performed. A physical mixture with a 3-MeCA:3-CF3CA ratio of 1:8 (sample I) was prepared and subjected to the same DSC treatment as sample G. The recovered material was shown by PXRD (Figure 4.29) to adopt a crystal structure similar to γ₂-3-CF₃CA, similar to the behaviour of pure 3-CF₃CA. This indicates that the threshold for 3-MeCA to inhibit the formation of the structure similar to γ₂-3-CF₃CA is between the ratios 3-MeCA:3-CF₃CA of 1:4-1:8.

As discussed in Chapter 3, in the γ₂ phase of 3-CF₃CA, the fluorine atoms are involved in C-F⋯F-C interactions, in addition to C-H⋯F which are present in both γ₁ and γ₂ structures. Thus, in 3-MeCA:3-CF₃CA, it is clear that the quantity of 3-MeCA in the case 1:4 (3-MeCA:3-CF₃CA) probably inhibit and the formation C-F⋯F-C interactions and the γ₁ solid solution dominates. However, the γ₂ solid solution structure is produced when the quantity of 3-MeCA present (for example, 1:8 3-MeCA:3-CF₃CA) does not significantly disturb the formation of C-F⋯F-C interactions. Such behaviour might indicate the importance of C-F⋯F-C interaction in the structure.[44]
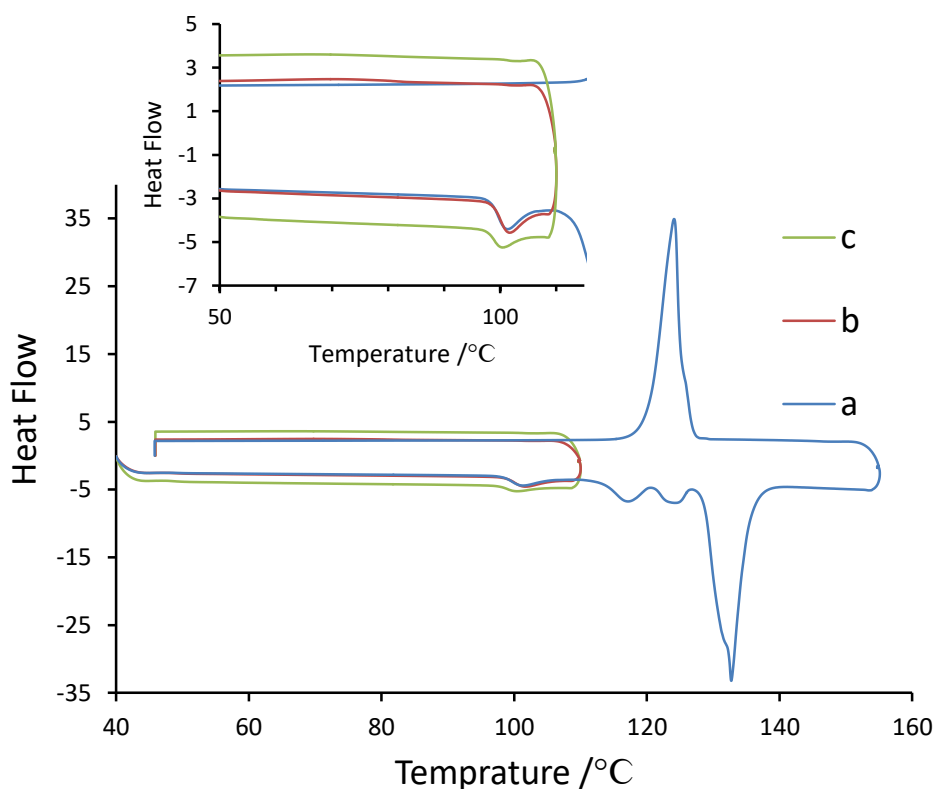
Figure 4.28. *Thermal analysis of (a) sample G with the DSC cycle from 40°C to 155°C and then to 40 °C again. (b) and (c) are for samples G₁ and I₁, respectively, with the DSC cycle from 40 to 110 °C and then to 40 °C again.*
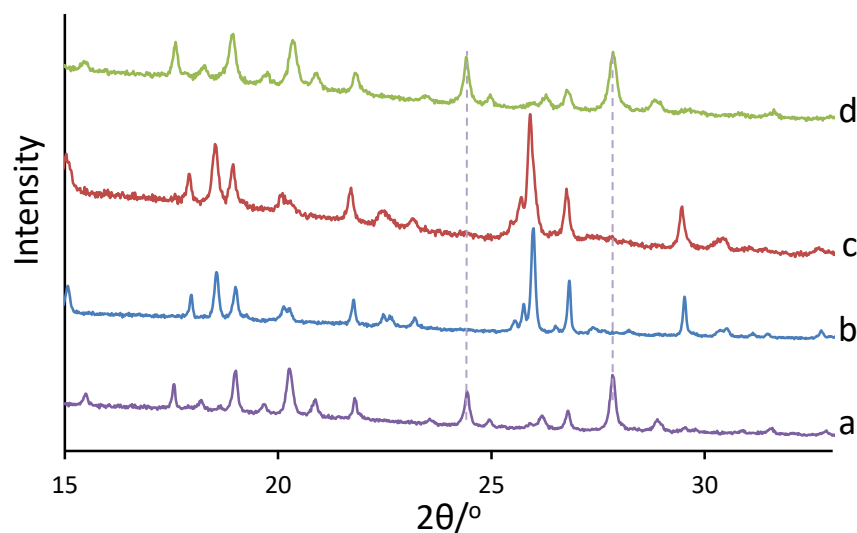
Figure 4.29. *The experimental PXRD pattern of (a)* γ_2*-3-CF₃CA. Patterns (b), (c) and (d) are for sample E, G and I respectively after the DSC cycle. The dashed lines show the missing of key peaks of* γ_2*-3-CF₃CA structure in E and G, while they are present in I.*

Sample G₁ and I₁ (physical mixture of 4:1 and 8:1 γ_1-3-CF₃CA:γ-3-MeCA respectively)

Further investigations were carried out in order to explain the DSC thermogram of sample G. DSC experiments on samples G₁ and I₁ (3-MeCA:3-CF3CA ratio of 1:4 and 1:8, respectively) with a heating rate of 20 °C/min from 40 to 110 °C and then cooling to room temperature, showed one endothermic peak around 100 °C in the heating cycle (Figure 4.28 b and c, respectively). PXRD analysis on the sample G₁ recovered after the DSC analysis revealed peaks similar to γ_1-3-CF₃CA, with additional peaks suggesting the existence of the solid solution of 3-MeCA/3-CF₃CA with a structure similar to sample E (Figure 4.30). Broadening of the peaks is observed, suggesting the formation of a solid solution similar to γ_1-3-CF₃CA structure with variant compositions of 3-MeCA:3-CF₃CA. Conversely, the recovered sample I₁ after DSC showed a PXRD pattern similar to the γ_2-3-CF₃CA structure. The results can be explained as follows; the endothermic event in the DSC cycle probably corresponds to the melting of 3-MeCA and a shift of the peak was observed compared with the pure acid, since the pure acid melts at about 122°C. The lowering in the melting temperature of 3-MeCA is due to the contamination with 3-CF₃CA. Thus, for sample G₁ (Figure 4.28b) the 3-MeCA melts and 3-CF₃CA is dissolved in the molten material which then cocrystallizes to produce a solid solution material similar to γ_1-3-CF₃CA. Interestingly, form γ_1 was obtained in this case rather than γ_2 form. However, in the case of I₁ (Figure 4.28c), when 3-MeCA

melts, it dissolved 3-CF$_3$CA and, since the quantity of 3-MeCA in the mixture is 1/8 the 3-CF$_3$CA, cocrystallization leads to a structure similar to γ_2-3-CF$_3$CA structure.

Thus, the results here support the hypothesis that introducing 3-MeCA into 3-CF$_3$CA destabilizes the formation of the structure that is similar to γ_2-3-CF$_3$CA and the greater the quantity of 3-MeCA, the greater the destabilization effect.
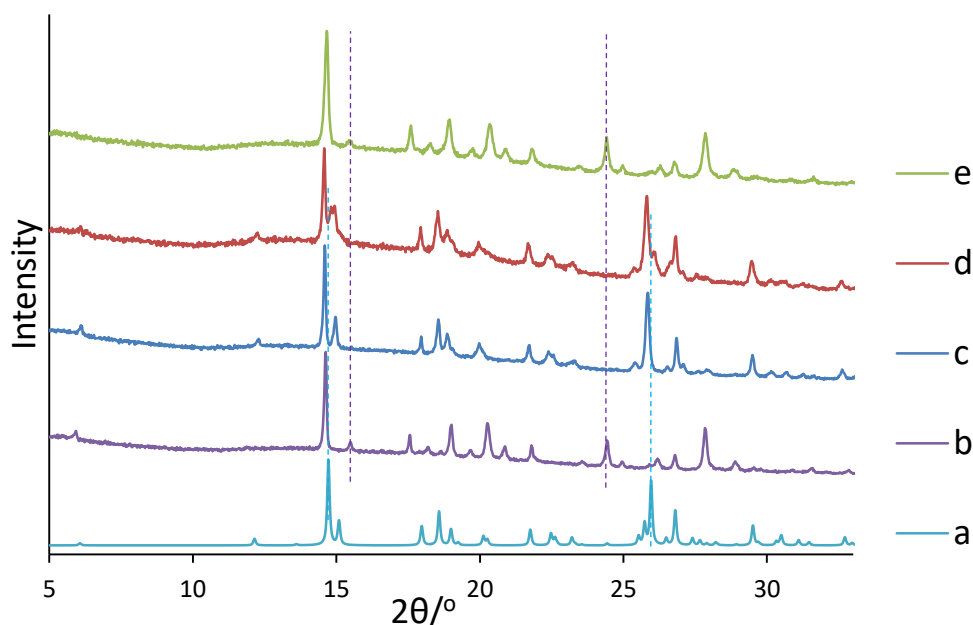
Figure 4.30. *(a) The calculated PXRD pattern of sample E, and the experimental PXRD pattern of (b) γ_2-3-CF$_3$CA, (c) γ_1-3-CF$_3$CA (d) sample G$_1$ after DSC heat until 100 °C and (e) sample I$_1$. The dashed lines indicate the existence of the phase corresponding to the colour.*

F and H (solid solution prepared by 3-CF$_3$CA:3-MeCA starting ratio of 1:4 and the physical mixture of γ_1-3-CF$_3$CA:γ-3-MeCA ratio of 1:4)

Similar thermograms for both samples F and H were produced from DSC experiments, with broad melting peaks observed around 118 °C, corresponding to the melting of the materials. However, in the case of F, the melting peak is more symmetrical, indicating of the existence of one entity material (see Figure 4.31). The cooling cycle of both F and H showed two exothermic peaks; a smaller peak present at around 113°C and a bigger one at about 99 °C. PXRD analysis of both samples F and H after DSC gave identical PXRD patterns to the calculated PXRD pattern of the solid solution structure determined previously for F.
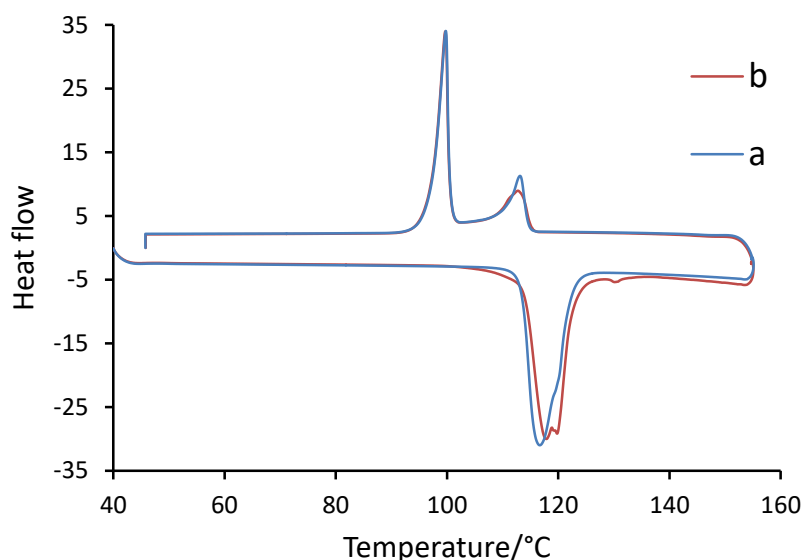
Figure 4.31. *Thermal analysis of (a) sample F and (b) samples H with the DSC cycle from 40 to 155 °C and then back to 40 °C.*

4.3.4. Investigation of cocrystallization of binary systems of different *meta-cinnamic acids*

4.3.4.a. Cocrystallization from solution

β forms of cinnamic acids can undergo photodimerzation reaction upon exposure to UV light. Both 3-BrCA and 3-ClCA are crystallized mainly in the *β* form from a solution in GAA. Additionally, they cocrystallized in the *β* form with a structure similar to 3-BrCA, from GAA solution. However, 3-MeCA and 3-CF$_3$CA were crystallized only in the *γ* forms. Structural mimicry has been used to transform the photochemical properties of the materials.[45] Thus, 3-ClCA/3-MeCA, 3-ClCA/3-CF$_3$CA, 3-BrCA/3-MeCA and 3-BrCA/3-CF$_3$CA were cocrystallized in an attempt to generate *β* forms of solid solutions. 1:1 ratios in MeOH and GAA were used. Characterization was by SC-XRD analysis using crystals selected from each batch and by PXRD to characterize the whole batch.

In all cases, SC-XRD determination showed the formation of *γ* phases of solid solutions with disordered substituents in the *meta*-position of the benzene ring. Table 4.11 shows the composition of the crystals and the crystallographic data are shown in Table 4.12.

Obtained solid solution (A/B)	Occupancies		Crystallization solvent
	(A)	(B)	
γ-3-ClCA/3-MeCA	0.67(1)	0.33(1)	MeOH
	0.34(1)	0.66(1)	GAA
γ-3-ClCA/3-CF₃CA	0.48(1)	0.52(1)	MeOH
	0.30 (1)	0.70(1)	GAA
γ-3-BrCA/3-MeCA	0.679 (3)	0.327(3)	MeOH
	0.46(1)	0.54(1)	GAA
γ-3-BrCA/3-CF₃CA	0.28(1)	0.72(1)	MeOH
	0.318(4)	0.682(4)	GAA

PXRD characterization of the cocrystallized samples of 3-ClCA/3-MeCA and 3-BrCA/3MeCA from MeOH, as well as from GAA, revealed similar patterns to those calculated for γ-3-ClCA/3-MeCA and γ-3-BrCA/3MeCA solid solutions (Figure 4.32 and 4.33, respectively).
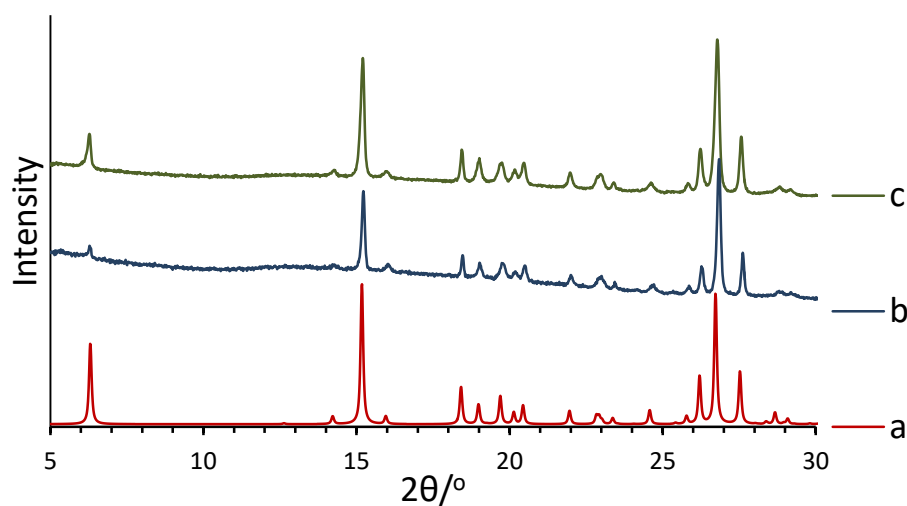
Figure 4.32. (a) The experimental PXRD pattern of γ-3-ClCA/MeCA solid solution crystallized from MeOH, (c) and (d) are the experimental PXRD patterns of a 1:1prep of 3-ClCA/3-MeCA from MeOH and from GAA, respectively.
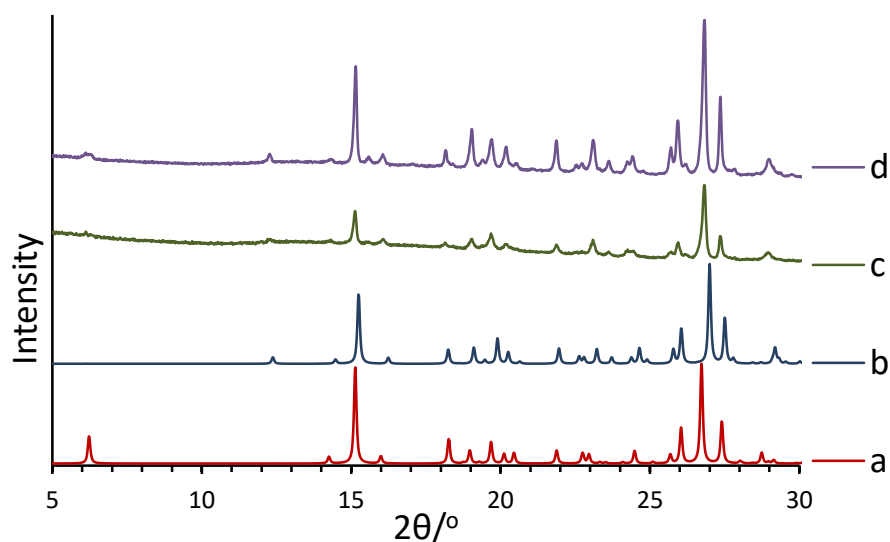
Figure 4.33. *The calculated PXRD pattern of γ-3-BrCA/MeCA solid solution crystallized from (a) MeOH, (b) GAA. (c) and (d) are the experimental PXRD patterns of a 1:1 prep of 3-BrCA/3-MeCA from MeOH and from GAA, respectively.*

Cocrystallization of 3-ClCA/3-CF₃CA from MeOH and GAA showed PXRD results similar to that calculated for γ-3-ClCA/3-CF₃CA solid solution, which cocrystallized from MeOH. The broad peaks suggest the existence of variant 3-ClCA/3-CF₃CA composition of the same phase of solid solution (Figure 4.34).
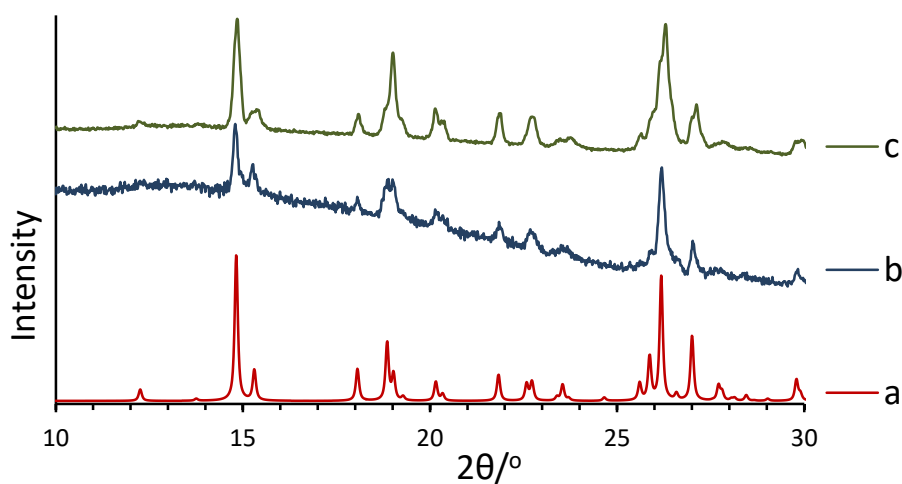
Figure 4.34. *The calculated PXRD pattern of (a) γ-3-ClCA/CF₃CA solid solution crystalized from MeOH, (b) and (c) are the experimental PXRD patterns of a 1:1 initial ratio of 3-ClCA:3-CF₃CA crystallization from MeOH and GAA, respectively.*

The PXRD pattern of 3-BrCA/3-CF$_3$CA crystallized from MeOH showed a pattern similar to that calculated for the γ-3-BrCA/3-CF$_3$CA solid solution. Additional peaks were also observed, indicating the existence of a solid solution with a structure similar to γ-3-BrCA, and shifts in the peaks in relation to the calculated PXRD pattern of γ-3-BrCA can be observed (Figure 4.35, compare a, b, c and e). Cocrystallization of 3-BrCA/3-CF$_3$CA from GAA also showed a PXRD pattern similar to that calculated for γ-3-BrCA/3-CF$_3$CA solid solution. However, Additional peaks were also observed in this case, indicating the existence of a crystalline material isostructural with β-3-BrCA. Shifts in the peaks suggested the formation of a solid solution material with a structure similar to β-3-BrCA. (Figure 4.35, compare a, b, d and f patterns). Unfortunately, the β crystal structure of the solid solution comprising 3-BrCA/3-CF$_3$CA was not determined by SC-XRD because suitable crystals could not be found.
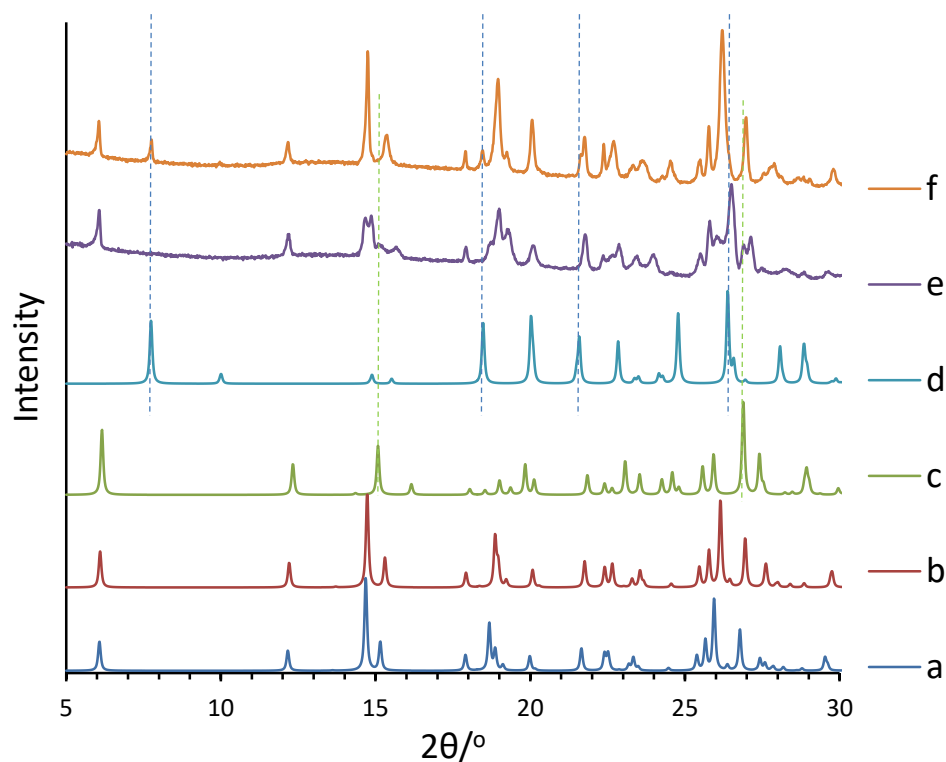
Figure 4.35. *The calculated PXRD pattern of (a) γ-3-BrCA/CF$_3$CA crystalized from MeOH, (b) γ-3-BrCA/CF$_3$CA crystallized from GAA, (c) γ-3-BrCA and (d) β-3-BrCA. (e) and (f) are the experimental PXRD patterns of a 1:1 prep of 3-BrCA/3-CF$_3$CA from MeOH and GAA, respectively.*

Table 4.12. *Crystallographic data for the crystal structure determination of some solid solutions.*

	γ-3-ClCA/3MeCA (MeOH)	γ-3-ClCA/3-MeCA (AA)	γ-3-ClCA/3-CF$_3$CA (MeOH)
Formula	$C_{9.33}H_{7.99}Cl_{0.67}O_2$	$C_{9.65}H_{8.96}Cl_{0.34}O_2$	$C_{9.52}H_{7.47}Cl_{0.48}F_{1.54}O_2$
Formula weight	175.86	169.22	200.35
Temperature, (K)	293(2)	293(2)	293(2)
λ, Å	0.71073	0.71073	1.54184
Crystal system	Monoclinic	Monoclinic	Monoclinic
Space group	P2$_1$/c	P2$_1$/c	P2$_1$/c
a, (Å)	13.8829(12)	14.0353(18)	14.4431(12)
b, (Å)	4.9214(5)	4.9551(7)	4.9249(3)
c, (Å)	12.3713(9)	12.4727(17)	12.8777(10)
α, (°)	90	90	90
β, (°)	94.019(5)	93.848(12)	92.457(7)
γ, (°)	90	90	90
Volume, (Å^3)	843.17(13)	865.5(2)	915.16(12)
Z	4	4	4
Density (calculated), (Mg/m^3)	1.385	1.299	1.454
Absorption coefficient, (mm^{-1})	2.672	0.192	2.301
F(000)	365	355	411
Crystal size, (mm^3)	0.7 x0.3 x0.08	0.30 x 0.16 x 0.08	0.18 x 0.05 x 0.03
Reflections collected	2950	3941	3106
Independent reflections	1880	2044	1739
R(int)	0.0308	0.0627	0.0220
Goodness-of-fit on F^2	1.074	1.015	1.115
Final R$_1$ indices [I>2sigma(I)]	0.0581	0.0771	0.0521
Final wR$_2$	0.1585	0.1897	0.1588
R$_1$ indices (all data)	0.0701	0.1595	0.0737
wR$_2$ (all data)	0.1780	0.2399	0.1752

	γ-3-ClCA/3-CF$_3$CA (AA)	γ-3-BrCA/3-MeCA (MeOH)	γ-3-BrCA/3-MeCA (AA)
Formula	$C_{9.70}H_7Cl_{0.30}F_{2.09}O_2$	$C_{9.33}H_{7.98}Br_{0.67}O_2$	$C_{9.54}H_{8.61}Br_{0.46}O_2$
Formula weight	205.74	205.81	192.19
Temperature, (K)	293(2)	293(2)	150(2)
λ, Å	1.54184	0.71073	0.71073
Crystal system	Monoclinic	Monoclinic	Monoclinic
Space group	P2$_1$/c	P2$_1$/c	P2$_1$/c
a, (Å)	14.4998(9)	14.4231(10)	14.332(2)
b, (Å)	4.9391(3)	4.9128(3)	4.9108(11)
c, (Å)	12.9365(7)	12.3548(11)	12.250(3)
α, (°)	90	90	90
β, (°)	92.211(5)	94.836(7)	95.00(2)
γ, (°)	90	90	90
Volume, (Å^3)	925.77(9)	872.32(11)	858.9(3)
Z	4	4	4
Density (calculated), (Mg/m^3)	1.476	1.567	1.486
Absorption coefficient, (mm^{-1})	1.892	3.165	2.238
F(000)	420	414	392
Crystal size, (mm^3)	0.21 x 0.13 x 0.03	0.25 x 0.10 x 0.06	0.33 x 0.26 x 0.17
Reflections collected	3303	4441	4860
Independent reflections	1781	2108	1601
R(int)	0.0275	0.0257	0.1164
Goodness-of-fit on F^2	1.088	1.160	1.175
Final R$_1$ indices [I>2sigma(I)]	0.0571	0.0440	0.0975
Final wR$_2$	0.1696	0.0847	0.2667
R$_1$ indices (all data)	0.0811	0.0779	0.1379
wR$_2$ (all data)	0.1924	0.0938	0.2984

Continue Table 4.12

	γ-3-BrCA/3-CF₃CA(MeOH)	γ-3-BrCA/3-CF₃CA(AA)
Formula	$C_{9.72} H_7 Br_{0.28} F_{2.15} O_2$	$C_{9.68} H_7 Br_{0.32} F_{2.04} O_2$
Formula weight	219.31	219.69
Temperature, (K)	293(2)	293(2)
λ , Å	1.54184	1.54184
Crystal system	Monoclinic	Monoclinic
Space group	P2₁/c	P2₁/c
a, (Å)	14.540(2)	14.5066(8)
b, (Å)	4.9564(7)	4.9396(3)
c, (Å)	13.011(2)	12.9200(8)
α, (°)	90	90
β, (°)	92.475(14)	92.926(6)
γ, (°)	90	90
Volume, (Å³)	936.7(2)	924.60(10)
Z	4	4
Density (calculated), (Mg/m³)	1.555	1.578
Absorption coefficient, (mm⁻¹)	2.527	2.715
F(000)	442	443
Crystal size, (mm³)	0.30 x 0.12 x 0.01	0.31 x 0.26 x 0.07
Reflections collected	2581	3087
Independent reflections	1589	1768
R(int)	0.0198	0.0133
Goodness-of-fit on F²	1.086	1.096
Final R₁ indices [I>2sigma(I)]	0.0719	0.0776
Final wR₂	0.1999	0.2063
R₁ indices (all data)	0.0835	0.0813
wR₂ (all data)	0.2093	0.2084

4.3.4.b. Cocrystallization from melt

The results from Chapter 3 revealed that both 3-ClCA and 3-BrCA crystallized in the *β* form from the melt. Therefore, described in this section is a further study that was carried out to investigate the cocrystallization from melt of these acids with other acids, with the aim of obtaining the *β* form of the solid solution material.

For this, 1:1 molar ratios of different acids were prepared (*γ*-3-ClCA:*γ*-3-MeCA, *γ*-3-ClCA:*γ*₁-3-CF₃CA, *γ*-3-BrCA:3MeCA and *γ*-3-BrCA:*γ*₁-3-CF₃CA) and then subjected to two DSC cycles. The first cycle was to heat the material from 40 °C until they melted and then cooling to 40 at 20 °C/min. The second cycle was a repeat of the first cycle on the product. The samples from the DSC pans were recovered after these two cycles and characterized by PXRD analysis.

3-ClCA/3-MeCA

For the *γ*-3-ClCA:*γ*-3-MeCA mixture, the first heating cycle showed multiple endothermic peaks, corresponding to the melting of the constituent materials in the mixture. In contrast, the second DSC cycle showed only one endothermic peak, suggestive of only one entity. PXRD of the sample after the DSC experiments showed

a pattern identical to that calculated for γ-3-ClCA/3-MeCA solid solution (the structure was discussed in Section 4.3.4.a) and, interestingly, there was no indication of the formation of the β-3-ClCA structure. This suggests an inhibitory effect of 3-MeCA on the formation the β-3-ClCA structure during cocrystallization from the melt (see Figure 4.36). The pure 3-ClCA crystallized in the β form from the melt (discussed in Chapter 3).
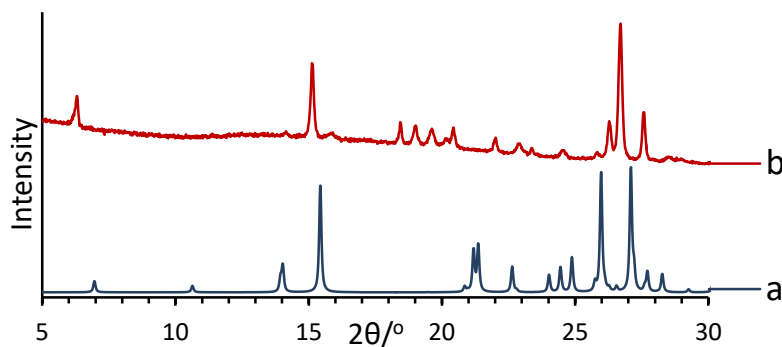
Figure 4.36. *(a) The calculated PXRD pattern of β-3-ClCA. (b) The experimental PXRD patterns of 1:1 physical mixture of γ-3-ClCA:γ-3-MeCA, after a second DSC cycle.*

3-ClCA/3-CF₃CA

The DSC experiment for the γ-3-ClCA:γ-3-CF₃CA mixture showed thermograms with multiple endothermic peaks in the first heating cycle but just one endothermic peak in the second heating cycle, indicating the formation of one entity from the melt. PXRD on the sample recovered after the DSC showed the existence of a solid solution of 3-ClCA/3-CF₃CA with a γ structure (similar to both γ-3-ClCA and γ₁-3-CF₃CA). β-3-ClCA and γ₂-3-CF₃CA were obtained for the pure acids from the melt and hence the acids prevented each other from behaving like the pure acids (see Figure 4.37).
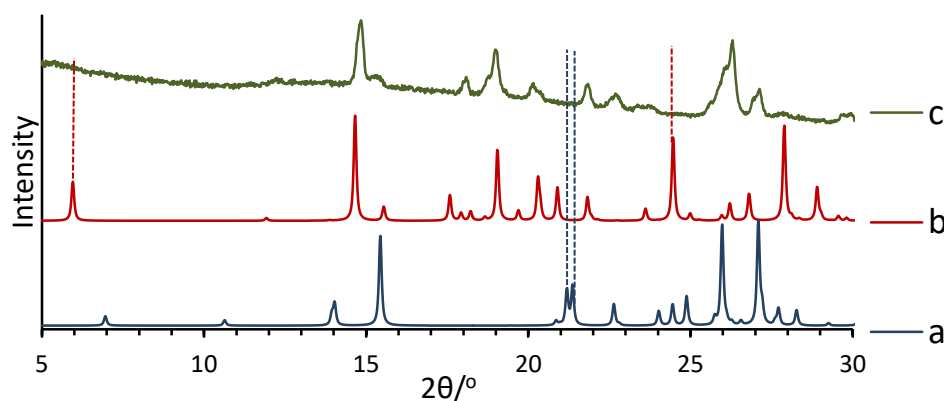
Figure 4.37. *The calculated PXRD pattern of (a) β-3-ClCA and (b) γ₂-3-CF₃CA. (c) The experimental PXRD patterns of 1:1 physical mixture of γ-3-ClCA:γ₁-3-CF₃CA after the second DSC cycle. Dashed lines show the missing peaks, indicating the absence of the phase.*

3-BrCA/3-MeCA

The heating cycle of the DSC experiment for the mixture comprising of γ-3-BrCA:γ-3-MeCA showed the expected multiple peaks in the first cycle corresponding to the melting of the distinct materials. However, two endothermic peaks were clearly observed in the second cycle, indicating the possibility of the existence of two distinct materials. PXRD of the sample recovered after the second cycle of DSC showed that the pattern with two sets of peaks; one for a crystal structure similar to both γ-3-BrCA and γ-3-MeCA and another for a crystal structure similar to β-3-BrCA (Figure 4.38). The result in this case indicates that the 3-MeCA has only some inhibitory effect on the crystallization of 3-BrCA in the β form from melt. Thus, instead of forming one structure similar to β-3-BrCA, two structures were produced. Unfortunately, the structure of a solid solution similar to β-3-BrCA could not be determined directly because of the powdery nature of the material recovered after the DSC experiment.
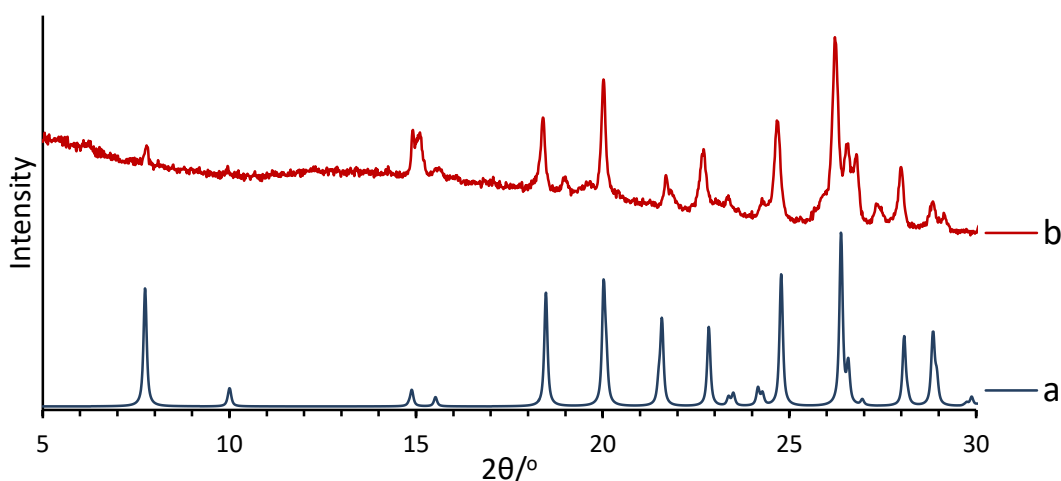
Figure 4.38. *(a) The calculated PXRD pattern of β-3-BrCA. (b) The experimental PXRD patterns of a 1:1 physical mixture of γ-3-BrCA:γ-3-MeCA after the second DSC cycle.*

3-BrCA/3-CF₃CA

For a mixture that comprises γ-3-BrCA:γ_1-3-CF$_3$CA, a similar behaviour in the thermogram to γ-3-BrCA:γ-3-MeCA was observed in the two DSC cycles. Unfortunately, the PXRD of the samples recovered after DSC showed a pattern that was different from the PXRD patterns of any possible known structures (such as γ, γ_2 and β 3-BrCA and γ_1-3-CF$_3$CA). However, some peaks in the pattern showed a similarity to γ_2-3-CF$_3$CA but not conclusively (Figure 4.39)
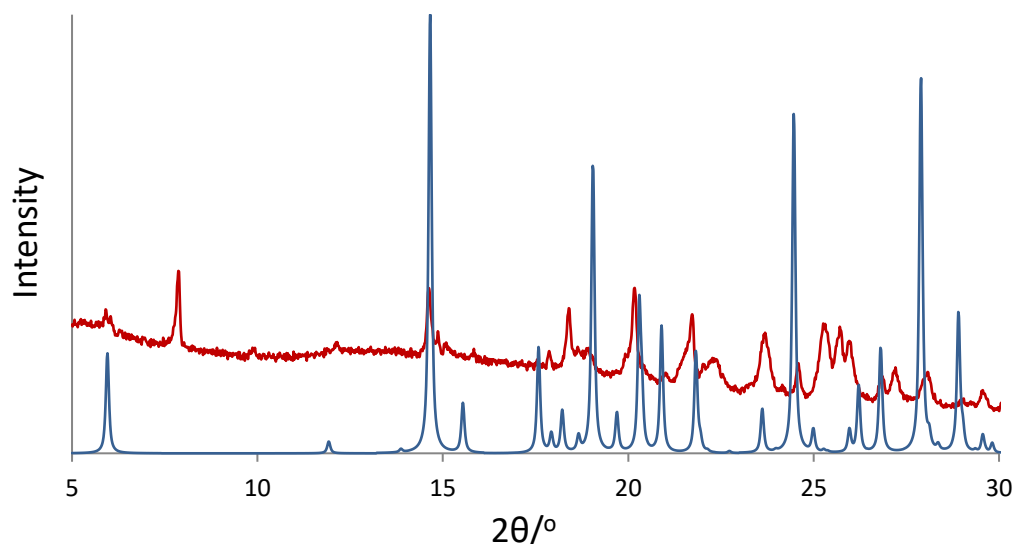
Figure 4.39. *The calculated PXRD pattern of γ₂-3-CF₃CA in blue, and the experimental PXRD pattern of a 1:1 physical mixture of γ-3-BrCA:γ₁-3-CF₃CA after the second DSC cycle in red.*

4.4. Conclusion

In this chapter the cocrystallization of different acids in binary systems resulting in a total of 12 crystal structures of solid solutions has been achieved. The general observations can be summarized as follows:

1- Solid solutions observed in this study showed that binary system of chloro/bromo, fluoro/bromo, methyl/trifluoromethyl, chloro/methyl, chloro/trifluoromethyl, bromo/methyl and bromo/trifluoromethyl *meta*-substituted cinnamic acid can occupy the same crystal with different ratios. Each substituent has electronic and size factor effects and, thus, different contributions of different substituents is expected, in term of interactions and close-packing. This has an influence on the structure of the solid solution material obtained. In other words, the identity of the substituents can influence the structure formed. This study showed that a solid solution of a binary system that comprises different parent forms of cinnamic acids is isostructural to either one or other of the parent materials.

2- For a binary system of γ-3-BrCA/3-ClCA solid solution, it is not surprising that a continuous γ solid solution is formed due to the isostructurality of γ-3-ClCA and γ-3-BrCA, consistent with the Kitaigorodsky proposal[41,28]. However, the combination of thermal analysis (DSC) with PXRD indicates that 3-BrCA and 3-ClCA form two types of substitutional *β*-solid solutions, one isostructural with *β*-3-BrCA and the

other with β-3-ClCA. The crystal structure of the solid solution obtained depends on the relative amounts of the two components. Starting with the structure of β-3-BrCA, molecules of 3-ClCA can be introduced up to a molar ratio of *ca.* 3:1 (3-ClCA/3-BrCA) beyond which the switch occurs to a structure similar to that of β-3-ClCA. The β-3-ClCA/3-BrCA solid solution was obtained from cocrystallization from solution, from melt, and interestingly, from sublimation as well. Surprisingly, SC-SC transformation of the γ-3-ClCA/3-BrCA solid solution to the β-3-ClCA/3-BrCA solid solution was confirmed by single crystal structure determination. The C=C groups of the adjacent molecules of β-3-ClCA/3-BrCA solid solution shows an optimum geometry for the photodimerization reaction.

3- Similarly and surprisingly, the study of the 3-BrCA/3-FCA binary system revealed the preference for formation of solid solution rather than a stoichiometric cocrystal. Thus, four types of substitutional solid solutions were observed for this binary system; three structures showed isostructurality to the 3-BrCA polymorphs (γ, γ_2 and β), and another substitutional solid solution to β-3-FCA. In contrast, thermal analysis using DSC with PXRD indicated that there is a limit to the amount of one type of molecule that can be accommodated into the structure of another. Thus, 3-BrCA and 3-FCA form two types of substitutional β-solid solutions and the maximum amount of 3-FCA molecules that can be introduced in the structure of 3-BrCA is only up to 1 molecule for 8 of 3-BrCA. This ratio is consistent with the result obtained from the determination of the structure for several crystals from different crystallization batches. It is also worth noting that structure determination showed that the solid solution that comprises 3-BrCA/3-FCA can also be obtained with a structure that is isostructural to β_1-3-FCA. In this structure, up to approximately 1 molecule of 3-BrCA can be introduced for every 10 molecules of 3-FCA. It also worth noting that the formation of a solid solution of a binary system of 3-BrCA and 3-FCA was possible despite the fact that none of the 3-BrCA polymorphs shows isostructurality to the 3-FCA polymorphs.

4- The results from the study of the cocrystallization from the melt of some binary systems showed that introducing small amounts of one acid to another as a molten mixture can lead to different structural products than would be expected when compared to the pure acids. In the case of a binary system of 3-MeCA/3-CF$_3$CA, for

example, cocrystallization from melt by introducing a small amount of 3-MeCA to 3-CF_3CA (in approximately a 1:4 molar ratio) produced a solid solution with a structure similar to γ_1-3-CF_3CA, rather than γ_2-3-CF_3CA which pure 3-CF_3CA crystallized in the γ_2 form from melt. Introducing a smaller amount of 3-MeCA (1:8) leads to solid solutions of γ_2-3-CF_3CA. Clearly, 3-MeCA here has a destabilizing effect on the formation of the γ_2-3-CF_3CA structure.

5- The results also showed that it is difficult to form the pure β structure of solid solutions of binary systems that comprise 3-ClCA/3-MeCA, 3-ClCA/3-CF_3CA, 3-BrCA/3-MeCA and 3-BrCA/3-CF_3CA. However, cocrystallization of 3-BrCA and 3-CF_3CA from GAA indicated by PXRD analysis the existence of a β structure (may be 3-BrCA/3-CF_3CA solid solution) similar to β-3-BrCA, together with γ-3-BrCA/3-CF_3CA. Similarly, cocrystallization of 3-BrCA and 3-MeCA from melt produced the β structure of 3-BrCA/3-MeCA commitment with the γ solid solution as shown by PXRD.

4.5. References

1   D. B. Varshney, G. S. Papaefstathiou and L. R. MacGillivray, *Chem. Commun.*, 2002, **646**, 1964–1965.

2   S. Chen, H. Xi, R. F. Henry, I. Marsden and G. G. Z. Zhang, *CrystEngComm*, 2010, **12**, 1485–1493.

3   A. V. Trask, W. D. S. Motherwell and W. Jones, *Int. J. Pharm.*, 2006, **320**, 114–123.

4   J. A. R. P. Sarma and G. R. Desiraju, *J. Am. Chem. Soc*, 1986, **108**, 2791–2793.

5   E. Schur, E. Nauha, M. Lusi and J. Bernstein, *Chem. Eur. J.*, 2015, **21**, 1735–1742.

6   D. Cinčić, T. Friščić and W. Jones, *New J. Chem.*, 2008, **32**, 1776–1781.

7   J. A. R. P. Sarma and G. R. Desiraju, *J. Chem. Soc. Perkin Trans. II.*, 1987, 1187–1193.

8   C. Vithana, H. Uekusa, A. Sekine and Y. Ohashi, *Acta Crystallogr. Sect. B*, 2002, **58**, 986–997.

9   Y. Maekawa, P.-J. Lim, K. Saigo and M. Hasegawa, *Macromolecules*, 1991, **24**, 5752–5755.

10   R. D. Willett, R. E. Butcher, C. P. Landee and B. Twamley, *Polyhedron*, 2006,

25, 2093–2100.

11   J. D. Hung, M. Lahav, M. Luwisch and G. M. J. Schmidt, *Isr. J. Chem.*, 1972, **10**, 585–599.

12   M. D. Cohen and R. Cohen, *J. Chem. Soc. Perkin II*, 1976, 1731–1735.

13   S. Ahn, K. D. M. Harris, B. M. Kariuki and D. M. S. Zin, *J. Solid State Chem.*, 2001, **156**, 10–15.

14   A. Pedretti, L. Villa and G. Vistoli, *J. Mol. Graph. Model.*, 2002, **21**, 47–49.

15   S. Ebenezer, P. T. Muthiah and R. J. Butcher, *Cryst. Growth Des.*, 2011, **11**, 3579–3592.

16   G. M. J. Schmidt, *J. Chem. Soc.*, 1964, 2014–2021.

17   C. J. Pickard and F. Mauri, *Phys. Rev. B Condens. Matter Mater. Phys.*, 2001, **63**, 245101/1–245101/13.

18   J. R. Yates, C. J. Pickard and F. Mauri, *Phys. Rev. B Condens. Matter Mater. Phys.*, 2007, **76**, 024401/1–024401/11.

19   S. Kanao, S. Kashino and M. Haisa, *Acta Crystallogr. Sect. C*, 1990, **46**, 2436–2438.

20   A. Dey and G. R. Desiraju, *CrystEngComm*, 2004, **6**, 642–646.

21   E. Lu, N. Rodríguez-Hornedo and R. Suryanarayanan, *CrystEngComm*, 2008, **10**, 665–668.

22   A. Fuliaş, G. Vlase, T. Vlase, L.-M. Şuta, C. Şoica and I. Ledeţi, *J. Therm. Anal. Calorim.*, 2015, **121**, 1081–1086.

23   H.-L. Lin, G.-C. Zhang and S.-Y. Lin, *J. Therm. Anal. Calorim.*, 2015, 679–687.

24   A. R. Denton and N. W. Ashcroft, *Phys. Rev. A*, 1991, **43**, 3161–3164.

25   L. Padrela, M. A. Rodrigues, S. P. Velaga, H. A. Matos and E. G. de Azevedo, *Eur. J. Pharm. Sci.*, 2009, **38**, 9–17.

26   F. Giordano, R. Bettini, C. Donini, A. Gazzaniga, M. R. Caira, G. G. Z. Zhang and D. J. W. Grant, *J. Pharm. Sci.*, 1999, **88**, 1210–1216.

27   M. a. Oliveira, M. L. Peterson and D. Klein, *Cryst. Growth Des.*, 2008, **8**, 4487–4493.

28   A. I. Kitaigorodsky, *Mixed Crystals*, Springer-Verlag, Berlin Heidelberg, 1984.

29   J. J. Kinnun, A. Leftin and M. F. Brown, *J. Chem. Ed.*, 2013, **90,** 123–128.

30   C. E. Hughes, P. A. Williams, V. L. Keast, V. G. Charalampopoulos, G. R. Edwards-Gau and K. D. M. Harris, *Faraday Discuss.*, 2015, **179**, 115–140.

31   R. K. Harris, *Analyst*, 2006, **131**, 351–373.

32   A. E. Aliev, K. D. M. Harris, P. J. Barrie and S. Camus, *J. Chem. Soc. Faraday trans*, 1994, **90**, 3729–3730.

33   H. Eckert, J. P. Yesinowski, D. J. Sandman and C. S. Velazquez, *J. Am. Chem. Soc.*, 1987, **109**, 761–768.

34   A. E. Aliev, K. D. M. Harris, R. K. Harris, S. A. Carss and A. C. Olivieri, *J. Chem. Soc. Faraday trans.*, 2000, **91**, 3167–3176.

35   R. P. Chapman, C. M. Widdifield and D. L. Bryce, *Prog. Nucl. Magn. Reson. Spectrosc.*, 2009, **55**, 215–237.

36   U. Sukkha, W. Vittayakorn, R. Muanghlua, S. Niemcharoen, B. Boonchom and N. Vittayakorn, *J. Am. Ceram. Soc.*, 2012, **95**, 3151–3157.

37   Y. J. Zhou, Y. Zhang, F. J. Wang and G. L. Chen, *Appl. Phys. Lett.*, 2008, **92**, 241917/1–241917/3.

38   S. Aitipamula, A. B. H. Wong, P. S. Chow and R. B. H. Tan, *CrystEngComm*, 2012, **14**, 8193–8198.

39   A. Buanz, T. J. Prior, J. C. Burley, B. T. Raimi-Abraham, R. Telford, M. Hart, C. C. Seaton, P. J. Davies, I. J. Scowen, S. Gaisford and G. R. Williams, *Cryst. Growth Des.*, 2015, 3249–3256.

40   D. Braga, F. Grepioni, L. Maini, M. Polito, K. Rubini, M. R. Chierotti and R. Gobetto, *Chem. Eur. J.*, 2009, **15**, 1508–1515.

41   A. I. Kitaigorodsky, *Physical Chemistry: Molecular Crystals and Molecules*, Academic Press, New York and London, 1973.

42   J. A. R. P. Sarma and G. R. Desiraju, *J. Am. Chem. Soc.*, 1985, 1905–1912.

43   B. Omondi, A. Lemmerer, M. A. Fernandes, D. C. Levendis and M. Layh, *Acta Crystallogr. Sect. B*, 2014, **70**, 106–114.

44   C. Capacci-Daniel, S. Dehghan, V. M. Wurster, J. A. Basile, R. Hiremath, A. A. Sarjeant and J. A. Swift, *CrystEngComm*, 2008, **10**, 1875–1880.

45   W. Jones, C. R. Theocharis, J. M. Thomas and G. R. Desirajub, *J. Chem. Soc., Chem. Commun.,* 1983, 1443–1444.

Chapter 5: Investigation of cinnamates: phase characterization, the role of cations and anions, supramolecular assembly and cocrystallization of mixed cation and anions

5.1. Introduction

In organic solid state chemistry, the chemical properties of the crystalline solids depend on the mode of the crystal packing. Salt formation of the organic acid has been used as an effective tool for the modification of structures, bringing the functional groups together in order for the reaction to occur in the solid state.[1–3] The basis for much of the reasoning that linked the structure and reactivity in solid-state is the pioneering work of Schmidt.[4,5] Thus, ionic interactions in an organic salt can be used to influence the packing of the molecules as interaction is strong and comparable with the hydrogen bonds due to the charge association.[6,7]

Salt formation of some organic acids has been shown to be an effective tool in steering the molecules, in order to bring the reactive group (such as C=C), into a favourable arrangement for a solid-state photodimerization reaction. For instance, converting azastilbenes to their HCl salts enables the reactive double bonds to undergo the photodimerization reaction in solid state.[1] In another example, ethylenediamine and several cinnamic acids produced cinnamate salts that underwent the photodimerization reaction to yield β-truxinic acid derivatives.[8] Additionally, several cinnamates show an ideal arrangement of reactive double bonds (for example, K-3-Br-cinnamate,[9] K-3-Cl-cinnamate[9] NH$_4$-3-Br-cinnamate,[10] NH$_4$-3-Cl-cinnamate, NH$_4$-3-Br-cinnamte/cinnamic acid[10] and Na-2-Cl-cinnamate[11]). This is however not always the case, Mg-cinnamate,[11] and Mg-4-Cl cinnamate[12] for example, show a non-optimum arrangement of double bonds of adjacent units.

The prime aim of the work described in this chapter was to investigate the effect of utilizing cations (K$^+$ and NH$_4^+$) to influence packing of the different *meta*-substituted cinnamic acids investigated in Chapter 3. The hope was that this may lead to different crystal structures with appropriate properties for the topochemical reaction. The study was extended to examine the effect of the aromatic *meta*-ring substituents (Cl, Br, F, CH$_3$

and CF$_3$) on the crystal architecture, with an overall goal of applying the knowledge gained in designing crystalline materials with ideal double bond geometry for a 2+2 photodimerization reaction.

For the study, K$^+$ and NH$_4^+$ salts of different substituted cinnamic acids (3-BrCA, 3ClCA, 3-FCA, 3-MeCA and 3-CF$_3$CA) were prepared and crystallized. Characterization was by SC-XRD, followed by PXRD to characterize the bulk of the materials. The structures were analysed with the aim of exploring the structural properties of different related salts.

Investigation was then carried out to assess the feasibility of cocrystallization of the K$^+$ or NH$_4^+$ salt of binary anion systems. 3-BrCA was one of anion in these binary systems in this study.

Finally, the formation of the mixed cation (K$^+$/NH$_4^+$) solid solution salt of 3-BrCA and 3-ClCA, was also investigated.

5.2. Experimental Methods

A wide range of crystallization experiments were carried out in order to prepare different *meta*-substituted cinnamic acid salts and their solid solutions, with the aim of obtaining single crystals suitable for SC-XRD. The slow solvent evaporating method was used for all crystallization experiment in this chapter.

5.2.1. Preparation of potassium and ammonium salts of *meta*-substituted cinnamic acid

3-ClCA salts

Based on the reported preparation,[9] a solution of 3-ClCA in EtOH was added to a solution of KOH in water in a molar ratio of 1:1. On crystallization, PXRD showed a pattern similar to that of the known structure of K-3-chloro cinnamate[9] (K-3-ClCate), denoted as structure I. There were additional peaks in the pattern corresponding to the structure of K-3-chloro cinnamate/3-chloro cinnamic acid (K-3-ClCate/3-ClCA), denoted as structure II, which will be discussed later in this chapter (Section 5.3.1.a). Repeating the same procedure, using a solution of 3-ClCA in 50/50v MeOH/EtOH instead of EtOH, gave a mixture of the same two structures (I and II). However,

preparation by dissolving the acid in a solution of KOH produced structure I contaminated with traces of structure II.

Preparation of the NH_4^+ salt of 3-ClCA was achieved by adding a solution of the acid in MeOH to a NH_4OH solution to produce the known phase of NH_4-3-chloro cinnamate/3-chloro cinnamic acid (NH_4-3-ClCate/3-ClCA). In this study, preparation of NH_4-3-chloro cinnamate (NH_4-3-Clcate)[10] was not successful.

3-BrCA salts

It was reported that adding a solution of 3-BrCA in EtOH to a solution of KOH in water in a molar ratio of 1:1 and then allowing the solvent to evaporate, yielded crystals of K-3-bromo cinnamate[9] (K-3-BrCate). In this study the results showed that either repeating this procedure or instead, dissolving the 3-BrCA in a solution of KOH, resulted in a monophasic sample of K-3-BrCate.

In order to prepare the NH_4^+ salt of 3-BrCA, the first attempt at preparation was carried out according to the reported procedure.[10] A solution of 3-BrCA in MeOH was added to a solution of NH_4OH. The crystallized material was shown by PXRD to have the structure of NH_4-3-bromo cinnamate/3-bromo cinnamic acid (NH_4-3-BrCate/3-BrCA), denoted as phase I. However, repeating the preparation (2nd attempt) of the salt using the same method produced a new phase of NH_4-3-BrCate/3-BrCA (designated as phase II), and is discussed later in this chapter (Section 5.3.1.b). For a further investigation the preparation was repeated (3rd attempt) but this time with new glass ware in a different laboratory, to avoid the seeding effect. Surprisingly, this mainly resulted in phase II. Another preparation of the salt (4th attempt), by dissolving the acid in a solution of NH_4OH, resulted again in the crystals of phase II. It was not possible to produce NH_4-3-BrCA[10] despite many attempts.

3-FCA, 3-MeCA and 3-CF₃CA salts

The K^+ salt of 3-FCA was obtained by either adding a solution of 3-FCA in MeOH to a solution of KOH or dissolving the acid directly in a KOH solution. A similar procedure was followed in order to prepare NH_4^+ salt by using a solution of NH_4OH in water instead of KOH. The same procedures were followed in the preparation of NH_4^+ and K^+ salts of 3-MeCA and 3-CF₃CA. Apart from the K^+ salt of 3-CF₃CA, characterization of

the materials from all crystallization attempts by PXRD revealed mono phasic samples (detailed in the Results and Discussion section). However, in the case of the K^+ salt of 3-CF$_3$CA, KHCO$_3$[13] was observed in addition to anther phase (discussed in Section 5.3.1.e).

5.2.2. Preparation of potassium and ammonium salts of binary systems of *meta*-substituted cinnamic acids

Solid solutions of the K^+ salt were prepared by dissolving of 1:1 molar ratios of 3-BrCA:3-ClCA, 3-BrCA:3-FCA, 3-BrCA:3-MeCA and 3-BrCA:3-CF$_3$CA in a solution of KOH. The solvent was then allowed to evaporate at room temperature. Different molar ratios of some binary systems were also prepared (details in the Result and Discussion section). The solid solutions of the NH$_4^+$ salt were prepared similarly to the K^+ salt using NH$_4$OH instead of KOH solution. The material was characterized by both SC-XRD and PXRD.

5.2.3. Preparation of mixed potassium/ammonium cation salts of 3-BrCA and 3-ClCA

A solution of 1:1 molar ratio of KOH:NH$_4$OH was first prepared and then used to dissolve appropriate amounts of acids (3-BrCA or 3-ClCA). The resultant solutions were stirred until clear and the solvent then allowed to evaporate slowly at room temperature for several days until the sample crystallized.

5.3. Results and Discussion

5.3.1. Potassium and ammonium salts of some *meta*-substituent cinnamic acids: crystal structural determination and structural relations

5.3.1.a 3-Cl cinnamic acid salts

Potassium salts

Preparation of the K^+ salt of 3-ClCA, as shown in the experimental section, resulted in two distinct structure types, denoted in this study as structures I and II. K-3-ClCate (structure I) has been reported previously,[9] whereas K-3-ClCate/3-ClCA (structure II) was determined in this study.

For structure I, the asymmetric unit comprises two cations (K^+ ion) and two anions (3-Clcate). In this structure each cation is coordinated by 6 oxygen atoms. The cations and

carboxylate groups are arranged into a layered structure which is separated by a bilayer of Cl atoms.

In structure II, the asymmetric unit consists of the K^+ cation site, located on the 2-fold rotation axis, and a 3-ClCate/3-ClCA unit. The carboxylic acid proton site lies on an inversion centre of symmetry and is equidistant from the two oxygen atoms of the carboxylic acid/carboxylate group. In this structure, each K^+ cation is coordinated by six oxygen atoms from five different molecules, with the K-O distances 2.708-2.776. Similar to phase I, a layered structure is also observed in form (II). Looking at the structural packing along the b-axis, as seen in Figure 5.1, the contents are arranged to form layers of K^+ cations parallel to the bc plane which are separated by a bilayer of anion/acid units.
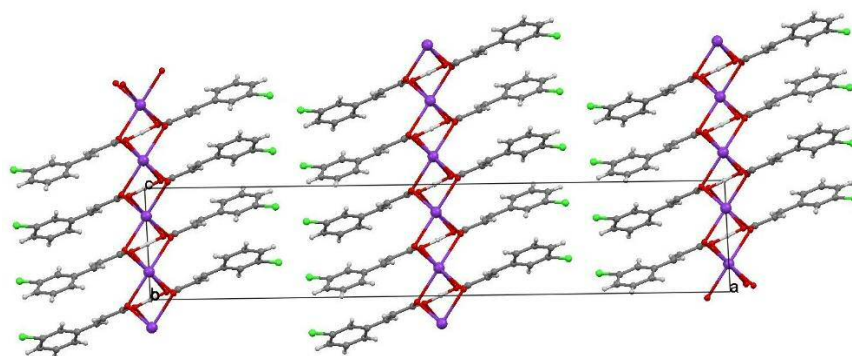
Figure 5.1. *Crystal packing of K-3-ClCate/3-ClCA (structure II) viewed along the b-axis.*

These anion/acid bilayers are interfaced with a bilayer of chlorine atoms in the middle. The shortest distance between Cl in adjacent layers is 3.733Å, making the angles C-Cl···Cl and Cl···Cl-C of 160.49° and 88.33° respectively (Figure 5.2a). Forming a type ii halogen···halogen interaction (discussed in Chapter 1). Viewing the structure along the c-axis, the planes of the anion units in the stack are not parallel and form an angle of approximately 131° to each other. The arrangement of the double bonds is criss-cross, with a 3.996Å distance between the double bond centroids.

Although the structures, II and I[9], have generally similar layered packing, differences exist; (a) Structure II accommodates acid units in addition to the carboxylate units. (b) The acid units in structure II form a hydrogen bond, in the catemer fashion, involving two neighbouring anion/acid units. The distance of O_2···O_2 is 2.460Å and the O_2-H_9···O_2 angle is 180° (Figure 5.2b). The existence of these hydrogen bond interactions may play a possible role in generating the structure. In this structure the double bonds of

neighbouring 3-ClCate/3-ClCA units are not parallel to each other. However, parallel double bond arrangements are observed for structure I with a separation distance of less than 4Å. (c) At the halogen-halogen interface between the bilayers in structure I, the shortest Cl⋯Cl contact is arranged to form type i halogen-halogen interaction. However, in structure II the Cl⋯Cl contact are arranged of type ii (type i and ii of halogen-halogen interaction is discussed in Chapter 1).

It is worth noting that structure II is the only protonated structure that has been discovered among K^+ salts of *meta*-substituents of cinnamic acids. The crystallographic data for structure II is shown in Table 5.1.
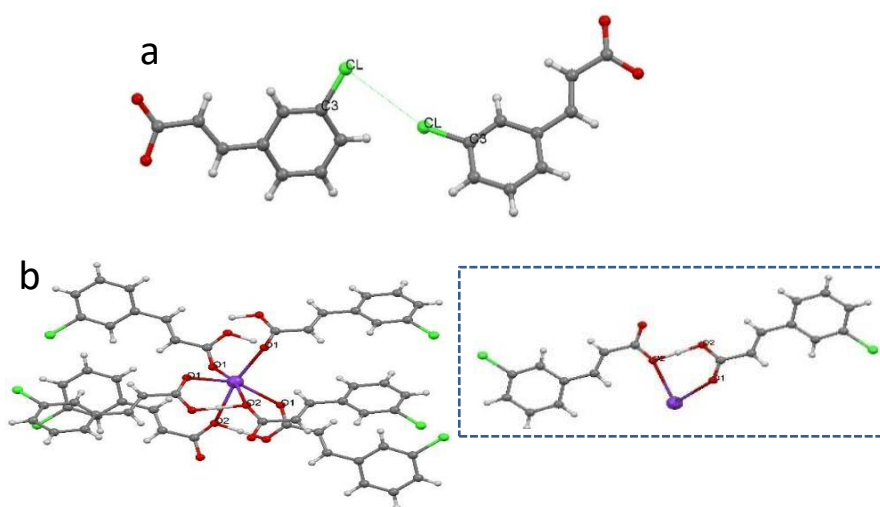
Figure 5.2. *(a) Cl⋯Cl contact geometry. (b) Coordination around K^+ in (K-3-ClCate/3-ClCA) (structure II). The dashed box shows the catemer arrangement.*

Table 5.1. *Crystallographic data for the crystal structure determination of K-3-ClCate/3-ClCA.*

Formula	$C_{18} H_{13} Cl_2 K O_4$	Z	4
Formula weight	403.28	Density (calculated), (Mg/m³)	1.568
Temperature, (K)	150(2)	Absorption coefficient, (mm⁻¹)	0.644
λ, Å	0.71073	F(000)	824
Crystal system	Monoclinic	Crystal size, (mm³)	0.25 0.22 0.14
Space group	C2/c	Reflections collected	2264
a, (Å)	38.9107(16)	Independent reflections	1512
b, (Å)	5.8905(2)	R(int)	0.0135
c, (Å)	7.4585(3)	Goodness-of-fit on F^2	1.074
α, (°)	90	Final R_1 indices [*I*>2sigma(*I*)]	0.0298
β, (°)	92.214(2)	Final wR_2	0.0743
γ, (°)	90	R_1 indices (all data)	0.0326
Volume, (Å³)	1708.24(11)	wR_2 (all data)	0.0761

PXRD analysis of the bulk materials from the crystallization batch from EtOH, as illustrated in Figure 5.3, confirmed the concomitant existence of crystals I and II.
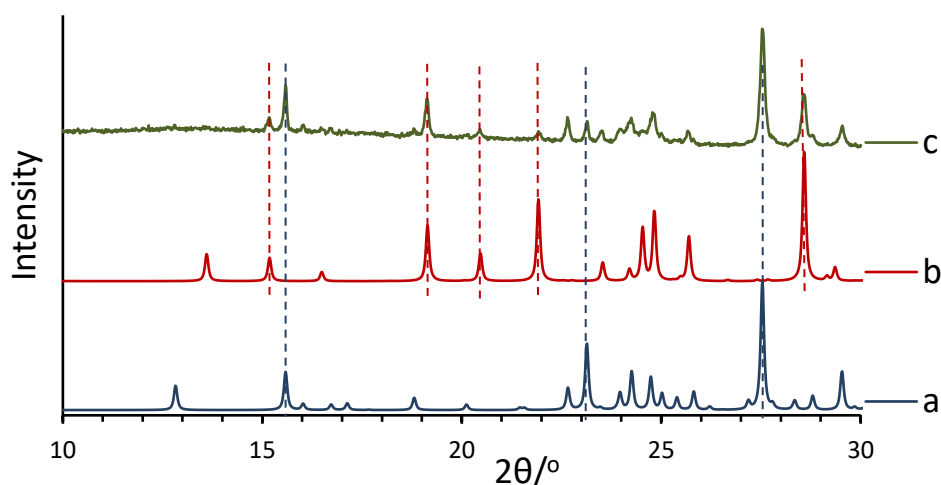
Figure 5.3. *The calculated PXRD pattern of (a) K-3-ClCate[9], (b) K-3-ClCate/3-ClCA (determined at room temperature) and (c) the experimental PXRD of the crystallization of K⁺ salt of 3-ClCA from EtOH. Dashed lines indicate the presence of the phase according to the corresponding colour.*

Ammonium salts

Two structures have been reported for the NH_4^+ salts of 3-ClCA; NH_4-3-ClCate and NH_4-3-ClCate/3-ClCA.[10]

When comparing the NH_4^+ salts of 3-ClCA with the K^+ salts, the structures can be classified in two groups; in one case the acid units are absent from the structure and present in the other. In the former case, K-3-ClCate and NH_4-3-ClCate have been reported by Chowdhury et al.[10] to be isostructural to each other. Similarly, considering the unit cell parameters and packing mode, in the latter case, K-3-ClCate/3-ClCA and NH_4-3-ClCate/3-ClCA are isostructural. On the other hand, in the NH_4-3-ClCate and K-3-ClCate structures, the double bond groups within the stack are parallel and separated by less than 4Å, whereas they are misaligned in the structures of NH_4-3-ClCate/3-ClCA and K-3-ClCate/3-ClCA.

5.3.1.b 3-Br cinnamic acid salts

Potassium salt

One crystal structure of K-3-BrCate has been reported.[9] In this structure the anion units and K^+ ion are accommodated in a layered structure. The double bonds are parallel to

each other in molecular stacks and separated by the ideal distance for the photodimerization reaction (as it will be discussed in Chapter 6).

Ammonium salts

The crystal structures of NH_4-3-BrCate and NH_4-3-BrCate/3-BrCA (designed in this study as phase I), have been determined previously.[10] In both structures, the double bonds of the adjacent anions (in NH_4-3-BrCate) and adjacent cinnamic acid/cinnamate units (in NH_4-3-BrCate/3-BrCA, phase I) are parallel and separated by less than 4Å.

However, investigation of salt preparation and crystallization revealed a crystal structure of NH_4-3-BrCate/3-BrCA (designed as phase II) which is different from the one previously reported[10]. In the structure, an NH_4^+ ion site lies on the 2-fold rotational axis, resulting in the presence of half an NH_4^+ ion in the asymmetric unit. The asymmetric unit also contains a 3-Br-Cate anion with the carboxylic acid proton disordered between two oxygen atoms of the carboxylic acid/carboxylate group. Crystallographic data is shown in Table 5.2.

Table 5.2. *Crystallographic data for the crystal structure determination of NH_4-3-BrCate/3-BrCA (phase II).*

Formula	$C_{18} H_{17} Br_2 N O_4$	Z	4
Formula weight	471.15	Density (calculated), (Mg/m³)	1.704
Temperature, (K)	293(2)	Absorption coefficient, (mm⁻¹)	5.797
λ, Å	1.54148	F(000)	936
Crystal system	Monoclinic	Crystal size, (mm³)	0.19 x 0.14 x 0.02
Space group	C2/c	Reflections collected	3458
a, (Å)	39.911(2)	Independent reflections	1817
b, (Å)	6.0097(2)	R(int)	0.0326
c, (Å)	7.6700(5)	Goodness-of-fit on F²	1.062
α, (°)	90	Final R_1 indices [I>2sigma(I)]	0.0993
β, (°)	93.211(6)	Final wR_2	0.2857
γ, (°)	90	R_1 indices (all data)	0.1033
Volume, (Å³)	1836.78(17)	wR_2 (all data)	0.2903

In this structure, NH_4^+ ions form layers parallel to the bc plane, separated by bilayers of cinnamate/cinnamic acid units, in a similar manner to the structure of NH_4-3-ClCate/3-ClCA. However, in this structure as seen in Figure 5.4b, the stacks of units along the c-axis show that the cinnamate/acid units are not aligned. They are rotated by 139.23° in relation to each other, which results in an unparallel alignment of the double bond through the stack. Viewing the structure along the [010] direction, the cinnamate/acid units are interfaced by a hydrophobic bilayer of bromine atoms. In these bilayers, the Br atoms are in contact via type ii halogen-halogen interaction (Figure 5.4b, shown by the

dashed line), making an angle of *ca.* 88° for C-Br···Br and 159.4° for Br···Br-C. The distance between Br···Br (3.849Å) is just longer than the sum of Br radii (3.7Å)[14]. Each NH_4^+ cation is in contact with four oxygen atoms from different cinnamic acid/cinnamate units with hydrogen bond distances ranging from *ca.* 2.8 to 2.9 Å. The cinnamic acid/cinnamate units form a catemer arrangement with a distance between the $O_1···O_1$ of 2.519Å and an angle O_2-$H_1···O_2$ of 176.27°. A similar arrangement is observed for phase I.

Comparing the NH_4^+ protonated salts, NH_4-3-BrCate/3-BrCA (phase I and II), shows that both structures have a similar layered structure. However, the two structures are not identical. The most striking difference between the structures is that, through the arrangement of the molecules (referred as stack) along the c-axis, the cinnamate/cinnamic acid units in one half of a bilayer are aligned in parallel to each other in phase I, but their alignment are not parallel in phase II (see Figure 5.4 a and b). This arrangement provides an ideal double bonds geometry for photodimerization in phase I and, in contrast, a criss-cross arrangement of double bonds for phase II.
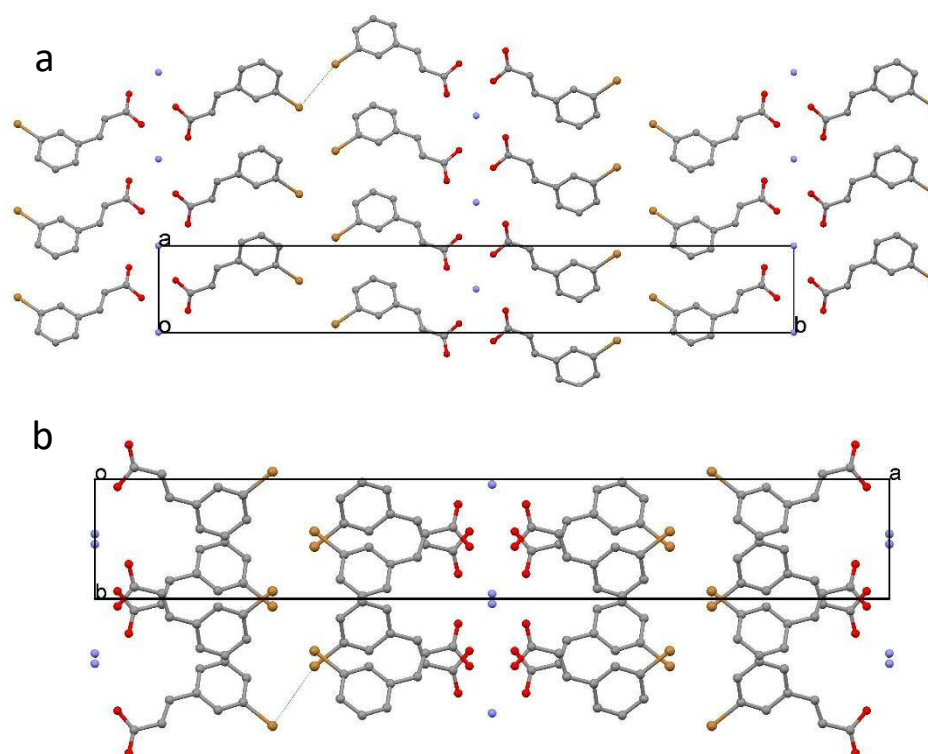
Figure 5.4. *Crystal packing of NH_4-3-BrCate/3-BrCA (a) phase I and (b) phase II showing the layered structure. Hydrogen atoms are omitted for clarity.*

Another important difference of these structures relates to the π-interactions of the benzene rings (Figure 5.5 a and b). In phase I, $\pi\cdots\pi$ interactions (offset stacks) are observed and the distance between the benzene ring centroid is only 3.954Å. However C–H$\cdots\pi$ interactions (edge-to-face interactions) are observed in phase II, where the distance of C(2)$\cdots\pi$ is 3.821Å. In contrast, the Br$\cdots$Br contacts in the interface bilayer are similar in both structures where type ii geometry (discussed earlier in the Chapter 1) is seen.
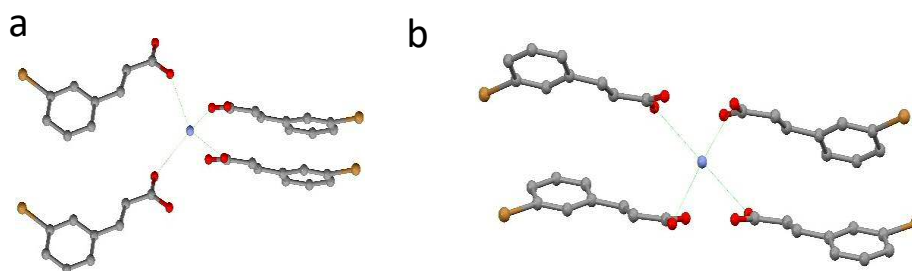
Figure 5.5. *The arrangement of molecules in NH₄-3-BrCate/3-BrCA (a) phase I and (b) phase II.*

PXRD analysis of the bulk materials from various crystallization attempts, as seen in Figure 5.6, confirmed the existence in phases I and II of NH₄-(3-BrCate/3-BrCA).
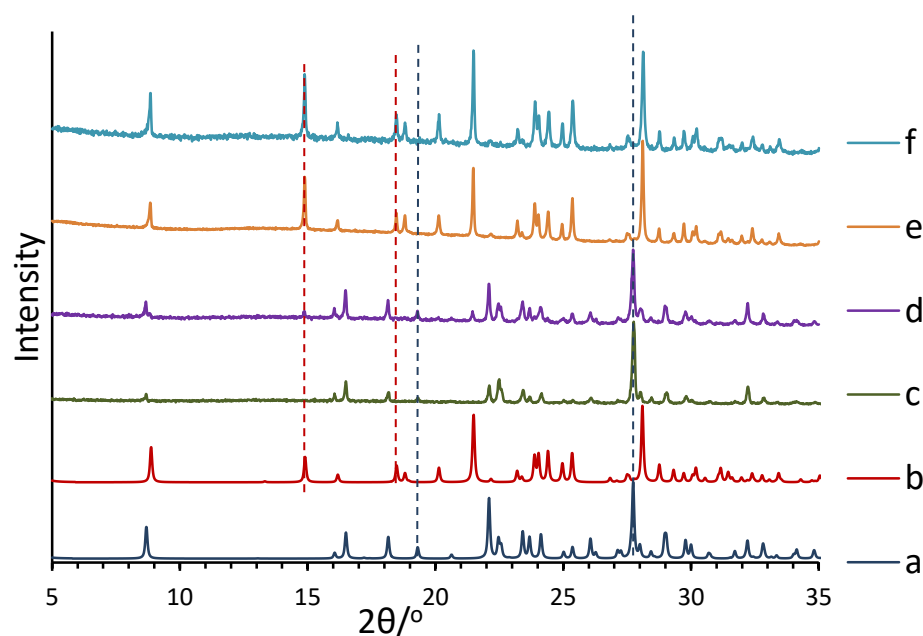
Figure 5.6. *The calculated PXRD pattern of (a) NH₄-3-BrCate/3-BrCA,[10] (b) NH4-3-BrCate/3-BrCA (phase II). (c), (d), (e) and (f) are the experimental PXRD of 1ˢᵗ, 2ⁿᵈ, 3ʳᵈ and 4ᵗʰ crystallization attempts as presented in the experimental section. Dashed lines aid in the identification of the phases.*

5.3.1.c 3-F-cinnamic acid salts

No crystal structure has been reported for either the NH_4^+ or K^+ salts of 3-FCA. The preparation of these salts and crystallization by SC-XRD and PXRD was therefore carried out.

Potassium salt

K-3-Fluoro cinnamate (K-3-FCate) crystallized in space group $P2_1/c$ with a 3-fluoro-cinnamate anion and one K^+ cation in the asymmetric unit. Crystallographic data is summarized in Table 5.3. In the crystal structure each K^+ cation is surrounded by five 3-fluoro-cinnamate anions and coordinated by six oxygen atoms, with K–O distances ranging from 2.67 to 2.79Å and one with a longer distance of 2.9Å.

Table 5.3. *Crystallographic data for the crystal structure determination of K-3-FCate.*

Formula	$C_9 H_6 F K O_2$	Z	4
Formula weight	204.24	**Density (calculated), (Mg/m^3)**	1.536
Temperature, (K)	293(2)	**Absorption coefficient, (mm^{-1})**	5.127
λ , Å	1.54184	**F(000)**	416
Crystal system	Monoclinic	**Crystal size, (mm^3)**	0.53 x 0.32 x 0.06
Space group	$P2_1/c$	**Reflections collected**	2983
a, (Å)	19.6467(7)	**Independent reflections**	1706
b, (Å)	5.8244(2)	**R(int)**	0.0216
c, (Å)	7.7179(3)	**Goodness-of-fit on F^2**	1.100
α, (°)	90	**Final R_1 indices [I>2sigma(I)]**	0.0356
β, (°)	90.628(3)	**Final wR_2**	0.0926
γ, (°)	90	**R_1 indices (all data)**	0.0422
Volume, ($Å^3$)	883.11(6)	**wR_2 (all data)**	0.0999

The carboxylate anions and K^+ cations form layers parallel to the bc plane, which are separated by bilayers of fluorine atoms. F⋯F atoms in the bilayer are in contact, and the shortest F⋯F distance is 3.074Å (greater than the sum of the Van der Waals radii of fluorine atoms)[14] and the angle C(3)-F(1)⋯F(1)=F(1)⋯F(1)-C(3) is 175.04°. Additionally, fluorine atoms from one layer form weak hydrogen interactions with the H atoms from another layer via C(4)-H(4)⋯F(1), with H⋯F distance of 2.648Å (approximately similar to the sum of the F and H radii 2.67)[14] and a C(4)-H(4)⋯F(1) angle of 148.75° (Figure 5.7). Both C-H⋯F and F⋯F interactions exist here. C-H⋯F reported[15] to be more important in structure direction than F⋯F.
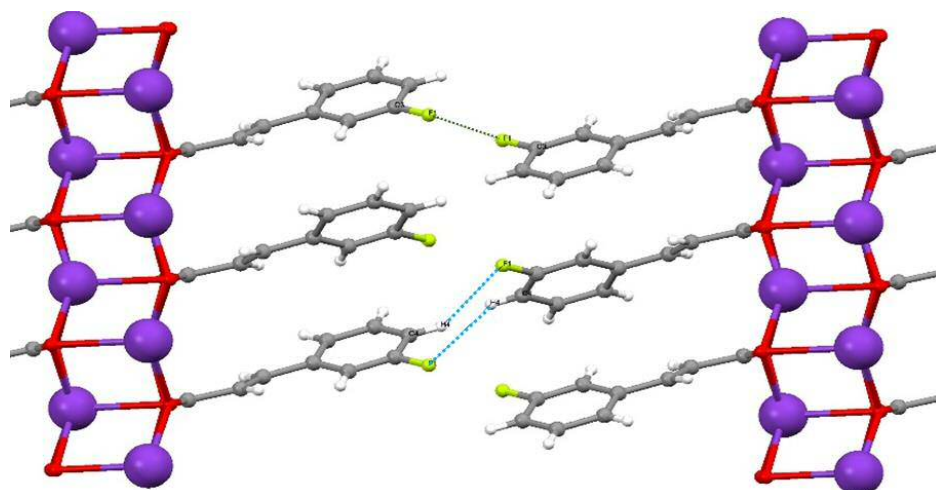
Figure 5.7. *A view of the structure along the b-axis, the blue line represent weak hydrogen interaction, while the green line show the F⋯F contact.*

Viewing the structure along the b-axis (see figure 5.7) shows that the adjacent anions in the stack are not parallel. Their planes form an angle of 138.96° and, as a result, the (C=C) double bonds of the neighbouring anions are not parallel but the distance between their centroids is 4.089Å.

Characterization of the bulk materials produced from the preparation of the K^+ salt of 3-FCA using PXRD revealed a mono-phasic material with the structure determined by SC-XRD.

Ammonium salt

A suitable single crystal of the NH_4^+ salt of 3-FCA was selected and the crystal structure was determined. The result showed that it crystallized in space group of C2/c, with an NH_4^+ cation site and 3-FCate/3-FCA units with a carboxylic acid proton. The proton is disordered between the two hydrogen bonded oxygen atoms of different 3-FCate/3-FCA units, leading to the formation of a catemer pair of two units, with a distance $O_1⋯O_1$ of 2.613Å and an angle $O_1-H_1⋯O_1$ of 173.15°. The 3-FCA/3-FCate unit is disordered in two different conformations of the 3-FCate/3-FCA unit (Figure 5.8). However, the cation is ordered and is positioned on the 2-fold rotational axis. Crystallographic data is shown in Table 5.4.
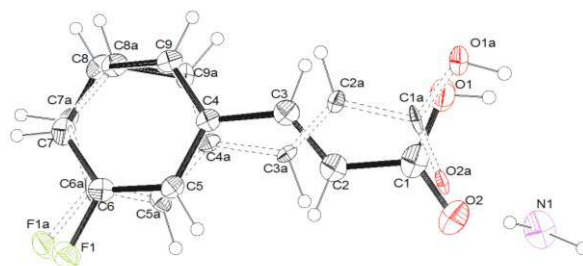
Figure 5.8. Asymmetric unit showing the disorder in 3-FCate/3-FCA unit.

In the description of the crystal structure, only the major component of the disordered group 3-FCate/3-FCA is considered. In the crystal structure, each NH_4^+ cation is surrounded by four 3-FCate/3-FCA units and hydrogen bonds to four oxygen atoms from different carboxylate groups, with two N⋯O distances of *ca.* 2.79 and ca 2.81Å.

Table 5.4. Crystallographic data for the crystal structure determination of NH_4-3-FCate/3-FCA.

Formula	$C_{18} H_{17} F_2 N O_4$	Z	4
Formula weight	349.33	Density (calculated), (Mg/m³)	1.395
Temperature, (K)	150(2)	Absorption coefficient, (mm⁻¹)	0.113
λ , Å	0.71073	F(000)	728
Crystal system	Monoclinic	Crystal size, (mm³)	0.36×0.2×0.1
Space group	C2/c	Reflections collected	3022
a, (Å)	38.7362(17)	Independent reflections	1827
b, (Å)	5.8631(3)	R(int)	0.0248
c, (Å)	7.3578(2)	Goodness-of-fit on F²	1.096
α, (°)	90	Final R_1 indices [I>2sigma(I)]	0.0495
β, (°)	95.576(2)	Final wR_2	0.1122
γ, (°)	90	R_1 indices (all data)	0.0606
Volume, (Å³)	1663.15(12)	wR_2 (all data)	0.1205

Bilayers of 3-FCate/3-FCA and a layer of NH_4^+ cations, parallel to the bc plane, are formed. The hydrophilic layers are separated by bilayers of cinnamate/acid units (see Figure 5.9a). The 3-FCate/3-FCA units are stacked along the c-axis and, within a stack, neighbouring molecules are not aligned parallel to each other but, instead, they are rotated by *ca.* 130° in relation to each other. This arrangement leads to unparalleled double bonds through the stack, separated by a distance of *ca.* 3.737Å.

Another feature of the structure is observed at the interphase in the middle of the bilayer of cinnamate/cinnamic acid units. The shortest F⋯F distance is 3.356Å, longer than the sum of radii of F atoms.[14] On the other hand, each three interphase molecule contact via two (C-H⋯F) weak hydrogen bonds, with a distance of 2.651Å for H(7)⋯F(1) (shorter than the sum of the F and H radii 2.67[14]) and forming a C(7)-H(7)⋯F(1) angle of

153.57° (Figure 5.9b). Consistence with the result observed in the structure of K-3-FCate, both (C-H⋯F) weak hydrogen bonds and F⋯F contacts were observed in the structure.

PXRD showed that the bulk of the material was mono-phasic with the structure determined by SC-XRD.
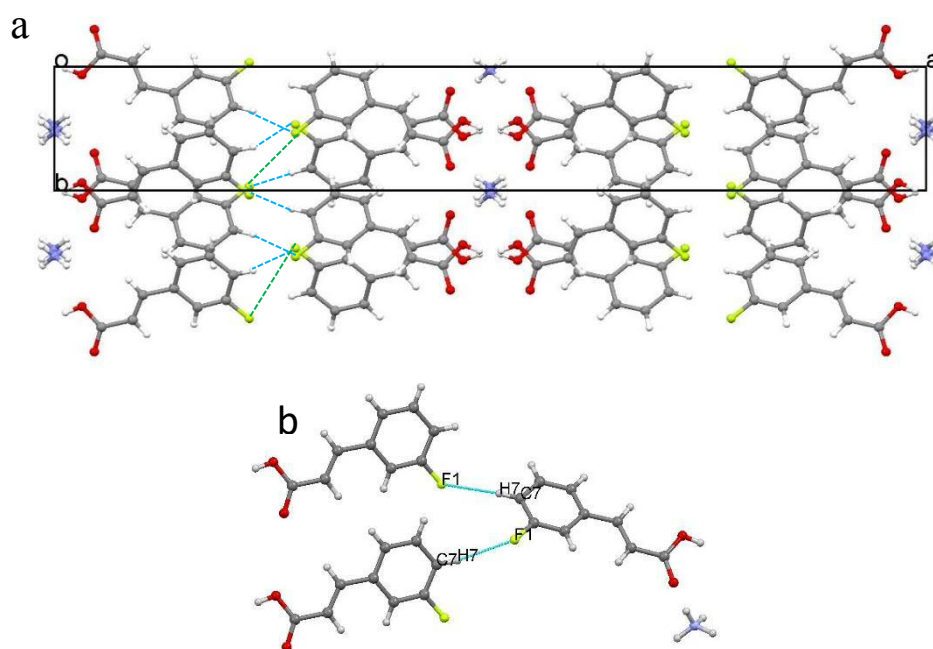
Figure 5.9. *(a) A view of the structure of NH₄-3-FCate/3-FCA along the c-axis. The blue dashed lines represent C-H⋯F weak hydrogen interactions, while green shows the F⋯F contacts. (b) A fragment of the structure showing C-H⋯F interaction.*

Although the structures of both the K⁺ and NH₄⁺ salts of 3-FCA have non-parallel arrangements of the double bond groups, they are different. Thus, the NH₄⁺ salt is protonated with cinnamate/cinnamic acid units while only the cinnamate anion is present in the structure of the K⁺ salt.

5.3.1.d. 3-Methyl cinnamic acid salts
Potassium salt

A suitable single crystal was selected from the crystallization of K-3-methyl-cinnamate (K-3-MeCate), and subjected to SC-XRD analysis. It crystallized in the monoclinic crystal system, space group $P2_1/c$. One 3-MeCate anion and one K⁺ cation constitute the asymmetric unit. Crystallographic data seen in Table 5.5.

Table 5.5. *Crystallographic data for the crystal structure determination of K-3-MeCate.*

Formula	$C_{10} H_9 K O_2$	Z	4
Formula weight	200.27	Density (calculated), (Mg/m³)	1.382
Temperature, (K)	293(2)	Absorption coefficient, (mm⁻¹)	0.514
λ , Å	0.71073	F(000)	416
Crystal system	Monoclinic	Crystal size, (mm³)	0.25 x 0.13 x 0.08
Space group	P2₁/c	Reflections collected	2388
a, (Å)	21.062(4)	Independent reflections	1374
b, (Å)	5.8530(11)	R(int)	0.0611
c, (Å)	7.939(2)	Goodness-of-fit on F²	1.093
α, (°)	90	Final R₁ indices [*I*>2sigma(*I*)]	0.0840
β, (°)	100.44(2)	Final wR₂	0.2372
γ, (°)	90	R₁ indices (all data)	0.1196
Volume, (Å³)	962.5(3)	wR₂ (all data)	0.3166

In the crystal structure, each K^+ cation is surrounded by five cinnamate anions and coordinated by six oxygen atoms with K–O distances of between 2.682 and 2.92Å. A layered arrangement is also observed in this structure, similar to the one observed for K-3-FCate. Thus, carboxylate anions and K^+ cations form layers parallel to the bc plane, and these layers are separated by bi-layers of methyl groups. In the bilayer of methyl groups, the shortest $C_{(Me)}\cdots C_{(Me)}$ distance is *ca.* 4.051 Å, and the $C(3)$-$C_{(Me)}$ bond from one half of bilayer is related perpendicularly to a $C(3)$-$C_{(Me)}$ in another half of the bilayer (see Figure 5.10). This geometry is similar to the type ii of halogen-halogen interaction (regardless of the actual distances) but, in this case, the arrangement is not determined by the electrostatic interaction, present in the case of the halogen. Therefore, the generation of such an arrangement is due to the close packing principle suggested by Kitaigorodsky[16].
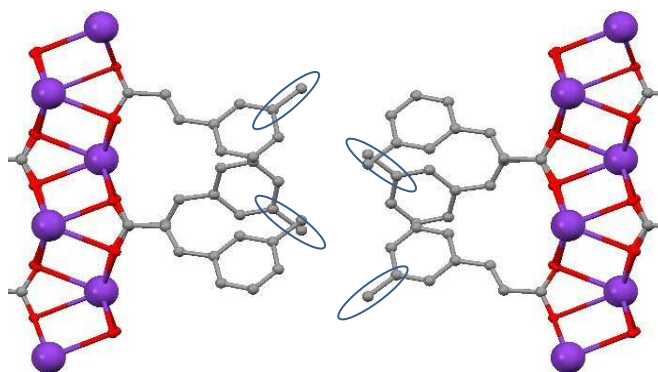
Figure 5.10. *A view of the K-3-MeCate structure along the c-axis. The blue circles show the perpendicular arrangement of C(3)-C(Me) bonds in the methyl bilayer.*

Along the c-axis, the adjacent anions through the stacks are not in parallel alignment but show a rotation by *ca.* 135.42° alternately along the stack. This arrangement results in

non-parallel C=C of the neighbouring molecules in the stacks. π edge-to-face interactions are observed between adjacent molecules with a distance of C(5)···benzene ring centroid of 3.558Å and forming an angle of 130.7° (Figure 5.11).
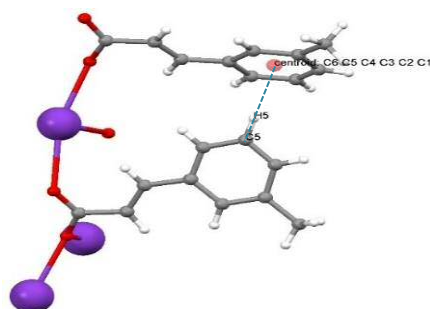
Figure 5.11. *A C-H···π interaction in the structure of K-3-MeCate presented as a dashed line.*

Ammonium salt

NH_4-3-methyl cinnamate/3-methyl cinnamic acid (NH_4-3-MeCate/3-MeCA) crystallized in the C2/c space group. Similarly to 3-FCate/3-FCA, the asymmetric unit consists of; half a NH_4^+ cation, as a result of being on a 2-fold rotation element, and a 3-MeCate/3-MeCA unit, with the carboxylic acid proton disordered between the two oxygen atoms of the carboxylic acid/carboxylate group. Hydrogen atoms of the methyl group are disordered in two positions with 54/54 occupancy. Crystallographic data is summarized in Table 5.6.

Table 5.6. *Crystallographic data for the crystal structure determination of NH_4-3-MeCate/3-MeCA.*

Formula	$C_{20} H_{23} N O_4$	Z	4
Formula weight	341.39	**Density (calculated), (Mg/m³)**	1.237
Temperature, (K)	293(2)	**Absorption coefficient, (mm⁻¹)**	0.054
λ , Å	1.54184	**F(000)**	728
Crystal system	Monoclinic	**Crystal size, (mm³)**	0.42 x 0.19 x 0.03
Space group	C2/c	**Reflections collected**	6101
a, (Å)	41.1302(18)	**Independent reflections**	1839
b, (Å)	5.9651(3)	**R(int)**	0.0224
c, (Å)	7.6959(3)	**Goodness-of-fit on F²**	1.057
α, (°)	90	**Final R_1 indices [I>2sigma(I)]**	0.0726
β, (°)	103.901(4)	**Final wR_2**	0.2110
γ, (°)	90	**R_1 indices (all data)**	0.0917
Volume, (Å³)	1832.86(14)	**wR_2 (all data)**	0.2334

In the crystal, six 3-MeCate/3-MeCA surround each NH_4^+ cation, with the N···O distance in the range of 2.855-3.051Å (Figure 5.12). In the structure, a catemer hydrogen bonded pair of two 3-MeCate/3-MeCA units is observed, with a distance O_2···O_2 of 2.547Å and a O_2-H_1···O_2 angle of 175.58°.

The molecules are packed such that the 3-MeCate/3-MeCA units and NH_4^+ cations form layers parallel to the ab plane, which are separated by bi-layers of methyl groups. Within the stack of 3-MeCate/3-MeCA units along the c-axis, the planes of neighbouring units are rotated by 140.53° with respect to each other. Therefore, the double bonds (C=C) of the adjacent units are not parallel and their centroids are 3.899Å apart.

In the methyl group bilayer, the distance between the nearest methyl group from one half of bilayer to another is 3.929Å and the $C-C_{(Me)}\cdots C_{(Me)}-C$ are in approximately linear arrangement. π edge-to-face interactions are also observed between adjacent anions, similarly to K-3-MeCate. The C(5)$\cdots$ (ring-centroid) is 3.557Å distance and the angle C(5)-H(5)$\cdots$centroid of the benzene ring is 130.3°.

Characterization of the bulk materials using PXRD revealed a pattern identical to that calculated for the crystal structure, indicating the existence of a mono-phasic material.
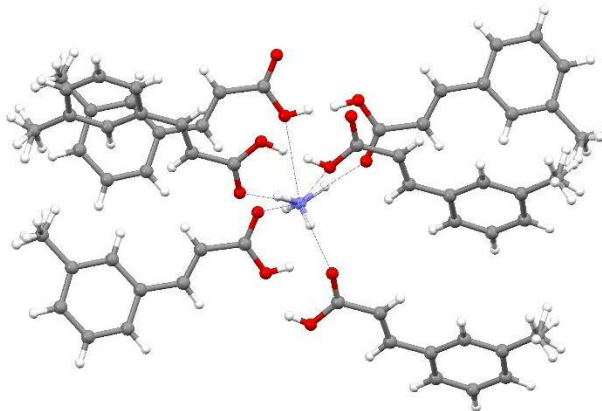
Figure 5.12. *The coordination around the NH_4^+ cation in the NH_4-(3-MeCate/3-MeCA). Note the disordered methyl group.*

5.3.1.e. 3-Trifluoromethyl cinnamic acid salts

Potassium salt

The determination of the crystal structure was a challenge, as the crystal showed a decay in diffraction intensity during the data collection. The result of SC-XRD determination revealed an uncommon crystal structure when compared with others K^+ and NH_4^+ cinnamate salts determined in this study or reported previously in the literature[9,10]. It crystallized in the triclinic crystal system with a P$\bar{1}$ space group. The

asymmetric unit, as shown in Figure 5.13 comprises six independent $3\text{-}CF_3Cate$ anions, 6 independent K^+ cations and four water molecules. Crystallographic data are shown in Table 5.7.
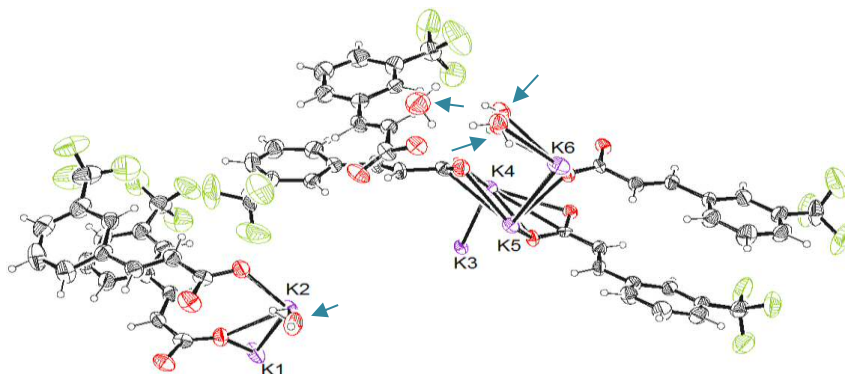
Figure 5.13. *Asymmetric unit of K-CF3Cate, showing 6 cinnamate units, 6 K^+ cations and 4 water molecules indicated by the blue arrows.*

Table 5.7. *Crystallographic data for the crystal structure determination of K-3-CF$_3$Cate.*

Formula	$C_{30} H_{22} F_9 K_3 O_8$	Z	4
Formula weight	798.78	Density (calculated), (Mg/m^3)	1.577
Temperature, (K)	293(2)	Absorption coefficient, (mm^{-1})	4.497
λ, Å	1.54184	F(000)	1616
Crystal system	Triclinic	Crystal size, (mm^3)	0.24 x 0.04 x 0.03
Space group	P$\bar{1}$	Reflections collected	10117
a, (Å)	7.7362(11)	Independent reflections	5816
b, (Å)	20.8674(13)	R(int)	0.1254
c, (Å)	21.058(3)	Goodness-of-fit on F^2	0.956
α, (°)	97.453(7)	Final R$_1$ indices [I>2sigma(I)]	0.0605
β, (°)	93.197(11)	Final wR$_2$	0.1218
γ, (°)	91.160(8)	R$_1$ indices (all data)	0.1289
Volume, (Å^3)	3364.2(7)	wR$_2$ (all data)	0.1583

A layered structure is also observed for this material. Viewing the structure down the a-axis shows that the cation and cinnamate anions form layers parallel to ab plane. In this way, the bilayer of K^+ cations and bilayers of cinnamate anion alternate within the structure. The cation bilayer accommodates water molecules, generating an ordered arrangement, as illustrated in Figure 5.14 (a, b, c and b), and then repeating to form a ribbon along the b-axis. F···F and C-H···F contact occurs in the anion bilayer.
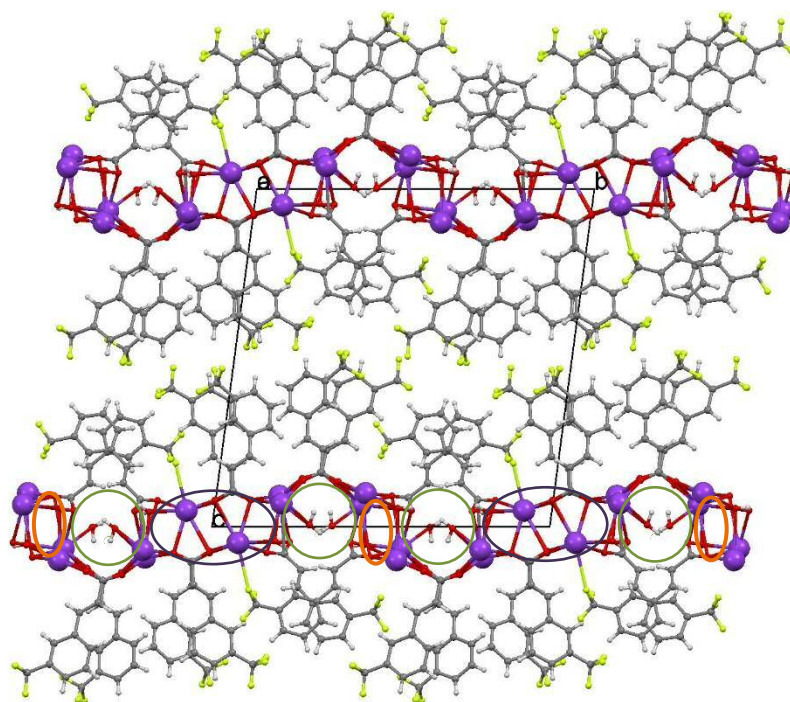
Figure 5.14. *Crystal structure of K-3-CF₃Cate down the a-axis, showing a-layered structure. The shown circles of K⁺ arrangements as follows; (a) orange, (b) green and (c) blue.*

A striking feature of the structure is the flexibility of the coordination around the K^+ cation. Thus, as illustrated in Figure 5.15 and Table 5.8, each K^+ cation present in asymmetric unit has a different coordination. For example, the F(12) atom is involved in the coordination of K(3) (Figure 5.15) since the highly electro-negative fluorine can approach the positively charged K^+ cation. Such interaction between $C\text{-}F\cdots M^{n+}$ has been widely observed[17,18] and it could be of general application in the field of host/guest chemistry.[19] This type of interaction has not been observed for the other K^+ cinnamate salts investigated in this study.

Another feature of the structure is that the anion units adopt different conformations (Figure 5.16). Thus, in the asymmetric unit, two molecules show anti-conformation, while the remaining four show syn-conformation. The arrangement of the cinnamate units does not allow the parallel arrangement of the double bonds of neighbouring units.

PXRD of the bulk material from the crystallization did not fully match the calculated pattern for the structure, due the existence of a significant amount of $KHCO_3$ and possible traces of other phases which could not be identified.
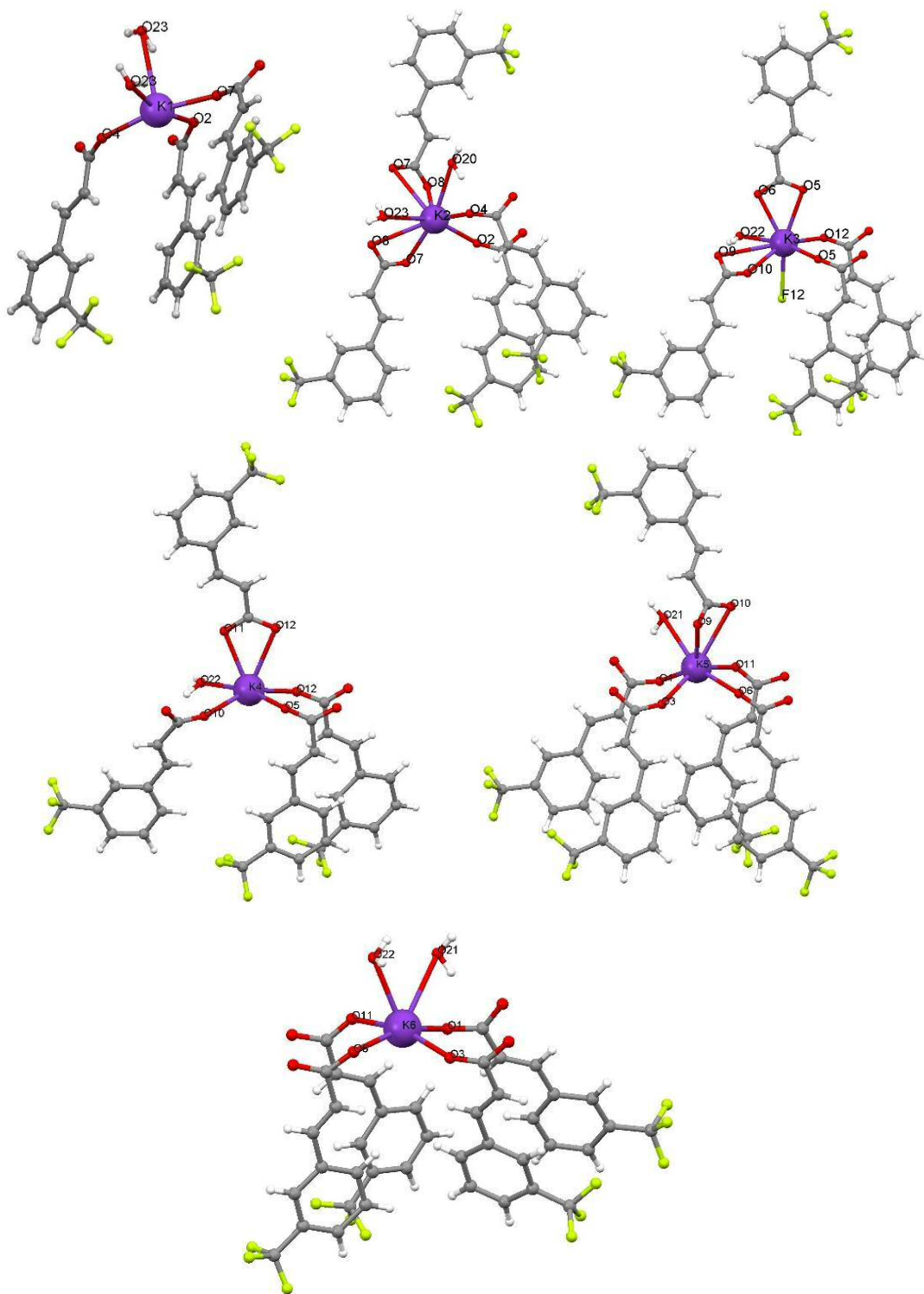
Figure 5.15. *The coordination around independent K⁺ cations.*

Table 5.8. *K⁺ coordination, the distance is measured in Å.*

K(1)-O(7)[2]	2.588(8)	K(4)-O(12)[1]	2.670(7)
K(1)-O(4)[2]	2.623(7)	K(4)-O(10)	2.676(8)
K(1)-O(2)	2.698(8)	K(4)-O(5)[3]	2.706(6)
K(1)-O(23)[7]	2.726(10)	K(4)-O(11)	2.779(7)
K(1)-O(23)[5]	3.206(11)	K(4)-O(22)[2]	2.834(8)
K(2)-O(2)	2.676(7)	K(4)-O(10)	2.676(8)
K(2)-O(7)[2]	2.742(7)	K(5)-O(6)	2.721(7)
K(2)-O(4)	2.798(8)	K(5)-O(3)[5]	2.729(8)
K(2)-O(8)[5]	2.819(8)	K(5)-O(11)	2.746(7)
K(2)-O(20)	2.983(9)	K(5)-O(1)[6]	2.781(8)
K(2)-O(8)[2]	3.165(6)	K(5)-O(9)	2.799(8)
K(2)-O(23)[2]	3.236(10)	K(5)-O(21)[2]	3.027(8)
K(2)-O(7)[5]	3.297(9)	K(5)-O(10)	3.190(9)
K(3)-O(5)[1]	2.638(7)	K(6)-O(3)[5]	2.573(9)
K(3)-O(12)[1]	2.697(6)	K(6)-O(11)[4]	2.608(7)
K(3)-O(10)[2]	2.753(7)	K(6)-O(1)[5]	2.643(8)
K(3)-O(6)[2]	2.754(7)	K(6)-O(6)	2.652(8)
K(3)-O(5)[2]	2.887(6)	K(6)-O(22)	2.819(10)
K(3)-F(12)[2]	3.043(12)	K(6)-O(21)	3.143(10)
K(3)-O(22)[2]	3.136(9)		
K(3)-O(9)[2]	3.238(6)		

1= -x+3,-y+2,-z+2   2= x+1,y,z   3= -x+2,-y+2,-z+2   4= x-1,y,z   5= -x+2,-y+1,-z+2

6= -x+3,-y+1,-z+2 7= x+2,y,z   8= -x+4,-y+1,-z+2   9= x-2,y,z
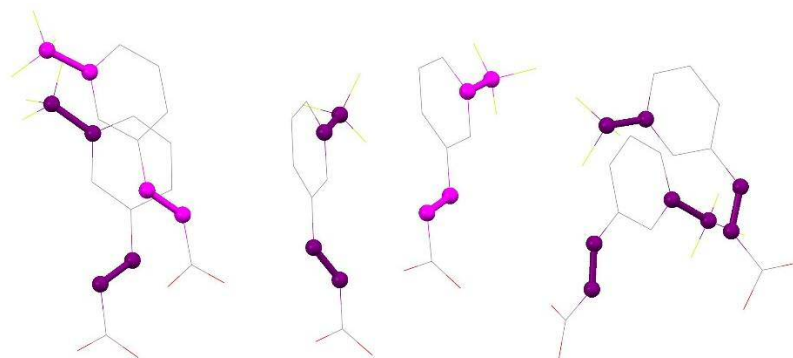
Figure 5.16. *The different 3-CF₃Cate anions in the asymmetric unit, showing two different conformations. The C-CF₃ and C=C bonds are illustrated in pink for the anti-conformational and in purple for syn-conformational.*

Ammonium salt

Initial attempts at determining the crystal structure of the NH_4^+ salt of 3-CF_3CA by SC-XRD at room temperature showed that the intensity of diffraction spots decayed as data collection proceeded. To investigate this, photos of the crystal were recorded over time. The crystal decreased in size and, after 8 days, disappeared completely. Therefore, data were recorded at low temperature (at 150K). Crystallographic data are summarized in Table 5.9. Data at 250K were also recorded as a means of comparison with experimental PXRD which was recorded at room temperature. The two structures (at 150 and 250K) are the same, although low quality data was obtained at 250K.

***Table 5.9.** Crystallographic data for the crystal structure determination of NH_4^+ salt of 3-CF_3CA determined at 150K.*

Formula	$C_{20} H_{17} F_6 N O_4$	Z	4
Formula weight	449.35	Density (calculated), (Mg/m^3)	1.576
Temperature, (K)	150(2)	Absorption coefficient, (mm^{-1})	0.148
λ , Å	0.71073	F(000)	920
Crystal system	Triclinic	Crystal size, (mm^3)	0.33 x 0.04 x 0.02
Space group	P$\bar{1}$	Reflections collected	8943
a, (Å)	6.8701(8)	Independent reflections	5603
b, (Å)	16.995(2)	R(int)	0.0709
c, (Å)	17.434(2)	Goodness-of-fit on F^2	1.078
α, (°)	72.846(12)	Final R_1 indices [I>2sigma(I)]	0.0824
β, (°)	79.489(10)	Final wR_2	0.1791
γ, (°)	79.335(11)	R_1 indices (all data)	0.1688
Volume, ($Å^3$)	1893.6(4)	wR_2 (all data)	0.2272

The salt crystallized in the triclinic crystal system, space group P$\bar{1}$. The crystal structure is different from the K^+ and NH_4^+ cinnamate salts, investigated in this study and discussed previously[9,10]. Thus, two 3-CF_3Cate anions, two 3-CF_3CA and two NH_4^+ cations comprised the asymmetric unit. Viewing the structure along the a-axis, as is seen in Figure 5.17, shows that the molecules are arranged parallel to the (011) plane. In this structure, a group of four molecules form sets (enclosed by the blue and orange rectangles) which alternate in the form of a butterfly shape; the hydrophilic parts of the sets face each other to form the body whereas the rest of the molecules are arranged to form the butterfly's wings. In other words, the set of molecules in the blue box and the set in the orange box have two different orientations.

Within each set of molecules, the double bonds are approximately parallel with respect to each other. However, they are less than 4Å apart for three neighbouring molecules

and more than 5Å for the fourth molecule. This indicates that the solid-state photoreaction can be induced to a certain extent (details of the photo reaction will be discussed in Chapter 6). Neighbouring molecules that are in a head-to-tail orientation (Figure 5.17 indicated by the red oval) have parallel double bonds separated by more than 5Å, suggesting photo-stability for these molecules.

F···F contact in the hydrophobic CF_3 bilayer is observed with the shortest F···F distance being 2.868Å (shorter than the sum of F radii[14]). Weak hydrogen bonds (C-H···F) are also observed in these bilayers, with distance F(2)···H(14) of about 2.53Å (less than the sum of the F and H radii[14]) and a F(2)···H(14)-C(14) angle of 169.93°.
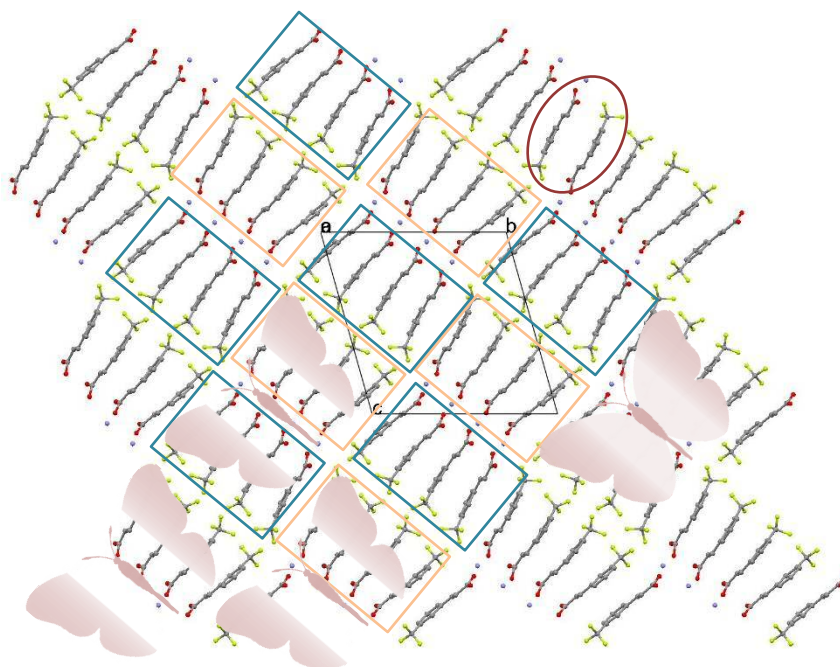
Figure 5.17. *Crystal structure of the NH_4^+ salt of 3-CF$_3$CA viewed down the a-axis, showing the butterfly like arrangements. The blue and orange boxes show the sets of four molecules, discussed in the text. The red oval shows head-to-tail related molecules.*

One NH_4^+ group is coordinated by 4 oxygen atoms from different anions/acid units with N···O distance in the range 2.82-2.89Å, while the other NH_4^+ group is coordinated by 6 oxygen atoms from different anions/acid units, with distances in the range 2.87-3.06Å. On the other hand, in the hydrophilic bilayer (butterfly body) pairs of molecules are in contact via hydrogen bonds, forming a catemer (Figure 5.18 and Table 5.10).
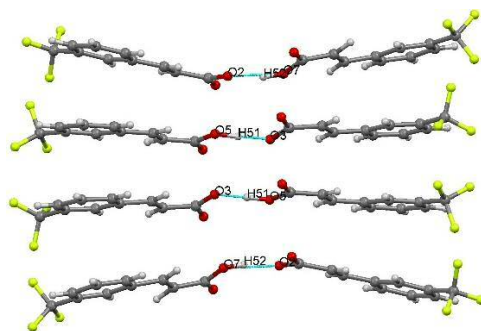
Figure 5.18. *Fragment of the crystal structure of the NH$_4^+$ salt of 3-CF$_3$CA showing the catemer arrangement. Blue lines show the hydrogen bonds.*

Table 5.10. *Hydrogen bonds present in the structure of the NH$_4^+$ salt of 3-CF$_3$CA.*

A-B···D	A-D (Å)	A-B···D (°)
O$_5$-H$_{52}$···O$_3$	2.568	178.95
C$_7$-H$_{51}$···O$_2$	2.575	169.06

PXRD analysis of the bulk sample from the crystallization from MeOH and NH$_4$OH solution revealed monophasic material and the resultant pattern was identical to that calculated for the single crystal structure determination; shifts in the peak positions were observed as a result of the different temperatures used for the PXRD (room temperature) and the SC-XRD (150 or 250K) experiment (see Figure 5.19).
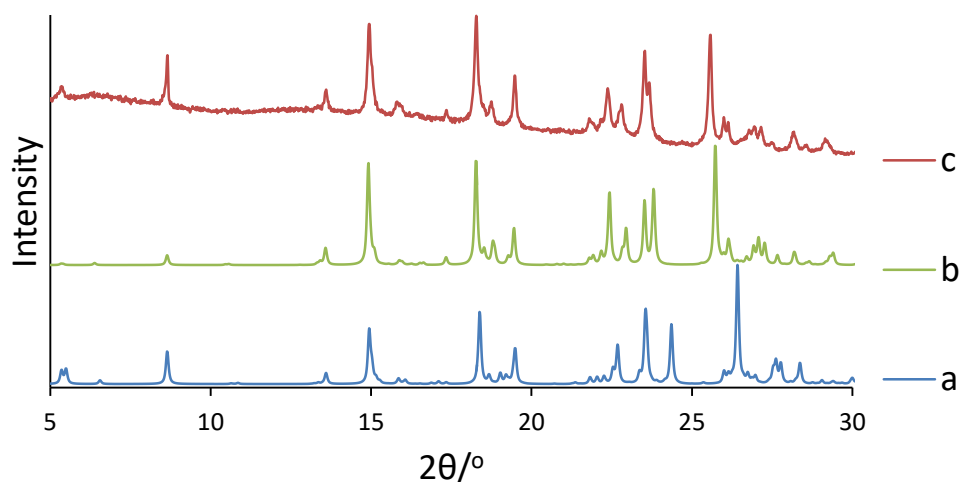
Figure 5.19. *The calculated PXRD pattern of the NH$_4^+$salt of 3-CF$_3$CA at (a) 150K and (b) 250K. (c) The experimental PXRD of the prepared NH$_4^+$salt of 3-CF$_3$CA.*

5.3.1.f. Discussion of the *meta*-substituent effect on the crystal structures of K-cinnamate

The substituent effect of halogen atoms (Br, Cl, F) and the methyl group on the crystal structure of K^+ cinnamate is discussed through consideration of crystal packing and intermolecular interaction. It has been observed[9] that, although K-3-BrCate and K-3-ClCate adopt similar arrangements regarding the hydrophilic layers, the overall arrangement of the molecules in the two structures are not identical. The key difference here may be attributable to the Br⋯Br and Cl⋯Cl interactions observed in the interface-region in the middle of the anion bilayers. Thus, a perpendicular arrangement (about 92°) of the C-Br bond, from the two halves of the bilayer, was observed in K-3-BrCate. In the structure of K-3-ClCate a collinear contact was clearly observed for C-Cl⋯Cl-C and the C-Cl⋯Cl and Cl⋯Cl-C angles were *ca.* 146°.

Comparing K-3-BrCate and K-3-ClCate with K-3-MeCate and K-3-FCate, it is clear that layered arrangements are observed in all of these structures. Additionally, despite the fact that alkali metals have the ability to coordinate in a random and unpredictable manner,[20,21] these structures adopted fixed synthons around the K^+ ion. As shown in Figure 5.20, the topology that results from the coordination around the K^+ cation with six oxygen atoms (from five units of cinnamate anions) is a square pyramid. Thus, the base of the pyramid is the result of K^+ ion coordination by four single oxygen atoms, each from a different cinnamate unit. The pyramid apex is generated from the coordination of the K^+ ion by two oxygen atoms from a carboxylate group of the same cinnamate unit. The K-O distances and the side of the base of the pyramid (Figure 5.20 and Table 5.11) in different structures are in approximately the same range, suggesting a fixed arrangement for the K^+-carboxylate group of structures.
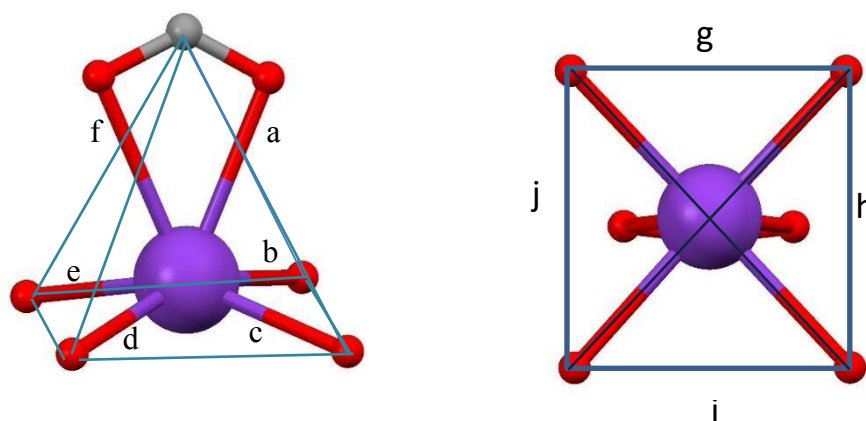
Figure 5.20. *Definition of K-O coordination geometry and other parameters associated with it.*

Table 5.11. *Geometry measured for the K-O coordination and other parameters, as defined in Figure 5.20.*

Structure	K coordinate						Pyramid base dimensions			
	a	**b**	**c**	**d**	**e**	**f**	**g**	**h**	**i**	**j**
K-3-BrCate (K1)	2.731	2.751	2.704	2.678	2.719	3.111	3.552	3.983	3.552	3.983
K-3-BrCate (K2)	2.708	2.707	2.733	2.656	2.742	3.109	3.535	3.983	3.535	3.983
K-3-ClCate (K1)	2.749	2.767	2.744	2.720	2.667	3.155	3.649	3.938	3.649	3.938
K-3-ClCate (K2)	2.663	2.666	2.635	2.725	2.681	3.040	3.460	3.938	3.460	3.938
K-3-FCate	2.790	2.729	2.672	2.671	2.705	2.899	3.607	3.855	3.607	3.867
K-3-MeCate	2.771	2.805	2.682	2.711	2.746	2.920	3.621	3.956	3.621	3.991

Although all structures showed a fixed arrangement of the K^+ bilayer, as illustrated in Figure 5.21, the arrangement of the vinyl-benzene segments vary between the different structures. In both K-3-BrCate and K-3-ClCate the anion molecules attached to the K^+ layer are stacked parallel to each other. Thus, $\pi\cdots\pi$ offset interactions for the phenyl motif along the stack occurs with distances between the benzene ring centroids of 3.982Å and 3.937Å in the K-3-BrCate and K-3-ClCate, respectively.

In contrast, in the structures of K-3-FCate and K-3-MeCate the molecules do not stack with the same orientation relative to each other. Instead, the molecules are rotated, relative to their neighbour in the stack (Figure 5.21 dashed rectangles), by 138.96° in the K-3-FCate structure and by 135.42° in the K-3-MeCate structure. This arrangement leads to C–H$\cdots\pi$ interactions (i.e. edge-to-face interactions), with distances from phenyl

centroid to C(5) of 3.513Å in the case of 3-FCate and 3.558Å in the case of 3-MeCate (Figure 5.11). This dissimilar behaviour is a result of the presence of polarizable groups (Br and Cl) in the K-3-BrCate and K-3-ClCate structures, respectively. So, the electrostatic interaction between the Br···Br and Cl···Cl in the stack of the anion molecules may play a role in bringing the molecules into parallel arrangement.

On replacing Br or Cl with Me in K-3-MeCate or F atom in K-3-MeCate, the effect of polarizability of the substituents becomes clear. Thus, Br, Cl and methyl have comparable sizes, but the polarizability of the methyl group and F is low in comparison to Cl and Br. If 3-MeCate units, for example, are arranged in the stacks with the same orientation, it is likely to increase unfavourable interaction between the groups through the stack. Therefore, the cinnamate units prefer to be packed with different orientations in relation to each other, in order to minimize this effect. Thus, through the stack of the anions, in the case of K-3-MeCate and K-3-FCate, C–H···π interactions predominate and help in stabilizing the structure, in the absence of halogen···halogen interaction through the stack as in the case of K-3-BrCate and K-3-ClCate.

From these comparisons, although all structures have the same synthon regarding the attachment of the anion unit to the K^+ cation, the identity of the substituent clearly affects the packing of the vinyl-benzene motifs of the anion units. Thus, similar substitutes (Cl and Br) have the same structural behaviour, whereas switching from these substituents to Me group and F has a greater effect on the structural packing. The change can in turn affect the chemical properties of the materials (discussed in Chapter 6).
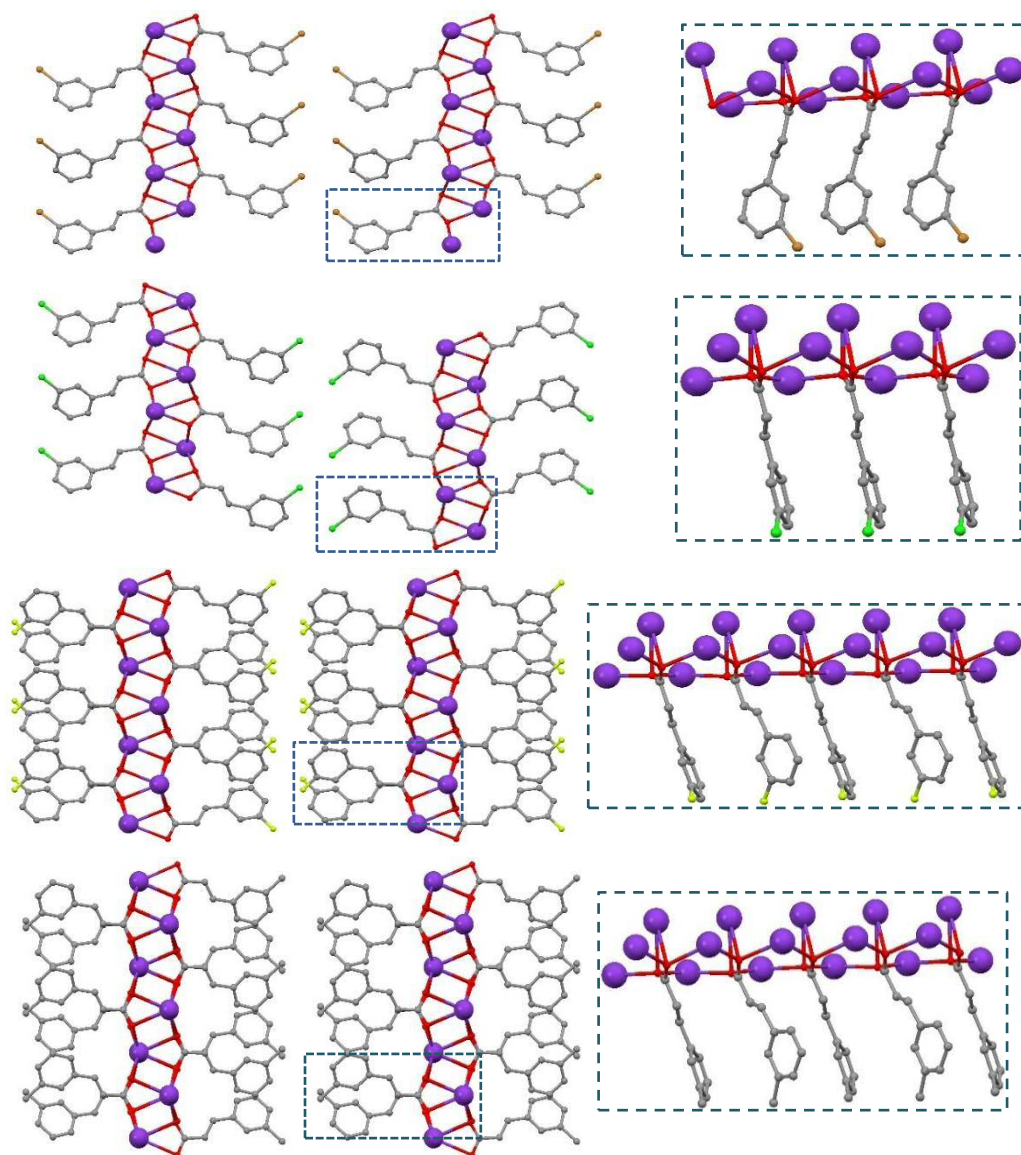
Figure 5.21. *Crystal structures of (from the top) K-3-BrCate[9], K-3-ClCate[9], K-3-FCate and K-3-MeCate. The dashed rectangles are the sections viewed perpendicularly in the figures on the right. Hydrogen atoms are omitted for clarity.*

5.3.1.g. Discussion of the *meta*-substituent effect on the crystal structures of NH₄-cinnamate/cinnamic acid

In contrast to NH$_4$-3-BrCate/3-BrCA[10] (phase I), the structures of NH$_4$-3-BrCate/3-BrCA (phase II), NH$_4$-3-ClCate/3-ClCA,[10] NH$_4$-3-FCate/3-FCA and NH$_4$-3-MeCA/3-MeCate showed similar structures in term of their unit cell parameters and structural architectures (Figure 5.22).

This similarity may allow the observation of slight differences in the structures generated in response to interchange of the substituents on the ring. The main

174

differences in the structures are the contacts between the different substituents in the bilayers of the anion/acid molecules. In the case of NH_4-3-BrCate/3-BrCA and NH_4-3-ClCate/3-ClCA, the shortest distance between Br···Br and Cl···Cl are 3.85 and 3.79Å, respectively, in a type ii of halogen-halogen interaction. However, in the case of NH_4-3-FCate/3-FCA the shortest F···F distance in the type ii arrangement is 4.563 Å, and 3.56Å for type i arrangement. Both distances are longer than the sum of F···F radii (2.94)[14]. In contrast, in NH_4-3-MeCA/3-MeCate, the shortest distance between the methyl carbon is 3.916Å, showing a collinear arrangement of C-Me···Me-C in the bilayer.
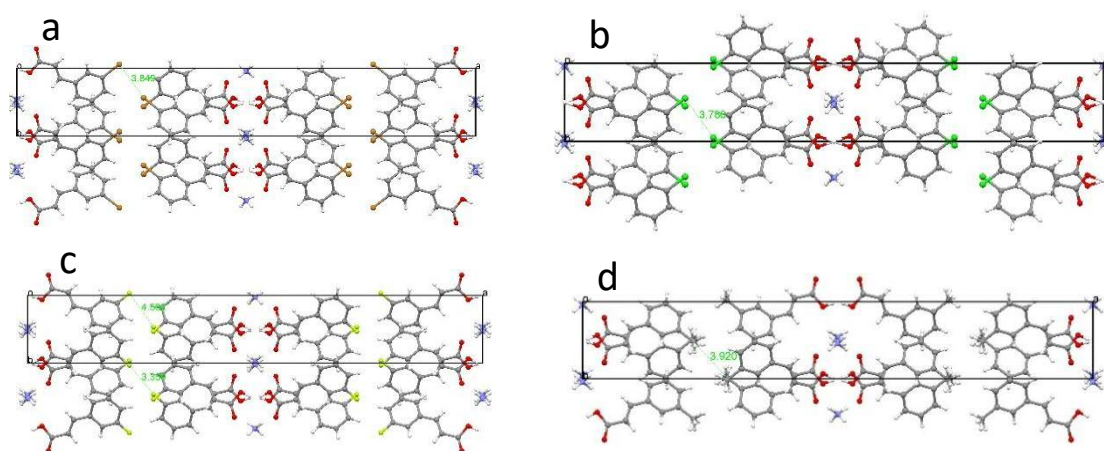
Figure 5.22. *Crystal structure of (a) NH_4-3-BrCate/3-BrCA (phase II), (b) NH_4-3-ClCate/3-ClCA*[10]*, (c) NH_4-3-FCate/3-FCA and (d) NH_4-3-MeCA/3-MeCate.*

NH_4-3-BrCate (phase I) and NH_4-3-ClCate[10] adopt a similar crystal structure with very close unit cell parameters, although they crystallized in different crystal systems. The most striking differences is attributable to the Br···Br and Cl···Cl interactions between the halogen atoms in the bilayer at the anion interphase. The Br···Br contact is a type ii, whereas a type i interaction is observed for the Cl structure (types i and ii are discussed in Chapter 1).

5.3.1.h. Discussion on the general effect of salts formation

The data presented in Table 5.12 shows twist angle 1 and 2 (see scheme 5.1) for some cinnamic acids and salts. Twist angle 1 is the angle between the planes of the 3-substituted phenyl ring (only the atom that is attached to the ring of the substituted group is taken in the plane measurement) and the vinyl group of the cinnamic acid or cinnamate anion respectively, while twist angle 2 is the angle between the planes of vi-

nyl group and carboxylic acid or carboxylate groups, excluding the H of the cinnamic acid.

The data for different cinnamic acids and salts are listed in Table 5.12. In general, cinnamic acids show approximately planer molecules and the maximum twist is seen in β_1 and β_2 3-FCA, where the twist angle 1 is approximately 6°.

However, in most of the salts, larger intra-acid/intra-anion twist angles 1 or 2 are observed. The K^+ cation has a greater effect on the twist angles than the NH_4^+ cation. The NH_4-(3-Br-Cate/3-BrCA)[10] salt shows a very low twist angles.

For the K^+ salts in general (including K^+/H salts), twist angle 1 is larger than the twist angle 2. Interestingly, a similar trend is also observed for the NH_4^+ non-protonated salts (NH_4-3-BrCate and NH_4-3-ClCate)[10]. Deviation from this trend is observed for K-3-MeCate and three cinnamate units of the K-3-CF$_3$Cate salt; K-3-MeCate and one cinnamate unit of K-3-CF$_3$Cate which show approximately similar twist angles 1 and 2 values (Table 5.3 highlighted in blue). The other two molecules of K-3-CF$_3$Cate show a twist angle 2 greater than twist angle 1 (Table 5.12 highlighted in green). The NH_4/H-salts generally have almost the same trend as K^+ salts, i.e. twist angle 1 is greater than twist angle 2. However, three cinnamate/cinnamic acid units out of the four in the structure of NH_4-(3-CF$_3$Cate/3-CF$_3$CA) and NH_4-(3-Br-Cate/3-BrCA)[10] showed the opposite behaviour where twist angle 2 was greater than twist angle 1. The results suggest that in general, salt formation has an effect on the twist angles 1 and 2, which in turn, affects the structure.
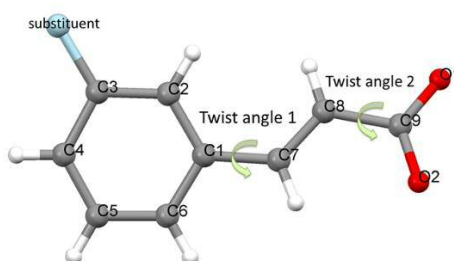
Scheme 5.1. *3-substituted-cinnamate unit showing twist angles 1 and 2.*

Table 5.12. *The twist angles 1 and 2.*

Acids

Compounds	Twist angle 1 (°)	Twist angle 2 (°)
γ-3-BrCA[22]	2.26	3.18
γ_2-3-BrCA	2.44	3.86
β-3-BrCA[23]	3.94	4.72
γ-3-ClCA	1.84	3.95
β-3-ClCA	5.13	1.50
γ-3-MeCA	1.92	3.09
β_1-3-FCA	6.48	2.08
β_2-3-FCA	6.05	2.47
γ_1-3-CF$_3$CA	2.35	3.55
γ_2-3-CF$_3$CA	1.22	1.04

K-salts

Compounds	Twist angle 1 (°)	Twist angle 2 (°)
K-3-BrCate [9]	M_1 20.70	14.57
	M_2 34.76	10.17
K-3-ClCate [9]	M_1 17.71	4.36
	M_2 25.59	5.88
K-3-MeCate	12.05	14.34
K-3-FCate	15.77	10.11
K-3-CF$_3$Cate	M_1 0.48	10.29
	M_2 5.79	14.06
	M_3 8.92	3.85
	M_4 15.74	11.40
	M_5 15.88	15.13
	M_6 18.85	5.91

K/H-salt

Compounds	Twist angle 1 (°)	Twist angle 2 (°)
K-3-ClCate/3-ClCA	16.92	1.91

NH$_4$-salts

Compounds	Twist angle 1 (°)	Twist angle 2 (°)
NH$_4$-3-BrCate [10]	M_1 20.65	2.37
	M_2 13.61	3.59
NH$_4$-3-ClCate [10]	M_1 16.36	3.11
	M_2 16.22	0.75

NH₄/H-salts

NH$_4$-(3-Br-Cate /3-BrCA)[10]	3.77	6.38
NH$_4$-3-BrCate /3-BrCA$^{(PhaseII)}$	10.65	5.31
NH$_4$-(3-ClCate /3-ClCA)[10]	12.03	5. 47
NH$_4$-(3-MeCate/3-MeCA)	12.54	3.13
NH$_4$-(3-FCate/3-FCA)	12.69	4.68
NH$_4$-(3-CF$_3$Cate/3-CF$_3$CA)	M$_1$ 3.37	6.24
	M$_2$ 6.74	8.47
	M$_3$ 4.38	6.20
	M$_4$ 12.17	0.57

5.3.2. Potassium and ammonium salts of binary *meta*-substituent cinnamic acids: crystal structure analysis

Understanding the principles that govern the packing of organic solids is a fundamental requirement in crystal engineering. The role of the cation (K$^+$ and NH$_4^+$) in linking the hydrophilic ends of the anion, as well as the effect of the ring substituent, on the structure were investigated in the previous section. In this section the effect of cocrystallization of K$^+$ or NH$_4^+$ salts of binary anions was investigated.

5.3.2.a. 3-ClCA/3-BrCA salts

Potassium salts

The information in Sections 5.3.1.a and from the literature[9] shows that different structures have been observed for K$^+$ salts of 3-BrCA and 3-ClCA. The salts are not isostructural[9] despite the similarity of Br and Cl regarding their electronic and geometric properties. Therefore, in this section the investigation was carried out to determine the effect of cocrystallization of a binary system of 3-BrCA and 3-ClCA as a K$^+$ salt.

-   *K$^+$ salt prepared from a 1:1 mixture of 3-BrCA/3-ClCA*

The material from the crystallization of 1:1 3-BrCA:3-ClCA in KOH solution (sample A) was characterized by both SC-XRD and PXRD. Single crystal structure determination of a suitable crystal (crystal A) showed that it crystallized in space group Cc with two independent K$^+$ cations and two 3-halo-cinnamate ions in the asymmetric unit. The substituent in the *meta*-position of the ring was disordered, with refined Br/Cl occupancies of 0.48(1)/0.52(1) for the first anion and 0.42(1)/0.58(1) for the second

anion. As shown in Figure 5.23, molecules are packed in a structure similar to that of K-3-BrCate so that the C-(Br/Cl) bond from the two halves of the anion bilayers are oriented perpendicular to each other.
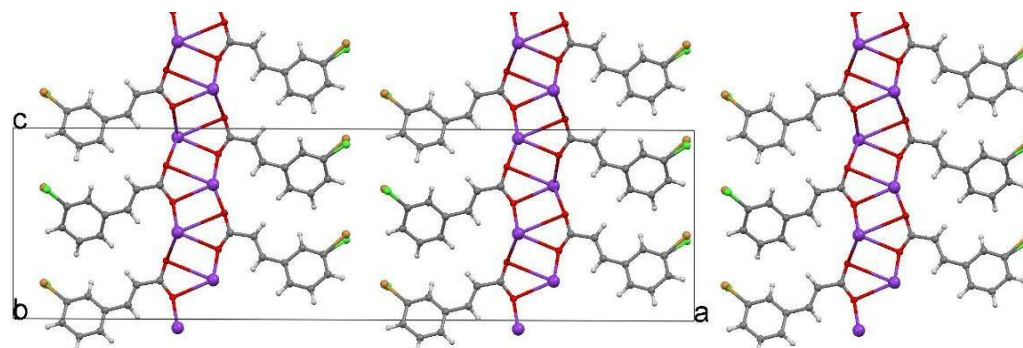
Figure 5.23. *Crystal structure of crystal A (K-(3-BrCate/3-ClCate) solid solution) viewed along the b-axis.*

PXRD of the material from the crystallization revealed an identical pattern to the calculated pattern of crystal A. This calculated pattern is similar to that of K-3-BrCate and the normal shift in the peak positions was observed (Figure 5.24).
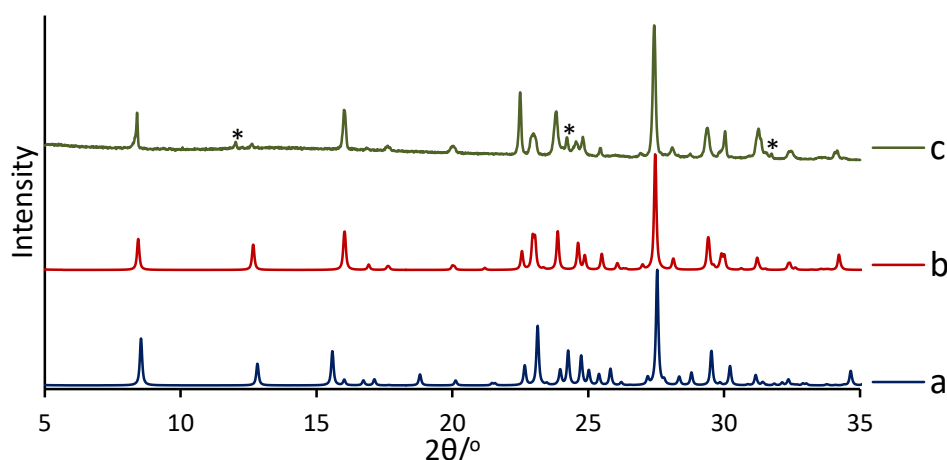
Figure 5.24. *The calculated PXRD patterns of (a) K-3-BrCate[9], and (b) crystal A. (c) The experimental PXRD of sample A. Stars mark the peaks associated with contamination by KHCO₃[13].*

- K⁺ salt preparation of other ratio of 3-BrCA:3-ClCA

A single crystal (crystal B) from a sample prepared from a 1:2 ratio of 3-BrCA:3-ClCA (sample B) was determined by SC-XRD. The result showed that it cocrystallized, like crystal A, with a similar structure to K-3-BrCate. The refined occupancies of Br/Cl were 0.33(2)/0.67(2) and 0.26(2)/0.74(2) for the first and second anion in the asymmetric

unit, respectively. The PXRD result of sample B suggested that both structures of solid solution similar to structures K-3-ClCate and K-3-BrCate (Figure 5.25) were presented.

Preparation of the K$^+$ salt using a 1:3 ratio of 3-BrCA:3-ClCA (sample C) gave a PXRD pattern (as illustrated in Figure 5.25), indicating two structures of K-(3-BrCate/3-ClCate) solid solutions: the main phase was similar to K-3-ClCate and was contaminated with K-3-BrCate. Crystal structure determination for a suitable single crystal (crystal C) showed a structure similar to K-3-ClCate. The asymmetric unit comprises two K$^+$ cations and two 3-halo-cinnamate anions with a substituted disordered Br/Cl in the *meta*-position of the ring. The refined occupancies of Br:Cl are 0.23(2):0.77(2) and 0.21(2):0.79(2) for the first and the second anion units, respectively. In the structure, as a result of a similar arrangement of the molecules to the structure of K-3-ClCate, the halogen atoms between the two halves of the anion bilayers are in contact via a co-linear arrangement for C-(Br/Cl)···(Br/Cl)-C.

Preparation of a solid solution using a 1:6 ratio of 3-BrCA:3-ClCA (sample D) and consequently PXRD analysis revealed a structure similar to K-3-ClCate (see Figure 5.25). Structure determination of a crystal from sample D showed it to be identical to C with disordered Br:Cl substituent and occupancies of 0.09(1):0.91(1) and 0.18(1): 0.82(1) for the two cinnamate anions present in the asymmetric unit.
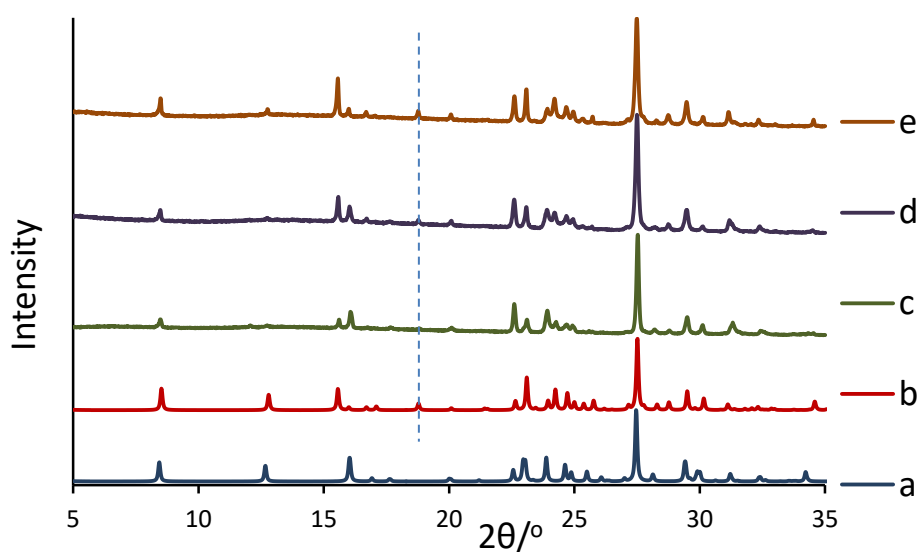
Figure 5.25. *The calculated PXRD pattern of (a) crystal A, (b) crystal D. (c),(d) and (e) Are the experimental PXRD pattern of sample B, C and D, respectively. The dashed line marks the peaks associated with the crystal A structure. (Table 5.13 explains the labels)*

As summarized in Table 5.13, the comparison of structures A, B, C and D showed the presence of K-3-BrCate:K-3-ClCate in ratios of 1:1 and 1:2.3 produced solid solution similar to K-3-BrCate structure. However, when the ratio of K-3-ClCate was increased to approximately 1:3.5 or greater, a different structure similar to K-3-ClCate was produced (see Figure 5.26). This indicates that the ratio of K-3-BrCate:K-3-ClCate where the switch from K-3-BrCate to K-3-ClCate occurs is between approximately 1:2.3 and 1:3.5. The change of the structure from K-3-BrCate to K-3-ClCate is associated with a change in the C-(Br/Cl)···(Br/Cl)-C bond contact from the perpendicular (type ii halogen-halogen interaction) to a collinear arrangement (type i halogen-halogen interaction). This suggests the influence of Cl and Br substituents in the formation of type i or type ii halogen-halogen interactions determines the resultant structure. It has been observed[24] that, as the polarization of the halogen increases I > Br > Cl, type ii halogen-halogen contact becomes more significant than type i. Another statistical study[25] of the CSD also showed that in Cl···Cl contacts type i occurs more often than type ii, whereas in Br···Br, approximately the same number of type i or type ii contacts are observed.

Table 5.13. *Summary of the disordered Br:Cl ratio in the A,B,C and D crystals, and the solid solution structure obtained.*

Label	Prep ratio Br:Cl	Br:Cl in the structure	The solid solution structure similar to:
A	1:1	≈1:1	K-3-BrCate structure
B	1:2	≈1:2.3	K-3-BrCate structure
C	1:3	≈1:3.5	K-3-ClCate structure
D	1:6	≈1:6.4	K-3-ClCate structure

Crystallographic data of the structure determination of the crystals A, B, C and D are shown in Table 5.14.

It is notable that, in the above solid solution structures which are similar to K-3BrCate or K-3-ClCate, molecules are arranged to have a head-to-head alignment with the required geometry for the [2 + 2] reaction.
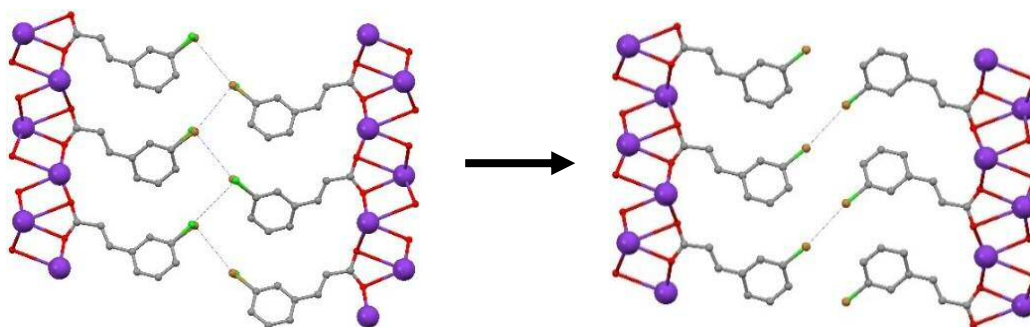
Figure 5.26. *Changing of the crystal packing mode as a result of increasing the ratio of the K-3-ClCate in the structure of A.*

Table 5.14. *Crystallographic data for the crystal structures determination of K-(3-ClCate/3-BrCate).*

	K-(3-BrCate/3-ClCate) (1:1) (Crystal A)	K-(3-BrCate/3-ClCate) (1:2)(Crystal B)	K-(3-BrCate/3-ClCate) (1:3)(Crystal C)	K-(3-BrCate/3-ClCate) (1:6)(Crystal D)
Formula	$C_9 H_6 Br_{0.45} Cl_{0.55} K O_2$	$C_9 H_6 Br_{0.30} Cl_{0.70} K O_2$	$C_9 H_6 Br_{0.22} Cl_{0.78} K O_2$	$C_9 H_6 Br_{0.13} Cl_{0.87} K O_2$
Formula weight	240.58	233.91	230.41	226.30
Temperature, (K)	293(2)	293(2)	293(2)	293(2)
λ , Å	1.54184	1.54184	1.54184	1.54184
Crystal system	Monoclinic	Monoclinic	Orthorhombic	Orthorhombic
Space group	Cc	Cc	$Pna2_1$	$Pna2_1$
a, (Å)	41.884(3)	41.837(3)	11.4911(14)	11.4857(4)
b, (Å)	3.9555(3)	3.9524(2)	3.9365(5)	3.9405(2)
c, (Å)	11.4525(11)	11.4617(11)	41.571(4)	41.4563(17)
α, (°)	90	90	90	90
β, (°)	90.219(7)	90.297(7)	90	90
γ, (°)	90	90	90	90
Volume, (Å³)	1897.4(3)	1895.2(2)	1880.4(4)	1876.29(14)
Z	8	8	8	8
Density (calculated), (Mg/m³)	1.684	1.640	1.628	1.602
Absorption coefficient, (mm⁻¹)	8.243	7.900	7.776	7.574
F(000)	960	939	928	914
Crystal size, (mm³)	0.22 x 0.05 x 0.04	0.21 x 0.08 x 0.02	0.27 x 0.06 x 0.02	0.23 x 0.07 x 0.03
Reflections collected	2963	2034	3984	3880
Independent reflections	2061	1596	2514	2299
R(int)	0.0392	0.0152	0.0321	0.0258
Goodness-of-fit on F^2	1.059	1.145	1.073	1.094
Final R_1 indices [I>2sigma(I)]	0.0683	0.0694	0.0770	0.0524
Final wR_2	0.1875	0.2078	0.2260	0.1589
R_1 indices (all data)	0.0739	0.0709	0.0819	0.0571
wR_2 (all data)	0.1955	0.2092	0.2324	0.1636

Ammonium salts

As shown in sections 5.3.1.a and 5.3.1.b, the structure of NH₄-3-BrCate/3-BrCA (phase II) and NH₄-3-ClCate/3-ClCA[10] adopt similar unit cells and crystal packing. However, other structures of NH₄⁺ salts of both 3-ClCA and 3-BrCA are also observed and they show different crystal structures. Therefore, in this section the cocrystallization of NH₄⁺ salts of 3-BrCA/3-ClA was studied to investigate the possible structures.

- *Ammonium salt prepared from a 1:1 mixture of 3-BrCA/3-ClCA*

Single crystal structure determination of a suitable crystal from a preparation contaning NH_4^+ and a 1:1 mixture of 3-BrCA:3-ClCA (sample E) gave a NH_4-(3-BrCate/3-ClCate)/(3-BrCA/3-ClCA) solid solution. The space group is C2/c and the molecules are arranged in a layered structure as shown in Figure 5.27, with cation layers (NH_4^+) separated by bilayers of anion/acid (3-halo-Cate/3-halo-CA) units. The Br and Cl are disordered in the *meta*-position of the ring by a Br:Cl ratio of 0.517(4):0.483(4), indicating formation of a solid solution salt. The structure is similar to that of both NH_4-3-BrCate/3-BrCA (designed as phase II) and NH_4-3-ClCate/3-ClCA[10] and therefore it is not surprising that a solid solution with a similar structure is formed.
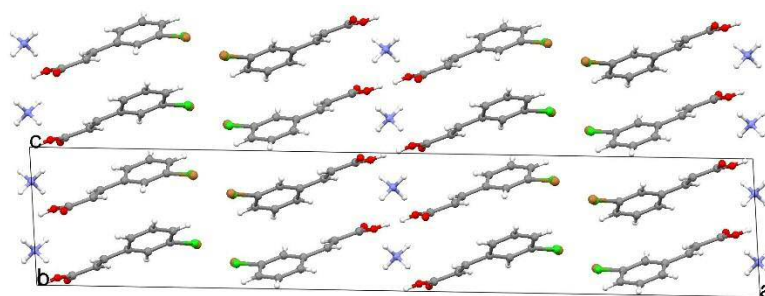
Figure 5.27. *Crystal structure of crystal A [NH_4-(3-Br Cate/3-ClCate)/(3-BrCA/3-ClCA)] solid solutions) viewed along the b-axis.*

PXRD analysis of the crystallized material gave an identical pattern to the calculated one from the single crystal determination and these patterns are similar to those calculated from both NH_4-3-BrCate/3-BrCA (phase II) and NH_4-3-ClCate/3-ClCA[10] (illustrated in Figure 5.28). Shifts in the PXRD peak positions of the solid solutions relative to their pure salts are observed, and indicate formation of solid solutions.
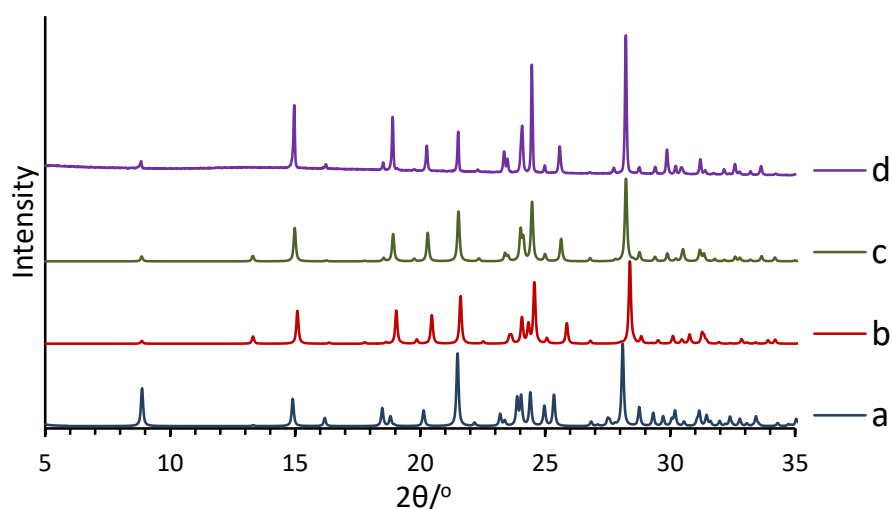
Figure 5.28. *The calculated PXRD patterns of (a) NH_4-3-BrCate/3-BrCA (phase II), (b) NH_4-3-ClCate/3-ClCA[10] and (c) crystal of sample E. (d) Is experimental PXRD patterns of sample E*

- *Ammonium salt prepared from other 3-BrCA:3-ClCA ratios*

The materials from the crystallization with ratios 1:4, 1:6 and 2:1 of 3-ClCA:3-BrCA in NH₄OH solution (samples F, G and H, respectively) were characterized by both SC-XRD and PXRD. Single crystal structure determination for the crystals from samples F, G and H indicated the formation of NH₄-(3-BrCate/3-BrCA)/(3-ClCate /3-ClCA) solid solutions, with similar crystal structures to the one observed for sample A. The only difference between the structures A, F and G was the amount of Br and Cl in the structure. The disordered Br:Cl ratios in the F,G and H crystals are summarized in Table 5.15. In contrast with the K(3-ClCate/3-BrCate) solid solution, in the NH₄-(3-BrCate/3-BrCA)/(3-ClCate/3-ClCA) solid solution structure, the arrangement of molecules does not form a parallel alignment of double bonds of neighbouring molecules.

Table 5.15. Summary of the disordered Br:Cl ratio in the F,G and H crystals.

Crystal	Prep ratio Cl:Br	Cl:Br in the structure
F	1:4	0.18(1) :0.82(1)
G	1:6	0.27(1):0.73(1)
H	2:1	0.709(4):0.209(4)

PXRD analysis of the bulk materials of samples F,G and H showed similar PXRD patterns, indicating the formation of solid solution materials with a structure that is similar to structure A. The normal expected shifts in the peak positions were observed, consistent with the different initial preparation ratios of the acids (Figure 5.29).
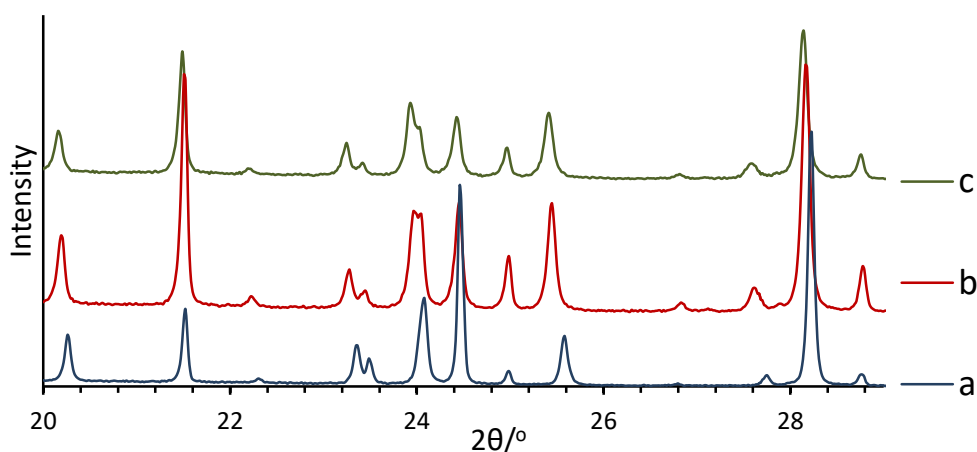
Figure 5.29. The experimental PXRD pattern of (a) sample E, (b) sample F and (c) sample G, showing shifts in the peak positions.

The results showed that although there is different polymorphism of NH$_4$-3-BrCate/3-BrC[10] phase I (discussed in Section 5.3.1.b), the structures obtained for the NH$_4^+$ salt of 3-BrCA/3-ClCA prepared in the range of 6:1–1:2 are isostructural to NH$_4$-3-BrCate/3-BrC phase II and NH$_4$-3-ClCate/3-ClCA. The crystallographic data of the structure determination of the crystals E, F, G and H are shown in Table 5.16.

Table 5.16. *Crystallographic data for the crystal structure determination of NH$_4$-(3-BrCate/3-BrCA)/(3-ClCate/3-ClCA) solid solutions.*

	NH$_4$-(3-BrCate/3-BrCA)/(3-ClCate/3-ClCA) (Cl:Br) (1:1)	NH$_4$-(3-BrCate/3-BrCA)/(3-ClCate/3-ClCA) (Cl:Br) (1:4)	NH$_4$-(3-BrCate/3-BrCA)/(3-ClCate/3-ClCA) (Cl:Br) (1:6)	NH$_4$-(3-BrCate/3-BrCA)/(3-ClCate/3-ClCA) (Cl:Br) (2:1)
Formula	C$_{18}$ H$_{17}$ Br$_{1.03}$ Cl$_{0.97}$ N O$_4$	C$_{18}$ H$_{17}$ Br$_{1.63}$ Cl$_{0.37}$ N O$_4$	C$_{18}$ H$_{17}$ Br$_{1.47}$ Cl$_{0.53}$ N O$_4$	C$_{18}$ H$_{17}$ Br$_{0.43}$ Cl$_{1.57}$ N O$_4$
Formula weight	428.13	454.70	447.47	401.23
Temperature, (K)	293(2)	293(2)	293(2)	293(2)
λ , Å	1.54184	1.54184	1.54184	1.54184
Crystal system	Monoclinic	Monoclinic	Monoclinic	Monoclinic
Space group	C2/c	C2/c	C2/c	C2/c
a, (Å)	39.989(4)	39.9321(11)	39.948(2)	39.961(2)
b, (Å)	5.9746(5)	6.0015(2)	5.9974(4)	5.9546(3)
c, (Å)	7.6164(6)	7.6503(3)	7.6422(3)	7.5830(4)
α, (°)	90	90	90	90
β, (°)	93.936(7)	93.296(3)	93.450(4)	94.121(6)
γ, (°)	90	90	90	90
Volume, (Å^3)	1815.4(3)	1830.38(11)	1827.64(17)	1799.73(17)
Z	4	4	4	4
Density (calculated), (Mg/m^3)	1.566	1.650	1.626	1.481
Absorption coefficient, (mm^{-1})	4.680	5.367	5.178	3.973
F(000)	866	909	898	823
Crystal size, (mm^3)	0.59 x 0.36 x 0.09	0.22 x 0.14 x 0.04	0.23 x 0.15 x 0.08	0.28 x 0.10 x 0.03
Reflections collected	6152	3267	3170	3073
Independent reflections	1823	1788	1789	1757
R(int)	0.0157	0.0108	0.0125	0.0116
Goodness-of-fit on F^2	1.063	1.032	1.179	1.021
Final R$_1$ indices [I>2sigma(I)]	0.0370	0.0308	0.0457	0.0513
Final wR$_2$	0.1023	0.0777	0.1258	0.1371
R$_1$ indices (all data)	0.0380	0.0317	0.0469	0.0573
wR$_2$ (all data)	0.1035	0.0786	0.1269	0.1438

5.3.2.b. 3-MeCA/3-BrCA salts

Photostability of the pure 3-MeCA has been notable during this study due to its existence only in γ form (Chapter 3). Cocrystallization of the acid with 3-BrCA and 3-ClCA showed that the resultant solid solution favoured crystallization in γ form. Additionally, the crystal structures of K$^+$ and NH$_4^+$ salts of 3-MeCA did not contain a parallel double bond arrangement in neighbouring molecules. However, the crystal structures of K-3-BrCate, NH$_4$-3-BrCate and NH$_4$-3-BrCate/3-BrCA (phase I) showed ideal geometry for the photodimerization of the double bond groups of neighbouring molecules. Therefore, the challenge in this section was to use crystal design strategies in bringing the molecules into reactive orientations. This cocrystallization of the salt of 3-MeCA and 3-BrCA was attempted

Potassium salt

- *Sample prepared using a 1:1 ratio*

Structure determination of a solution-grown single crystal (crystal J) from a cocrystallization experiment with an initial 1:1 ratio of 3-BrCA:3-MeCA in KOH solution (sample J) revealed the formation of a solid solution. Surprisingly, the structure was similar to K-3-ClCate instead of K-3-BrCate (discussed below). The structure has space group Pna2$_1$, with two independent 3-substituted-Cate anions and two K$^+$ cations in the asymmetric unit, with disordered Br and Me in the *meta*-position of the ring. The refined occupancies of Br/Me were 0.42(1)/0.58(1) and 0.44(1)/0.56(1) for the first and second anions. The asymmetric unit is displayed in Figure 5.30.
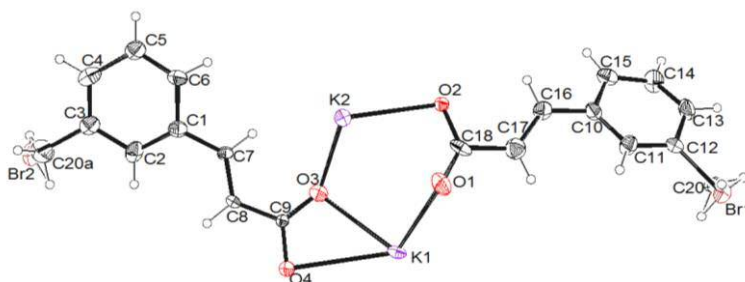
Figure 5.30. *Asymmetric unit of crystal J, showing disordered Br/Me in the 3-position of the ring.*

A layered structure is also observed in this solid solution, similarly to the K-3-ClCate and K-3-BrCate structures.[9] As seen in Figure 5.31, K$^+$ cations and cinnamate anions are arranged in layers parallel to the ab plane. In the middle of the anion bilayer Br atoms and methyl groups are disordered. A feature of the structure is that, at the interface of the bilayer, the Br and the methyl groups are in contact. Thus C-Br$\cdots$C$_{(Me)}$-C, C-Br$\cdots$Br-C or C$_{(Me)}\cdots$C$_{(Me)}$-C contacts are collinear.
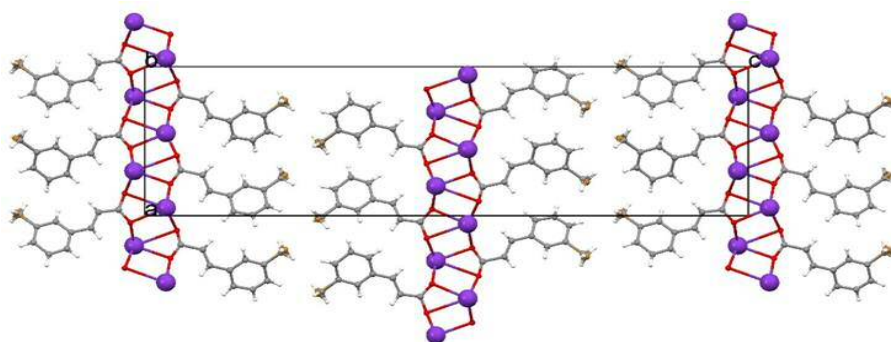
Figure 5.31. *Crystal structure of crystal J, the structure is viewed along the a-axis.*

The obtained structure of K-3-BrCate/3-MeCate is identical to K-3-ClCate[9]. This is an example of solid solution of a binary system that adopts different structure from the parent structures (see Figure 5.32).

This result also suggests that the nature of the substituents has an effect on the structure obtained. Thus, combining K-3-BrCate (where the C-Br···Br-C has a perpendicular arrangement) and K-3-MeCate (where the C-Me···Me-C has both collinear and perpendicular arrangements), resulted in K-3-BrCate/3-MeCate solid solution, in which the substituent arrangement (Br/Me) seems to behave like a group with combination of Br and Me properties. This produced a collinear arrangement of C-Y···Y-C where Y is disordered Br/Me (identical to the C-Cl···Cl-C arrangement in K-3-ClCate[9]).
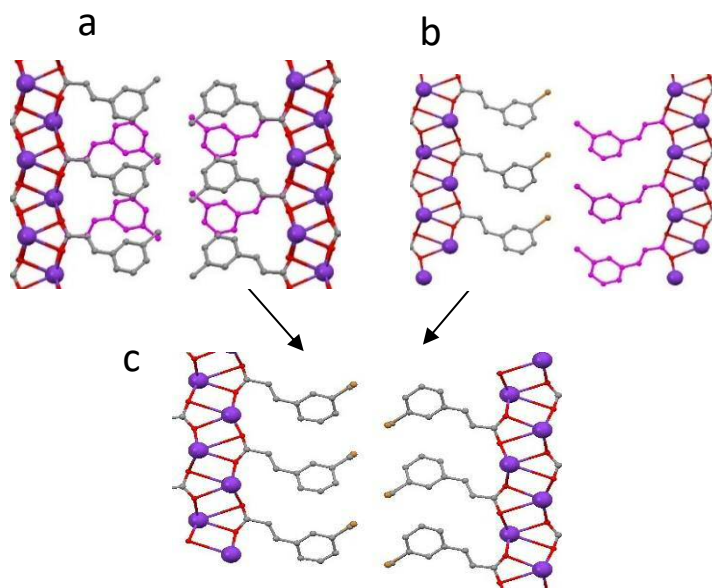
Figure 5.32. *Part of crystal structure of (a) K-3-MeCate, (b) K-3-BrCate and (c) K-(3-MeCate/3-BrCate) solid solution. Hydrogen atoms are omitted for clarity.*

Another striking feature of the structure is that, in the anion layers, the stacks of cinnamate units form along the b-axis. Such an arrangement brings the double bonds of double bond groups within the photoreactive distance (≈ 4Å) and parallel to each other, and thus a photodimerization reaction can be predicted. Details of the reaction are discussed in Chapter 6.

As shown in Figure 5.33, PXRD analysis of the bulk material (sample J) reveals a pattern that is similar to the PXRD pattern of K-3-ClCate rather than of K-3-BrCate. The PXRD pattern is identical to the calculated PXRD of crystal J, suggesting the formation a single phase of a solid solution.
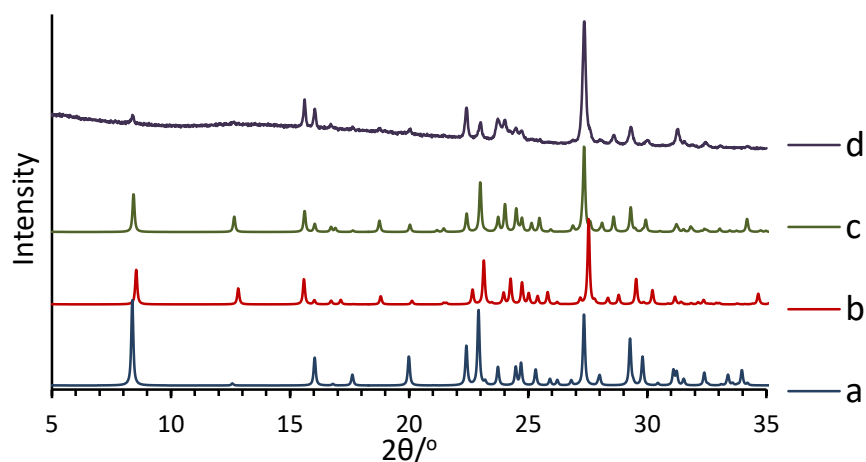
Figure 5.33. *The calculated PXRD pattern of (a) K-3-BrCate, (b) K-3-ClCate and (c) crystal J. (d) The experimental PXRD of sample J.*

- ***Samples prepared using other ratios***

The bulk material from the preparation using a 1:6 ratio of 3-BrCA:3-MeCA in a KOH solution (sample K) was characterized by PXRD. Two phases were clearly visible, one similar to crystal J and another similar to K-3-MeCate (crystal K), see Figure 5.34. A single crystal (crystal K) from the crystallization of sample K showed by SC-XRD analysis a structure similar to K-3-MeCate. In the structure traces of Br were detected in the *meta*-position of the benzene ring (refined occupancies of 0.032(2) for Br and 0.968(2) for Me group).

Cocrystallization of a 1:8 ratio of 3-BrCA:3-MeCA in a KOH solution (sample L) produced a structure similar to K-3-MeCate, as shown by PXRD. However, peaks associated with structure J were also observed (Figure 5.34), indicating the existence of both structures J and K. (summary of different initial preparation ratios are shown in Table 5.17).

Table 5.17. *Summary of initial Br:Me ratios prepration in the J, K and L sample and their results.*

Sample label	Prep ratio Br:Me	Br:Me in the structure	The solid solution structure similar to:
J	1:1	1:1.3	K-3-ClCate
K	1:6	1:30	K-3-MeCate
L	1:8	No SC-XRD was done	Both K-3-MeCate and K-3-ClCate
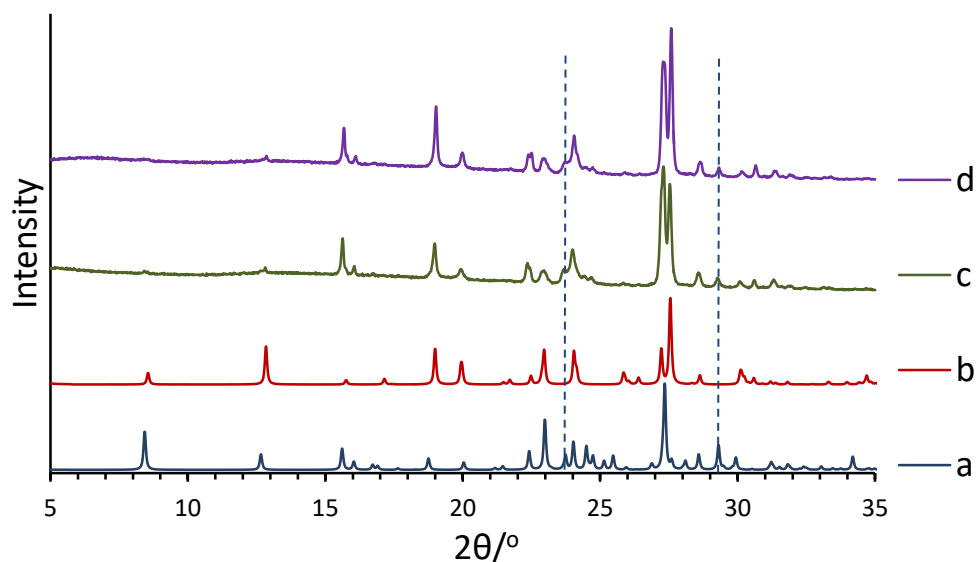
Figure 5.34. *The calculated PXRD pattern of (a) crystal J, (b) crystal K. (c) and (d) are the experimental PXRD patterns of samples K and L, respectively. Dashed lines mark some peak positions associated with the crystal J pattern.*

Crystallographic data for the structure determination of the crystals J and K are shown in Table 5.18.

Table 5.18. *Crystallographic data for the crystal structure determination of K-(3-BrCate/3-MeCate) solid solutions.*

	K-(3-BrCate/3-MeCate) (1:1) (crystal J)	*K-(3-BrCate/3-MeCate)* (1:6) (crystal K)
Formula	$C_{9.57} H_{7.72} Br_{0.43} K O_2$	$C_{9.97} H_{8.90} Br_{0.03} K O_2$
Formula weight	227.92	202.38
Temperature, (K)	293(2)	293(2)
λ , Å	1.54184	1.54184
Crystal system	Monoclinic	Monoclinic
Space group	P n a 2_1	P2_1/c
a, (Å)	11.4486(8)	21.0172(17)
b, (Å)	3.9807(3)	5.8403(3)
c, (Å)	41.928(3)	7.9031(7)
α, (°)	90	90
β, (°)	90	100.501(10)
γ, (°)	90	90
Volume, (Å³)	1910.8(2)	953.83(12)
Z	8	4
Density (calculated), (Mg/m³)	1.585	1.409
Absorption coefficient, (mm⁻¹)	6.658	4.736
F(000)	921	419
Crystal size, (mm³)	0.17 x 0.10 x 0.03	0.23 x 0.09 x 0.04
Reflections collected	3985	1803
Independent reflections	2637	1338
R(int)	0.0355	0.0179
Goodness-of-fit on F^2	1.152	1.062
Final R_1 indices [I>2sigma(I)]	0.0779	0.0572
Final wR_2	0.2204	0.1620
R_1 indices (all data)	0.0835	0.0616
wR_2 (all data)	0.2245	0.1692

Ammonium salts

A single crystal, from the crystallization from a solution with an initial ratio of 1:1 3-BrCA:3-MeCA in NH_4OH solution (sample M), was selected and the crystal structure was determined. The material crystallized in space group C2/c. The asymmetric unit consists of an NH_4^+ ion on the 2-fold rotational axis, and a 3-substituted-Cate/3-substituted-CA unit, with a carboxylic acid proton disordered between two oxygen atoms. The 3-substituted position is occupied by disordered Br/Me with a ratio of 0.588(4)/0.411(4). It is not surprising that the structure is similar to both NH_4-3-BrCate/3-BrCA (phase II) and NH_4-3-MeCA/3-MeCate structures, which have similar unit cell parameters and packing.

The experimental PXRD of sample M showed an identical pattern to that calculated for the structure determined, suggesting a mono-phasic sample (see Figure 5.35). The study then aimed to investigate the possibility of forming solid solution material comprising 3-MeCate/3-BrCate, with the structure similar to phase (I) of the NH_4-3-BrCate/3-BrCA or NH_4-3-BrCate (both have ideal geometry of double bonds for a photodimerization reaction). Thus, an initial ratio of 1:6 3-MeCA:3-BrCA in ammonia solution (NH_4OH) (sample N) was prepared and crystallized.

SC-XRD of a suitable crystal (crystal N) revealed a similar structure to the crystal from sample M. The disordered Br/Me in the asymmetric unit were in the ratio 0.899(4)/0.100(4). Additionally, as seen in Figure 5.35, PXRD of the material showed a pattern identical to that calculated for crystal N. This result indicates that this structure is more favorable for this binary system of the salts, at least with the preparation ratios in the range 1:1-1:6 (3-MeCA:3-BrCA).

Crystallographic data for the structure determination of the crystals M and N are shown in Table 5.19.
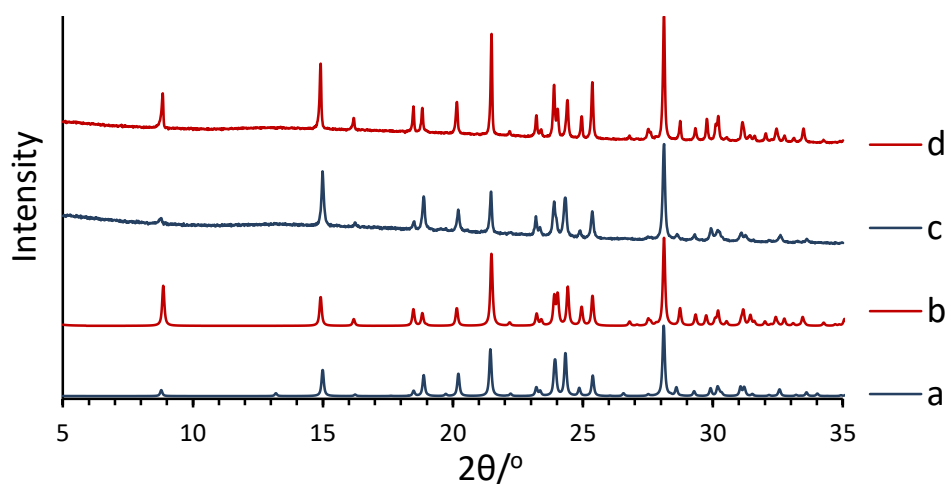
Figure 5.35. *The calculated PXRD pattern of (a) crystal M and (b) crystal N. (c) and (d) are the experimental PXRD of sample M and N respectively.*

Table 5.19. *Crystallographic data for the crystal structure determination of NH₄-(3-BrCate/3-BrCA)/(3-MeCate/3-MeCA) solid solutions.*

	NH₄-(3-BrCate/3-BrCA)/(3-MeCate/3-MeCA) (1:1)(crystal M)	NH₄-(3-BrCate/3-BrCA)/(3-MeCate/3-MeCA) (1:6)(crystal N)
Formula	$C_{18.82}H_{19.47}Br_{1.18}NO_4$	$C_{18.20}H_{17.60}Br_{1.80}NO_4$
Formula weight	417.79	458.01
Temperature, (K)	293(2)	293(2)
λ , Å	1.54184	1.54184
Crystal system	Monoclinic	Monoclinic
Space group	C2/c	C2/c
a, (Å)	40.316(2)	39.9565(14)
b, (Å)	5.9697(3)	6.0028(2)
c, (Å)	7.6734(3)	7.6666(3)
α, (°)	90	90
β, (°)	93.584(5)	93.221(3)
γ, (°)	90	90
Volume, (Å³)	1843.20(15)	1835.94(11)
Z	4	4
Density (calculated), (Mg/m³)	1.506	1.657
Absorption coefficient, (mm⁻¹)	3.687	5.283
F(000)	850	915
Crystal size, (mm³)	0.24 x 0.04 x 0.03	0.22 x 0.04 x 0.03
Reflections collected	3145	3053
Independent reflections	1774	1803
R(int)	0.0200	0.0184
Goodness-of-fit on F²	1.045	1.043
Final R₁ indices [*I*>2sigma(*I*)]	0.0514	0.0336
Final wR₂	0.1292	0.0839
R₁ indices (all data)	0.0690	0.0393
wR₂ (all data)	0.1423	0.0896

5.3.2.c. 3-FCA/3-BrCA salts

Results in Chapter 4 indicate the ability of forming a solid solution of a binary system of 3-BrCA and 3-FCA with the ratio of 8:1 to produce a structure that is similar to 3-BrCA. A ratio of *ca.* 1:10 produced a structure similar to 3-FCA. Therefore, the aim here is to investigate how this binary system behaves as K^+ and NH_4^+ salts.

Potassium salts

The PXRD pattern of the crystalline material from crystallization of a solution with an initial ratio of 1:1 (3-BrCA:3-FCA) in KOH solution (sample O) revealed the formation of two distinct structures. One with structure is similar to K-3-FCate and the other is similar to K-3-BrCate. Thus, as shown in Figure 5.36, by comparing the experimental PXRD pattern of sample O contains peak from both K-3-FCate and K-3-BrCate. Interestingly, shifts in peak positions in the PXRD of sample O, relative to their positions in the pattern of K-3-FCate and K-3-BrCata, were observed. Peaks assigned to the K-3-BrCate structure shifted to higher 2θ, whereas those related to K-3-FCate shifted to lower 2θ. This trend clearly indicates the formation of solid solutions, consistent with the results observed in Section 4.3.2 of Chapter 4.
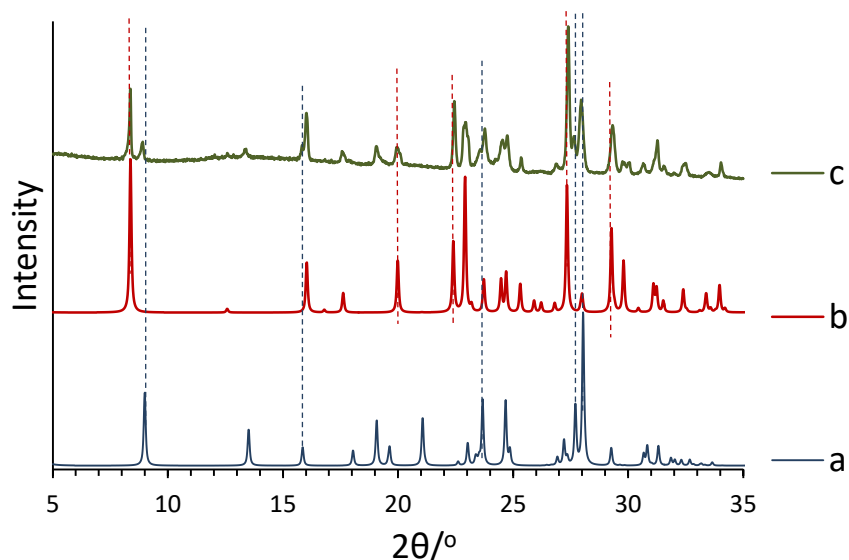
Figure 5.36*. The calculated PXRD pattern of (a) K-3-FCate and (b) K-3-BrCate, and (c) the experimental PXRD pattern of sample O. Dashed lines help in the comparison.*

Unfortunately, single crystal structure determination was not possible due to the powdery nature of the products.

Ammonium salts

The crystallized materials from a solution with an initial 1:1 ratio of 3-FCA:3-BrCA in NH_4OH solution (sample P) was characterized by PXRD. Similarly to the K^+ salt of the same binary system (discussed in the previous section), the pattern showed that the material crystallized into two structural types. One was similar to NH_4-3-BrCate/3-BrCA (phase II) and the other to NH_4-3-FCate/3-FCA. Shifts in the PXRD peak positions were also observed, indicating solid solution formation (see Figure 5.37). To

confirm the observation, SC-XRD structure determination was carried out. The material (crystal P) crystallized in monoclinic space group C2/c. Similar to the NH_4-3-BrCate/3-BrCA (phase II) structure, the NH_4 cation and one 3-halo-anion/3-halo-acid unit are present in the asymmetric unit. Br and F are disordered in the *meta*-position of the ring with a refined occupancy of 0.903(4) for Br and 0.097(4) for F. In the crystal structure, the 3-halo-anion/3-halo-acid unit and NH_4 cation form a layered structure, similar to the packing observed for NH_4-3-BrCate/3-BrCA (phase II).

Unfortunately, a suitable crystal of the solid solution salt with a similar structure to NH_4-3-FCate/3-FCA could not be found due to the general poor quality of the crystals. Therefore, preparation of an 8:1 of 3-FCA:3-BrCA in NH_4OH solution (sample Q) was performed. The crystallized material was then characterized using PXRD and SC-XRD. The crystal structure determination of a suitable single crystal (crystal Q) revealed a similar structure to NH_4-3-FCate/3-FCA. F and Br were disordered in the meta-position of the benzene ring of the 3-halo-Cate/3-halo-CA unit with occupancies of 0.951(3) and 0.049(3), respectively, confirming the formation of solid solution. As seen in Figure 5.37, PXRD analysis showed the existence of mainly the NH_4-3-FCate/3-FCA structure.

It is notable that the quantity of disordered Br and F in these structures (P and Q) showed a good agreement with the results observed from the cocrystallization of 3-BrCA and 3-FCA (discussed in Chapter 4). Thus, there is a limit to the quantity of one component that can be introduced into crystals of the other to form a solid solution, with a single structure form that is isostructural to either of the crystal forms of the pure component. This limit is *ca.* 1:8 for F-substituted:Br-substituted to form a structure that isostructural to a pure Br-substituted structure (here the F:Br ratios is *ca.* 1:10). In contrast the limit is *ca.* 10:1 for F-substituted:Br-substituted to form a single solid solution structure that is isostructural to a pure F-substituted structure (here the F:Br ratios is *ca.* 20:1).
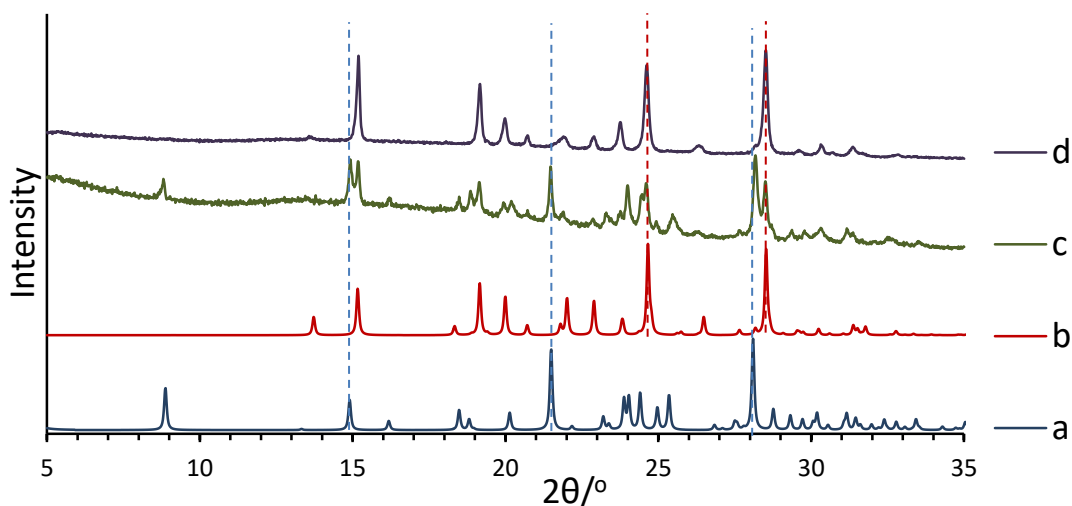
Figure 5.37. *The calculated PXRD patterns of (a) NH$_4$-3-BrCate/3-BrCA (phase II) and (b) NH$_4$-3-FCate/3-FCA. (c) and (d) Are the experimental PXRD patterns of sample P and Q, respectively. Dashed lines show the similarity of the pattern.*

Crystallographic data of the structure determination of the crystals P and Q are shown in Table 5.20.

Table 5.20. *Crystallographic data for the crystal structure determination of NH$_4$-(3-BrCate/3-BrCA)/(3-FCate/3-FCA) solid solutions.*

	NH$_4$-(3-BrCate/3-BrCA)/(3-FCate/3-FCA) (1:1)(Crystal P)	NH$_4$-(3-BrCate/3-BrCA)/(3-FCate/3-FCA) (1:8)(Crystal Q)
Formula	C$_{18}$ H$_{17}$ Br$_{1.77}$ F$_{0.23}$ N O$_4$	C$_{18}$ H$_{17}$ Br$_{0.10}$ F$_{1.90}$ N O$_4$
Formula weight	457.29	355.57
Temperature, (K)	293(2)	293(2)
λ , Å	1.54184	1.54184
Crystal system	Monoclinic	Monoclinic
Space group	C2/c	C2/c
a, (Å)	40.0547(11)	39.025(7)
b, (Å)	5.99210(10)	5.8832(7)
c, (Å)	7.6363(2)	7.5140(7)
α, (°)	90	90
β, (°)	93.566(2)	95.362(11)
γ, (°)	90	90
Volume, (Å^3)	1829.25(8)	1717.6(4)
Z	4	4
Density (calculated), (Mg/m^3)	1.660	1.375
Absorption coefficient, (mm^{-1})	5.258	1.205
F(000)	912	739
Crystal size, (mm^3)	0.19 x 0.08 x 0.02	0.16 x 0.10 x 0.02
Reflections collected	6248	2957
Independent reflections	1836	1657
R(int)	0.0125	0.0268
Goodness-of-fit on F^2	1.102	1.050
Final R$_1$ indices [I>2sigma(I)]	0.0358	0.0886
Final wR$_2$	0.0857	0.2372
R$_1$ indices (all data)	0.0369	0.1178
wR$_2$ (all data)	0.0865	0.2661

5.3.2.d. 3-CF₃CA/3-BrCA salts

The results from section 5.3.1.e, showed that determination of the crystal structure of K-3-CF₃CA and NH₄-3-CF₃Cate was challenging. However, the crystal structure of K-3-CF₃CA and NH₄-3-CF₃Cate shows differences from all other salt structures and, of 3-substituted-cinnamate structures discussed in this chapter. Since the K-3-CF₃CA showed flexibility of the K⁺ coordination including F-K coordinate and, a layer formed by K⁺ in the structure showed different arrangements of K⁺ throughout the layer. This layer is accommodated by water molecules. In the NH₄⁺ salt of 3-CF₃CA, segments layers are showed in the structure. Thus, the study here aimed to investigate the effect of the cocrystallization of 3-CF₃CA and 3-BrCA as a K⁺ or NH₄⁺ salts on the structure obtained.

Potassium salt

The product of material from crystallization of a preparation with an initial 1:1 ratio of 3-CF₃CA:3-BrCA in a KOH solution (sample R) was characterized using PXRD. The pattern had some peaks similar to those observed for K-3-BrCate (see Figure 5.38). However, additional peaks were also observed (marked by * in Figure 5.38) but they did not match any known phases (such as $KHCO_3$[13], γ_1-3-CF₃CA, γ_2-3-CF₃CA and K-3-CF₃Cate). Additionally, due to the powdery nature of the crystallized material, it was not possible to find a suitable single crystal for structure determination by SC-XRD.
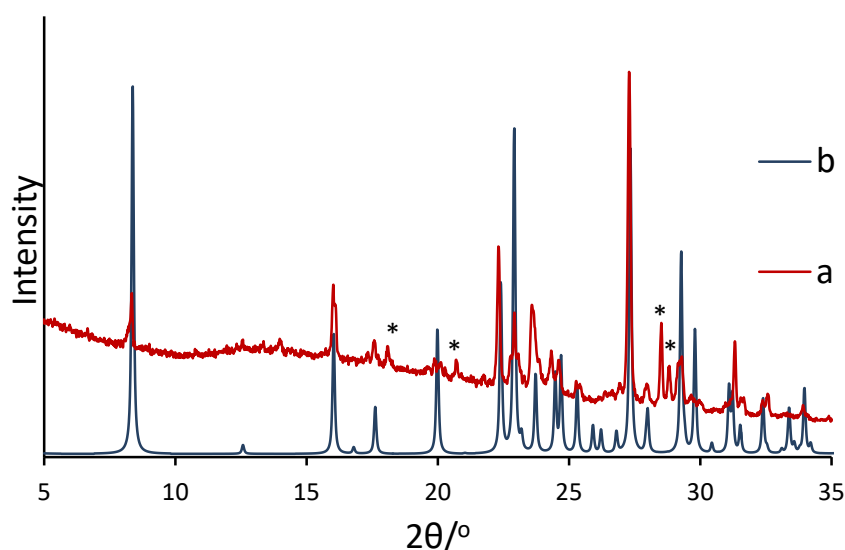
Figure 5.38. *(a) The experimental PXRD of sample R. (b) The calculated PXRD pattern of K-3-BrCate.*

Ammonium salts

A suitable crystal of the crystalline material prepared from an initial 1:1 ratio of 3-BrCA:3-CF$_3$CA in NH$_4$OH solution (sample S) was selected (crystal S) and the structure was determined. The result showed that it crystallized in space group C2/c. The 3-substituted-CA/3-substituted-Cate unit present in the asymmetric unit included disordered Br and CF$_3$ at the 3-substituted site in the ratio 0.85(1):0.15(1), indicating the formation of a solid solution. The structure is similar to NH$_4$-3-BrCate/3-BrCA (phase II), in which the double bonds of neighboring molecules are not in a parallel relationship.

PXRD analysis of sample S (Figure 5.39) showed that the pattern contained some peaks that matched the calculated PXRD of the structure determined, and some additional peaks. Unfortunately it was not possible to assign these peaks to any other known phases (for example: γ_1-3-CF$_3$CA, γ_2-3-CF$_3$CA, different structures of NH$_4^+$ salts of 3-BrCA and 3-CF$_3$CA). No other suitable single crystal was found with a different structure from the one found for crystal S. This result indicates that the crystallized material (S) contains solid solutions of NH$_4$-(3-BrCate/3-BrCA)/(3-CF$_3$Cate/3-CF$_3$CA) with a structure similar to NH$_4$-3-BrCate/3-BrCA (phase II), and another unknown crystallized material.

Crystallographic data for the structure determination of the salt solid solution is summarized in Table 5.21.
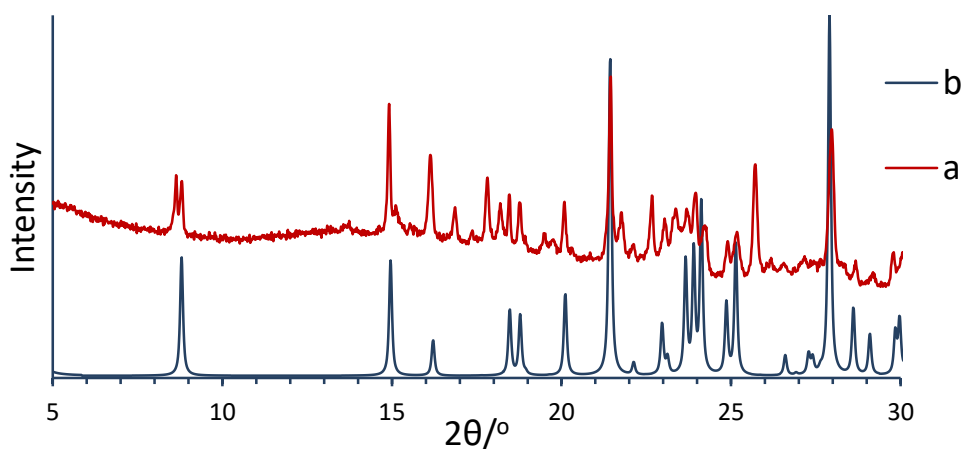
Figure 5.39*. The experimental PXRD of sample S in blue and the calculated PXRD pattern of crystal S in red.*

Table 5.21. *Crystallographic data for the crystal structure determination of NH₄-(3-BrCate/3-BrCA)/(3-CF₃Cate/3-CF₃CA) solid solution.*

Formula	$C_{18.33} H_{17} Br_{1.67} F N O_4$	Z	4
Formula weight	467.54	Density (calculated), (Mg/m³)	1.666
Temperature, (K)	293(2)	Absorption coefficient, (mm⁻¹)	4.984
λ , Å	1.54184	F(000)	933
Crystal system	Monoclinic	Crystal size, (mm³)	0.37 x 0.08 x 0.01
Space group	C2/c	Reflections collected	5720
a, (Å)	40.255(2)	Independent reflections	1864
b, (Å)	5.9826(3)	R(int)	0.0228
c, (Å)	7.7524(4)	Goodness-of-fit on F²	1.176
α, (°)	90	Final R₁ indices [*I*>2sigma(*I*)]	0.0462
β, (°)	93.477(5)	Final wR₂	0.1122
γ, (°)	90	R₁ indices (all data)	0.0622
Volume, (Å³)	1863.59(17)	wR₂ (all data)	0.1172

5.3.3. Investigation of crystallization of cinnamic acid salt of mixed cations (potassium/ammonium)

In NH_4^+ organic carboxylate salts, a dual function of the NH_4^+ ion is expected. In addition to being charged, it can also form hydrogen bonds with adjacent surrounding oxygen atoms which are directional interaction. On the other hand, only electrostatic interaction links K^+ ions to adjacent anions in the case of the K^+ carboxylate salts. It has been reported that metal coordination geometry and phase formation can be altered by the formation of mixed-metal materials. An example is the use of mixed metals (Co and Zn) to form $[\{(4,4`-bipy)-Co_{1-x}Zn_xCl_2\}_n]$.[26] Therefore, preparing *meta*-substituted cinnamic acid salts of mixed cations (K^+ and NH_4^+) may help in farther understanding of the role of the cations on the crystal structures obtained.

5.3.3.a. 3-BrCA salts of mixed cations

Preparation of the 3-BrCate salt of a mixture of a 1:1 molar ratio of NH_4OH:KOH solution and crystallization revealed, by optical microscopy, (Figure 5.40) the existence of two crystal morphologies; plate-like and needle-like (V and W, respectively).

The crystal structure determination of a suitable single crystal of V showed it to crystallize in space group C2/c with a cation site and a 3-BrCate/3-BrCA unit, with the carboxylic acid proton disordered between two oxygen atoms of the carboxylic acid/carboxylate group of the hydrophilic layers. Disordered K^+/NH_4^+ ions 0.755(3)/0.245(3) are present in the cation site. Determination of another single crystal, showed a K^+:NH_4^+ ratio of 0.853(4):0.147(4).

In this structure, the disordered mixed cations form layers parallel to the bc plane and are separated by bilayers of cinnamate/cinnamic acid units. An interesting observation is

that the crystal structure obtained is isostructural with that of NH$_4$-3-BrCate/3-BrCA (phase II) rather than K-3-BrCate, although the amount of K$^+$ in the crystals is 4-6 times more than NH$_4^+$. This suggests that the presence of the NH$_4^+$ ion influences the structure obtained (Figure 5.41) in favour of the structure similar to the protonated structure of NH$_4$-3-BrCate/3-BrCA (phase II).
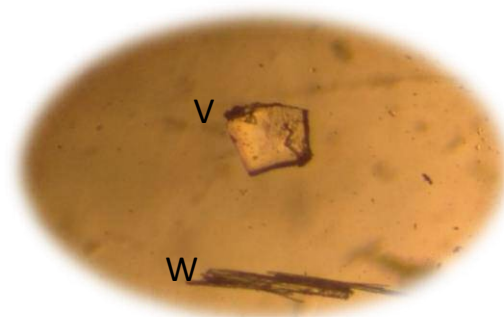
Figure 5.40. *A picture of the two habits of the crystalline materials.*
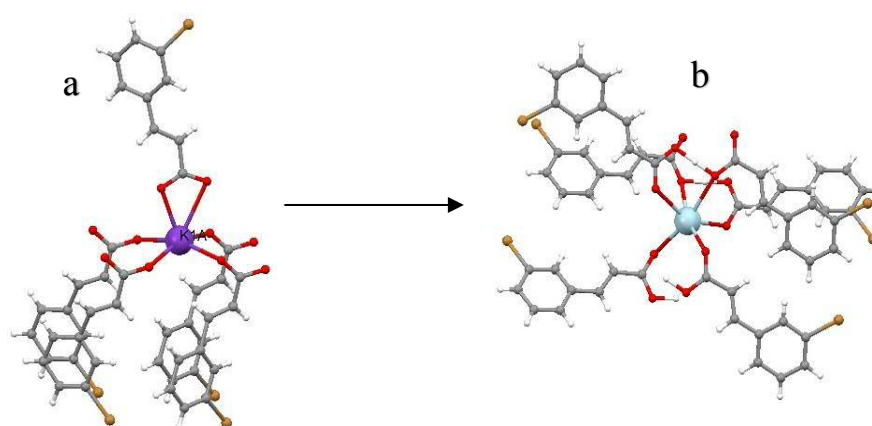
Figure 5.41. *The change of the cation coordination from (a) K-3BrCate to (b) sample V, the blue sphere in b is the disordered K$^+$/NH$_4^+$ ion.*

On the other hand, analysis of a suitable single crystal of W revealed that it crystallized in space group Cc. The asymmetric unit comprises two independent 3-BrCate anions and two K$^+$ cations. The crystal structure is identical to K-3-BrCate[9] (see section 5.3.1.b). Surprisingly, only K$^+$ was presented in the structure and no NH$_4^+$ was observed.

Thus, as observed in the crystals of V, the presence of a small amount of NH$_4^+$ gave structure similar to NH$_4$-3-BrCate/3-BrCA (phase II), whereas the structure similar to

K-3-BrCate[9] was obtained in the absence of the NH_4^+ ion. Crystallographic data for the crystals V and W are summarized in Table 5.22.

As seen in Figure 5.42, PXRD analysis of the 3-BrCA salts of mixed cations indicates the existence of both phases V and W.
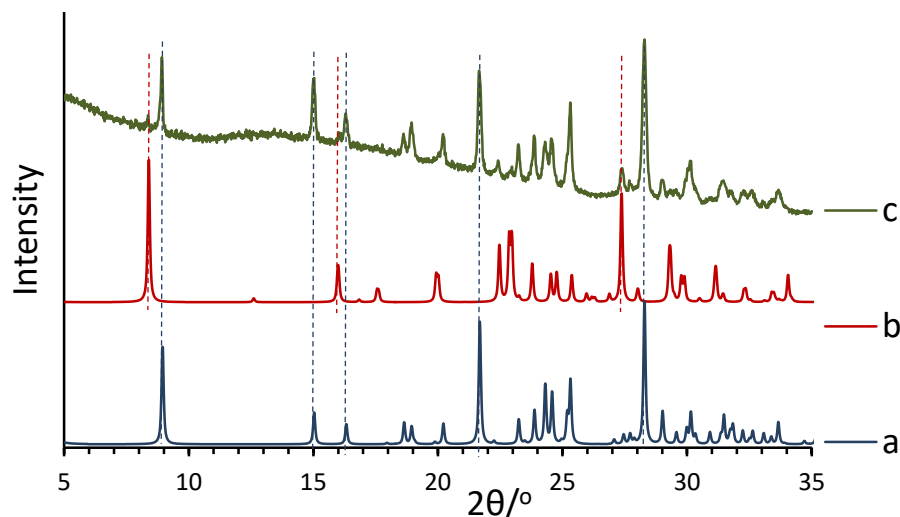
Figure 5.42. *The calculated PXRD pattern of crystals of (a) sample V and (b) sample W. (c) The experimental PXRD of the material from 3-BrCA salts of mixed cations. Dashed lines show matching peaks.*

Table 5.22. *Crystallographic data for the crystal structure determination of 3-BrCate salt of mixed cations.*

	(K/NH₄)-(3-BrCA-3-BrCate)(sample V)	K-3-BrCate (sample W)
Formula	$C_{18} H_{13.96} Br_2 K_{0.76} N_{0.24} O_4$	$C_9 H_6 Br K O_2$
Formula weight	487.89	265.15
Temperature, (K)	293(2)	293(2)
λ , Å	1.54184	1.54184
Crystal system	Monoclinic	Monoclinic
Space group	C2/c	Cc
a, (Å)	39.5270(14)	42.090(2)
b, (Å)	5.9548(2)	3.9712(3)
c, (Å)	7.6537(2)	11.4759(8)
α, (°)	90	90
β, (°)	92.474(3)	90.268(6)
γ, (°)	90	90
Volume, (Å³)	1799.81(10)	1918.1(2)
Z	4	8
Density (calculated), (Mg/m³)	1.801	1.836
Absorption coefficient, (mm⁻¹)	7.546	9.435
F(000)	961	1040
Crystal size, (mm³)	0.20 x 0.11 x 0.05	0.23 x 0.03 x 0.01
Reflections collected	3437	3044
Independent reflections	1606	2246
R(int)	0.0118	0.0339
Goodness-of-fit on F²	0.980	1.076
Final R₁ indices [I>2sigma(I)]	0.0223	0.0758
Final wR₂	0.0585	0.2141
R₁ indices (all data)	0.0234	0.0806
wR₂ (all data)	0.0596	0.2209

5.3.3.b. 3-ClCA salts of mixed cations

The 3-ClCA salt prepared from a 1:1 molar ratio mixture of $NH_4OH:KOH$ and crystallized. The material was characterized using optical microscopy, SC-XRD and PXRD. Two crystal morphologies; plate-like and needle-like crystals (Y and Z, respectively) were identified using optical microscopy (Figure 5.43).
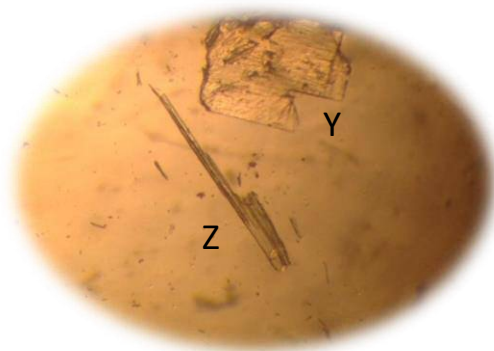
Figure 5.43. A picture of the two habits of the crystalline material.

Crystal structures were determined for suitable single crystals of Y and Z. Two crystals were analysed for Z and both crystallized in space group C2/c. The asymmetric unit includes a disordered cation site with refined K^+/NH_4^+ occupancies of 0.766(2)/0.234(2) for the first crystal and 0.82(3)/0.18(3) for a second crystal. The cation site lies on a 2-fold rotation axis. The asymmetric unit also contains a 3-ClCate/3-ClCA unit with a carboxylic acid proton lying on an inversion centre, equidistant from two oxygen atoms of the carboxylic acid/carboxylate group.

On the other hand, single crystal structure determination of a crystal of Z showed that it was similar to K-3-ClCate, where the asymmetric unit contains of two independent 3-ClCate anions and two cation sites, one with a refined K^+/NH_4^+ occupancy of 0.96(3)/0.04(3), while the other has full K^+ occupancy, indicating that only traces of NH_4^+ ion are present in the structure.

This results suggests that the identity of the cation influences the resultant structure. For example, inserting the NH_4^+ as a mixed cation with K^+, was found to lead to the formation of structures isostructural with NH_4-3-ClCate/3-ClCA[10] and K-3-ClCate/3-ClCA (NH_4-3-ClCate/3-ClCA[10] and K-3-ClCate/3-ClCA are isostructural).

However, a structure similar to K-3-ClCate was preferred in the case of absent or traces of the NH_4^+ cations. Crystallographic data for crystals Y and Z are shown in Table 5.23.

As shown in Figure 5.44, PXRD analysis of the 3-ClCA salts of mixed cations indicates the existence of both Y and Z.
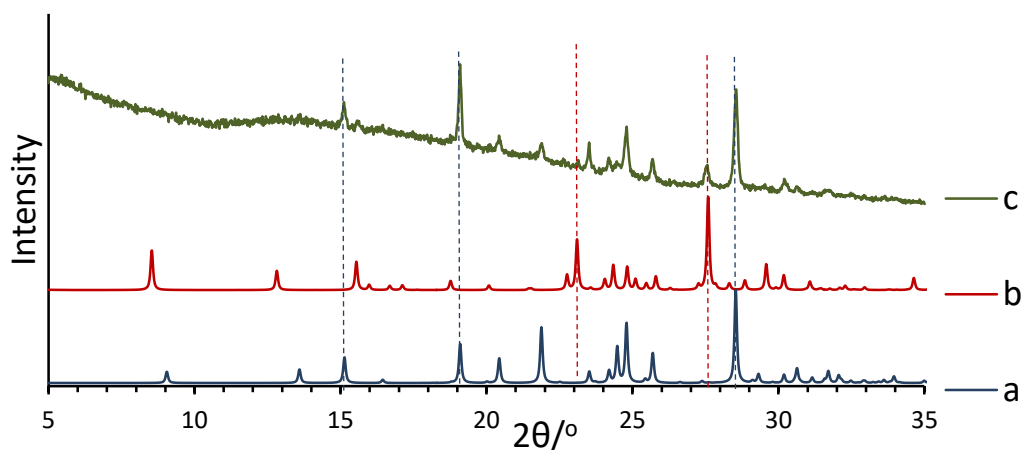
Figure 5.44. *The calculated PXRD pattern of crystal of (a) Y and (b) Z. (c) is the experimental PXRD of 3-ClCA salts of mixed cations. Dashed lines show similar peak positions.*

Table 5.23. *Crystallographic data for the crystal structures determination of 3-ClCate salt of mixed cations.*

	(K/NH₄)-(3-ClCA-3-BrCate)(Sample Y)	(K/NH₄)-3-ClCate (Sample Z)
Formula	$C_{18} H_{13.96} Cl_2 K_{0.76} N_{0.24} O_4$	$C_9 H_{6.05} Cl K_{0.99} N_{0.01} O_2$
Formula weight	398.34	220.42
Temperature, (K)	293(2)	293(2)
λ , Å	1.54184	1.54184
Crystal system	Monoclinic	Orthorhombic
Space group	C2/c	P n a 2₁
a, (Å)	39.105(2)	11.502(6)
b, (Å)	5.9156(3)	3.9215(15)
c, (Å)	7.5689(4)	41.403(13)
α, (°)	90	90
β, (°)	92.982(6)	90
γ, (°)	90	90
Volume, (Å³)	1748.53(17)	1867.5(13)
Z	4	8
Density (calculated), (Mg/m³)	1.513	1.568
Absorption coefficient, (mm⁻¹)	5.160	7.259
F(000)	816	895
Crystal size, (mm³)	0.10 x 0.07 x 0.03	0.18 x 0.03 x 0.01
Reflections collected	2953	3912
Independent reflections	1713	1554
R(int)	0.0182	0.2077
Goodness-of-fit on F²	1.053	0.914
Final R₁ indices [*I*>2sigma(*I*)]	0.0321	0.0779
Final wR₂	0.0891	0.1685
R₁ indices (all data)	0.0405	0.1947
wR₂ (all data)	0.0946	0.2533

5.4. Conclusion

The investigation of the K^+ and NH_4^+ salts of different cinnamic acids revealed eight new structures of cinnamate salts. Four of the structures are K salts; K-(3-ClCate/3-ClCA), K-3-FCate, K-3-MeCate and K-3-CF$_3$Cate. The others four are NH_4^+ salts: NH$_4$-(3-BrCate/3-BrCA) (phase II), NH$_4$-(3-FCate/3-FCA), NH$_4$-(3-MeCate/3-MeCA) and NH$_4$-(3-CF$_3$Cate/3-CF$_3$CA).

Comparison of the structures of K^+ salts of different 3-substituted cinnamic acids (Br, Cl, F, Me) shows many characteristics in common; all generally adopt layered structures and, additionally, have similar coordination around the K^+ ions. However, the structures are not identical. In fact, different arrangements of the benzene-vinyl group in the structures suggest that a change of the *meta*-substituent of the benzene ring can influence the structure obtained. K-3-CF$_3$Cate and NH$_4$-3-CF$_3$Cate/3-CF$_3$CA are different from any other cinnamate structures observed in this study or reported previously[9,10] for K^+ or NH_4^+ salts of the 3-substituted cinnamic acid.

Although a layered structure is also observed for K-3-CF$_3$Cate, it is a tetra-hydrate with six cinnamate cations in the asymmetric unit in addition to six independent K^+ cations, each adopting a different coordination. In contrast, NH$_4$-3-CF$_3$Cate/3-CF$_3$CA showed a layered segments in the structure, in which 8 cinnamate/cinnamic acid units are arranged in a bilayer arrangement.

The results from the cocrystallization investigation of NH_4^+ salts indicate that it is feasible to form a solid solution of a binary system of containing [3-BrCA/(3-ClCA, 3-MeCA, 3-FCA or 3-CF$_3$CA). Furthermore, since the structure of NH$_4$-3-BrCate/3-BrCA (phase II) is isostructural with the pure NH_4^+ salts of 3-ClCA, 3-MeCA and 3-FCA, it is not surprising that the solid solutions obtained adopted a similar structure. A comparable structure was also obtained for the NH_4^+ salt of a binary system of 3-BrCA/3-CF$_3$CA, although the pure the NH_4^+ salt of 3-CF$_3$CA showed different crystal structure. On the other hand, the cocrystallization of a NH_4^+ salt of 3-BrCA/3-FCA supports the result observed in Chapter 3; in the case of forming a solid solution of a binary system that comprises F:Br substituents group, there is a limit to the quantity of one component that can be introduced into the structure of the other to form a solid solution that is isostructural with either of the pure components.

For the K$^+$ salt of a binary system of 3-BrCA/3-ClCA, two structures of solid solutions were obtained. One is similar to K-3-BrCate and the other to K-3-ClCate. The result also indicated that the crystal structure of the solid solution obtained, and hence the halogen-halogen interaction geometries, depend on the relative quantity of the two salt components.

The results also show the ability to design crystals via the formation of K$^+$ salts of the binary system that comprise $\approx$ 1:1 K-3-BrCate and K-3-MeCate. The solid solution obtained had a structure similar to K-3-ClCate, where the double bonds of neighbouring molecules adopted ideal geometry for the photo-dimerization reaction. However, in this system, the solid solution with the structure similar to K-3-MeCate was also observed. This indicates that the quantity from the two components of a binary system controlled the structures obtained.

The work on the investigation of the competition between K$^+$ and NH$_4^+$ in salts of 3-BrCA and 3-ClCA showed that the co-cation (mixed cation) crystal can exist. The K$^+$ cation is the greater component in these mixed cation crystalline salts. In the case of the 3-BrCA mixed cation salt, although the NH$_4^+$ ion content was low (ratio of 1/6 of K$^+$) it had a great effect on the structure obtained. Thus the structure in this case is similar to NH$_4$-3-BrCate/3-BrCA (phase II) rather than K-3-BrCate. This result indicates the possibility of accessing the cinnamate salt structure by introducing only a small amount of another cation.

5.5. References:

1   B. Mondal, B. Captain and V. Ramamurthy, *Photochem. Photobiol. Sci.*, 2011, **10**, 891–894.

2   Y. Ito and G. Olovsson, *J. Chem. Soc. Perkin Trans. 1*, 1997, 127–133.

3   S. d'Agostino, F. Spinelli, E. Boanini, D. Braga and F. Grepioni, *Chem Commun*, 2016, **52**, 1899–1902.

4   M. D. Cohen and G. M. J. Schmidt, *J. Chem. Soc.*, 1964, 1996–2000.

5   M. D. Cohen, G. M. J. Schmidt and F. I. Sonntag, *J. Chem. Soc.*, 1964, 2000–2013.

6   H. Ihmels, D. Leusser, M. Pfeiffer and D. Stalke, *Tetrahedron*, 2000, **56**, 6867–6875.

7   G. K. Kole, G. K. Tan and J. J. Vittal, *CrystEngComm*, 2011, **13**, 3138–3145.

8   Y. Ito, B. Borecka, J. Trotter and J. R. Scheffer, *Tetrahedron Lett.*, 1995, **36**, 6083–6086.

9   D. Crowther, M. Chowdhury and B. M. Kariuki, *J. Mol. Struct.*, 2008, **872**, 64–71.

10   M. Chowdhury and B. M. Kariuki, *Cryst. Growth Des.*, 2006, **6**, 774–780.

11   B. M. Kariuki, J. B. Valim, W. Jones and J. King, *Acta Crystallogr. Sect. C*, 1995, **51**, 1051–1053.

12   B. M. Kariuki, J. B. Valim, W. Jones and J. King, *Acta Crystallogr. Sect. C*, 1994, **50**, 1665–1667.

13   J. O. Thomas, R. Tellgren and I. Olovsson, *Acta Crystallogr. B*, 1974, **30**, 1155–1166.

14   A. Bondi, *J. Phys. Chem.*, 1964, **68**, 441–451.

15   V. R. Thalladi, H.-C. Weiss, D. Bläser, R. Boese, A. Nangia and G. R. Desiraju, *J. Am. Chem. Soc.*, 1998, **120**, 8702–8710.

16   A. I. Kitaigorodsky, *Molecular Crystals and Molecules*, Academic Press, New York, 1973.

17   P. Murray-rust, I. P. W. C. Stallings, C. T. Monti, R. K. Preston and J. P. Glusker, *J. Am. Chem. Soc.*, 1983, **105**, 3206–3214.

18   E. Bernhardt, D. J. Brauer, M. Köckerling and G. Pawelke, *Z. Anorg. Allg. Chem.*, 2007, **633**, 947–954.

19   H. Takemura, N. Kon, M. Yasutake, H. Kariyazono, T. Shinmyozu and T. Inazu, *Angew. Chem. Int. Ed.*, 1999, **38**, 959–961.

20   M. K. Kim, V. Jo, D. W. Lee, I. Shim and K. M. Ok, *CrystEngComm*, 2010, **12**, 1481–1484.

21   A. Chanthapally, H. S. Quah and J. J. Vittal, *Cryst. Growth Des.*, 2014, **14**, 2605−2613.

22   S. Ahn, K. D. M. Harris, B. M. Kariuki and D. M. S. Zin, *J. Solid State Chem.*, 2001, **156**, 10–15.

23   S. Kanao, S. Kashino and M. Haisa, *Acta Crystallogr. Sect. C*, 1990, **46**, 2436–2438.

24   V. R. Pedireddi, D. S. Reddy, B. S. Goud, D. C. Craig, A. D. Rae and G. R. Desiraju, *J. Chem. Soc. Perkin Trans. II*, 1994, **2**, 2353–2360.

25   S. Tothadi, S. Joseph and G. R. Desiraju, *Cryst. Growth Des.*, 2013, **13**, 3242–

3254.

26   C. J. Adams, A. L. Gillon, M. Lusi and A. G. Orpen, *CrystEngComm*, 2010, **12**, 4403–4409.

Chapter 6: Investigation of solid-state photochemistry of cinnamates and acids

6.1. Introduction

The [2+2] solid-state photodimerization reaction is one of the most intensely studied in organic solid state chemistry. The main advantages of solid-state reactions over the solution-state reactions emanate from the relatively more rigid environment leading to higher selectivity, novel products, stereochemically pure products and high efficiency.[1–3]

With the aid of the topochemical principle, prediction of the reaction outcome of many solid-state reactions is possible. According to the principle, the reaction pathway (and hence the specific product obtained) is controlled by the spatial arrangement of molecules in the reactant crystal structure.[4–15] As discussed in Chapter 1 Section 1.4, *trans*-cinnamic acid and its derivatives played a significant role in rationalizing the relationships between the structure and properties of crystalline organic solids,[8] particularly in relation to photochemical reactivity.

Aside from generation of new organic materials through the direct solid-state photodimerization reaction of pure materials, other potential applications are accessible through crystal engineering strategies in which reactant molecules are prearranged in the solid state, prior to effecting a chemical transformation to generate a targeted product.[1,2,16,17] In this regard, the synthesis of unsymmetrical derivatives, in which two different *trans*-cinnamic acids, for example, undergo photodimerization, is a greater challenge. Nevertheless, they can be obtained by solid-state reactions by following crystal engineering principles as exemplified by the synthesis of 3-(3`,5`-dinitrophenyl)-4-(2`,5`-dimethoxyphenyl) cyclobutane-1,2-dicarboxylic acid from a stoichiometric cocrystal of the two reactant molecules prearranged through donor-acceptor interactions.[18] An alternative approach to asymmetric synthesis is through the formation of solid solutions, utilizing materials that are already known to crystallize with appropriate geometry for a photodimerization reaction.[19–24] For example, p-methyl, p-Br substitution of 2-benzyl-5-benzylidenecyclopentanon (1) crystallized in a photoactive crystal structure, but p-Cl, p-Br substituted of 2-benzyl-5-benzylidenecyclopentanon (2) crystallized in a photostable modification. Mixed crystallization of 1 and 2 produced a cocrystalline material with a

structure similar to (1) and underwent a solid-state photoreaction.[20] In another approach,[25] organization of the reagents for a photodimerization reaction in a solid solution was accessed via the introduction of a third component in the crystal. Thus, the crystal structures of pure 4-Cl-stilbazole and 4-methyl-stilbazole, showed unfavourable molecular packing for a photoreaction. However, cocrystallization of 4-Cl-stilbazole and 4-methyl-stilbazole with resorcinol, as a trinary system in the form of cocrystal solid solution, templated the structure by bringing the olefin groups of 4-Cl-stilbazole and 4-methyl-stilbazole into appropriate geometry for a photodimerization reaction.

Herein, we explore the photochemical behaviour of the materials discussed previously in this study, for which the photodimerization reaction was predicted from the crystal structures. For ease of discussion these materials were divided in three categories;

1) β_1 and β_2 3-FCA (discussed in Chapter 3), K-3-BrCate, NH$_4$-3-BrCate/3-BeCA (phase I)[26] and the NH$_4^+$ salts of 3-CF$_3$CA (discussed in Chapter 5) were investigated since the arrangement of the molecules in the crystal structure produced optimal geometry for a photodimerization reaction (parallel double bonds separated by less than 4.2Å).

2) The binary system of β-3-BrCA/3-ClCA (discussed in Chapter 4) showed that the molecules in the crystal structure adopted ideal geometry for the photodimerization reaction. In another binary system of K-3-BrCate/3-MeCate, the design strategy through salt formation was applied to obtain optimum geometry for the photodimerization reaction (discussed in Chapter 5). However, in both systems, the information obtained from SC-PXRD and PXRD was not conclusive regarding the molecular distribution in the crystal (i.e. whether the two components in the binary system form domains throughout the crystal or whether they are distributed randomly as a homogeneous solid solution). Therefore, the reaction was explored as a tool to probe how the molecules are distributed in the crystal. Additionally a potential outcome is the production of a heterodimer product, in which two different *meta*-substituted benzene rings are present in the same molecule, which is of interest from the synthetic chemistry point of view.

3) The result of the crystal structure determination of K$^+$ and NH$_4^+$ salts of 3-FCA and 3-MeCA (discussed in Chapter 5) showed a non-optimal arrangement of the reactive double

bonds. Therefore, a study was carried out, firstly, to investigate the possibility of the reaction to occur and, secondly, to determine any products obtained.

6.2. Experimental Methods

6.2.1. UV Irradiation

The solid material of the appropriate sample was ground to a fine powder using a pestle and mortar and then spread in a thin layer on a glass dish and exposed to UV radiation from a high pressure mercury vapour lamp (λ = 300-700 nm). The irradiation was continued for several hours with periodic agitation of the powder (typically every 45 minutes to 6 hours) to promote uniform irradiation. All samples were analysed using PXRD, prior to the irradiation, to ensure mono phasic material.

6.2.2. Spectroscopic analysis

IR spectroscopy, solution-state ^{1}H NMR or electrospray mass spectrometry (ES-MS) were used to monitor the reaction and analyze the products. IR spectra were recorded on a Shimadzu IR Affinity-1 Fourier Transform Infrared spectrometer. Solution-state ^{1}H NMR spectra were recorded on a Bruker AM 400 MHz, with the sample dissolved in deuterated methanol [CD_3OD]. For the material after HPLC separation a Bruker AM 600 MHz solution-state ^{1}H NMR was used. ES-MS was carried out using a Waters LCT Premier XE mass spectrometer.

^{1}H NMR results of the products of irradiated K-(3-MeCate/3-BrCate) after HPLC separation

For the product in the HPLC peak (i) (as mentioned in Section 6.3.5.b): ^{1}H NMR (600 MHz, MeOD) δ 6.95 (t, J = 7.6 Hz, 2H), 6.85 – 6.74 (m, 6H), 4.26 (d, J = 6.2 Hz, 2H), 3.76 (d, J = 6.3 Hz, 2H), 2.17 (s, 6H), while for the material in the HPLC peak (ii):^{1}H NMR (600 MHz, MeOD) δ 7.16 (d, J = 7.7 Hz, 2H), 7.00 (dd, J = 12.4, 6.8 Hz, 3H), 6.84 (dd, J = 19.5, 7.1 Hz, 3H), 4.38 – 4.19 (m, 2H), 3.77 (dt, J = 16.1, 9.9 Hz, 2H), 2.20 (s, 3H). Some other peaks due to contamination during sample transfer were also observed but only peaks of products were selected.

6.2.3. Separation of the irradiated products by HPLC

HPLC analysis was carried out using an Agilent Technology 1200 series liquid chromatograph. Chromatographic separation was achieved using Rf-HPLC (Phenomenex, Luna C18 (2) column, 5μ, 250 mm × 4.6 mm). Gradient elution was carried out using solvents A (0.1% formic acid in water) and B (acetonitrile) with a gradient elution of A:B from 51:49 to A:B 49:51, for 25 minutes at a flow rate of 1.0 ml/min. Samples were prepared, prior to HPLC analyses by dissolving the materials in Acetonitrile. Drops of formic acid were added in the case of the salts to ensure the hydrolysis of salts to the corresponding acid, and the samples was filtered using a 0.2μm syringe filter before injection into the HPLC.

6.2.4. Crystallization of the photoproducts

Product from irradiation of *β*-3-FCA

Two structures, solvated and non-solvated, were determined for the dimeric products of the *β*$_1$-3-FCA, after irradiation. The solvated structure was crystallized from glacial acetic acid as colourless, plate-like crystals. In contrast, the non-solvated structure was obtained when the irradiated material was added to hot water in a vial, with continuous agitation of the vial to produce a brown deposit. The vial was then covered using para-film and left at room temperature. A day later, plate-like crystals were observed on the surface of the deposit.

Product from irradiation of *β*-3-ClCA/3-BrCA

The product from irradiation of *β*-3-ClCA/3-BrCA was crystallized from acetonitrile by slow evaporation of the solvent, leading to colourless, plate-like crystals denoted in this study as *β*-3-ClCA/3-BrCA-D.

Product from irradiation of NH$_4$-3FCate/3-FCA

The irradiated sample of NH$_4$-3FCate/3-FCA was dissolved in hot water by agitating the vial, until a precipitate of brown material was observed in the solution. The solution then was cooled to room temperature, covered with para-film, and left under ambient laboratory conditions. Several days later, thin plate-like crystals appeared.

6.3. Result and Discussion

6.3.1. Solid-state [2+2] photodimerization reactions of *β*-3-FCA

The crystal structures of both the β_1 and β_2 polymorphs of 3-FCA have the ideal geometry for solid-state [2+2] photodimerization reactions. The reactive neighbouring molecules along the stacks are related by unit cell translation (a-axis for β_1 and b-axis for β_2). The C=C bonds of neighbouring molecules along the stack are parallel to each other and the distance between the centres of the C=C bonds is 3.843Å for the β_1 polymorph and 3.775Å for the β_2 polymorph (Figure 6.1). As both polymorphs of 3-FCA meet the structural criteria characteristic of *β*-type structures, it would be expected, on topochemical grounds, that the photoproduct obtained in each case would be the mirror-symmetric dimer 3,3`-difluoro-*β*-truxinic acid (Scheme 6.1).
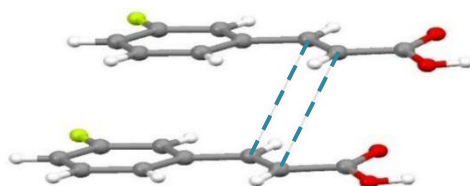
Figure 6.1. *The arrangement of two molecules in β_1-3-FCA showing the parallel double bonds. The same feature was observed in the β_2 structure.*
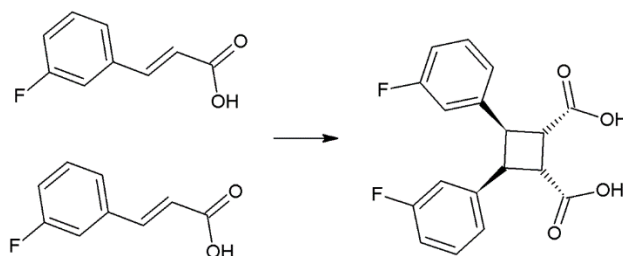
Scheme 6.1. *The photodimerization reaction of 3-FCA to give 3,3`-difluoro-β-truxinic acid.*

The photochemical reactivity of both the β_1 and β_2 polymorphs of 3-FCA under UV irradiation was studied. The sample was ground prior the photodimerization reaction, since greater reactivity is expected as a result of increasing of the exposure surface (i.e. increasing the surface area).[27] An initial indication that a photoreaction occurred in each case was the observation of a colour change from white to yellow, which become increasingly noticeable as the irradiation time increased. For each polymorph, analysis of the photoproduct by ES-MS confirmed that a dimer is indeed obtained, characterized by a significant M^+ peak at m/z = 331.06 (together with a residual monomer at m/z = 165.02 for incomplete reactions).

6.3.1.a. Monitoring the reaction by IR studies

The results from IR spectroscopy also demonstrated the progressive consumption of the monomer and formation of the dimer, as a function of irradiation time. The C=C stretching band (1633 cm^{-1}, Figure 6.2, band **4**) decayed consistent with the loss of the C=C bond on reaction. The C=O stretching band (*ca*. 1696 cm^{-1}, Figure 6.2, band **3**) concurrently shifted to a higher frequency (*ca*. 1710 cm^{-1}, Figure 6.2, band **2**) and another band developed at 1750 cm^{-1} (Figure 6.2, band **1**). A sample of the photoproduct crystallized from acetic acid displayed only band 2 (i.e. no bands **1** or **3**), indicating that the shift from *ca*. 1696 cm^{-1} to *ca*. 1710 cm^{-1} was due to the loss of conjugation during the dimerization reaction. Band **1** (1750 cm^{-1}) may be associated with changes in the crystal environment and disruption of hydrogen bonding that accompanies the loss of crystallinity revealed by PXRD (shown in Section 6.3.1.b). Thus, the shift of the C=O stretching band from *ca*. 1696 cm^{-1} to *ca*. 1750 cm^{-1} could be a result of loss of the hydrogen bonds between two molecules carboxylic acids. Another possible explanation for the appearance of band **1** may be due to the formation of acid anhydride through dehydration.
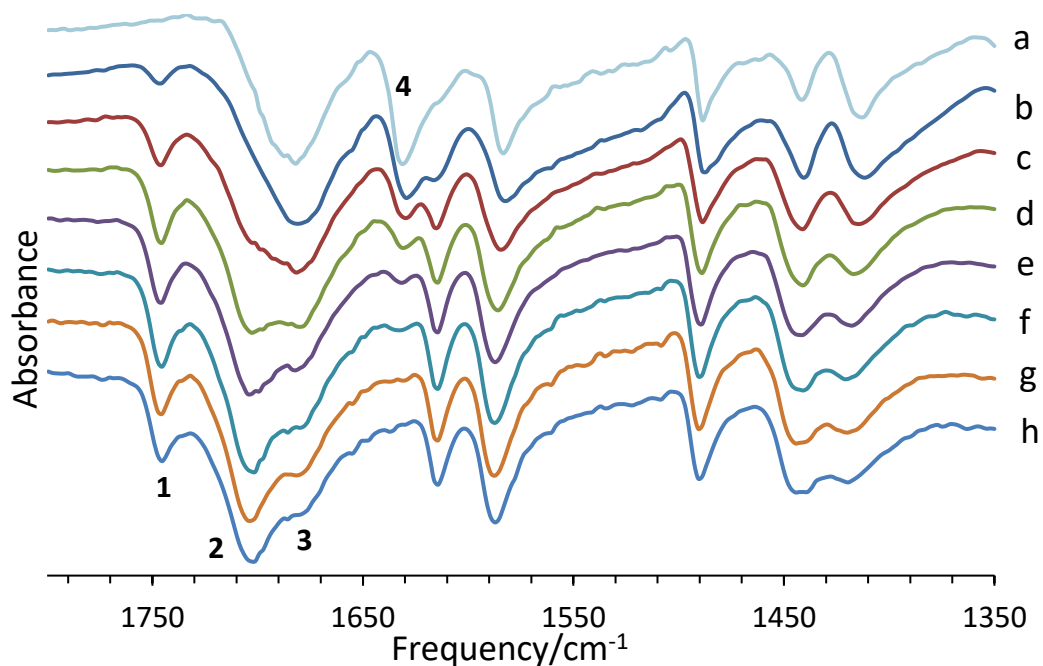
Figure 6.2. *IR spectra showing the region from 1350 to 1800 cm^{-1} for (a) the β$_1$ polymorph of 3-FCA, and for samples collected following UV irradiation for (b) 6 hrs, (c) 12 hrs, (d) 18 hrs, (e) 24 hrs, (f) 30 hrs, (g) 36 hrs and (h) 42 hrs.*

6.3.1.b. Monitoring the reaction by solution-state ^{1}H NMR

The loss of crystallinity during the photodimerization reactions for both the β_1 and β_2 polymorphs of 3-FCA, as illustrated in Figure 6.3, prevents the use of SC-XRD or PXRD for monitoring the progress of the solid-state reaction and for determining the crystal structure of the directly produced photoproduct in each case. Under such circumstances, solid-state NMR spectroscopy has often been used to monitor the evolution of solid-state reactions of *trans*-cinnamic acids[28–31] due to the sensitivity of this technique to probe changes in the local environment. In the study, solution-state ^{1}H NMR has proved to be an effective technique for monitoring the photoreaction.
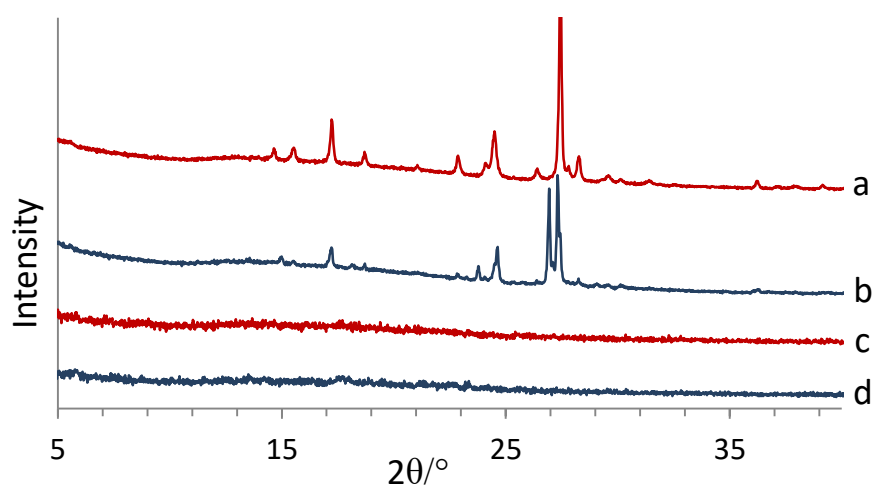
Figure 6.3. *Powder XRD patterns for: (a) the β_1 polymorph of 3-FCA, (b) the β_2 polymorph of 3-FCA, (c) the product following UV irradiation of the β_1 polymorph, and (d) the product following UV irradiation of the β_2 polymorph. From (c) and (d), it is clear that crystallinity is lost after irradiation of both the β_1 and β_2 polymorphs.*

The ^{1}H NMR spectra recorded (*ex-situ*) for samples before and during irradiation of the β_1 polymorph showed that the ^{1}H resonances due to vinyl hydrogens from *ca.* 6.8 and 8 ppm (labelled **i** in Figure 6.4) disappeared during the reaction, while ^{1}H resonances due to the hydrogens of the cyclobutane ring at *ca.* 4.3-4.7 ppm (labelled **ii** in Figure 6.4) appeared and increased in intensity as a function of irradiation time. Similar results was observed for the β_2 polymorph of the acid, indicating the occurrence of the photodimerization reaction. The progression of the photoreaction in both cases will be discussed later in this section.

On the other hand, during the irradiation of the samples (β_1 and β_2 polymorphs of 3-FCA), evidence of the isomerization process was observed (transformation of 3-FCA molecules from *Trans* to *Cis* isomers). This was indicated by the observation of small peaks in the

^{1}H NMR spectra as the irradiation proceeded, corresponding to the proton that attached to the vinyl group (Hα) of the *cis* isomer of the acid, around 6.4 ppm (see Figure 6.4 of β_1-3-FCA results). This process is discussed later in Section 6.3.5.a.
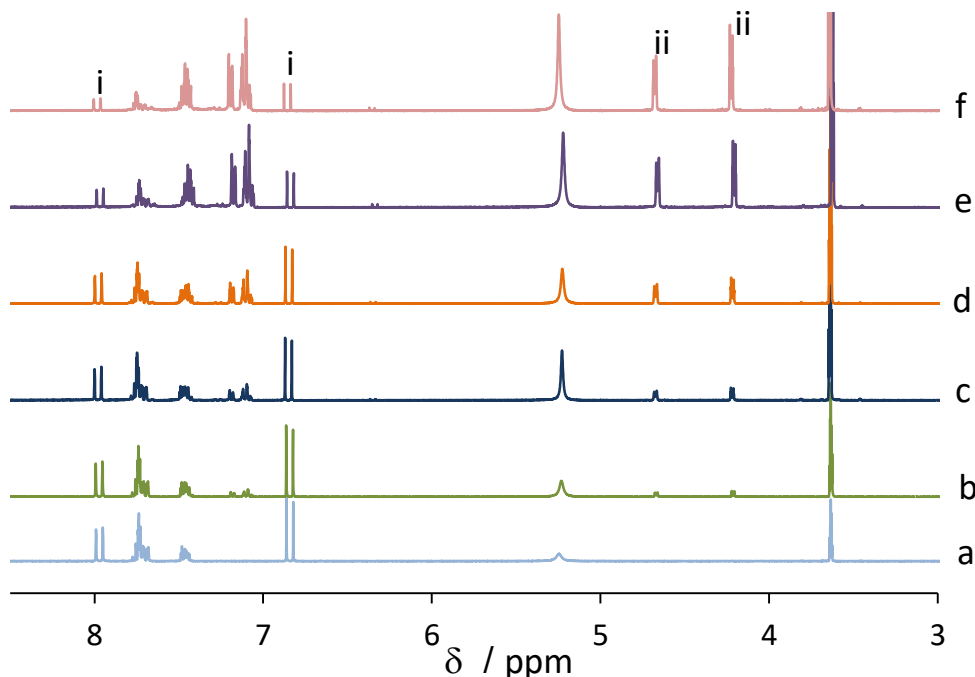
Figure 6.4. *Solution-state ^{1}H NMR spectra recorded (ex-situ) for (a) the β₁ polymorph of 3-FCA, and for samples collected after UV irradiation for (b) 60 mins, (c) 105 mins, (d) 195 mins, (e) 510 mins and (f) 720 mins.*

The effect of mixing on photoreaction progress

The effectiveness of solid-state photochemistry in synthesis depends on its applicability to bulk samples. In this work, solution-state ^{1}H NMR was used as a method for monitoring the progress of the reaction in bulk samples.

- β₁-3-FCA

Two experiments were done using β_1 polymorph of 3-FCA. In the first experiment, *ca.* 100 mg of material was spread evenly in a Petri dish of diameter 5.5 cm, and in the second experiment, about 300 mg of sample in a dish of diameter 7.5 cm was used (the density of material in each case was approximately similar, *ca.* 6.5 mg/cm^2). For the first experiment, 10 samples were collected over a period of 12 hours. The first sample was collected 60 mins after initiating UV irradiation, followed by sampling at intervals of 45, 45, 45, 45, 90, 90, 90, 90 and 120 mins. The solid was mixed thoroughly before collecting each sample or at 45 min intervals between sample collections. The collected samples were

dissolved in deuterated methanol and ^{1}H NMR spectra were recorded. The percentage of unreacted monomer was determined from integrated peak intensities and is shown in blue in Figure 6.5a [reactant% = 100 × reactant/(reactant + product)]. The results show that over 93% of the monomer was consumed after 12 hours. A plot of ln(reactant%) *versus* time is linear (blue line in Figure 6.5b) with R^2 = 0.9986, consistent with a first order reaction. The result is consistent with F.-L. Hu and co-workers observation[32] of a first order process behaviour of [2+2] photocycloaddition reaction in the solid state. In another study,[33] β-2-fluoro- and β-4-fluoro-*trans*-cinnamic acids also showed first order kinetics for a photodimerization reaction.

For the second experiment, the same conditions for irradiation were replicated and the same sample collection procedure was followed. After initiating irradiation, eight samples were collected at intervals of 6 hours, with the final sample being collected after a total of 106 hours. In this case, over 96% of the monomer had been consumed after 36 hours (black line in Figure 6.5a) and a plot of ln(reactant%) against time (black line in Figure 6.5b) is also linear (R^2 = 0.9986) for the first 30 hours. For longer exposure times, the data deviate from linearity, possibly due to increasing sampling errors as the amount of reactant diminishes. Interestingly, the reaction takes about three times longer for this sample, although the sample density was the same in each experiment. Nevertheless, the final conversion is again close to 100% and the slower rate may be attributed to the fact that the intervals mixing of the sample were longer. The implication is that fast reaction rates may be achievable for relatively large quantities of sample with continuous agitation.

- β_2-3-FCA

The progress of the reaction was also investigated by solution-state ^{1}H NMR for a sample of β_2 obtained by thermal phase transformation of β_1. The results indicate that over 90% of the reactant was consumed after 12.5 hours (figure 6.6a) and the plot of ln(reactant%) against time (figure 6.6b) is also linear (R^2 = 0.994) for the first 10 hours (again, the deviation from linearity for longer exposures may be attributed to sampling errors). Although the reaction appears to proceed more slowly for the β_2 polymorph, conclusions could not be drawn regarding the relative reaction rates for the β_1 and β_2 polymorphs, on the basis of the present data, due to the dependence of the observed reaction rates on the efficiency of sample mixing.
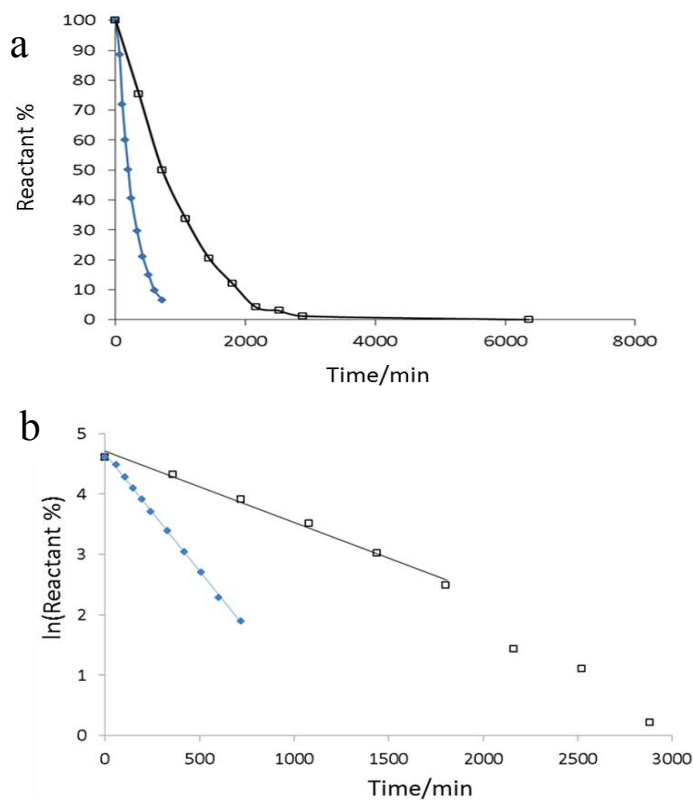
Figure 6.5. *(a) The percentage of reactant phase remaining as a function of UV irradiation time for short (blue) and long (black) intervals mixing of samples of the β₁ polymorph of 3-FCA, and (b) the corresponding plot of ln(reactant%) as a function of time.*
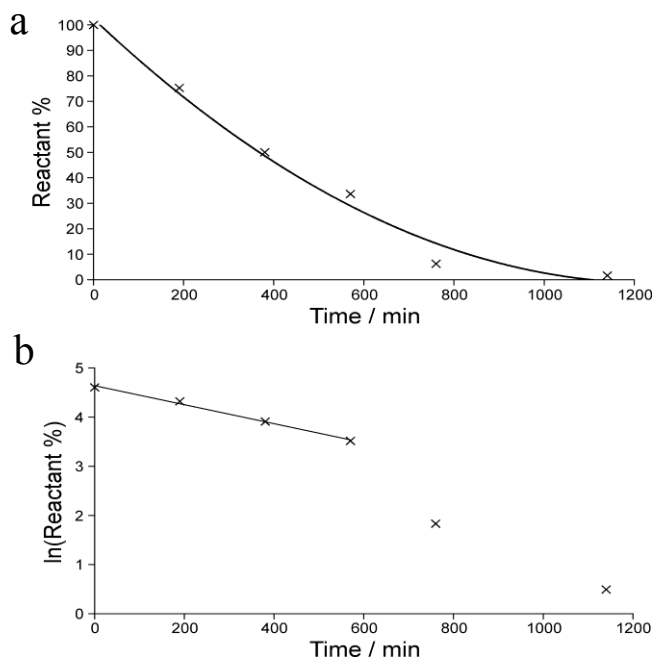
Figure 6.6. *(a) The percentage of reactant phase remaining as a function of UV irradiation time for the β₂ polymorph of 3-FCA, and (b) the corresponding plot of ln(reactant%) as a function of time.*

6.3.1.c. The crystal structure of the photodimerization product

To confirm that the photoproduct is, indeed, 3,3`-difluoro-$\beta$-truxinic acid, the crystal structure of a recrystallized sample of the photoproduct was determined from SC-XRD data. Crystallization of the photoproduct from glacial acetic acid (GAA) gave solvated structure of 3,3`-difluoro-β-truxinic acid, in contrast non-solvated structure of 3,3`-difluoro-β-truxinic acid was crystallized using hot water.

Structure determination of a crystal obtained from GAA showed that it crystallized in space group P$\bar{1}$. In this structure the asymmetric unit is comprised of one molecule of 3,3`-difluoro-$\beta$-truxinic acid and one molecule of acetic acid (Figure 6.7a). The two 3-fluorophenyl groups of the 3,3`-difluoro-β-truxinic acid molecule are disordered between two orientations related by 180° rotation about the C(phenyl)–C(cyclobutane) bond, with occupancies of 0.564(5) and 0.435(5) for F1/F1A and occupancies of 0.584(4) and 0.416(4) for F2/F2A. The C–C–C bond angles within the cyclobutane ring deviate only slightly from 90°, ranging from 87.86 to 90.59°. The carboxylic acid groups of neighbouring 3,3`-difluoro-β-truxinic acid molecules are linked to each other by hydrogen bonding with O(2)···O(1) and O(4)···O(3) distances of 2.680Å and 2.655Å, respectively, and O(2)–H(2A)···O(1) and O(4)–H(4)···O(3) angles of 172.9° and 178.3°, respectively, to form zig-zag chains. Adjacent chains interact in a zip-like fashion via the fluorophenyl groups, to form layers parallel to the (112) plane (Figure 6.7b).

The acetic acid molecules exist as hydrogen bonded pairs with O(6)···O(5) distance of 2.641Å and O(6)–H(6)···O(5) of 165.4°. There is no direct hydrogen bonding between the acetic acid molecules and dimer molecules. Nevertheless, the oxygen atoms of the solvent dimer (O(6) and O(5)) and O(3) from the truxinic acid are in contact, forming a triangular shape with the sides of O(6)···O(3): 2.980Å , O(3)···O(5):3.020 and O(6)–···O(5): 2.641Å (see Figure 6.8a). The refined structure revealed an ordered OH group for both the photoproduct and acetic acid.

In the structure, the acetic acid (solvent molecule) readily occupies spaces located above and below the layers of the dimer molecules (Figure 6.8b). The incorporation of other molecules (in this case, acetic acid) into the crystal structure is a common feature of the structures of other derivatives of β-truxinic acid.[18,34,35] For example, the structure of the

dimeric product 3-(3`,5`-dinitrophenyl)-4-2`,5`-dimethoxyphenyl)cyclobutane-1,2-di-carboxylic acid is a solvated structure with water and toluene,[18] both 3,3`-dibromotruxinic acid and 3,3`-dichlorotruxinic acid structures are water-acetic acid solvated[34]and, tetrahydrofuran and water are incorporated in the structure of 4,4'-dibromo-β-truxinic acid[35].
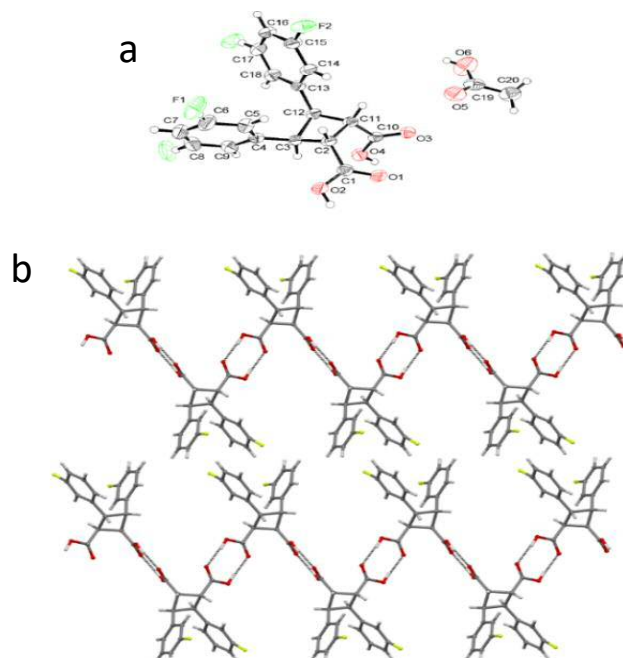
Figure 6.7. (a) The asymmetric unit in the crystal structure of the acetic acid solvate of 3,3` difluoro-β-truxinic acid. (b) Part of the crystal structure showing a layer of chains. Only the orientation of the fluorophenyl rings corresponding to the major disorder component is shown, and dashed lines represent hydrogen bonds.
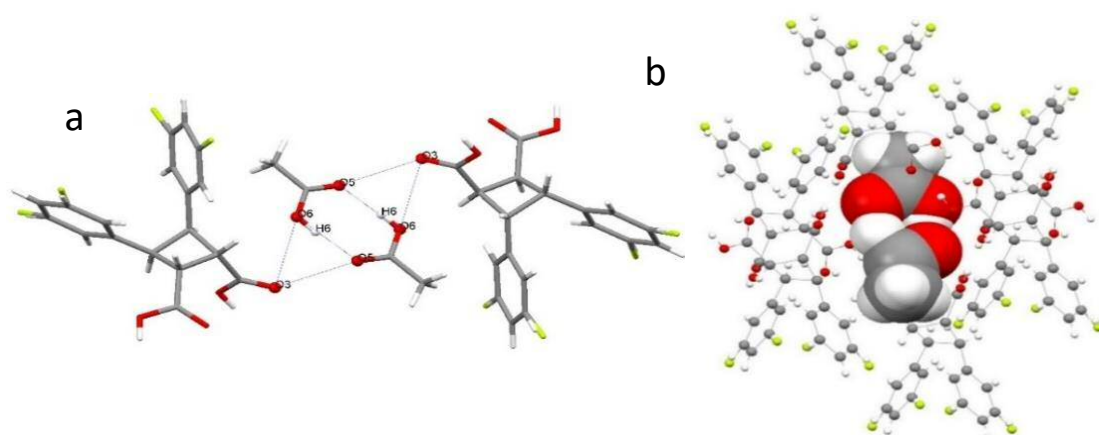
Figure 6.8. (a) Illustration of the hydrogen bonds of the acetic acid solvent molecules and the triangular shape formed by the contact of the solvent with the dimer molecules. (b) The acetic acid solvent, in a space filling style, accommodated in the spaces between the 3,3`difluoro-β-truxinic acid molecules.

On the other hand, crystallization of the product from water produced a non-solvated structure. SC-XRD determination showed that the photoproduct crystallized from water in space group P$\bar{1}$ and only one 3,3`-difluoro-*β*-truxinic acid molecule comprised the asymmetric unit. Similarly to the solvated structure of the dimer, the two 3-fluorophenyl groups of the 3,3`-difluoro-*β*-truxinic acid molecule are disordered between two orientations related by a 180° rotation about the C(phenyl)–C(cyclobutane) bond, with occupancies of 0.675 (5) and 0.324(5) for F1/F1A and occupancies of 0.844(5) and 0.155 (5) for F2/F2A. The C-C-C bond angles within the cyclobutane ring deviate only slightly from 90°, ranging from 87.82° to 89.16°. To our knowledge, no other non-solvated truxinic acid structure has been reported.

In the structure, each 3,3`-difluoro-*β*-truxinic acid molecule is in contact with two other molecules via hydrogen bond interactions in a zig-zag fashion (Figure 6.9) similar to that seen in the solvated structure. Relative to a central molecule, chain of the dimer molecule extends in an "across the page" for the solvated structure (Figure 6.10a) and "into the page" for the non-solvated one (Figure 6.10b) to allow efficient packing. Crystallographic data for the photoproducts (solvated and non-solvated) are summarized in Table 6.1.
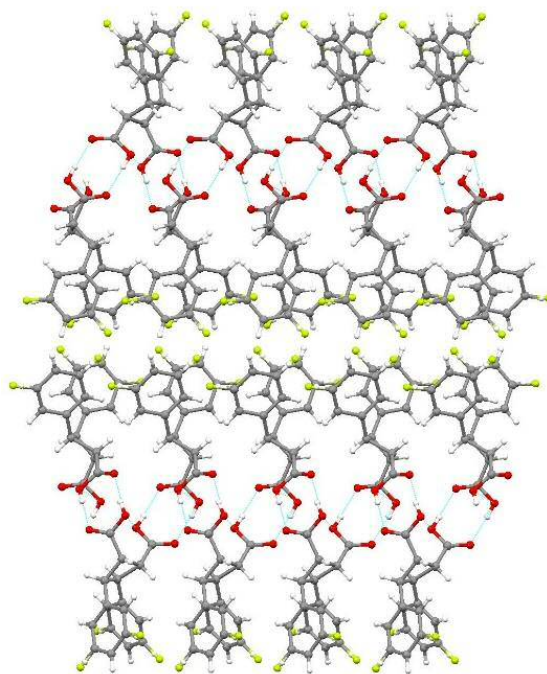
Figure 6.9. *The crystal structure of 3,3`-difluoro-β-truxinic acid. Dashed lines represent hydrogen bonds.*
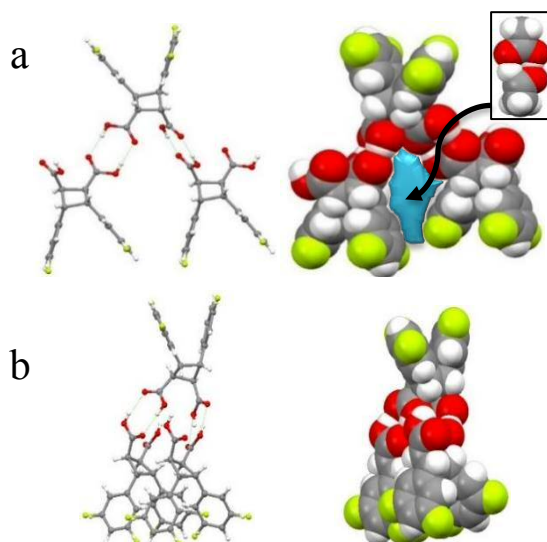
Figure 6.10. *Part of the crystal structure of 3,3`-difluoro-β-truxinic acid in ball and stick and space fill styles, (a) the solvated structure, showing the space in the structure that is occupied by the solvent molecule and (b) the non-solvated structure.*

Table 6.1. *Crystallographic data for the crystal structure determination of 3,3`-difluoro-β-truxinic acid structures.*

	3,3`-difluoro-β-truxinic acid/ acetic acid solvate	3,3`-difluoro-β-truxinic acid
Formula	$C_{20} H_{18} F_2 O_6$	$C_{18} H_{14} F_2 O_4$
Formula weight	392.34	332.29
Temperature, (K)	150(2)	150(2)
λ , Å	1.54184	1.54184
Crystal system	Triclinic	Monoclinic
Space group	$P\bar{1}$	C2/c
a, (Å)	7.6159(5)	32.304(3)
b, (Å)	8.6685(4)	5.5057(4)
c, (Å)	15.1547(9)	16.4308(10)
α, (°)	77.057(5)	90
β, (°)	77.346(5)	91.745(7)
γ, (°)	74.730(5)	90
Volume, (Å^3)	926.91(9)	2920.9(4)
Z	2	8
Density (calculated), (Mg/m^3)	1.406	1.511
Absorption coefficient, (mm^{-1})	0.999	1.052
F(000)	408	1376
Crystal size, (mm^3)	$0.19 \times 0.13 \times 0.02$	0.11 x 0.07 x 0.02
Reflections collected	6905	4942
Independent reflections	3618	2870
R(int)	0.0470	0.0426
Goodness-of-fit on F^2	1.028	1.039
Final R$_1$ indices [I>2sigma(I)]	0.0520	0.0627
Final wR$_2$	0.1247	0.1523
R$_1$ indices (all data)	0.0860	0.0830
wR$_2$ (all data)	0.1477	0.1690

6.3.2. Solid-state photodimerization of NH4+ and K+ salts of 3-BrCA

It was reported that, in both NH4-3-BrCate/3-BeCA (phase I)[26] and K-3-BrCate[36] structures, the C=C double bonds of neighbouring anion units in the stack fulfilled the Schmidt criteria for the [2+2] photodimerziation reaction. The alignment of the anions is a head-to-head and, therefore, mirror-symmetric dimeric products are expected (Scheme 6.2). In order to study their photodimerization, both salts were prepared and characterized by PXRD. Powdered samples were spread on a glass Petri dish and subjected to the UV light of a high pressure mercury vapor lamp.
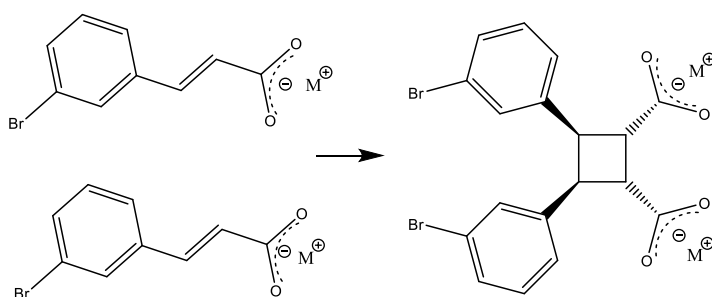
Scheme 6.2. The photodimerization reaction of M-3-BrCate to give M-3,3`-dibromo-β-truxinate. M+ represents the K+ or NH4+ cations.

The progress of the reaction was monitored by solution-state ^{1}H-NMR spectroscopy. As seen in Figure 6.11a and 6.12a, the ^{1}H-NMR spectra of NH4-3-BrCate/3-BeCA (phase I) and K-3-BrCate, before sample irradiation showed resonances of vinyl hydrogen atoms (hydrogen atoms attached to sp^2 carbons), at *ca*. 6.5 ppm and 7.7 ppm . As the reactions progressed, the gradual disappearance of these peaks was clearly observed, and in addition, the intensity of the peaks associated with the hydrogen atoms bonded to sp^3 carbon atoms of the resultant cyclobutane ring (4.3–3.8 ppm) increased (Figure 6.11(b-d) and 6.12(b-d), respectively). This result indicated that the photo-dimer products are formed and was supported by analysis of both samples obtained after the irradiation, using mass spectrometry. Peaks at *m/z* = 452.9 were observed in both samples indicating the existence of the dimeric product 3,3`-dibromo-β-truxinate.

In the case of the K+ salt, the reaction was much cleaner than for the NH4+ salt. Irradiation of the NH4+ salt generated traces of the *cis* isomer of the 3-BrCA as indicated by the

appearance of the peaks marked **i** in Figure 6.12b-d. In contrast, no such reaction was seen in the case of the K⁺ salt (this is discussed later in Section 6.3.5.a).
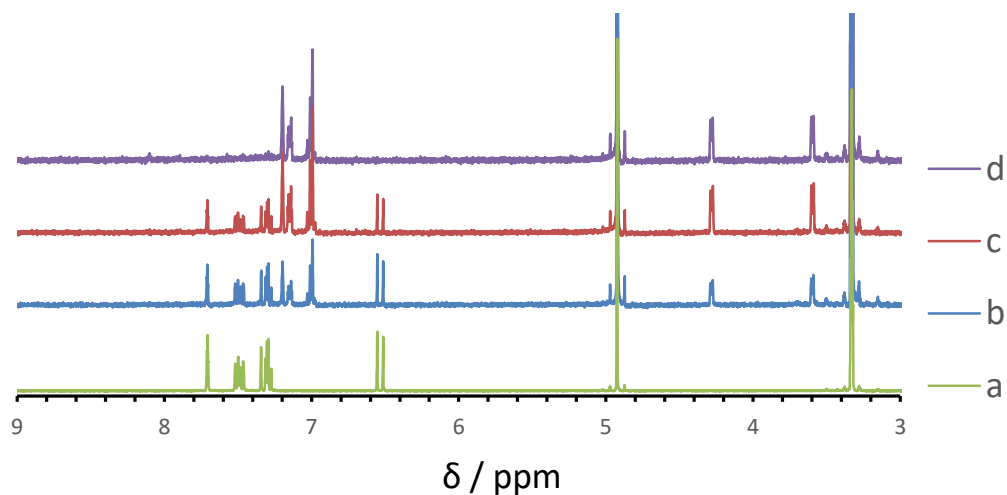
Figure 6.11. *Solution-state ^{1}H NMR spectra recorded (ex-situ) for K-3-BrCate sample collected (a) before UV irradiation, (b), (c) and (d) at different stages during UV irradiation.*
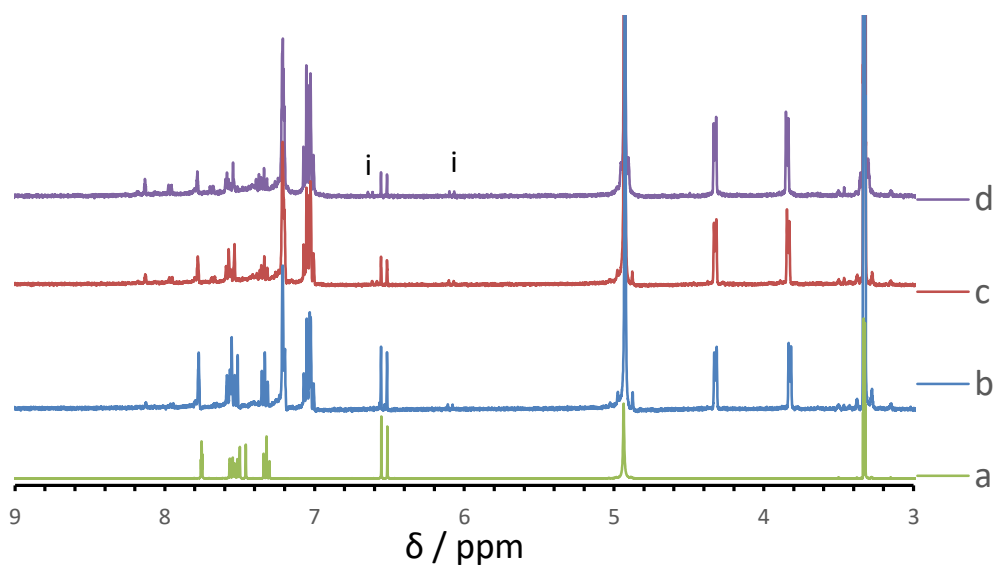
Figure 6.12. *Solution-state ^{1}H NMR spectra recorded (ex-situ) for NH₄-3-BrCate/3-BrCA (phase I) sample collected (a) before UV irradiation, (b), (c) and (d) at different stages during UV irradiation.*

6.3.3. Solid-state photodimerization of the NH₄⁺ salt of 3-CF₃CA

The structural analysis of NH₄-3-CF₃Cate/3-CF₃Cate, discussed previously in Chapter 5, revealed that a potential for solid-state photodimerization. Figure 6.13 shows the crystal structure of the salt and illustrates a favourable arrangement of the double bonds for photoreaction for three out of four neighbouring molecules in each set of four molecules. In

this structure the molecules are aligned in a head-to-head orientation in the column of a small stack with a double bond distance of less than 3.875Å apart.
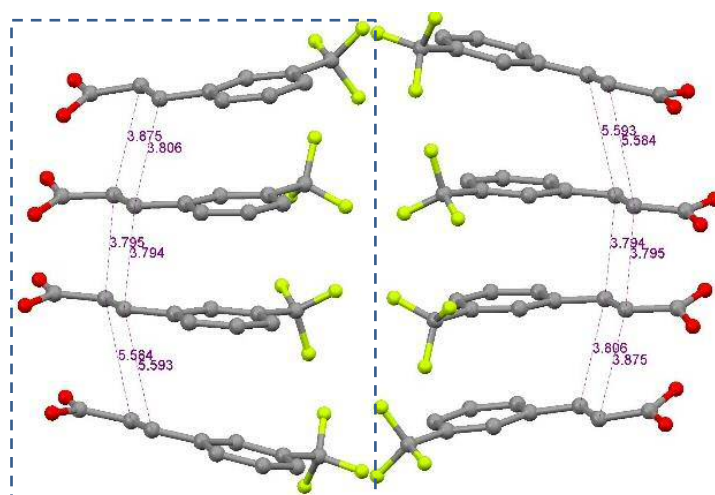
Figure 6.13. *The arrangement of the molecules in NH₄-3-CF₃Cate/3-CF₃CA, showing the double bond arrangement.*

Therefore, an investigation of the photodimerization reaction was carried out with the expectation of producing the truxinate (Scheme 6.3). Thus, a ground sample of the salt was spread out into a thin layer on a glass Petri dish and exposed to the UV light. Mixing of the material during the irradiation was done every 3-4 hours to obtain uniform irradiation.
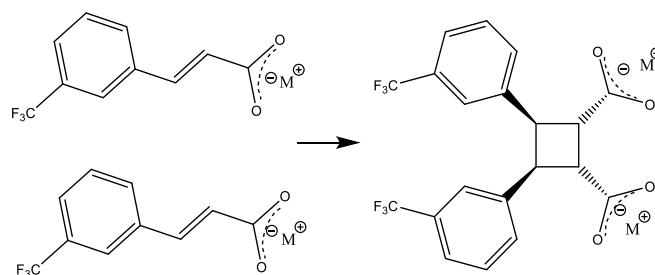
Scheme 6.3. The photodimerization reaction of NH₄-3-CF₃CA/3-CF₃Cate to give corresponds NH₄⁺salt of 3,3`-di-CF₃-β-truxinic acid. M⁺ represent the NH₄⁺ cation.

The photoproduct was analysed by ES-MS which confirmed that a dimer had, indeed, been obtained, as characterized by a significant M^+ peak at $m/z = 431$. The reaction progression was investigated by ^{1}H NMR spectroscopy. As seen in Figure 6.14b, the sample collected after 20 hours of irradiation time showed new resonance peaks around 3.95-4.47 ppm, which correspond to hydrogen atoms bonded to the sp^3 carbon atoms of the cyclobutane ring of the dimeric product. The sample collected after 40 hours of irradiation

time (Figure 6.14b) showed further progress in the reaction. However, very little progress was observed for the sample collected a further 12 hours, when compared to previous samples (Figure 6.14c), indicating that the reaction did not proceed to completion.

PXRD on the sample irradiated for 52 hours showed that it comprised both the starting salt and γ_2-3-CF$_3$CA, with no other crystalline material. The presence of the acid can be explained and is discussed later in Section 6.3.7. The *cis* isomer was also observed by the solution ^{1}H NMR (Figure 6.14, the peaks labelled (iii)) and is discussed in Section 6.3.5.a.

The solution-state ^{1}H NMR data indicated that only about 53% of the reactant was consumed over the duration of 52 hours of irradiation. This can be explained with the aid of crystal structure of the starting material and PXRD data for the product after irradiation. Firstly, the production of the acid during irradiation lowers the yield as the acid in the γ form, (i.e. a photo stable form, as discussed previously in Chapter 3). Secondly, the crystal structure indicates that the reaction cannot proceed to 100%. As discussed earlier, a set of four molecules are aligned head-to-head (as represented in a dashed rectangle in Figure 6.13). Of the three with the right geometry, only two molecules can undergo photodimerization; either the top molecule with the molecule underneath it or the second molecule from the top with the molecule that is underneath it. The bottom molecule cannot react as the double bond distance with neighbouring molecules more than 5Å. Thus, only half the molecules can react. This result is in good agreement with the solution-state ^{1}H NMR results.
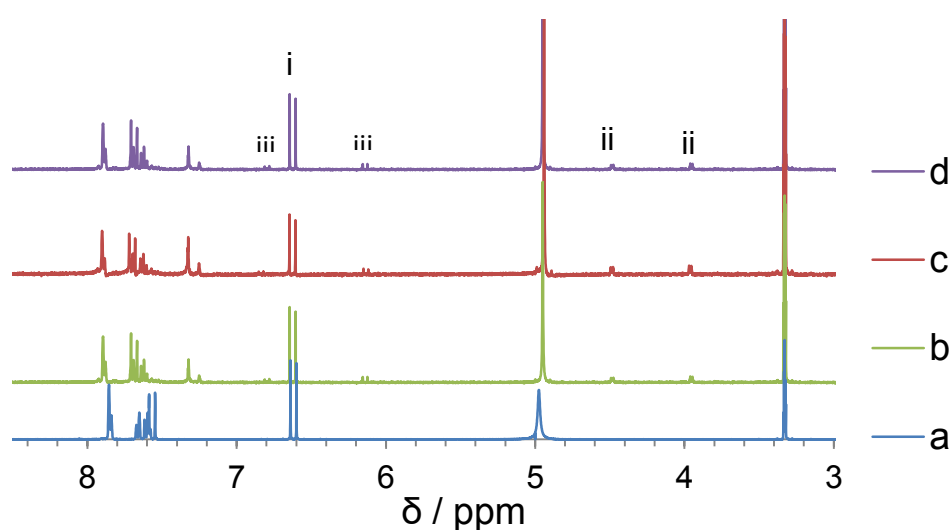
Figure 6.14. *Solution-state ^{1}H NMR spectra recorded (ex situ) for NH$_4$-3-CF$_3$CA/CF$_3$Cate sample collected (a) before UV irradiation, (b), (c) and (d) at different stages during UV irradiation.*

6.3.4. Solid-state photodimerization of *β*-3-ClCA/3-BrCA solid solution

The results from Chapter 4 (Section 4.3.1.c**)** showed the formation of solid solution ma-
terials of *β*-3-ClCA/3-BrCA, in which the molecules are aligned head-to-head. The C=C
bonds are parallel with a centre-to-centre separation of 3.865Å, corresponding to the ideal
geometric arrangement for a solid-state [2+2] photodimerization reaction, in accordance
with the topochemical principle (Figure 6.15). The crystal structure did not provide in-
formation on how the molecules are distributed within the crystal (domains or random
distribution) but the photoreaction can provide a direct route to information about the
nature of intra-crystal contacts at the molecular level. The rationale is that large separate
domains of 3-ClCA and 3-BrCA would give predominantly two products, namely 3,3′-
dibromo-*β*-truxinic acid and 3,3′-dichoro-*β*-truxinic acid whereas a completely random
distribution of components within the crystal would produce a significant amount of the
asymmetric dimer, 3-Cl-3′-Br-*β*-truxinic acid (Scheme 6.4).
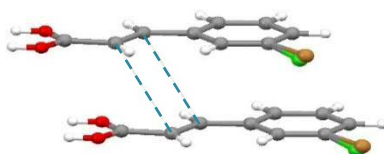
Figure 6.15. *The arrangement of the two molecules of disordered (3-Br/3-Cl)-CA showing, the
parallel double bonds.*
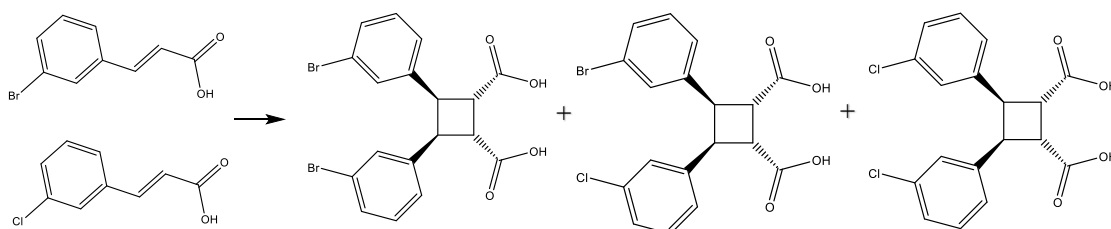
Scheme 6.4. *The photodimerization reaction of β-3-ClCA/3-BrCA to give 3,3'-dibromo-β-truxinic
acid, 3-Cl-3'-Br-β-truxinic acid and 3,3'-dichoro-β-truxinic acid.*

6.3.4.a. Monitoring the reaction by IR studies

A powder sample of *β*-3-ClCA/3-BrCA was subjected to UV irradiation and an early
indication of the occurrence of a reaction was a colour change from white to yellow. As
observed previously in the case of 3-FCA, PXRD showed that irradiation was associated
with loss of crystallinity of the cocrystalline material. In order to follow the progress of

the reaction, IR spectra were recorded for samples collected every 12 hours over a period of 60 hours.

The intensity of the band at *ca.* 1629 cm^{-1} (Figure 6.16, band **2**), due to the C=C stretching mode, decreases gradually as a function of irradiation time, indicating loss of the C=C bonds. In addition, the C=O stretching band (band **1**) shifts from *ca.* 1670 cm^{-1} to *ca.* 1695 cm^{-1}, consistent with the loss of conjugation associated with the dimerization reaction.
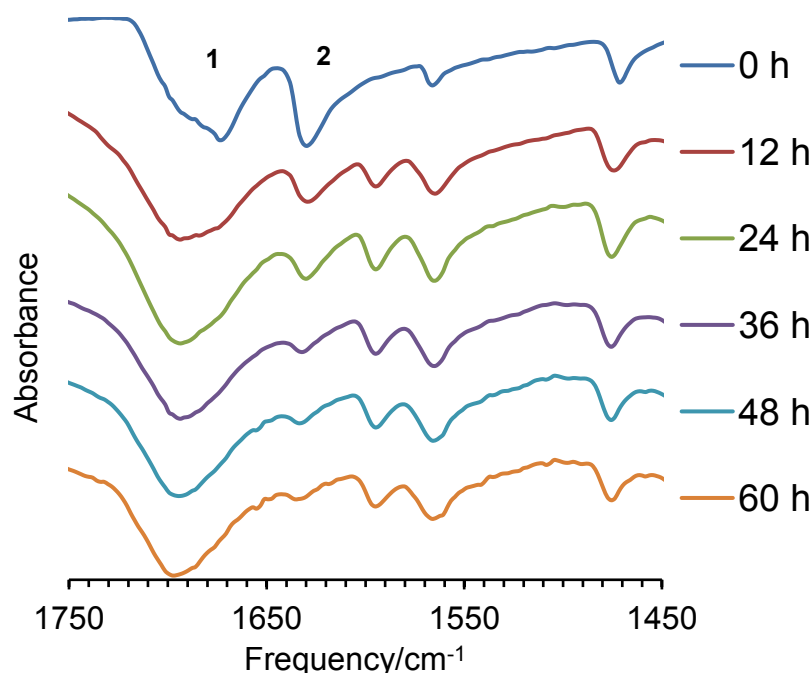
Figure 6.16. *IR plots recorded during photoirradiation of the β-3-ClCA/3-BrCA solid solution.*

6.3.4.b. The reactivity progress: solution-state ^{1}H-NMR study

Solution-state ^{1}H NMR studies were fully consistent with the occurrence of the photodimerization reaction. The ^{1}H NMR spectra for the initial 1:1 solid solution and the material sampled periodically during irradiation are shown in Figure 6.17. The resonances of vinyl hydrogen atoms (hydrogen atoms attached to sp^2 carbons) at *ca.* 6.8 ppm and 8 ppm (Figure 6.17 (i)) decrease in intensity, while those for hydrogen atoms bonded to the sp^3 carbon atoms of the cyclobutane ring (4.0-4.8 ppm) increase in intensity, as a function of irradiation time (Figure 6.17 (ii)). The solution-state ^{1}H NMR data indicate that over 95% of the reactant was consumed during the reaction (Figure 6.18a). A plot ln(reactant%) *versus* time, [where reactant% = 100 × reactant/(reactant + product)] is linear (with $R^2 = 0.995$), indicating first order kinetics (Figure 6.18b), similar with the reaction in the case of 3-FCA systems.
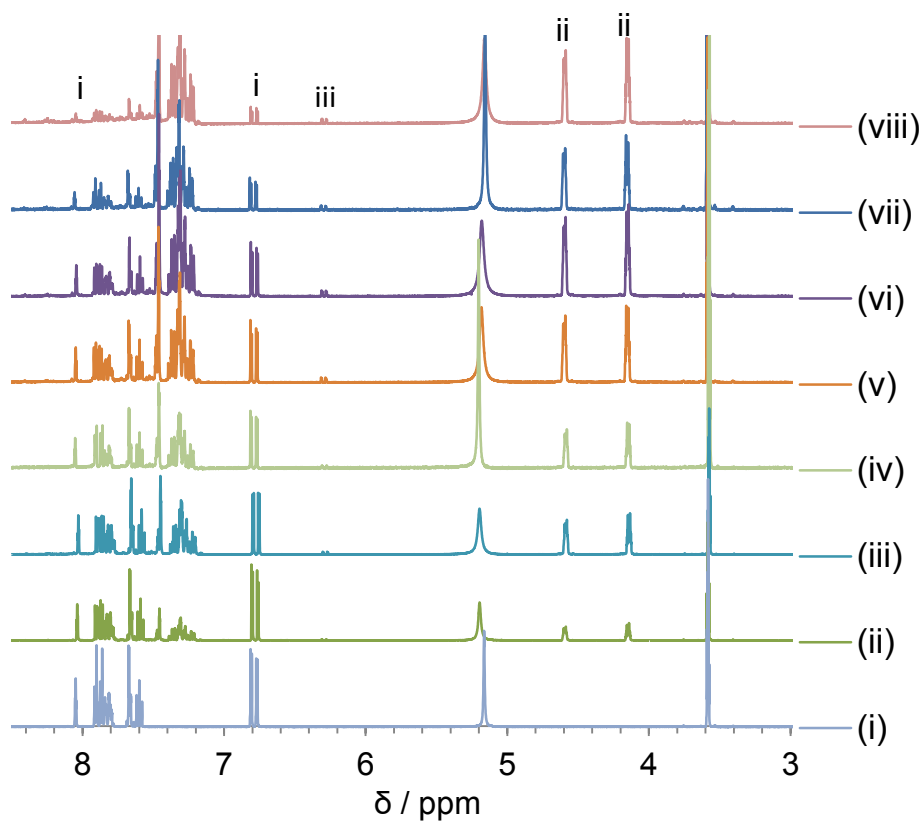
Figure 6.17. *Raw data of ¹H NMR studies of samples extracted at different stages during UV irradiation the β-3-ClCA/3-BrCA solid solution.*
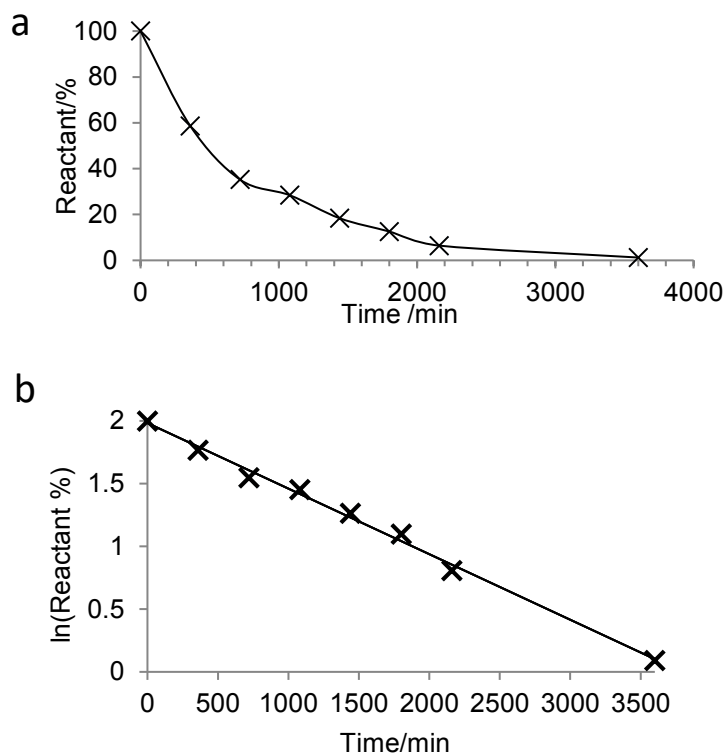
Figure 6.18. *(a) The percentage of reactant phase remaining as a function of UV irradiation time of β-3-ClCA/3-BrCA solid solution, and (b) a plot of ln(reactant %) against time.*

6.3.4.c. Photoirradiation in the solution-state *versus* solid-state

The aim was to compare the efficiency of the solid-state photoreaction with the process in solution. Thus, a 1:1 molar ratio of both 3-ClCA:3-BrCA was dissolved in MeOH and the resultant solution irradiated using the same UV light as used for the reaction in the solid state. The solution-state ^{1}H NMR spectra for the initial sample (before the irradiation) and the material sampled periodically during irradiation are shown in Figure 6.19. Clearly, in contrast with the results of the reaction in the solid state (Figure 6.17), for the solution reaction showed only small peaks for hydrogen atoms bonded to the sp^3 carbon atoms of the cyclobutane ring (around 4.0-4.8 ppm).

Mainly isomerization products were observed in the case of the solution reaction, rather than dimerization products. This is shown by the presence of the resonance peaks around *ca.* 5.9 and 6.9 (i and ii Figure 6.19) which are associated with the hydrogens of the vinyl group and show consistency with the results observed by Salum et al.[37] where the E/Z isomerization was observed from irradiation of a solution of E-3-methoxy-4-hydroxy-cinnamaic acid in acetonitrile and no competition from the photodimerization reaction was reported.

However, it is worth noting that traces of isomerization reaction was also observed in the case of the solid-state reaction. Thus, the peaks associated with the α(H) of the vinyl group in the *cis* isomer were observed as a function of irradiation time (Figure 6.17 indicated by iii). Isomerization in the crystal will be discussed in Section 6.3.5.a. The peaks associated with the *β*(H) of the *cis* isomer of the acid are expected to overlap with the peaks of hydrogens of the benzene ring. It is not surprising that photoisomerization takes place rapidly in solution, as the molecules are not constrained. For the isomerization to occur, rotation of the molecule around the double bond is required, in order to change conformation. For the photoisomerization to occur, a large free space around the relevant group is necessary.[38] Thus, although isomerization in the crystalline solid is possible,[39,40] it is expected to occur much less in the solid state, where molecular motion is restricted compared to the solution state.
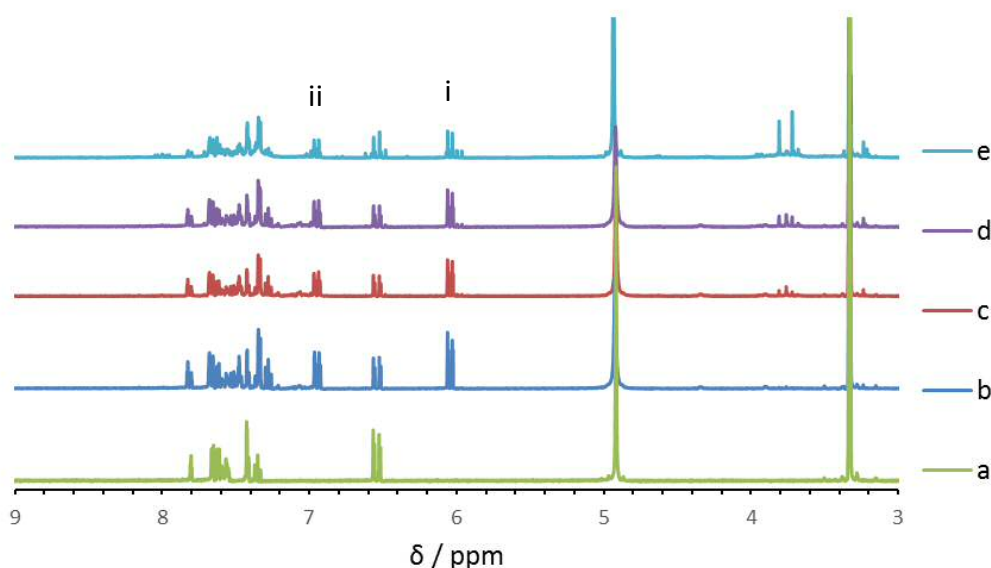
Figure 6.19. *Solution-state ^1H NMR spectra recorded (ex-situ) for samples collected during the irradiation of a solution of 3-ClCA/3-BrCA in methanol (a) before the irradiation and after (b) 8 hrs, (c) 27hrs, (d) 36 hrs, and (e) 60 hrs.*

6.3.4.d. Characterization the photochemical products: mass spectrometry and HPLC separation

Crystallization of the product after irradiation and determination of the crystal structure would not provide conclusive proof that the 3-Cl-3'-Br-β-truxinic acid heterodimer was present in the reaction product, as 3,3`-dichloro-$\beta$-truxinic acid and 3,3`-dibromo-β-trux-inic acid homodimers are also produced. Clearly, 3,3`-dichloro-$\beta$-truxinic acid and 3,3`-dibromo-β-truxinic acid could form a solid solution that may be indistinguishable, using diffraction techniques, from the 3-Cl-3'-Br-β-truxinic acid heterodimer (i.e. the average crystal structure could be the same in each case). Mass spectrometry and HPLC, however, can distinguish the three different types of dimer molecule.

Mass spectrometry

The ES-mass spectrum of the product sampled after 60 hours of irradiation is consistent with a mixture of the three different dimer molecules. Peaks due to 3-Cl-3'-Cl-β-truxinic acid and 3-Br-3'-Br-β-truxinic acid homodimers are observed at $m/z = 363.03$ and 452.94, respectively and a peak attributed to the 3-Cl-3′-Br-β-truxinic acid heterodimer is also observed at $m/z = 408.99$.

Separation of the products by HPLC

Analytical HPLC (Figure 6.20) shows a clear difference between the products obtained from the photoreaction of pure β-3-ClCA and pure β-3-BrCA, on the one hand, and the

228

3-ClCA/3-BrCA solid solution, on the other. The product from irradiation of β-3-ClCA has a retention time of 11.832 min whereas the product from irradiation of β-3-BrCA has a retention time of 13.693 min. (The results from a mixture of the two products is shown in Figure 6.20a). The product of the photochemical reaction of the β-3-ClCA/3-BrCA solid solution (Figure 6.20b) has an additional peak with a retention time of 12.715 min which lies between those of the products from β-3-ClCA and β-3-BrCA and is in good agreement with the expectation that the properties of the heterodimer product should fall between those of the homodimers. The integrated areas of the peaks at 11.83, 12.72 and 13.69 min are 18.8, 38.3 and 22.7%, respectively. This is approximately in the 1:2:1 ratio expected for a photodimerization in a 1:1 solid solution, with a random distribution of 3-ClCA and 3-BrCA molecules.
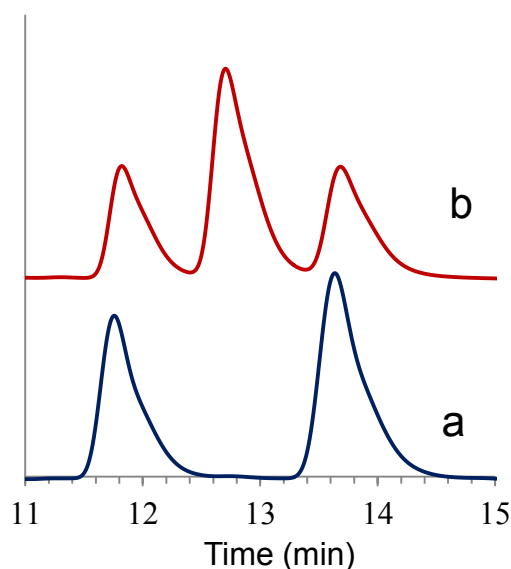
Figure 6.20. *HPLC plots showing (a) a mixture of the products from irradiation of pure β-3-ClCA and β-3-BrCA and (b) the products of irradiation of β-3-ClCA:3-BrCA.*

6.3.4.e. Crystal structure of the photodimerization product

The product obtained after irradiation of the 3-ClCA/3-BrCA solid solution for 60 hours was crystallized from acetonitrile and the crystal structure was determined from SC-XRD. The structure (Figure 6.21) is triclinic (space group $P\bar{1}$) and the asymmetric unit comprises one β-truxinic acid molecule with disorder of Cl and Br at both the 3-position and the 3'-position and one molecule of acetonitrile (which is disordered). The refined occupancies of Cl and Br at the 3-position and 3'-position of the β-truxinic acid molecule in were 0.464(3)/0.536(3) for one site and 0.500(3)/0.500(3) for the other site. The refined occupancies revealed that the quantity of Br is more than the quantity of Cl, this may indicate that the crystal contains more than one photo-dimer, which implies that the 3-

bromo-3`-chloro-β-truxinic acid heterodimer cannot be the only product from the reaction, as discussed above.

Crystallographic data are shown in Table 6.2. The unit cell shows similarity to the unit cells of 3,3`-dibromo-β-truxinic acid[34] and 3,3`-dichloro-β-truxinic acid[34] (Table 6.3).

Table 6.2. *Crystallographic data for the crystal structure determination of β-3-(Cl/Br)CA-D.*

Formula	$C_{19}H_{15.5}Br_{0.96}Cl_{1.04}N_{0.5}O_4$	Z	2
Formula weight	428.62	**Density (calculated), (Mg/m³)**	1.531
Temperature, (K)	296(2)	**Absorption coefficient, (mm⁻¹)**	2.305
λ , Å	0.71073	**F(000)**	433
Crystal system	Triclinic	**Crystal size, (mm³)**	$0.45 \times 0.30 \times 0.09$
Space group	$P\bar{1}$	**Reflections collected**	8237
a, (Å)	8.5769(6)	**Independent reflections**	4372
b, (Å)	14.2022(10)	**R(int)**	0.0214
c, (Å)	8.1299(5)	**Goodness-of-fit on F²**	1.019
α, (°)	103.985(5)	**Final R_1 indices [I>2sigma(I)]**	0.0440
β, (°)	102.631(5)	**Final wR₂**	0.0816
γ, (°)	79.990(6)	**R_1 indices (all data)**	0.0828
Volume, (Å³)	930.02(11)	**wR₂ (all data)**	0.0941

Table 6.3. *Unit cells parameters of 3,3`-dibromo-β-truxinic acid and 3,3`-dichloro-β-truxinic acid*

	3,3`-dibromo-β-truxinic acid[34]	3,3`-dichloro-β-truxinic acid[34]
a, (Å)	8.670(1)	8.634(1)
b, (Å)	14.253(1)	14.228(2)
c, (Å)	8.1895(8)	8.001(1)
α, (°)	104.567(8)	103.49(1)
β, (°)	102.545(8)°	102.91(1)
γ, (°)	79.379(9)	79.43(1)

In the crystal structure, each *β*-truxinic acid molecule is in contact with two others by hydrogen bonding through the carboxylic acid groups, leading to a zig-zag chain. The hydrophobic ends of the dimer molecules interact in a zip-like fashion through the aryl groups. The solvent molecules are located above and below the chains of *β*-truxinic acid and there is no direct hydrogen bonding between the *β*-truxinic acid and acetonitrile molecules.
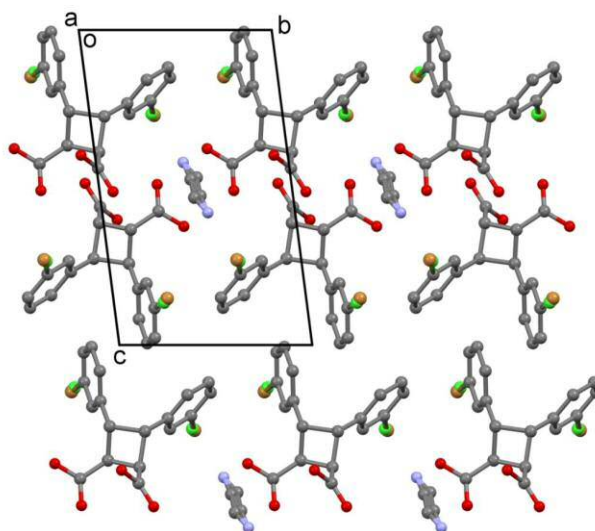
Figure 6.21. *The crystal structure of the heterodimer from irradiation of β-3-ClCA:3-BrCA solid solution. Hydrogen atoms are omitted for clarity.*

6.3.5. Photodimerization by design: photodimerization reaction of a solid solution of K-3-BrCate/3-MeCate solid solution

A continuing challenge is the development of methods to generate structures with desirable geometry of reactive double bonds. The results from Chapter 3 showed that 3-MeCA crystallized in the *γ* phase which is a photostable form. Cocrystallization of 3-MeCA with other *meta*-substituted cinnamic acids (as discussed in Chapter 4) showed the preference of forming *γ*-phase solid solutions, which are also photostable. Additionally, the results in Chapter 5 showed that, in the structures of both the K^+ and NH_4^+ salts of 3-MeCA, the cinnamate units were arranged with criss-cross double bonds for neighbouring molecules.

Therefore, in Chapter 5, an investigation was carried out into the design of cocrystalline materials containing 3-MeCate and 3-BrCate, with the aim of producing structures with optimum double bonds arrangements for the photodimerization reaction. Thus, cocrystallization of 3-MeCA and 3-BrCA as a K^+ salt produced a solid solution with the double bonds stacked parallel to each other and with a distance of only *ca.* 3.981Å (Figure 6.22).
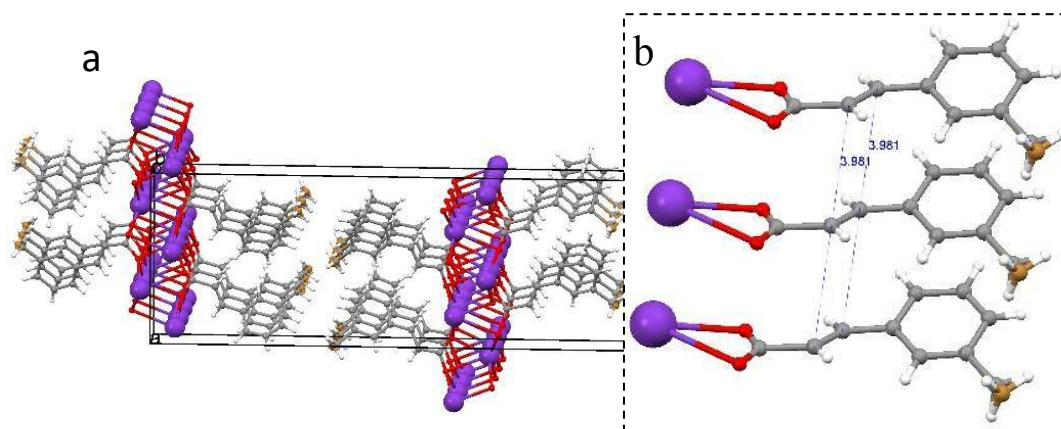
Figure 6.22. *(a) The crystal packing of K-(3-Br/3-Me)Cate solid solution. (b)Parts of the stack of the cinnamate units along the b-axis in the structure, showing the ideal geometry for [2+2] photoreaction.*

The photodimerization reaction of the solid solution K-(3-BrCate/3-MeCate) was investigated. The sample was powdered and spread in a thin layer on the glass Petri dish and then irradiated by UV with periodic mixing of the sample to ensure uniform irradiation and faster reaction. Consistent with the result obtained in Section 6.3.4, three dimeric products were expected for this binary system; K-3,3`-dibromo-*β*-truxinate, K-3-Br-3'-Me-*β*-truxinate and K-3,3`-di-Me-*β*-truxinate (see Scheme 6.5). The occurrence of the photodimerization reaction was studied first by solution-state ^{1}H NMR spectroscopy.

6.3.5.a. Monitoring the reaction using solution-state ^{1}H NMR spectroscopy

Figure 6.23a shows the solution ^{1}H NMR spectrum of the salt solid solution recorded before the irradiation, while (b) and (c) show the progression of the reaction. As seen previously in the case of K-3-BrCate, only the resonance peaks of the hydrogens that are associated with the monomers (K-3-BrCate and K-3-MeCate) were observed before the irradiation. The resonances of vinyl hydrogen atoms for both monomers (hydrogen atoms attached to sp^2 carbons) occurred at *ca*. 6.5 ppm and 7.7 ppm (Figure 6.23a). Additionally, the resonance of the hydrogens of 3-Me group in the K-3-BrCate was at *ca.* 2.4 ppm.

During irradiation, as seen in Figure 6.23 b and c, resonance peaks of the hydrogen atoms bonded to the sp^3 carbon atoms of the cyclobutane ring (at 3.6-4.3 ppm) grow, indicating the formation of dimeric products. Interestingly two singlet resonance peaks appeared around *ca.* 2.15-2.18 and were assigned to the two environmentally distinct groups of protons for the methyl groups.

To aid in understanding the growth of the singlet peaks at *ca.* 2.15-2.18, recall the result observed in Section 6.3.4.d; three dimeric products were obtained from the solid solution of *β*-3-ClCA/3-BrCA (two homodimers and one heterodimer). In the present case of the solid solution of K-(3-BrCate/3-MeCate), three dimeric products were also expected (Scheme 6.5); homodimers K-3,3`-dibromo-*β*-truxinate and K-3,3`-di-Me-*β*-truxinate and heterodimer K-3-Br-3'-Me-*β*-truxinate. Two resonance peaks (Figure 6.23c labelled i and ii), associated with the hydrogens of the methyl groups of the distinct dimeric materials (K-3,3`-di-Me-*β*-truxinate and K-3-Br-3'-Me-*β*-truxinate) are observed. As the ratio of the hydrogen atoms associated with the Me groups in these structures is 2 (for K-3,3`-di-Me-*β*-truxinate) to 1 for (K-3-Br-3`-Me-*β*-truxinate), it would be expected that the integral of peak i is double that of peak ii. Interestingly, peaks i and ii have the same intensities, suggesting the same total amount hydrogens associated with the methyl groups in both dimeric products. The results from the following section (6.3.5.b) explain this behaviour.
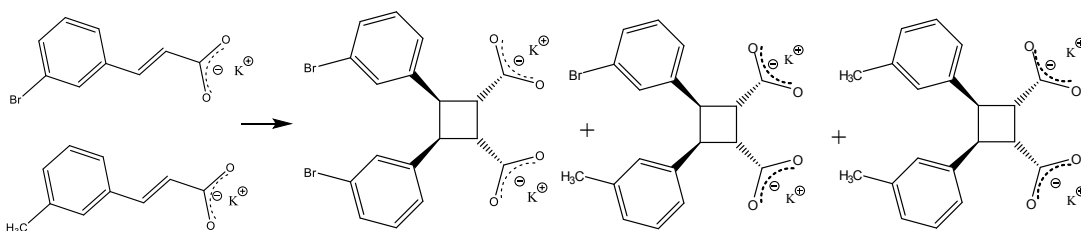
Scheme 6.5. *The photodimerzation reaction of K-(3-Br/3-Me)Cate solid solution to give K-3,3'-dibromo-β-truxinate, K-3-Br-3'-Me-β-truxinate and K-3,3'-di-Me-β-truxinate.*
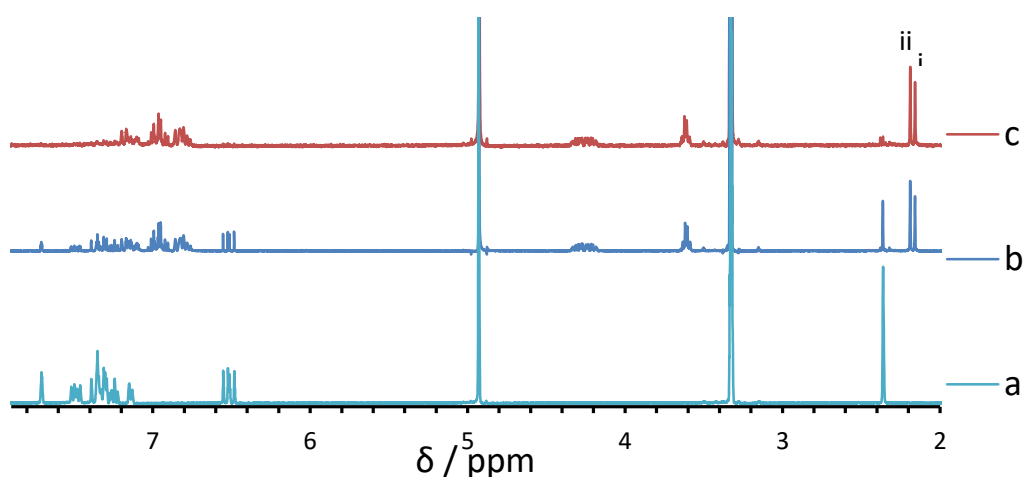
Figure 6.23. *Raw data of ^1H NMR studies of K-(3-Br/3-Me)Cate solid solutions; (a) sample before irradiation. (b) and (c) samples ncollected at different stages during UV irradiation.*

Photoisomerization reaction

The ^{1}H NMR spectrum of the samples after irradiation showed no evidence of the photoisomerization reaction, consistent with the result obtained from the irradiation of K-3-BrCate. In contrast, irradiation of β-3-FCA, β-3-BrCA/3-ClCA solid solution and NH_4^+ salts of 3-BrCA and 3-CF$_3$CA showed evidence of the isomerization reaction. It is clearly from the results of the work in this chapter that the isomerization reaction is more likely to occur in cases that involved acid than the cinnamate. (Note the observation that the NH_4^+in the ammonium salts can be lost during irradiation and this is discussed in Section 6.3.7). It is possible that the cation binds the ions restricting free movement and hence rotation about C$\overset{..}{-}$C.

6.3.5.b. HPLC separation of the photoproducts

In order to confirm the formation of the three dimeric products discussed in the previous section (6.3.5.a), the material obtained after photoirradiation was subjected to HPLC analysis. Figure 6.24a shows the chromatogram obtained after HPLC separation of the products. Three peaks were observed, indicating three distinct dimeric products; one has a retention time of 13.658 min, and was therefore assigned to the dimeric product of 3,3`-dibromo-$\beta$-truxinic acid, since it showed a very good agreement with the 3,3`-dibromo-β-truxinic acid produced from the irradiation of pure β-3-BrCA (see Figure 6.24; compare (b) with a (iii)). The properties of the heterodimer product should fall between those of the homodimers and hence the peak with a retention time of 12.200 (ii) was assigned to the 3-Br-3'-Me-β-truxinic acid. The one with a retention time 10.568 (i) was assigned to 3,3`-di-Me-β-truxinic acid (discussed in Section 6.3.5.a). The integrated areas of the peaks are 15.0, 38.7 and 16.1% for i, ii and iii, respectively, roughly in the 1:2:1 ratio expected for the photoproduct of a 1:1 solid solution of 3-BrCA:3-MeCA in which the components of a binary system are distributed randomly as a homogeneous solid solution. This result is consistent with the ^{1}H NMR result obtained in Section 6.3.5.a, where the integral of the ^{1}H NMR peaks of the methyl group in 3-Br-3'-Me-β-truxinate was similar to that of the methyl groups in 3,3`-di-Me-$\beta$-truxinate. This indicates that the concentration of 3-Br-3'-Me-$\beta$-truxinate was double that of 3,3`-di-Me-β-truxinate. This also demonstrates a homogeneous molecular distribution of K-3-MeCate and K-3-BrCate in the crystal.
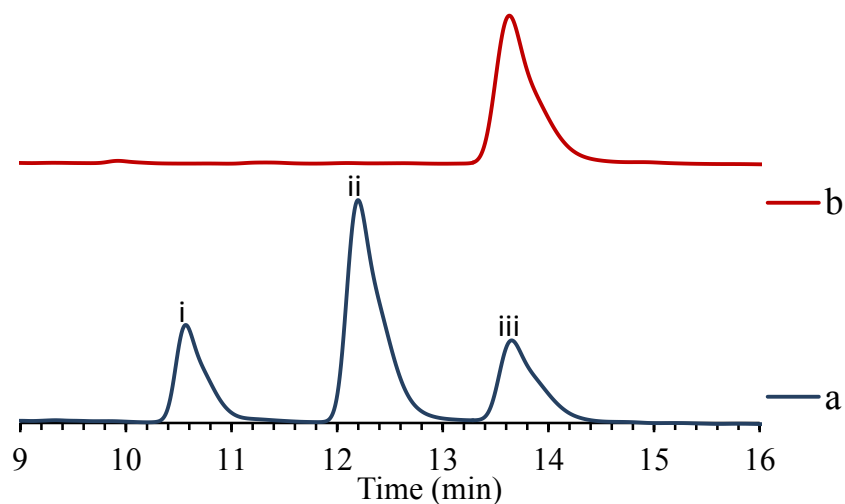
Figure 6.24. *HPLC chromatograms showing: (a) the products of irradiation of K-3BrCate/K-3MeCate. (b) The product from of the irradiation of pure β-3-BrCA.*

Mass spectrometry

The ES-mass spectrum of the product sampled after irradiation is consistent with the expectation of the presence of the three different dimer molecules. The fragments with $m/z = 323.11$ and 452.90 are due to 3,3`-di-Me-β-truxinic acid and 3,3`-dibromo-β-truxinic acid. The peak attributed to 3-Br-3'-Me-β-truxinic acid, the heterodimer, is also observed at $m/z = 389.00$.

6.3.5.c. Solution-state ^{1}H NMR studies of the separated materials

Peak iii was assigned to 3,3`-dibromo-β-truxinic acid as discussed in Section 6.3.5.b. Further investigation was carried out with the aim of confirming the identity of the materials giving rise to peaks i and ii (Figure 24a). To perform this, samples (i) and (ii) were collected after HPLC separation and analysed by solution-state ^{1}H NMR.

The results were in good agreement with the expectation. In both cases, two peaks were observed around *ca.* 3.8 and 4.3 and are associated with the hydrogen atoms of the cyclobutane ring, indicating the existence of dimeric products. On the other hand, each sample had only one resonance peak for the protons of the methyl groups. Interestingly, the integration of the peaks indicated 6 protons for (i) and 3 protons for (ii); a result in good agreement with the expected products. Thus, (i) is 3,3`-di-Me-β-truxinic acid where two methyl groups have 6 hydrogen atoms, and (ii) is 3-Br-3'-Me-β-truxinic acid where one methyl group has 3 hydrogen atoms.

6.3.6. Criss-crossed arrangement of the double bonds: solid-state photoreaction of NH_4^+ and K^+ salts of 3-FCA and 3-MeCA

The results from Chapter 5, showed that, in the crystal structures of the NH_4^+ and K^+ salts of 3-FCA and 3-MeCA, the closest contact between the double bonds involved neighbouring molecules with non-parallel alignment. Therefore, two questions arose: Do the crystals show any reaction on irradiation? If so, what would the products be?

Thus, an investigation was carried out to determine the effect of UV irradiation on the salts. As shown in Figure 6.25, examining the crystal structures of the NH_4^+ salt of 3-MeCA and the K^+ salts of 3-FCA and 3-MeCA showed an arrangement of double bonds through the stack in a way that could potentially form photoproducts (NH_4^+ salt of 3-FCA is discussed later as it is disordered). Thus, for example, in the case of K-3-FCate (Figure 6.25a), C(7) of molecule (R) and C(8) of molecule (R`) may form a single bond and then C(7) of molecule (R`) may form a single bond with the C(8) of molecule (R``). This reaction may continue in a similar manner through the stack, resulting in oligomers. The end of the chain would probably depend on defects in the crystal leading to the disruption of the reaction. Similar crystal packing is observed for NH_4-3-MeCate/3-MeCA and K-3-MeCate (see Figure 6.25 b and c, respectively) and, therefore, a similar photoreaction may occur. The results obtained by mass spectrometry for the products, after irradiation of the NH_4^+ salts of 3-MeCA and K^+ salt of 3-FCA and 3-MeCA, support the proposed hypothesis. Fragments of *m/z*, consistent with oligomers of different chain length of up to 8 molecules in some cases, were observed (Table 6.4).

A striking feature of the observed *m/z* peaks is that, in the case of the K^+ salts of 3-MeCate, the reaction gave dimer, trimer, tetramer, pentamer and hexamer product. In the case of K-3-FCate, similar products were observed in addition to heptamer and octamer oligomers. In contrast, NH_4-3FCate-3FCA and NH_4-3MeCate-3MeCA only produced dimer, trimer and or tetramer. This result is consistent with the observation that the NH_4^+ is lost during irradiation (as discussed in Section 6.3.7) which may affect the structure and therefore disrupt the reaction. The K^+ is retained, allowing the maintenance of structure and thereby resulting in the formation of longer chains of photoproduct.
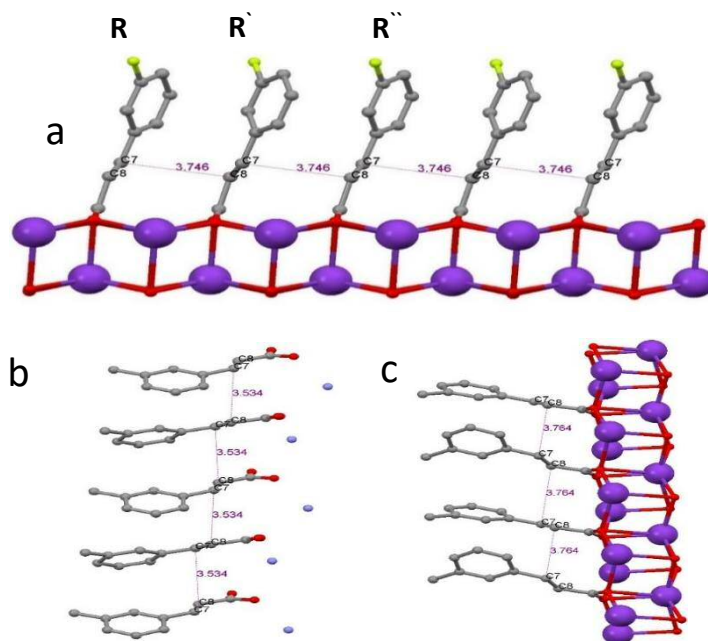
Figure 6.25. *Segments of the crystal structures of (a) K-3-FCate, (b) NH₄-3-FCate/3-FCA and (c) K-3-FCate, showing the arrangement of the double bond that may lead to the formation of photoproducts.*

Table 6.4. *The results obtained by mass spectrometry for the product after irradiation of different salts. (* refers to K⁺ adduct ion whereas ** refers to Na⁺ adduct ion)*

Salt	Irradiation time (hrs)	m/z peak	Chain length	Irradiation time (hrs)	m/z peak	Chain length
K-3-FCate	9	369*	2	49	369*	2
		573*	3		537*	3
		777*	4		777*	4
		981*	5		981*	5
		1185*	6		1185*	6
		1389*	7		-	-
		1594*	8		-	-
K-3-MeCate	7	361*	2	48	361*	2
		561*	3		561*	3
		761*	4		761*	4
		961*	5		961*	5
		1161*	6		1161*	6
NH₄-3FCate-3FCA	11	377**	2	31	331	2
		543**	3		663	4
NH₄-3MeCate-3MeCA	4	323	2	45	323	2
		485	3		647	4
		697*	4		-	-

237

Discussion of solution-state ¹H NMR and HPLC results

After irradiation of the salts, the products were also analysed using solution ¹H NMR. In all of the NH_4^+ and K^+ salts of 3-FCA and 3-MeCA, a photoreaction had clearly occurred. Since the peaks of protons attached to sp^3 carbon were clearly observed in all cases at around *ca.* 3.6 and 4.2, suggesting the formation of the saturated bond.

Analysis of the products from K-3MeCate, K-3FCate and NH₄-3-FCate-3-FCA after irradiation using HPLC clearly revealed some product peaks. These peaks were consistent with the corresponding dimeric peaks obtained previously from HPLC analysis for 3,3`-dimethyl-*β*-truxinic acid and 3,3`-difluoro-*β*-truxinic acid. (Figures 6.26 and 6.27).
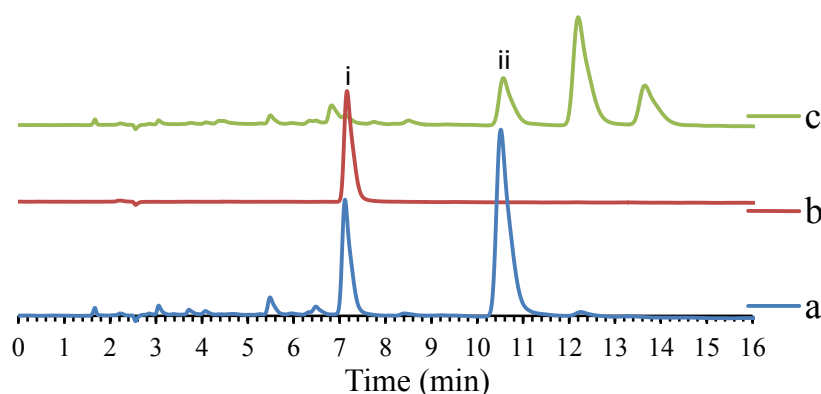
Figure 6.26. *HPLC plots for the products from (a)K-3-MeCA after 48 hrs of irradiation, showing monomer and dimer peaks, (b) 3-MeCA (monomer), (c) the products of irradiation of K-3BrCate/K-3MeCate solid solution, where (i) is 3-MeCA (monomer) and (ii) is 3,3`-di-Me-β-truxinic acid.*
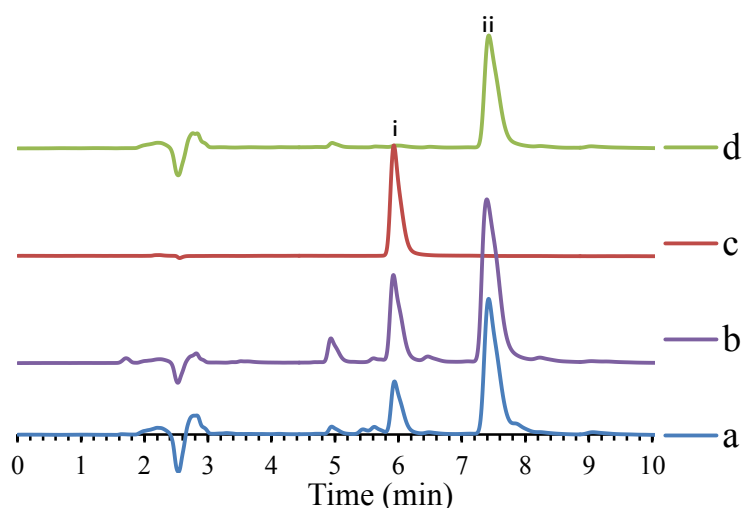
Figure 6.27. *HPLC plots showing (a) NH₄-3-FCate/3-FCA after 31 hrs of irradiation showing monomer and dimer peaks. (b) K-3-FCate after 49 hrs of irradiation showing monomer and dimer peaks (c) 3-FCA (monomer) (d) the products of irradiation of 3-FCA: (i) is 3-FCA (monomer) and (ii) is 3,3`-difluoro-β-truxinic acid.*

Mass spectrometry *versus* ^{1}H NMR and HPLC results

In the light of the mass spectrometry, ^{1}H NMR and HPLC results, it is clear that photoreaction takes place. Mass spec indicates the formation of dimers and oligomers but it was not possible to distinguish the products using HPLC and solution-state ^{1}H NMR. HPLC showed that only a dimer was present. A possible explanation could be low solubility for the other products. ^{1}H NMR may not be able to distinguish between oligomers as the relevant chemical environments may be similar.

Formation of the dimeric photoproduct

In the structures of NH_4^+ and K^+ salts of 3-FCA and 3-MeCA, the double bonds are not aligned. For the reaction to produce the *β*-dimer, a pedal motion of one of the double bonds can be proposed in order to align both prior to dimer formation (see Figure 6.28).
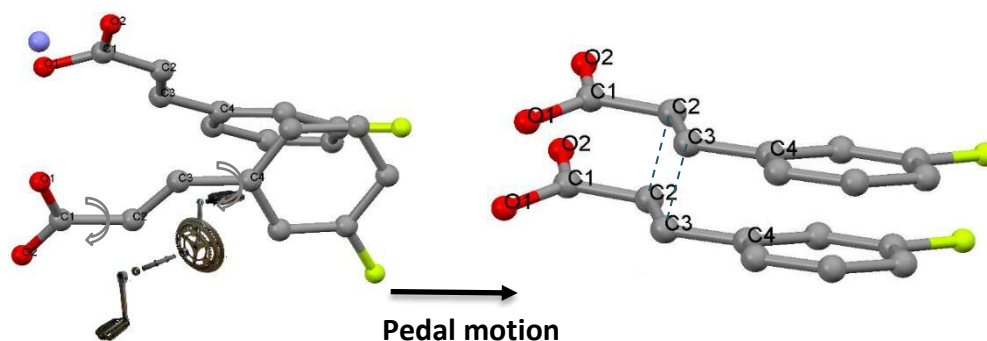
Pedal motion

Figure 6.28. *Two molecules extracted from the structure of NH₄-3-FCate-3FCA, showing non-parallel double bonds and the pedal motion required to produce alignment. Only atoms of the major component in the asymmetric unit are represented for clarity.*

If the reaction proceeds in this manner, a large motion is involved in the crystal prior to the reaction. This type of motion has been discussed previously in the literature[41]. For example, it was reported by Ito et al[42] that a paddle-like conformational change was required prior to the dimerization reaction of phthalic acid and *trans*-cinnamamide cocrystal to produce *β*-truxinnamide. Phthalic acid and *trans*-cinnamamide (1:2) were reported[43] to form a three-component assembly cocrystal, with two cinnamamide molecules linked to one phthalic acid molecule via hydrogen bond linkers. This cocrystalline material was confirmed, unambiguously, to undergo a SC-SC photoreaction although, in the crystalline state, the adjacent double bonds from the two cinnamamide molecules align in a criss-cross fashion.

In another example,[44] a pedal-like motion was also suggested to be involved in the mirror-symmetric β-dimer formation, induced by the photoirradiation reaction, of solid solutions of the diamine double salt of *trans*-2,4-dichlorocinnamic acid and *trans*-1,2-diaminocyclohexane at temperature above 50 °C.

Photodimerization reaction of NH₄-3-FCate/3-FCA,

The crystal structure of NH₄-3-FCate/3-FCA, showed disorder (discussed in Chapter 5). As shown in Figure 6.29a, the most striking feature of this disorder is the arrangement of the double bonds of the two disordered molecules in a criss-crossed arrangement. Such disorder in the crystal structure is an important indicator of pedal motion in the crystal.[41] Figures 6.29b and 6.29c show that when the molecules are packed in the crystal, at a local level there are four possible relationships between the adjacent double bonds. Close examination of the adjacent double bonds through the stack, regardless of the disorder, showed that these groups were arranged in the crystal with torsion angles for C(2A)-C(3A)-C(3)-C(2) of 40.14° and for C(3)-C(2)-C(2A)-C(3A) of 39.18° (the distances between the double bonds were *ca.* 3.898Å and 3.718Å, respectively). Accordingly, the photodimerization reaction might be possible[41,43] to yield β-3,3`-difluoro-truxinate. Solution ¹H NMR of the material after irradiation demonstrated the occurrence of the reaction. Interestingly, from the integration of the signals, the reaction was found to be approximately 90% complete after irradiation of the sample for 31 hours. Further irradiation of the sample did not increase the percentage of the photodimerized product. The reaction did not proceed to 100% conversion[45], possibly due to the requirement for the paddle motion which probably occurs partially.[41]
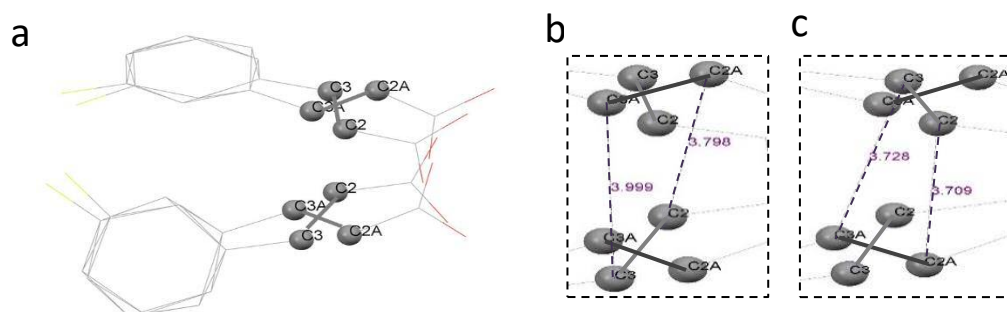
Figure 6.29. *(a) Two pairs of the disordered molecules in the crystal structure of NH₄-3-FCate/3-FCA. The carbons of the double bonds are represented in ball and stick style. (b) and (c) show the distances between the double bonds expected to undergo the photodimerization reaction.*

Crystal structure of the product

The product obtained after irradiation of the NH$_4$-3-FCate/3-FCA was crystallized from water and the crystal structure was determined by SC-XRD. This revealed a sodium salt of the dimer product which crystallized in the triclinic crystal system space group P$\bar{1}$. The asymmetric unit comprised of Na$^+$ cation, two molecules of 3,3`-difluoro-$\beta$-truxinic acid, one molecule of 3,3`-difluoro-β-truxinic acid/truxinate and three water molecules. As shown in Figure 6.30, in this structure, each sodium cation is coordinated by seven oxygen atoms, with distances in the range of 2.307Å to 2.425Å and a longer distance of 3.039Å. Four oxygen atoms are from three different 3,3`-difluoro-β-truxinic acid units while the other three are from three different water molecules. Crystallographic data are shown in Table 6.5.
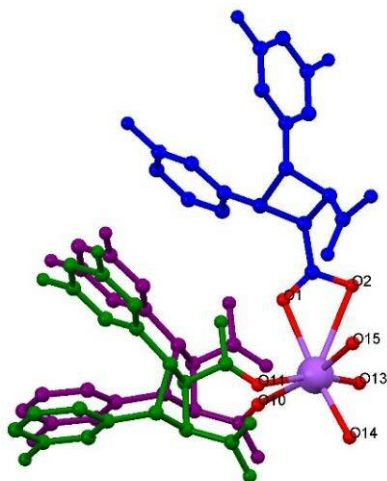
Figure 6.30. *Coordination of the sodium cation. Different dimeric molecules are represented in the asymmetric unit, and are displayed in different colours. Hydrogen atoms are omitted for clarity.*

Table 6.5. *Crystallographic data for the crystal structure determination of Na-3,3`-difluoro-$\beta$-truxinate/3,3`-difluoro-β-truxinic acid.*

Formula	C$_{54}$ H$_{47}$ F$_6$ Na O$_{15}$	Z	2
Formula weight	1072.91	Density (calculated), (Mg/m^3)	1.461
Temperature, (K)	150(2)	Absorption coefficient, (mm^{-1})	1.113
λ , Å	1.54184	F(000)	1112
Crystal system	Triclinic	Crystal size, (mm^3)	0.22 x 0.11 x 0.04
Space group	P$\bar{1}$	Reflections collected	13603
a, (Å)	5.9405(3)	Independent reflections	13603
b, (Å)	19.9177(8)	R(int)	0
c, (Å)	22.8276(13)	Goodness-of-fit on F^2	1.198
α, (°)	114.609(5)	Final R$_1$ indices [*I*>2sigma(*I*)]	0.1174
β, (°)	95.415(4)	Final wR$_2$	0.2790
γ, (°)	91.361(3)	R$_1$ indices (all data)	0.1312
Volume, (Å^3)	2438.8(2)	wR$_2$ (all data)	0.2921

A view of the crystal structure along the a-axis shows two sodium cations in indirect contact via the water molecules, forming a hydrophilic site. This hydrophilic site is surrounded by six units of 3,3`-difluoro-β-truxinic acid/3,3`-difluoro-β-truxinate arranged such that the hydrophilic end of the molecules (the carboxylate groups) are pointed towards the hydrophilic site and the hydrophobic ends point out to the circles of 2D micelle-like arrangements (Figure 6.31).
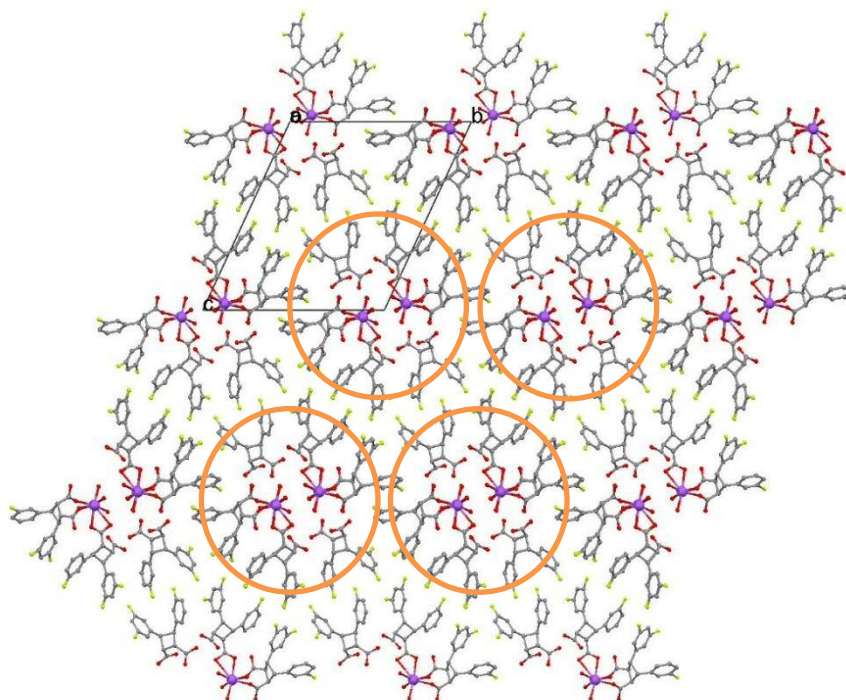
Figure 6.31: *The crystal structure of the Na-3,3`-difluoro-β-truxinate/3,3`-difluoro-β-truxinic acid viewed along the a-axis. Circles show the 2D micelles-like arrangements. Hydrogen atoms are omitted for clarity.*

6.3.7. Investigation of the effect of radiation on the NH$_4^+$ ion in NH$_4$-3-MeCate/3-MeCA

During the investigation of the photoreaction of the NH$_4^+$ salt of 3-MeCA and 3-FCA it was observed that the ^{1}H NMR resonance peak corresponding to Hβ in the cinnamic acid/cinnamate unit showed a shift during the irradiation but not for the K$^+$ salts. Therefore, the effect of irradiation was studied.

The NH$_4^+$ salt of 3-MeCA was chosen for this study. A powdered sample of the salt was spread on the glass Petri dish and exposed to the high pressure mercury UV light, as described in the experimental section. Samples were collected after 1.5, 3, 6, 9, 12, 45

and 56 hours of irradiation time and analysed using ^{1}H NMR. The shift in the resonance peaks of Hβ (Scheme 6.6) as a function of UV exposure time is plotted in Figure 6.32.
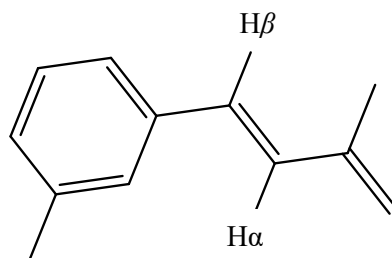
Scheme 6.6: *The unit of 3-MeCate/3-MeCA showing Hβ.*

As irradiation time increased the Hβ resonance shifted towards higher ppm. This suggested an increase in the amount of cinnamic acid units in the sample (this is explained now). The crystal structure of the salt NH$_4$-3-MeCate/3-MeCA (discussed in Chapter 5) contains both cinnamic acid and cinnamate units. Increasing the amount of cinnamic acid in the structure can occur only if the NH$_4$$^+$ ion is lost from the structure. UV irradiation may play a role in influencing of loss of the NH$_4$$^+$ ion. Thus, the cinnamate unit associated with the lost NH$_4$$^+$ ion is converted to cinnamic acid by capturing H atoms and releasing NH$_3$. The shift in the resonance of Hβ is, therefore, an indication of the changing of the cinnamate/cinnamic acid ratio. This was confirmed by a further experiment.

This experiment involved adding 3-MeCA to a solution of NH$_4$-3-MeCate/3-MeCA. The final molar ratios of 3-MeCA:NH$_4$-3-MeCate were 0:1, 0.5:1, 1:1, 2:1, 3:1 and 4:1. The mixtures were analysed by solution-state ^{1}H NMR and Figure 6.33 illustrates the shifts of the resonance peaks of Hβ versus the acid ratio. This confirms that as the acid in the mixture increases, resonance of the Hβ shifts towards higher ppm. This result supports the hypothesis that the NH$_4$$^+$ ion is lost during irradiation.
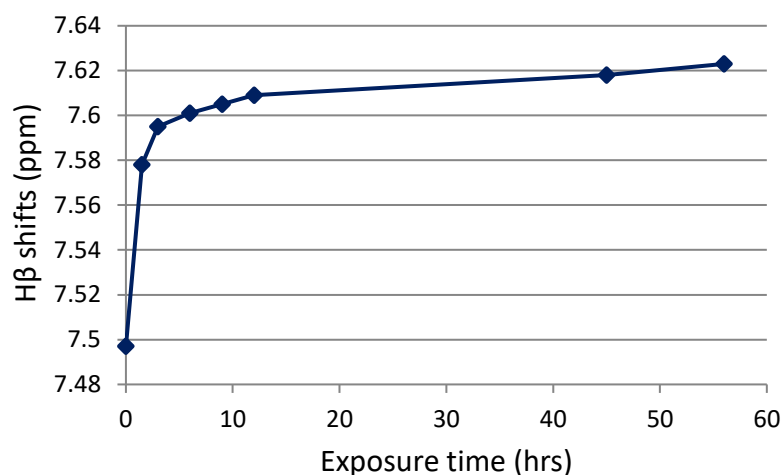
Figure 6.32: *The shift in the resonance peaks of Hβ of 3-MeCate/3-MeCA as a function of the UV exposure time.*
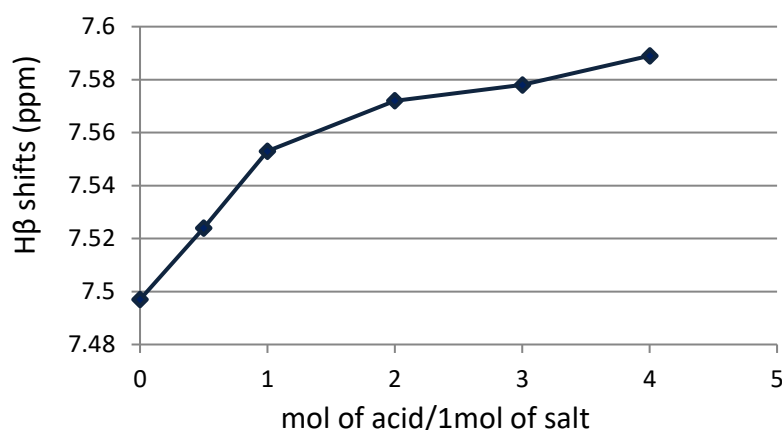
Figure 6.33: *The shift in the resonance peaks of Hβ for the mixture of 3-MeCA:1 molar of NH₄-3-MeCate.*

6.4. Conclusion

Herein solid-state photoreaction of distinct systems have been explored.

1) 3,3`-Difluoro-β-truxinic acid was obtained from the photodimerization reaction of β_1 and β_2 polymorphs of 3-FCA. In both cases the photoproduct obtained was in close to 100% yield. Similarly, both K^+ and NH_4^+ salts of 3-BrCA reacted in their crystalline state on exposure to UV irradiation to produce the corresponding β-dimeric photoproducts. However, the NH_4^+ salt of 3-CF$_3$CA showed crystal packing with the molecules arranged in segments of layers (as compare with the other salts discussed in this study where they have layered structure). In this structure three molecules out of four in the stack are in a

head-to-head orientation, which is suitable for a solid-state photodimerization reaction. ^{1}H NMR results showed that, after 52 hours of irradiation time, around only 50% of the reactant was consumed.

2) Both structures of β-3-ClCA/3-BrCA and K-(3-BrCate/3-MeCate) solid solutions have ideal geometry for photodimerization. Analysis of the product confirmed the random distribution of constituents throughout the crystal and demonstrated the applicability of the solid-state reaction in organic synthesis to generate asymmetrical molecules.

3) In the structures where the double bonds showed criss-crossed arrangements (K-3-MeCate, K-3-MeCat3-MeCA and K-3-FCate), photoirradiation of those materials showed, by mass spectrometry, the production of dimer and oligomers of different lengths. However, the identification of the all products by ^{1}H NMR and HPLC was not possible. On the other hand, in the disordered structure of NH4-3-FCate/3-FCA, the formation of the photoproduct of 3,3`-difluoro-β- truxinate was proved by SC-XRD and the paddle motion of the double bonds prior to the reaction was proposed.

4) In the case of β_1 and β_2 3-FCA, the photodimerization reaction was associated with complete loss of crystallinity, leading ultimately to an amorphous photoproduct. This limits the opportunity to apply SC-XRD or PXRD techniques to monitor the progress of the solid state reaction and to determine the structural properties of the directly produced dimer phase in each case.

6.5. References

1   K. Tanaka and F. Toda, *Chem. Rev.*, 2000, **100**, 1025–1074.

2   D. Braga, *Chem. Commun.*, 2003, 2751–2754.

3   F. Toda, *Ace. Chem. Res*, 1995, **28**, 480–486.

4   A. Mustafa, *Chem. Rev.*, 1952, **51**, 1–21.

5   M. D. Cohen and G. M. J. Schmidt, *J. Chem. Soc.*, 1964, 1996–2000.

6   M. D. Cohen, *Pure Appl. Chem.*, 1964, **9**, 567–574.

7   M. D. Cohen, G. M. J. Schmidt and F. I. Sonntag, *J. Chem. Soc.*, 1964, 2000–2013.

8   G. M. J. Schmidt, *J. Chem. Soc.*, 1964, 2014–2021.

9   F. L. Hirshfield and G. M. J. Schmidt, *J. Polym. Sci.*, 1964, **2**, 2181–2190.

10   G. M. J. Schmidt, *Pure Appl. Chem.*, 1971, **27**, 647–678.

11   J. M. Thomas, *Philos. Trans. R. Soc. A*, 1974, **277**, 251–287.

12   V. Enkelmann, G. Wegner, K. Novak and K. B. Wagener, *J. Am. Chem. Soc.*, 1993, **115**, 10390–10391.

13   F. Guo, J. Martı´-Rujas, Z. Pan, C. E. Hughes and K. D. M. Harris, *J. Phys. Chem. C*, 2008, **112**, 19793–19796.

14   K. Biradha and R. Santra, *Chem. Soc. Rev.*, 2013, **42**, 950–967.

15   V. Ramamurthy and K. Venkatesan, *Chem. Rev.*, 1987, **87**, 433–481.

16   D. B. Varshney, G. S. Papaefstathiou and L. R. MacGillivray, *Chem. Commun.*, 2002, **646**, 1964–1965.

17   M. Nagarathinam, A. M. P. Peedikakkal and J. J. Vittal, *Chem. Commun.*, 2008, 5277–5288.

18   C. V. K. Sharma, K. Panneerselvam, L. Shimoni, H. Katz, H. L. Carrell and G. R. Desiraju, *Chem. Mater.*, 1994, **6**, 1282–1292.

19   M. D. Cohen and R. Cohen, *J. Chem. Soc. Perkin II*, 1976, 1731–1735.

20   C. R. Theocharis, G. R. Desiraju and W. Jones, *J. Am. Chem. Soc.*, 1984, **106**, 3606–3609.

21   C. Vithana, H. Uekusa, A. Sekine and Y. Ohashi, *Cryst. Growth Des.*, 2005, **5**, 1755–1760.

22   W. Jones, C. R. Theocharis, J. M. Thomas and G. R. Desirajub, *J. Chem. Soc., Chem. Commun.,* 1983, 1443–1444.

23   M. D. Cohen, R. Cohen, M. Lahav and P. L. Nie, *J. Chem. Soc. Perkin II.*, 1973, 1095–1100.

24   Y. Ito, *Mol. Supramol. Photochem. Mol. Photochem.*, 1999, **3**, 1–70.

25   D.-K. Bučar, A. Sen, S. V. S. Mariappan and L. R. MacGillivray, *Chem. Commun. (Camb).*, 2012, **48**, 1790–1792.

26   M. Chowdhury and B. M. Kariuki, *Cryst. Growth Des.*, 2006, **6**, 774–780.

27   A. M. P. Peedikakkal and J. J. Vittal, *Chem. Eur. J.*, 2008, **14**, 5329–5334.

28   M. Bertmer, R. C. Nieuwendaal, A. B. Barnes and S. E. Hayes, *J. Phys. Chem. B*, 2006, **110**, 6270–6273.

29   K. D. M. Harris and J. M. Thomas, *J. Solid State Chem.*, 1991, **94**, 179–205.

30   M. Khan, G. Brunklaus, V. Enkelmann and H.-W. Spiess, *J. Am. Chem. Soc.*, 2008, **130**, 1741–1748.

31   R. C. Nieuwendaal, M. Bertmer and S. E. Hayes, *J. Phys. Chem. B*, 2008, **112**, 12920–12926.

32 F.-L. Hu, S.-L. Wang, J.-P. Lang and B. F. Abrahams, *Sci. Rep.*, 2014, **4**, 6815/1–6815/6.

33 S. L. Jenkins, M. J. Almond, S. D. M. Atkinson, M. G. B. Drew, P. Hollins, J. L. Mortimore and M. J. Tobin, *J. Mol. Struct.*, 2006, **786**, 220–226.

34 S. Kanao, S. Kashino and M. Haisa, *Acta Crystallogr. Sect. C*, 1990, **46**, 2439–2442.

35 J. L. R. Yates and H. A. Sparkes, *CrystEngComm*, 2013, **15**, 3547–3553.

36 D. Crowther, M. Chowdhury and B. M. Kariuki, *J. Mol. Struct.*, 2008, **872**, 64–71.

37 M. L. Salum, C. J. Robles and R. Erra-Balsells, *Org. Lett.*, 2010, **12**, 4808–4811.

38 A. Natarajan, J. T. Mague, K. Venkatesan, T. Arai and V. Ramamurthy, *J. Org. Chem.*, 2006, **71**, 1055–1059.

39 D. Furukawa, S. Kobatake and A. Matsumoto, *Chem. Commun.*, 2008, 55–57.

40 K. Tanaka, T. Hiratsuka, S. Ohba, M. R. Naimi-Jamal and G. Kaupp, *J. Phys. Org. Chem.*, 2003, **16**, 905–912.

41 J. Harada and K. Ogawa, *Chem. Soc. Rev.*, 2009, **38**, 2244–2252.

42 Y. Ito, H. Hosomi and S. Ohba, *Tetrahedron*, 2000, **56**, 6833–6844.

43 S. Ohba, H. Hosomi and Y. Ito, *J. Am. Chem. Soc.*, 2001, **123**, 6349–6352.

44 A. Natarajan, J. T. Mague, K. Venkatesan and V. Ramamurthy, *Org. Lett.*, 2005, **7**, 1895–1898.

45 M. Nagarathinam and J. J. Vittal, *Chem. Commun.*, 2008, 438–440.

Chapter 7: Mechanogrinding: a green chemistry approach in controlling phase transformation and cocrystallization

7.1. Introduction

Polymorphism of crystalline solids is one of the hot topics in organic materials chemistry. This is because different polymorphs, despite their identical molecular identity, could have different properties, such as solubility, melting point, chemical reactivity, etc. Therefore, the control of the specific polymorph remains a highly important area of research.[1–3]

Controlling polymorphism from solution crystallization is the most frequent method that has been used; for example, different solvents can produce different polymorphs. [4–8] However, in the push towards green chemistry,[9,10] where minimizing or eliminating harmful chemicals in the environment is the challenge, efforts have therefore been made to develop new methods.

Solvent-less systems are one such example. Therefore, mechanogrinding (solvent free) and solvent drop grinding (SDG, where a minimal amount of the solvent is used), can be applied as green chemistry, an alternative to solution crystallization. As an example, four polymorphs of benzidine were reported[11] to have been obtained via solvent drop grinding. In another approach,[12] selective conversion towards specific polymorphs of anthranilic acid and succinic acid was controlled using SDG. Behaviour was also investigated in cocrystalline material; Trask et al.[13] reported that caffeine and glutamic acid undergo cocrystallization via the mechanogrinding process and, with a minimal addition of a solvent, the polymorph obtained can be controlled.

Cinnamic acid and its derivatives are highly studied materials for aspects such as screening of polymorphs, particularly because of the correlation between their structures and the solid-state photodimerization reaction (discussed previously in Chapter 1).[14–16] However, to our knowledge, the effect of mechanogrinding and solvent drop grinding on the structures obtained of cinnamic acid derivatives, has not been specifically investigated.

Thus, the work described here was carried out with the aim of investigating the effect of neat grinding and solvent drop grinding on the γ and β polymorphs of two cinnamic acids (3-BrCA and 3-ClCA). The study was extended further with the objective of forming, via grinding, cocrystalline materials with different structures, and to understand the mechanism of such cocrystallization behaviour. Additionally, an investigation on the transformation in solid solution materials was also undertaken in this study.

7.2. Experimental Methods

A vibratory ball mill was used for the grinding process. Grinding frequency was set to 15 Hz and an appropriate amount of powder was ground in a grinding jar with two steel grinding balls of 10mm diameter. The material was ground for the duration required to meet the targets of the grinding experiment. For most of the experiments, one and a half hours of grinding time was applied or is otherwise as stated. Note that, a new powder sample was used for each new experiment, including different grinding times.

In the case of solvent drop grinding (SDG) the appropriate quantity of the solvents was added using a micro pipette. The ground materials were then exposed to allow any solvent present to evaporate. PXRD was used to characterize the resulting material after grinding.

7.3. Result and Discussion

7.3.1. Effect of grinding on the pure acids

Both acids, 3-BrCA and 3-ClCA, were of interest in this study. Two different polymorphs have been reported for 3-BrCA (γ[17] and β[18]), where the γ phase undergoes phase transformation to β form when heated[17]. Similarly, 3-ClCA was reported to crystallize in two different polymorphs (γ and β)[16,18], and this study (Chapter 3) indicated that heat induced a similar transformation to 3-BrCA, where the γ form transformed irreversibly to the β form. Interestingly, the γ forms of the acids (3-BrCA and 3-ClCA) are isostructural, whereas β forms are not. Therefore, the study here was carried out to gain more insight into the effect of grinding on the γ and β forms of each acid.

7.3.1.a. γ phase of 3-BrCA and 3-ClCA

The γ forms of both acids (3-BrCA and 3-ClCA) were ground separately for one and a half hours. PXRD analysis for the ground materials, as shown in Figure 7.1, indicated that no transformation occurred during grinding and both acids remained in their original form. It was also observed that the ground materials were stable after a storage duration of six months under ambient conditions of the laboratory.
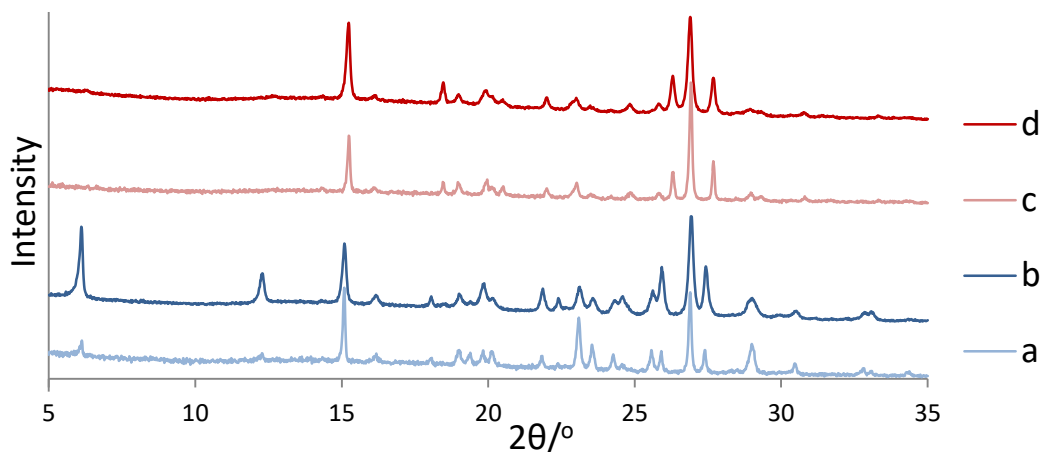
Figure 7.1. *Comparison of the PXRD patterns of (a) and (b) for γ-3-BrCA and (c) and (d) for γ-3-ClCA before and after grinding, respectively.*

7.3.1.b. β phase of 3-BrCA and 3-ClCA

No effect on the phase was observed on grinding β forms of both acids (3-BrCA and 3-ClCA) for a duration of one and a half hours. Thus, analysis of samples after grinding using PXRD showed the existence of monophasic material (β phase) in both samples and no other phases were detected. However, some γ-3-ClCA was observed after repeating PXRD on the ground β-3-ClCA that was left on the laboratory shelf for 7 days (PXRD was run on the same prepared sample in the tape) (see Figure 7.2). This was further investigated later. In fact, no phase transformation was observed in the unground β-3-ClCA that was left in the laboratory under ambient conditions for 40 days. This indicates an effect of grinding on β-3-ClCA in the process of transformation of the acid from β to γ. This is discussed in detail later in this section.
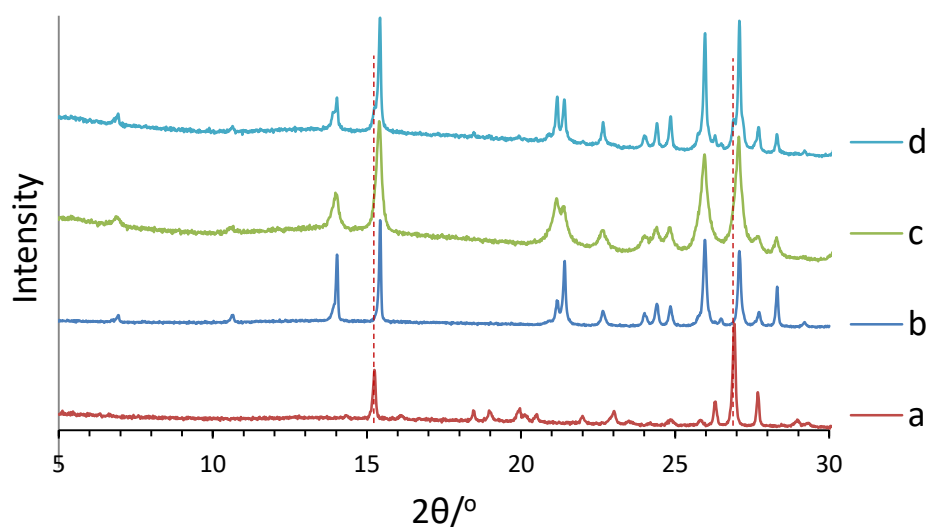
Figure 7.2. *Comparision of the PXRD patterns of: (a) and (b) for γ and β 3-ClCA, respectively, before grinding. (c) Immediately after grinding β-3-ClCA for 1.5 hrs. (d) Repeating PXRD of the same sample after 7 days.*

In contrast, no change to the *β*-3-BrCA was been observed for either the ground acid or the unground acid when the samples were left for more than 40 days in the laboratory under ambient conditions and the PXRD repeated on the same prepared tape of the sample.

Solvent drop grinding

The next study was carried out to investigate the effect of SDG on the *β* phases of both acids. 50μl of the solvent (MeOH or deionized H_2O (d.i.water)) was added to one mmol of *β*-3-BrCA and then ground for one and a half hours. The ground material was then analysed using PXRD. As seen in Figure 7.3, for all ground samples, just *β*-3-BrCA was observed after the course of SDG, illustrating the phase stability of *β*-3-BrCA. However-er, broadening in the PXRD peaks of the ground samples was observed (see, in particu-lar, the peak around 26.352˚ and 26.65˚ *2θ* in Figure 7.3). This broadening is expected due to either reduction in the particle size or the defect induced in the structure during the grinding process or both.[19]
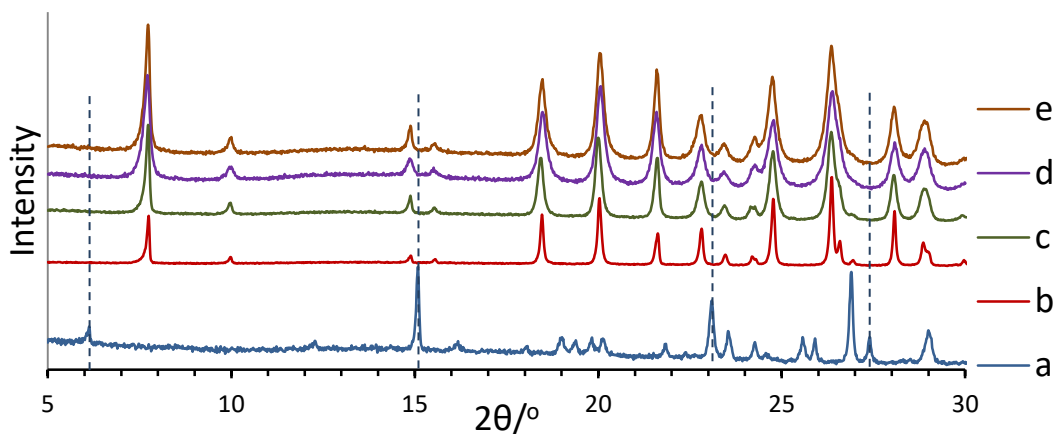
Figure 7.3. *PXRD of: (a) and (b) γ and β 3-BrCA, respectively, before grinding, (c) after neat grinding of β-3-BrCA for 1.5 hrs immediately, (d) and (e) after SDG of β-3-BrCA for 1.5 hrs using MeOH and d.i.water, respectively. Dashed lines indicate the absence of γ-3-BrCA.*

However, subjecting β-3-ClCA to the same experiment by grinding 1 mmol of β-3-ClCA with 50μl of the solvent (MeOH, d.i.water or hexane) for one and a half hours, produced pure monophasic γ-3-ClCA in all cases. Surprisingly, there was no indication of any peaks of β-3-ClCA, indicating a complete phase transformation. As there was no transformation observed immediately after the neat grinding of β-3-ClCA, this illustrates that the solvent here act as a catalyst in accelerating the process of transformation. Additionally, the results also revealed that all solvents used here caused a similar effect regarding transformation and no difference was observed whether the solvent used was polar or non-polar.

Further investigation was then performed in order to assess the quantity of the solvent that can induce the transformation in the case of β-3-ClCA. Hence, as summarized in Table 7.1, three solvents were selected for this study, MeOH, acetone (AC) and d.i. water. 1 mmol of β-3-ClCA was ground by the SDG method with the above mentioned solvents of various quantities and the products were then analysed using PXRD. The results showed that only 10 μl of AC was enough for the phase conversion to occur, while about 20 μl of MeOH was required to induce the transformation. On the other hand, using 20 μl water showed an incomplete transformation. Thus we can conclude that AC is the most effective catalyst while water is the least effective. As 3-ClCA is highly soluble in both MeOH and AC and, water was observed to be a poor solvent for 3-ClCA, the transformation may therefore be linked to solubility. It was reported[20] that the amount of the water added enhanced the transformation of Famotidine from one form (A) to another form (B) during the grinding process, as adding water leads to easi-

er polymorphic transformation. This observation showed good agreement with the result obtained in this study. Thus, increasing the amount of water from 20μl to 50μl/1mmol of γ-3-ClCA leads to full transformation of the acid from the γ form to β, regardless of the solubility effect.

Table 7.1. Summary of the ground β-3-ClCA via SDG.

Solvent	Amount of the solvent used		The phase observed by PXRD
	(μl)	(mmol)	
MeOH	10	0.25	Mixture of β-3-ClCA and γ-3-ClCA
	20	0.49	Pure γ-3-ClCA
AC	5	0.07	Mixture of β-3-ClCA and γ-3-ClCA
	10	0.14	Pure γ -3-ClCA
d.i.Water	20	1.11	Mixture of β-3-ClCA and γ-3-ClCA
	50	2.77	Pure γ-3-ClCA

Catalytic effect of the tape

The sample of β-3-ClCA ground for a duration of one and a half hours was checked by PXRD immediately after grinding and was found to be the β phase (Figure 7.4c), as mentioned previously. The sample in the tape (sample A) together with other ground material not in the tape were stored in a desiccator for investigation of any change with time. One week later, PXRD on the sample A showed that the β phase was present but the γ phase had started to grow (Figure 7.4d). PXRD recorded for the sample two and four weeks after grinding (labelled A_e and A_f, respectively) (Figure 7.4 e and f, respectively) indicated an increasing amount of the γ phase while the β phase was still present. However, when the original ground sample (not stored in the tape) was analysed after four weeks (labelled sample B), the PXRD surprisingly showed no transformation to the γ form and the acid was monophasic (β phase) (see Figure 7.4g). Thus, the question raised was: what caused the transformation in sample A?

In order to answer the question, first, the difference between the storage conditions of the two samples (A_f and B) were considered; both samples were stored in the desiccator, under laboratory ambient conditions for four weeks. Sample B was in a covered vial, while sample A_f was sandwiched between two pieces of transparent tape and then placed in a covered vial. On the other hand, sample A_f was measured four times by PXRD in the duration of the four weeks, while sample B was only measured once,

meaning sample A_f experienced more exposure to X-rays than sample B. Therefore, the two factors that were likely to have affected the transformation in sample A_f were either the material of the tape or the exposure to X-ray radiation during measurement.
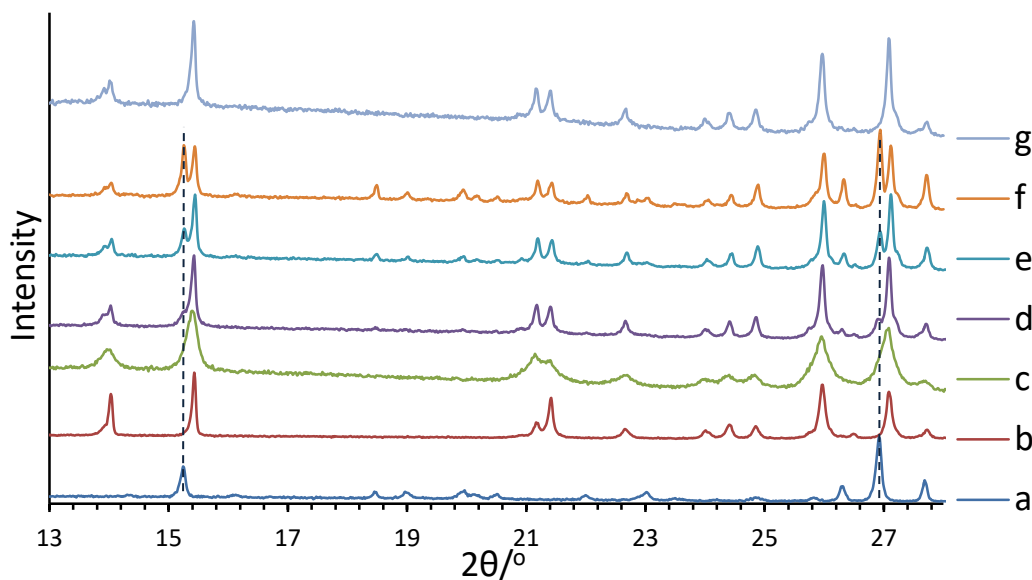
Figure 7.4. *Comparison of the PXRD of: (a) and (b) for γ and β 3-ClCA, respectively, before grinding. (c) Immediately after grinding β-3-ClCA for 1.5 hrs. (d), (e) and (f) repeated PXRD of the sample stored in the tape (sample A) after 1 week, 2 weeks (A_e) and 4 weeks (A_f), respectively. (g) Sample B (four weeks later after grinding). Dashed lines indicate the presence of γ-3-ClCA.*

Thus, in order to investigate the effect of X-rays and of the tape that was used to prepare the sample prior to PXRD analysis, *β*-3-ClCA was ground for three hours. First the sample was checked by PXRD which showed both *γ* and *β* 3-ClCA (the presence of both *γ* and *β* phases is because a longer duration of grinding, this will be discussed later in this section). Then some of the sample was sandwiched between pieces of the tape and kept in the desiccator (labelled C). The rest of the ground material was also kept in the desiccator (labelled D). Two weeks later, both samples (C and D) was analysed by PXRD. Interestingly, although both samples contained both phases (*β* and γ) of the acid, sample C seemed to contain more *γ* phase than sample D (see Figure 7.5). This result eliminates the effect of the X-ray exposure on the transformation, on the one hand, and emphasises the effect of the tape on the transformation, on the other hand. As both samples were exposed to X-rays only once, the effect of the X-ray was the same and the only difference then between them was that sample C was in contact with the tape during storage, while sample D was not. So, the differences in the PXRD showing more *γ* phase in sample C than sample D can be only attributable to the tape acting as a

catalyst to produce more γ phase. The tape was used here is a Scotch transparent tape and the adhesive material of the tape is a kind of polymer that composed a combination of complex chemical mixture composes of alcohol, acid, raw materials (that produced from a chemical treatment of distillated crude oil) water and hydrocarbon.[21]
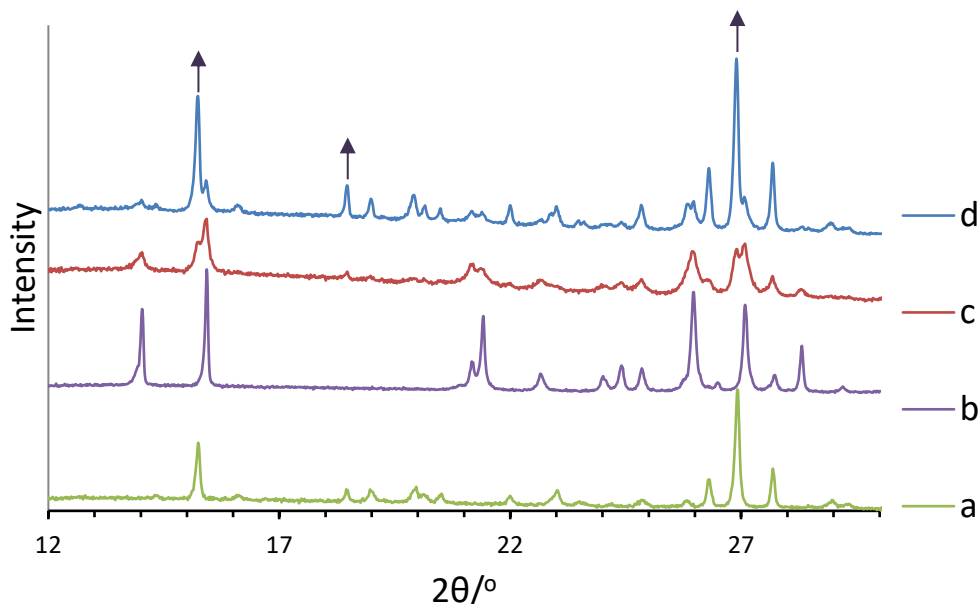
Figure 7.5. *PXRD of: (a) and (b) for γ and β 3-ClCA, respectively, before grinding. (c) and (d) Samples D and C, respectively, after grinding and storing for two weeks. Arrows indicate the growing of γ phase.*

Does increasing the grinding time enhance the transformation of β-3-ClCA?

The study in the previous section revealed that no phase transformation was observed when the sample was ground for a duration of one and half hours (when the catalytic effect of tape on the transformation was eliminated). Thus, an investigation was carried out to assess whether increasing the grinding time has any effect on the growth of the γ phase of the acid. To achieve this study β-3-ClCA was ground for one and a half hours (labelled H_A) and, for three hours (labelled H_b), then the samples were sealed in glass capillaries and analysed by PXRD at specific time intervals to monitor the change in the sample. The samples were sealed in capillaries to eliminate the tape effect.

PXRD analysis of both samples H_A and H_b, one day after grinding, showed that both samples were in their original β form (Figure 7.6c and 7.7c, respectively). However, sample H_b showed a gradual growth of the γ phase with time (Figure 7.7), while no transformation was noticed for sample H_A, as illustrated Figure 7.6.

These results are consistent with previously obtained result of *Catalytic effect of the tape*, where the PXRD of the freshly prepared ground sample, stored for two weeks, showed growth of the γ phase for the material that was ground for three hours. There was no observed indication of a γ phase for the sample ground for one and a half hours and stored for four weeks.

Grinding of *β*-3-ClCA for one and a half hours leads to no phase change, but a longer duration of grinding is required to initiate the transformation in the material during the storage time. Therefore, we can conclude that increasing the grinding time has a clear effect on the generation of the γ phase from ground *β*-3-ClCA. This can be explained as follows; increasing the grinding time induces more change in the crystalline materials, such as, a reduction in the particle size, defects, strains and partial amorphization[22] which may therefore enable the transformation to occur easily.

It is worth noting that, in the case of sample H_A, although the peak positions remain the same after grinding the sample, a change in the intensity of some peaks was observed (2θ of 21.2° and 21.4°) as shown in Figure 7.6, indicated by the dashed rectangle. This intensity change is probably attributed to the change in the crystal habit and the presence of defects in the crystals[23].
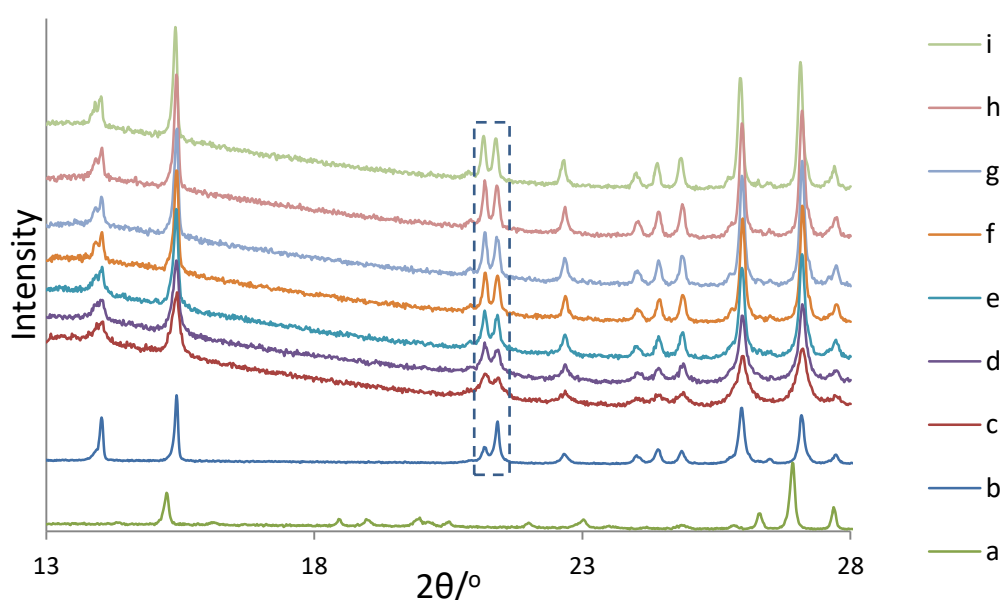
Figure 7.6. *The comparison of PXRD of: (a) and (b) for γ and β 3-ClCA, respectively, before grinding. (c), (d), (e). (f), (g), (h) and (i) for the sample after grinding for 1.5 hrs then stored in a sealed glass capillary for 1 day, 1 week, 3 weeks, 5 weeks, 7 weeks, 10 weeks and 15 weeks, respectively.*
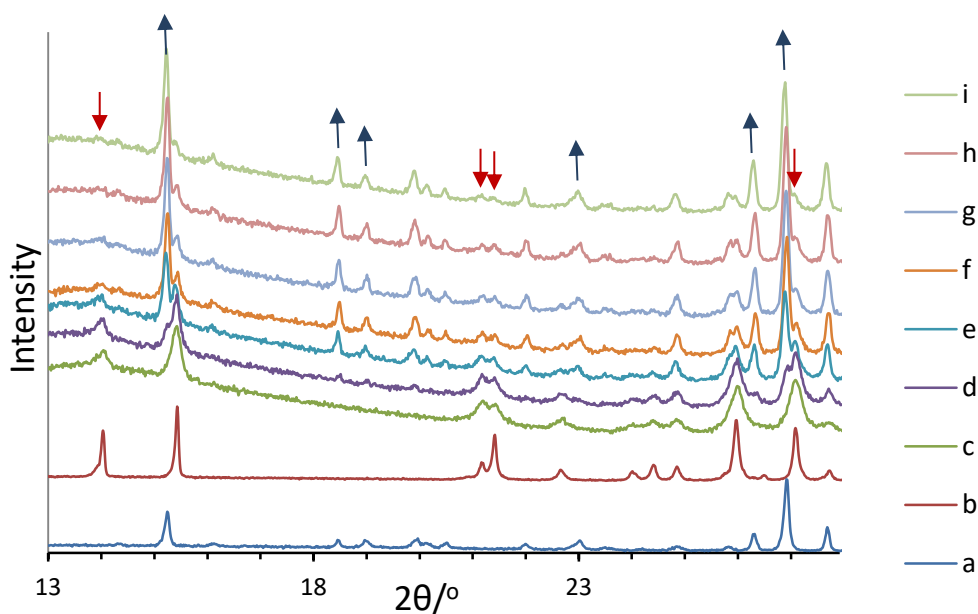
Figure 7.7. *The comparison of PXRD of: (a) and (b) for γ and β 3-ClCA, respectively, before grinding. (c), (d), (e). (f), (g), (h) and (i) for the sample after grinding for 3 hrs then stored in a sealed glass capillary for 1 day, 1 week, 3 weeks, 5 weeks, 7 weeks, 10 weeks and 15 weeks, respectively. Arrows indicate the growth of γ phase (blue), and the decay of β phase (red).*

7.3.1.c. Effect of phase contamination during grinding

The previous study in this chapter showed that *β*-3-ClCA undergoes phase transformation to produce *γ*-3-ClCA upon SDG, whereas *β*-3-BrCA does not change upon SDG. Thus, the study here was carried out to investigate the effect of grinding mixed phases of either same material or different materials.

As summarized in Table 7.2, grinding *γ* and *β* phases of 3-ClCA in a 1:1 molar ratio for one and a half hours produced the PXRD patterns of *γ*-3-ClCA, indicating the accelerated transformation of the *β* form of the acid into the *γ* form in the presence of the *γ* phase (Figure 7.8c). Additionally, grinding a mixture with a ratio of 1:8 of *γ*:*β* resulted in mainly the *γ* phase with a contamination of the *β* phase (see the PXRD comparison of the 1:8 of *γ*:*β* mixture before and after grinding in Figure 7.8 d and e, respectively). The results here showed that introduction of a small amount of the *γ* phase induces the transformation from *β* to *γ* upon grinding. As in this case, the *γ* phase plays a seeding role in accelerating the transformation via grinding. It was shown in the previous section that the *β* phase of 3-ClCA ground for one and a half hours is stable at least fifteen weeks.
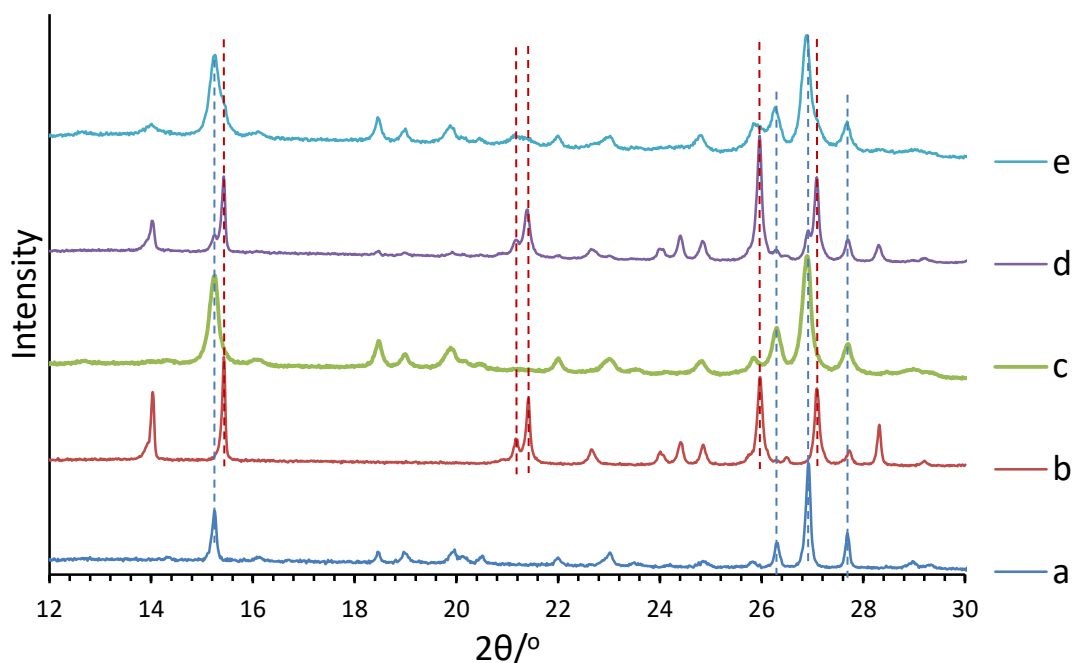
Figure 7.8*. The comparison of PXRD of: (a) and (b) for γ and β 3-ClCA, respectively before grinding. (c) Grinding of 1:1 γ:β 3-ClCA, (d) and (e) are 1:8 mixture of γ:β 3-ClCA before and after grinding, respectively. All grinding experiments are for 1.5 hrs. Dashed lines indicate the presence of the phase according to the corresponding colour.*

On the other hand, grinding mixtures of phases comprising 3-BrCA (γ:β) with ratios 1:1 and 8:1 showed no obvious effect on the product. (Figure 7.9 e and c respectively). The most interesting result here is that, in the 8:1 γ:β mixture, although the amount of the γ was eight times more than the β phase, the β structure was not induced to transform. PXRD patterns in Figure 7.9 d and e of the 1:8 ratio before and after grinding respectively, showed no obvious transformation (from β to γ), indicating a high stability for the β structure of 3-BrCA in the presence of γ contamination.

In a further investigation, β-3-ClCA was ground with γ-3-BrCA with a 1:1 molar ratio for one and a half hours. Analyses of the product using PXRD showed the formation of the γ-3-ClCA/3-BrCA solid solution. This indicated the transformation of β-3-ClCA to the γ structure of the solid solution (which is isostructural with the γ-3-ClCA and with γ-3BrCA structure). This result, in agreement with other observations, shows that β-3-ClCA has a preference to transform to γ-3-ClCA upon grinding, when contamination is present. Table 7.2 summarizes the experiments performed with phase contamination. (NB: The formation of solid solutions, via grinding, is discussed later in Section 7.3.2)
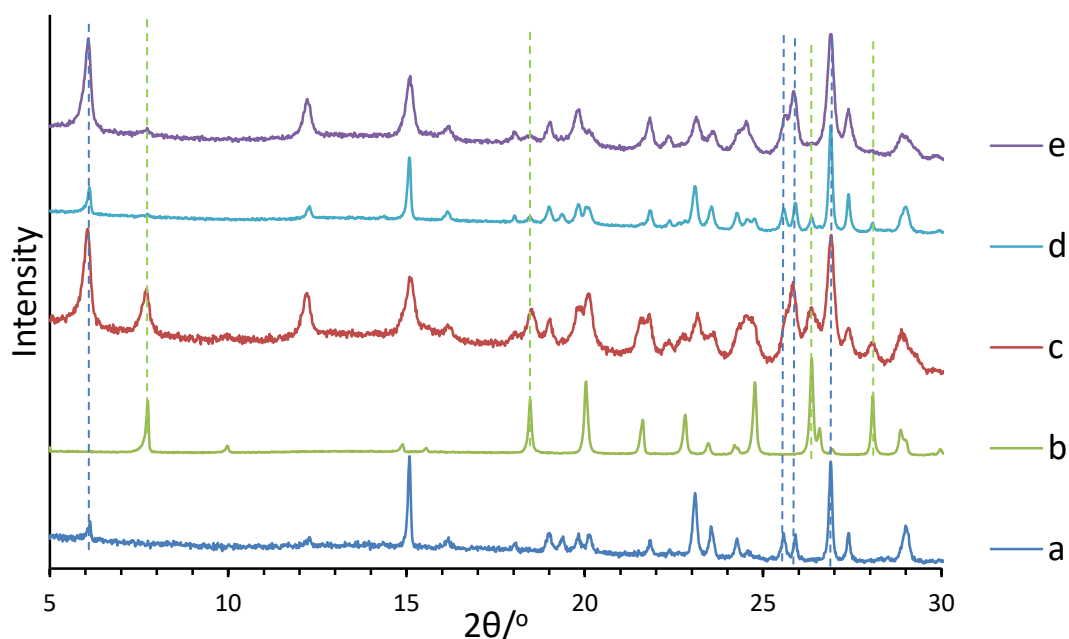
Figure 7.9. *The comparison of PXRD of: (a) and (b) for γ and β 3-BrCA, respectively, before grinding. (c) Grinding of 1:1 γ:β 3-BrCA. (d) and (e) 8:1 mixture of γ:β 3-BrCA before and after grinding, respectively. All grinding experiments are for 1.5 hrs. Dashed lines indicate the presence of the phase according to the corresponding colour.*

Table 7.2. *Summary of the ground mixtures comprising materials 1 and 2 and the products obtained based on PXRD analysis.*

Material 1	Material 2	Phase produced
1 mmol *β*-3-ClCA	1 mmol *γ*-3-ClCA	*γ*-3-ClCA
8 mmol *β*-3-ClCA	1 mmol *γ*-3-ClCA	Mostly *γ*-3-ClCA with traces of *β*-3-ClCA
1 mmol *β*-3-BrCA	1 mmol *γ*-3-BrCA	Mixture of *γ*-3-BrCA and *β*-3-BrCA
1 mmol *β*-3-BrCA	8 mmol *γ*-3-BrCA	Mostly *γ*-3-BrCA with traces of *β*-3-BrCA
1 mmol *β*-3-ClCA	1 mmol *γ*-3-BrCA	*γ*-solid solution (isostructural to *γ* form of 3-BrCA and 3-ClCA

7.3.2. Cocrystallization via grinding

Recalling the results from Chapter 4, it was observed that 3-ClCA and 3-BrCA undergo cocrystallization from solution, under different conditions, to produce three forms of solid solution (*β*, *γ*, *γ₂*). Mechanogrinding is considered to be a green effective tool in the formation of cocrystalline materials when it is accessible.[24,25] Therefore, the study in this section focused on cocrystallization of 3-ClCA and 3-BrCA and includes an explanation of the effect of neat grinding and SDG on the product obtained.

7.3.2.a. Grinding of a mixture of acids in their γ phase

Neat grinding

Solid state grinding of a mixture of γ-3-ClCA and γ-3-BrCA with a 1:1 ratio resulted in γ-3-ClCA/3-BrCA solid solution, as judged by comparison with PXRD of the γ-3-ClCA/3-BrCA solid solution that was obtained from the solution crystallization experiments reported in Chapter 4 (see Figure 7.10). This result is not surprising since, γ-3-ClCA and γ-3-BrCA are isostructural to each other and therefore the molecules of one acid can easily be replaced with molecules of the other acid, assisted by grinding and, accordingly, they are most likely to cocrystallize.
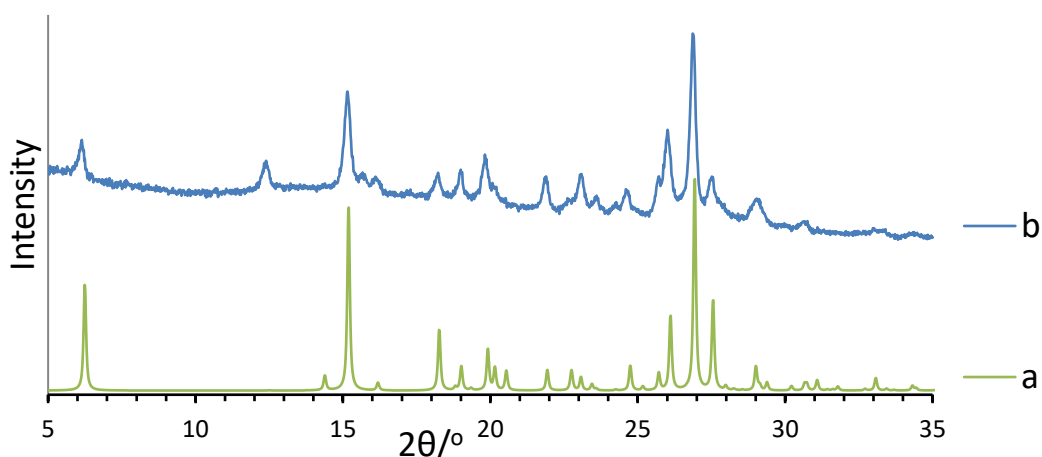
Figure 7.10. *(a) Simulated PXRD of SC-XRD of γ-3-ClCA/3-BrCA solid solution. (b) PXRD of ground 1:1 γ-3-ClCA:γ-3-BrCA.*

Solvent drop grinding

As shown in Chapter 4, cocrystallization of 1:1 of 3-BrCA:3-ClCA from a solution of glacial acetic acid (GAA) was shown by SC-XRD to produce a β-3-ClCA/3-BrCA solid solution with a ratio of ≈ 1:1 3-ClCA:3-BrCA. In contrast, SDG of a 1:1 mixture of γ-3-BrCA:γ-3-ClCA in the presence of 50μl of GAA was shown by PXRD to produce the γ-3-ClCA/3-BrCA solid solution. Similarly, SDG of these acids 3-BrCA:3-ClCA in their γ phase with a ratio 1:1 using 50μl MeOH or AC also produced γ solid solution. Introducing 50μl of water instead, also produced γ solid solution but some starting materials (γ-3-ClCA and γ-3-BrCA) remained (see Figure 7.11). The presence of these starting material after the grinding process indicates a semi-inhibitory effect of water in the formation of the cocrystalline material. This is a surprising result as, although it is a poorer solvent, it would be expected to enhance, not to partially inhibit the process of cocrystallization. It was reported that an increase in humidity (water) plays an important role in the cocrystallization via grinding, by facilitating the movement and subsequent

rearrangement of the molecules on the surface of the crystallites.[26,27] It was also shown[28] that grinding of cyclohexane-1,3cis,5cis-tricarboxylic acid (A) and 4,7-phenanthroline (B) using drops of acetonitrile as a solvent (in which both A and B are only partly soluble) accelerating the cocrystallization. Accordingly, in the present study, as 3-BrCA and 3-ClCA showed a slight solubility in water, it would be expected that adding drops of water enhances rather than inhibits the cocrystallization. Thus, this effect of water in the partial inhibition of a solid solution formation suggests that, it is probably the nature of the water molecules themselves and the way that they interact with the surface of the materials, which may hinder the two crystalline materials from undergoing complete cocrystallization.
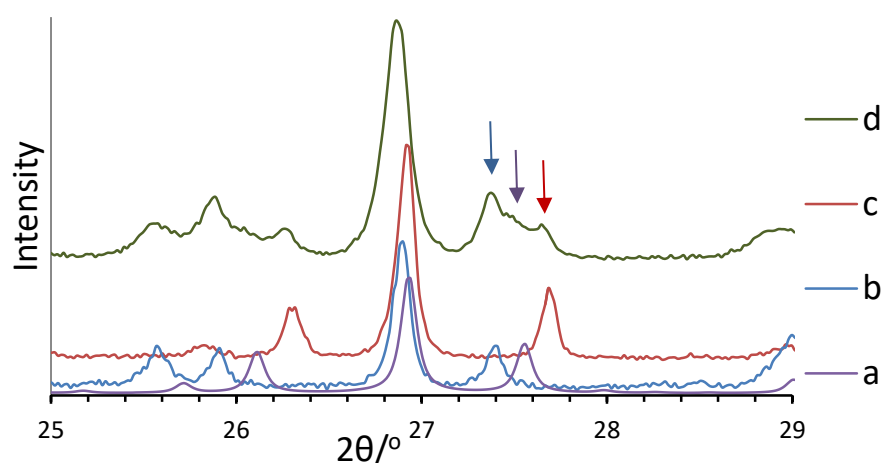
Figure 7.11. *Part of (a) Simulated PXRD of SC-XRD of γ-3-ClCA/3-BrCA solid solution. (b) and (c) PXRD of γ-3-BrCA and γ-3-ClCA, respectively. (d) PXRD of ground 1:1 γ-3-ClCA:γ-3-BrCA and 50μl d.i.water. Arrows indicate different phases purple (a), blue (b) and red (c).*

7.3.2.b. Grinding of mixture of acids in their *β* phase

Neat grinding of 1:1 mixtures

Solid state grinding of *β*-3-ClCA and *β*-3-BrCA with a ratio of 1:1 for one and half hours resulted in *β*-3-ClCA/3-BrCA solid solution with a PXRD similar to *β*-3-BrCA. This result was revealed by the comparison of the PXRD patterns of both the *β*-3-ClCA/3-BrCA solid solution obtained from the solution cocrystallization (reported in Chapter 4) and the mechanogrinding process (see Figure 7.12).
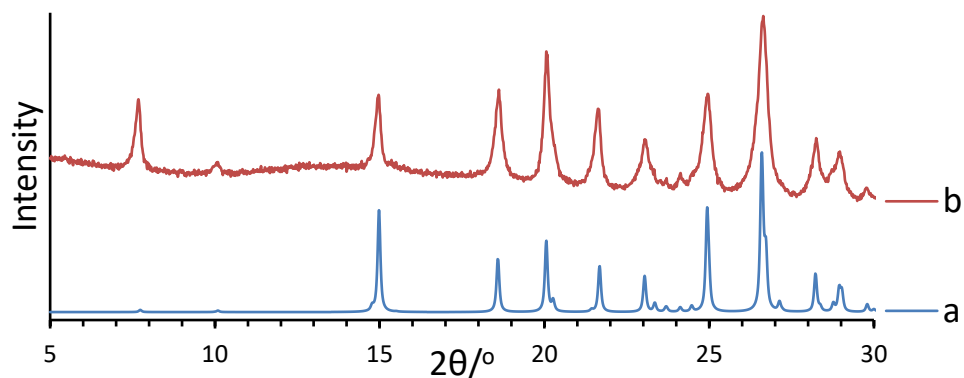
Figure 7.12. *(a) Simulated PXRD of SC-XRD of β-3-ClCA/3-BrCA solid solution. (b) PXRD of ground 1:1 β-3-ClCA:β-3-BrCA.*

As mentioned previously, *β*-3-ClCA and *β*-3-BrCA are not isostructural to each other and, additionally, the molecules have different conformations regarding their C-halogen bond and C=C bond (see Figure 7.13). It is, therefore, understandable that they form a solid solution with a structure similar to *β*-3-BrCA, from either solution or melt, since the molecules can move much more freely in a solution or melt state. So, in the course of cocrystallization, they are able to pack in the preferred crystal structure. However, during solid grinding, the molecules are constrained in comparison with the solution or melt state and, subsequently, their movement is expected to be much less. To pack *β*-3-ClCA molecules in a structure that is similar to *β*-3-BrCA to form a solid solution, two changes are required in the 3-ClCA molecules; in their conformation and their orientation. Nevertheless, the results indicate the formation of the cocrystalline material that comprises both acids with a structure that is similar to *β*-3-BrCA. This result illustrates that, in their solid state and under mechanical force, the 3-ClCA molecules exhibited the required movement to allow the formation of the cocrystalline material (in form of solid solution).
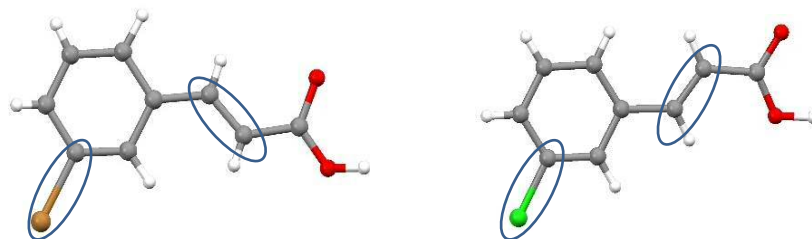
Figure 7.13. *Comparison of different conformation of the molecules of β-3-BrCA and β-3-ClCA structures.*

Neat grinding of different ratio mixtures

The result from Chapter 4 revealed that cocrystallization of 3-ClCA:3-BrCA from melt with ratios of 4:1 and 5:1 produced *β*-3-ClCA/3-BrCA solid solution isostructural to *β*-

3-ClCA. A further study was carried out to investigate the possibility of obtaining this structure of solid solution by neat grinding. Additionally, the effect of neat grinding of different ratios of *β*-3-ClCA and *β*-3-BrCA on the structure obtained was also investigated. As illustrated in Figure 7.14 b and c, *β*-3-ClCA/3-BrCA solid solution with a structure similar to *β*-3-BrCA was produced by grinding *β*-3-ClCA:*β*-3-BrCA, with starting ratios of 1:4 and 2:1. However, grinding *β*-3-ClCA:*β*-3-BrCA with starting ratios of 4:1 and 5:1 gave a mixture of three phases; *β*-3-ClCA/3-BrCA solid solution with a structure is similar to *β*-3-BrCA and *β*-3-ClCA, as well as a *γ*-3-ClCA/3-BrCA solid solution isostructural to both *γ*-3-ClCA and *γ*-3-BrCA (Figure 7.14 d and e). These results demonstrate, firstly, the possibility of forming *β*-3-ClCA/3-BrCA solid solution with a structure similar to *β*-3-ClCA. However, it was not pure, as it was contaminated with other phases. Secondly, the result shows the flexibility of forming solid solutions with different structures via grinding.
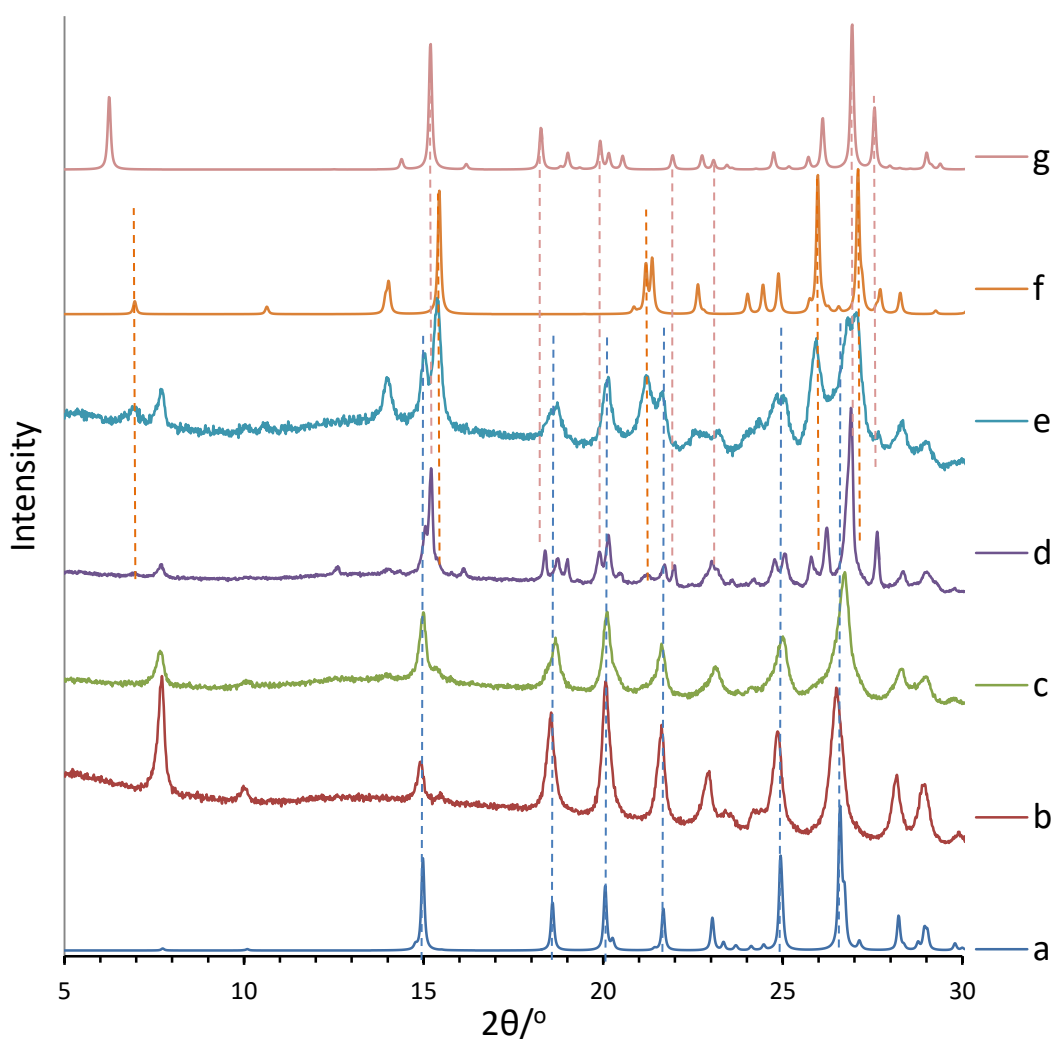
Figure 7.14. *Simulated PXRD of SC-XRD of (a) β-3-ClCA/3-BrCA solid solution, (f) β-3-ClCA and (g) γ-3-ClCA/3-BrCA solid solution. (b), (c), (d) and (e) are PXRD patterns of the ground β-3-ClCA:β-3-BrCA with the ratio of 1:4, 2:1, 4:1 and 5:1 respectively.*

Solvent drop grinding of mixtures of *β*-3-ClCA and *β*-3-BrCA and their *β* solid solutions

The effect of introducing a solvent when grinding mixtures of *β*-3-ClCA and *β*-3-BrCA as well as *β*-3-ClCA/3-BrCA solid solutions was also investigated. Thus, a 1mmol:1mmol ratio of *β*-3-ClCA:*β*-3-BrCA was ground and 50 µl of the solvents were introduced (MeOH, GAA or AC). The results obtained in all cases were identical in that *γ*-3-ClCA/3-BrCA solid solutions were produced as shown by PXRD analysis. In Figure 7.15 the PXRD pattern (c) illustrates the formation of *γ*-3-ClCA/3-BrCA solid solution upon MeOH SDG of a 1:1 molar ratio of *β*-3-ClCA:*β*-3-BrCA.

In contrast, grinding 1mmol:1mmol ratio of *β*-3-ClCA:*β*-3-BrCA with 50 µl of d.i.water gave a product (illustrated in Figure 7.15d) found to comprise *γ*-3-ClCA/3-BrCA solid solution and *β*-3-BrCA. The presence of *β*-3-BrCA suggests the possibility that water has some inhibitory effect on the formation of cocrystalline materials, similar to that seen in Section 7.3.2.a and, therefore, some *β*-3-BrCA did not undergo the cocrystallization process. Subsequently, this material did not transform to *γ* upon SDG but remained in its original phase (*β*). This is consistent with results of solvent drop grinding of *β*-3-BrCA, obtained in Section 7.3.1b.

To investigate the ability of the *β*-3-ClCA/3-BrCA solid solution to transform to *γ* solid solution, SDG of 1 mmol of *β*-3-ClCA/3-BrCA solid solution, prepared previously from solvent cocrystallization, was carried out by introducing 50 µl MeOH. PXRD analysis of the product showed only *γ*-3-ClCA/3-BrCA solid solution, indicating that the transformation from *β* solid solution to *γ* solid solution can be performed via SDG.

The results here are, interestingly, consistent with the SDG of *β*-3-ClCA, which produced *γ*-3-ClCA upon SDG. On the other hand, no transformation was observed for *β*-3-BrCA upon SDG. Thus, some questions arise: why does the transformation proceed in *β*-3-ClCA and not in *β*-3-BrCA? Is it due to the structural aspects or the effect of the molecular identity?

From the results observed in this study, it is clear that the structure has no effect on prevention of the transformation, as the *β*-3-ClCA/3-BrCA solid solution and *β*-3-BrCA are isostructural. *β*-3-BrCA showed phase stability upon SDG grinding while the *β*-3-

ClCA/3-BrCA solid solution transformed to the *γ*-solid solution upon SDG. Therefore, the transformation appears to be dependent on molecular identity, since introducing 3-ClCA molecules into the structure of *β*-3-BrCA leads to the structure transforming upon SDG.

A further experiment using 10 μl of MeOH upon grinding 1mmol of *β*-3-ClCA/3-BrCA solid solution produced a mixture of *γ*-3-ClCA/3-BrCA solid solution and *β*-3-ClCA/3-BrCA solid solution (illustrated in Figure 7.15e). This result indicates that the amount of solvent used clearly affects the transformation of *β*-3-ClCA/3-BrCA solid solution, consistent with pure *β*-3-ClCA.
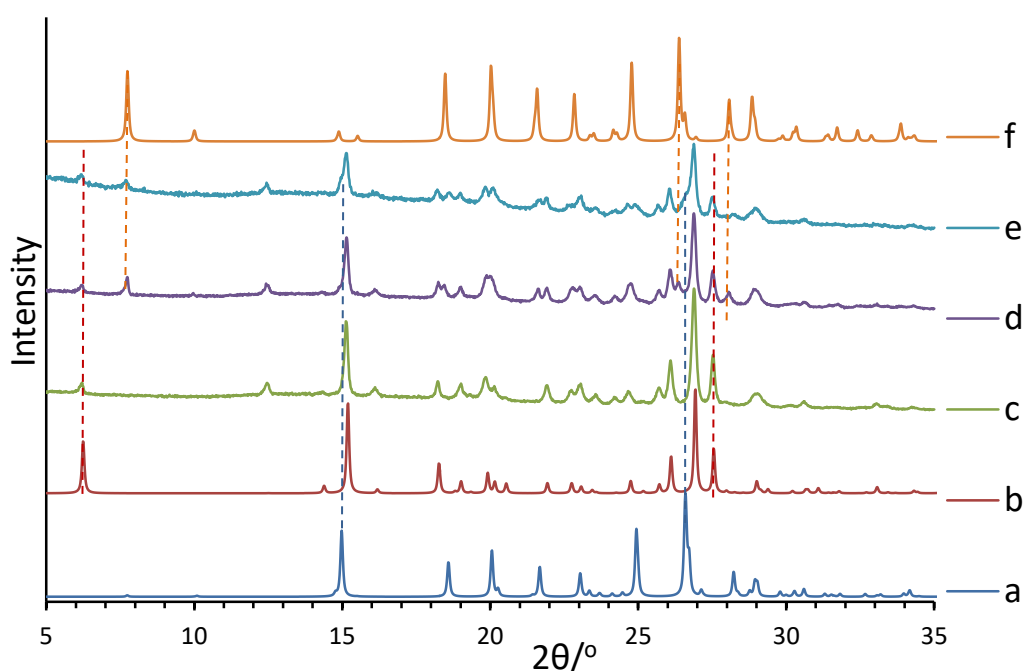
Figure 7.15. *Simulated PXRD of SC-XRD of (a) β-3-ClCA/3-BrCA solid solution, (b) γ-3-ClCA/3-BrCA solid solution and (f) β-3-BrCA. (c) and (d) are PXRD of SDG of 1:1 β-3-ClCA:β-3-BrCA using 50 μl MeOH and 50 μl d.i.water, respectively. (e) is PXRD of SDG of β-3-ClCA/3-BrCA solid solution using 10 μl MeOH. Dashed lines are to assist the identification of the phase shown in corresponding colours.*

Monitoring the cocrystallization of the *β* phase

The formation of *β* solid solutions via solid state grinding of the *β* phase of the corresponding acids was monitored as a function of the grinding time using *ex-situ* PXRD and a new powder sample each time. To perform these experiments, 1:1 molar ratios of *β*-3-ClCA:*β*-3-BrCA were ground for different grinding times: 1, 3, 7.5, 15, 30 and 90 minutes. Figure 7.16 shows the comparison between PXRD patterns obtained.

Only a mixture of *β*-3-ClCA and *β*-3-BrCA was clearly observed, by PXRD, for the materials ground for 1 and 3 minutes (Figure 7.16 d and e), indicating that the grinding time was too short to produce any visible change. However, increasing the grinding time to 7.5 minutes was found to produce broad peaks (e.g. around 26.7°, Figure 7.16f labelled *) and this was taken to correspond to the formation of the *β*-3-ClCA/3-BrCA solid solution. Additionally, both *β*-3-ClCA and *β*-3-BrCA were also observed for this ground material. However, a considerable decrease of the diffraction peaks of *β*-3-ClCA was observed at this stage, in contrast with the diffractions peaks of *β*-3-ClCA that were observed for the materials ground for 1 and 3 minutes (Figure 7.16f). Interestingly, *β* 3-ClCA/3-BrCA solid solution peaks were observed to grow remarkably when the grinding time was increased to 15 and 30 minutes (labelled * in Figure 7.16g and h). In contrast, *β*-3-ClCA peaks became much broader and harder to observe while the diffraction peaks of *β*-3-BrCA were still visible but with reduced intensities and were much broader (Figure 7.16 g and h, respectively). Finally, increasing the grinding time to 90 minutes produced only *β*-3-ClCA/3-BrCA solid solution (see Figure 7.16i).

The results above provide a glimpse into the mechanism of the formation of the solid solution of these particular acids. Thus, as seen for the grinding experiments of the acids for 7.5, 15 and 30 min, the *β*-3-ClCA structure disappeared first as its molecules occupied the structure of *β*-3-BrCA, in order to form a cocrystalline material. Solid solutions of different ratios of *β*-3-ClCA:*β*-3-BrCA were formed, as one acid (*β*-3-ClCA) was shown to disappear before the other (*β*-3-BrCA), the amount of the 3-ClCA in the structure of the solid solution was greater than that of 3-BrCA, at this stage. This is indicated by the shift in the peak position (the peak around 26.7° labelled * in the diffractograms f, g, h of Figure 7.16) to a higher 2θ which is consistent with the presence of more 3-ClCA molecules in the *β* solid solution structure (discussed previously in Chapter 4). This is supported by the results presented in Section 7.3.2.b (*neat grinding of different ratio mixtures*), where a *β* solid solution of a structure similar to *β*-3-BrCA was produced via grinding an initial 1:0.5 molar ratio of *β*-3-ClCA:*β*-3-BrCA. Finally, increasing the grinding time to 90 minutes was shown to be optimum for the formation of *β* cocrystalline material, with the initial ratio for acids of 1:1.

As no peaks of additional phases were observed during the formation of cocrystalline material, this leads to the conclusion that the cocrystalline material is produced without

any crystalline intermediate and that formation of the solid solution is produced directly by grinding the component materials. It is, however, unclear whether an amorphous intermediate is formed.
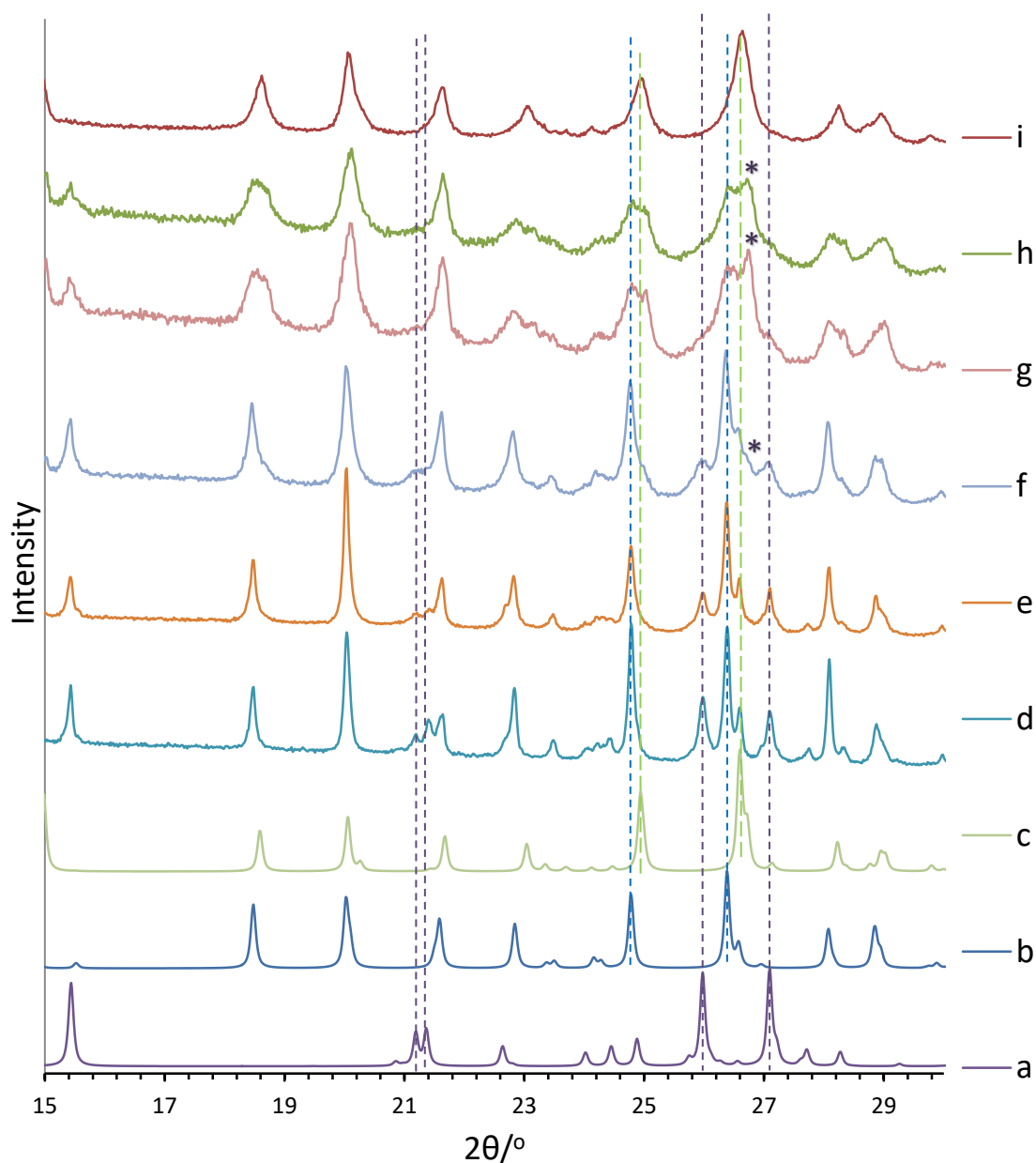
Figure 7.16. _Simulated PXRD of SC-XRD of (a) β-3-ClCA (b) β-3-BrCA and (c) β-3-ClCA/3-BrCA solid solution. (d), (e), (f), (g), (h) and (i) are PXRD of 1:1 β-3-ClCA:β-3-BrCA ground for 1, 3, 7.5, 15, 30 and 90 mins respectively. Dashed lines are to assist the identification of the phase shown in corresponding colour._

7.4. Conclusion

The results obtained in this chapter reveal information regarding polymorphic transformation and solid solution formation via a green chemistry approach (mechanogrinding and SDG techniques).

The γ phases of both acids (3-BrCA and 3-ClCA) showed stability on mechanogrinding and SDG and no transformation was observed. Similar behaviour was also observed for β-3-BrCA.

Different behaviour was observed for β-3-ClCA. Thus, grinding the β form of the acid together with a small quantity of certain solvents (approximately 50μl:1mmol of solid) has been demonstrated to assist the acid to fully transform to the γ form. Similarly, the transformation from β to γ 3-ClCA was also accelerated by introducing some γ phase of the same acid during neat grinding. On the other hand, neat grinding of β-3-ClCA for 90 minutes showed stability of the phase for a duration of 15 weeks at least, whereas, by doubling the grinding time, the ground β-3-ClCA showed a gradual transformation to the γ phase. Interestingly, the tape that was used to prepare the sample prior to PXRD analysis also enhanced the transformation of the ground β-3-ClCA.

The study here also demonstrated that neat grinding processes can be used as a means of obtaining a particular solid solution polymorph. Thus, grinding a 1:1 ratio of β-3-ClCA:β-3-BrCA produced β-3-ClCA/3-BrCA solid solution whereas grinding a 1:1 ratio of γ-3-ClCA:γ-3-BrCA produced γ-3-ClCA/3-BrCA solid solution. Interestingly, SDG of a 1:1 ratio of β-3-ClCA:β-3-BrCA mixture and, β-3-ClCA/3-BrCA solid solutions produced only γ-3-ClCA/3-BrCA solid solution.

The mechanism of the formation of β-3-ClCA/3-BrCA via neat grinding was proposed in this study, with the assistance of *ex-suit* PXRD analysis for materials ground for different durations. In this regard, direct transformation from mono crystalline materials (β-3-ClCA and β-3-BrCA) to cocrystalline materials (β-3-ClCA/3-BrCA solid solution) was observed with no crystalline intermediate present in the medium. On the other hand, there is no information regarding cocrystallization from the amorphous phase.

7.5. References

1   E. Simone, G. Steele and Z. K. Nagy, *CrystEngComm*, 2015, **17**, 9370–9379.

2   L. G. Tulli, N. Moridi, W. Wang, K. Helttunen, M. Neuburger, D. Vaknin, W. Meier and P. Shahgaldian, *Chem. Commun.*, 2014, **50**, 3938–3940.

3   M. Kitamura, *CrystEngComm*, 2009, **11**, 949–964.

4   N. Blagden, W. I. Cross, R. J. Davey, M. Broderick, R. G. Pritchard, R. J.

Roberts and R. C. Rowe, *Phys. Chem. Chem. Phys.*, 2001, **3**, 3819–3825.

5   N. Blagden and R. J. Davey, *Cryst. Growth Des.*, 2003, **3**, 873–885.

6   I. Weissbuch, V. Y. Torbeev, L. Leiserowitz and M. Lahav, *Angew. Chemie Int. Ed.*, 2005, **44**, 3226–3229.

7   M. Kitamura, T. Hara and M. Takimoto-kamimura, *Cryst. Growth Des.*, 2006, **6**, 1945–1950.

8   M. Trifkovic, S. Rohani and M. Mirmehrabi, *Org. Process Res. Dev.*, 2007, **11**, 138–143.

9   P. Anastas and N. Eghbali, *Chem. Soc. Rev.*, 2010, **39**, 301–312.

10   J. H. Clark, *Green Chem.*, 1999, 1–8.

11   M. Rafilovich and J. Bernstein, *J. Am. Chem. Soc.*, 2006, **128**, 12185–12191.

12   A. V. Trask, N. Shan, W. D. S. Motherwell, W. Jones, S. Feng, R. B. H. Tan and K. J. Carpenter, *Chem. Commun.*, 2005, 880–882.

13   A. V. Trask, W. D. S. Motherwell and W. Jones, *Chem. Commun.*, 2004, 890–891.

14   M. D. Cohen and G. M. J. Schmidt, *J. Chem. Soc.*, 1964, 1996–2000.

15   M. D. Cohen, G. M. J. Schmidt and F. I. Sonntag, *J. Chem. Soc.*, 1964, 2000–2013.

16   G. M. J. Schmidt, *J. Chem. Soc.*, 1964, 2014–2021.

17   S. Ahn, K. D. M. Harris, B. M. Kariuki and D. M. S. Zin, *J. Solid State Chem.*, 2001, **156**, 10–15.

18   S. Kanao, S. Kashino and M. Haisa, *Acta Crystallogr. Sect. C*, 1990, **46**, 2436–2438.

19   V. Mazel, C. Delplace, V. Busignies, V. Faivre, P. Tchoreloff and N. Yagoubi, *Drug Dev. Ind. Pharm.*, 2011, **37**, 832–840.

20   W. T. Cheng and S. Y. Lin, *Int. J. Pharm.*, 2008, **357**, 164–168.

21   American Chemical Society National Historic Chemical Landmarks. Scotch® Transparent Tape. *http://www.acs.org/content/acs/en/education/whatischemistry/landmarks/scotchtape.html*, 02/08/2016.

22   F. Delogu, C. Deidda, G. Mulas, L. Schiffini and G. Cocco, *J. Mater. Sci.*, 2004, **39**, 5121–5124.

23   Erizal, S. Y. Cahyati, S. S. Nurono and A. Halim, *Int. J. Pharmacol.*, 2008, **4**, 140–144.

24   D. Braga, L. Maini and F. Grepioni, *Chem. Soc. Rev.*, 2013, **42**, 7638–7648.

25   J. C. Espinosa-Lara, D. Guzman-Villanueva, J. I. Arenas-García, D. Herrera-Ruiz, J. Rivera-Islas, P. Román-Bravo, H. Morales-Rojas and H. Höpfl, *Cryst. Growth Des.*, 2013, **13**, 169–185.

26   C. Maheshwari, A. Jayasankar, N. A. Khan and N. Rodrıguez-Hornedo, *CrystEngComm*, 2009, **11**, 493–500.

27   I. Sarceviča, L. Orola, K. P. Nartowski, Y. Z. Khimyak, A. N. Round and L. Fabian, *Mol. Pharm.*, 2015, **12**, 2981−2992.

28   N. Shan, F. Toda and W. Jones, *Chem. Commun.*, 2002, 2372–2373.

Chapter 8: Outline on the future work

Throughout the research carried out in this thesis, many questions have been raised, which need a further investigation in the future. The discussion in this chapter highlights these questions together with proposed suggestions for the future work.

The investigation carried out on the 3-BrCA in Chapter 3 revealed a new γ form of the acid (γ_2). However, it was not possible during this work to produce this phase in a pure form, which, in turn, limits the opportunity of investigation of the thermal properties of this form. Investigation of suitable crystallization conditions to produce pure γ_2-3-BrCA would allow a study of the thermal properties.

The work presented in this chapter (Chapter 3) also revealed that the γ form of the isostructural *meta*-substituted cinnamic acids (3-CF$_3$CA, 3-MeCA, 3-ClCA and 3-BrCA) showed distinct thermal behaviours. Despite the fact that this study has gone some way towards enhancing our understanding of the role of the substituent groups in stabilizing of the final product, further investigation of theoretical computational work of this cinnamic acid family is strongly recommended, to assess the role of different interactions.

In the work carried out on cocrystallization of a binary *meta*-substituent cinnamic acids in Chapter 4, it was not possible to produce pure β forms of solid solutions comprising 3-ClCA/3-MeCA, 3-ClCA/3-CF$_3$CA, 3-BrCA/3-MeCA and 3-BrCA/3-CF$_3$CA. However, the PXRD analysis of some cocrystalline systems, such as 3-BrCA/3-CF$_3$CA from GAA and 3-BrCA/3-MeCA from the melt, revealed the formation of some β form contaminated with other structures. Thus, the future work would focus on adjusting the cocrystallization conditions to obtain pure β structures of these solid solutions, and hence to determine the crystal structures and study the photodimerization reaction.

Another interesting result presented also in Chapter 4 is that, PXRD characterization of the cocrystallized material of 3-BrCA:3-CF$_3$CA, from melt, showed a different phase from any known structures of the pure acids. The crystal structure of this phase remains undetermined and thus, identifying the structure is an importance for the future work.

In Chapter 5, crystallization of the K$^+$ salt of 3-CF$_3$CA revealed by PXRD a different PXRD pattern from the crystal structure. Similarly, cocrystallization of K$^+$ salt or NH$_4^+$ of a binary system of 3-BrCA/3-CF$_3$CA PXRD indicated a presence of another phase, which was not possible to assign to any other known structures presented in this study. Thus further investigations to identify these phases are recommended.

Combining the results of Chapter 3 and 6 illustrates that, 3-FCA underwent a rare case of thermotransformation among cinnamic acid derivatives in which the β form of the acid (β_1) transformed irreversibly to another β form (β_2). Both forms undergo photodimerization to produce an amorphous dimeric photoproduct. These results raised an interesting question as to whether experimental conditions could be found that would allow the solid-state photodimerization reactions of the β_1 and β_2 polymorphs to proceed without loss of crystallinity. An interesting subsequent question is whether the photodimerization reactions of the β_1 and β_2 polymorphs yield the same or different polymorphs of 3,3'-difluoro-β-truxinic acid. In this regard, the application of modern techniques for analysis of PXRD data may prove to be essential for carrying out complete crystal structure determination of the photoproduct phases.

In Chapter 6 traces of the photo isomerization during the photo irradiation was observed in some systems. Cinnamic acids and cinnamate/cinnamic acid systems showed such isomerization, but it was absence in the case of pure K$^+$ cinnamate systems. Therefore, further studies are needed to assess the role of K$^+$ cation in the process.

During the work described in Chapter 6, salt systems exhibiting the criss-cross arrangement for the adjacent double bond, underwent photoreaction upon irradiation. However, the identification of different products (for example, different length oligomers those proposed by mass spectroscopy) using HPLC and solution-state ^{1}H NMR was not possible. Further work should attempt the separation and characterization of these products.

The results presented in Chapter 7 demonstrate the effective of mechanogrinding and SDC as a tool in the cocrystallization process and control of polymorphism for both pure crystalline material and solid solutions. Therefore, It is recommended that further research should be applied, using mechanogrinding technique, to reveal significant new

insights on a range of systems of interest, particularly studies of the salt binary systems presented in Chapter 5.

On the other hand, during the work described in Chapter 7, it was discovered that a direct transformation from mono crystalline material (β-3-ClCA and β-3-BrCA) to cocrystalline materials (β-3-ClCA/3-BrCA solid solution), via mechanogrinding, was achieved with no crystalline intermediate present in the medium. However, there was no information whether the cocrystallization produced from the amorphous phase. This is an important issue that should be investigated in the future work.

Appendix A: Ellipsoid presentation of asymmetric unit of some cinnamic acids
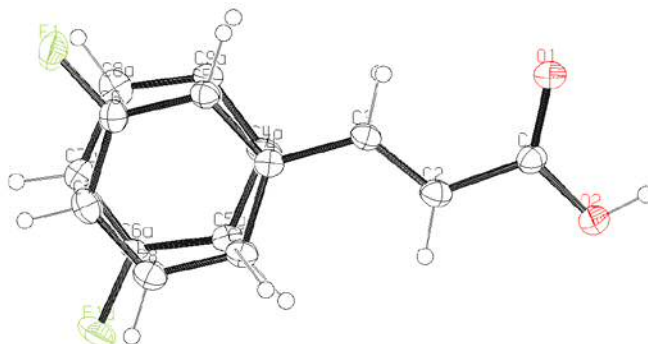
Figure A.1. *The asymmetric unit in the β₂ polymorph of 3-FCA showing the disorder.*
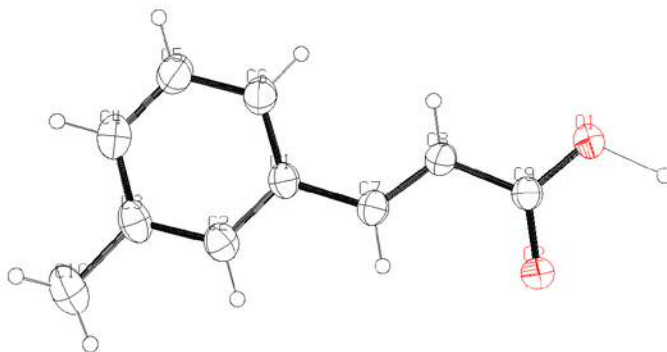
Figure A.2. *The asymmetric unit of the 3-MeCA.*
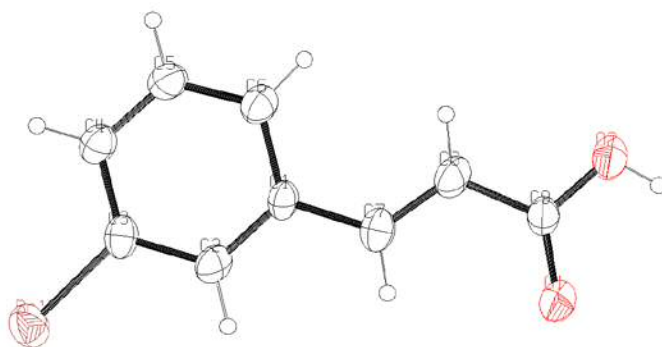
Figure A.3. *The asymmetric unit in the γ₂ polymorph of 3-BrCA.*

Appendix B: Ellipsoid presentation of asymmetric unit of some binary systems of cinnamic acids
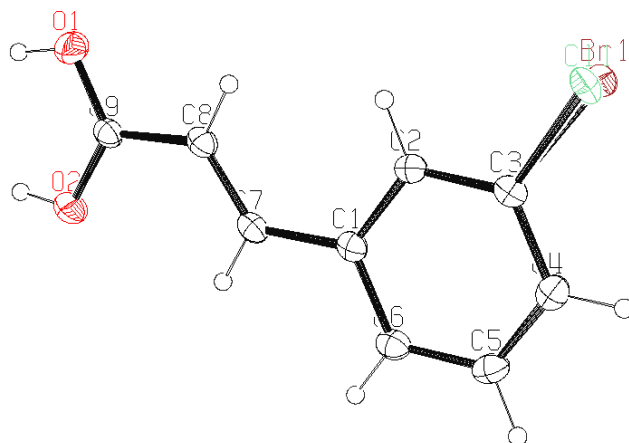
Figure B.1. *The asymmetric unit in the β-3-ClCA/3-BrCA showing the disorder.*
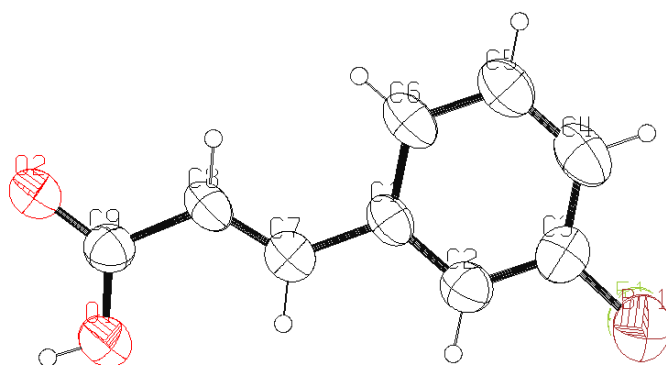
Figure B.2. *The asymmetric unit in the β₁-3-BrCA/3-FCA showing the disorder.*
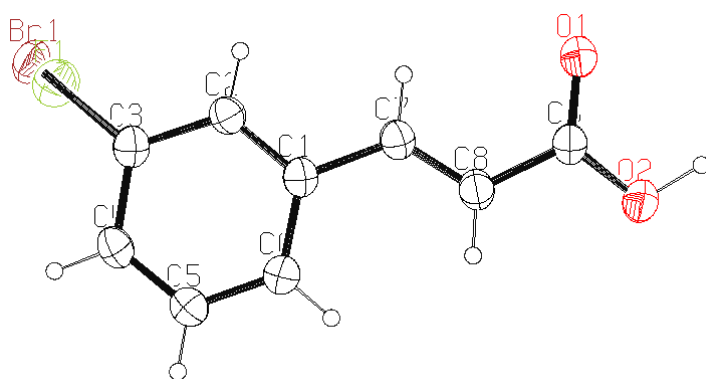
Figure B.3. *The asymmetric unit in the γ₂-3-BrCA/3-FCA showing the disorder.*
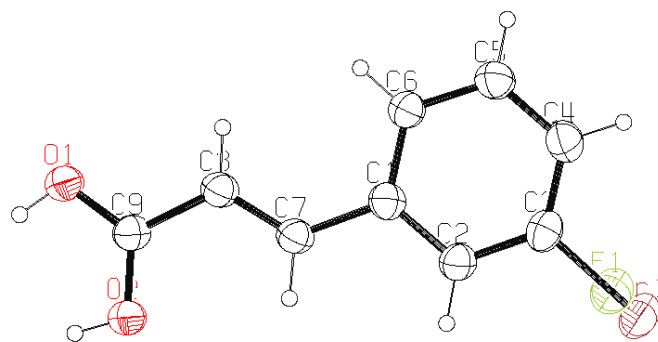
Figure B.4. *The asymmetric unit in the γ-3-BrCA/3-FCA showing the disorder.*
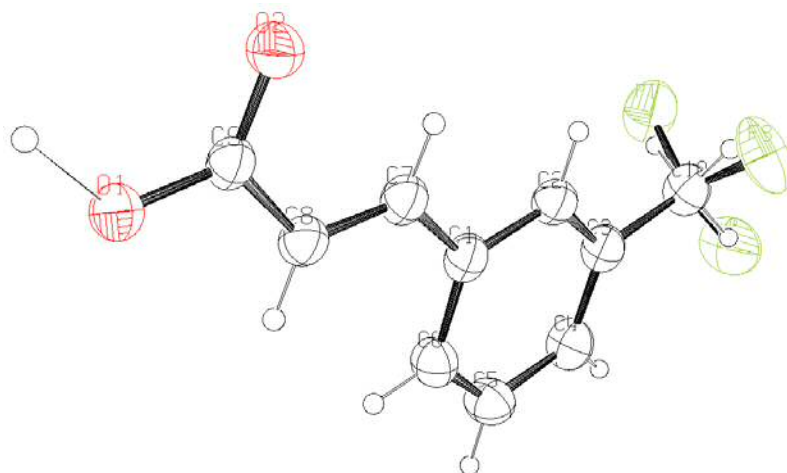
Figure B.5. *The asymmetric unit in the 3-CF₃CA/3-MeCA solid solution, 3-Me group and 3-CF₃ are disordered by 0.78(1):0.21(1) in the crystal.*
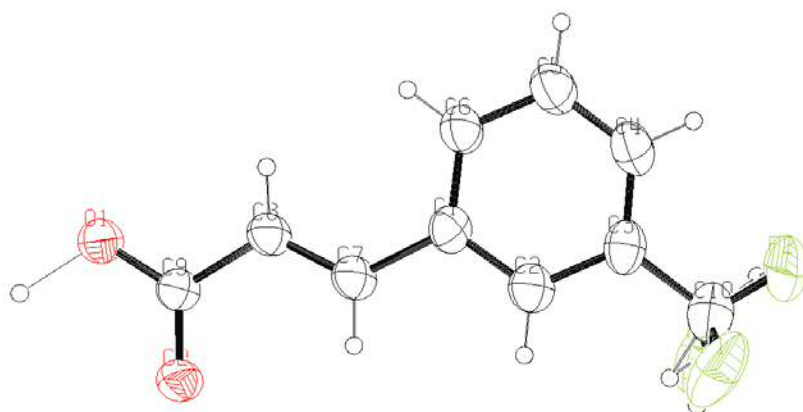
Figure B.6. *The asymmetric unit in the 3-CF₃CA/3-MeCA solid solution, 3-Me group and 3-CF₃ are disordered by 0.17(1):0.83(1) in the crystal.*

Appendix C: Ellipsoid presentation of asymmetric unit of some cinnamate and their binary systems
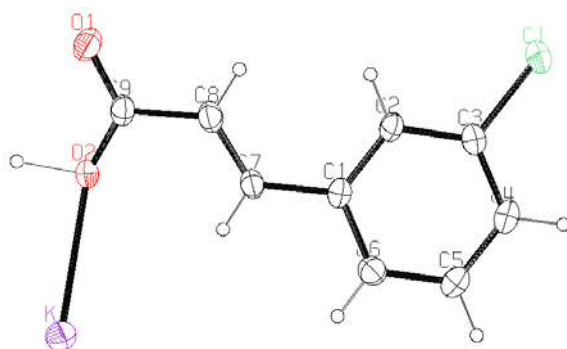
Figure C.1. The asymmetric unit in the K⁺ salt of 3-ClCA (structure II).
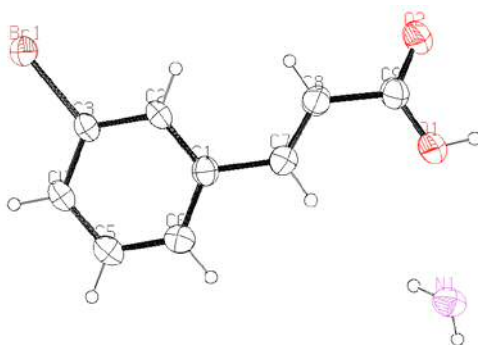
Figure C.2. The asymmetric unit in the K⁺ salt of 3-ClCA (structure II).
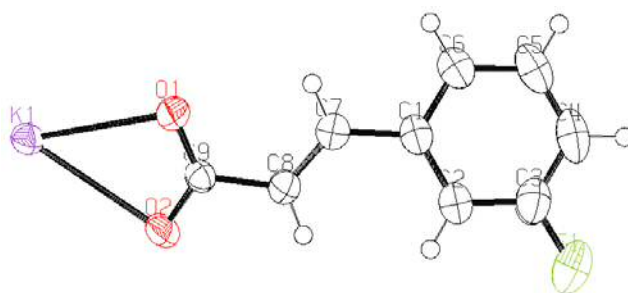
Figure C.3. The asymmetric unit in the K⁺ salt of 3-FCA.
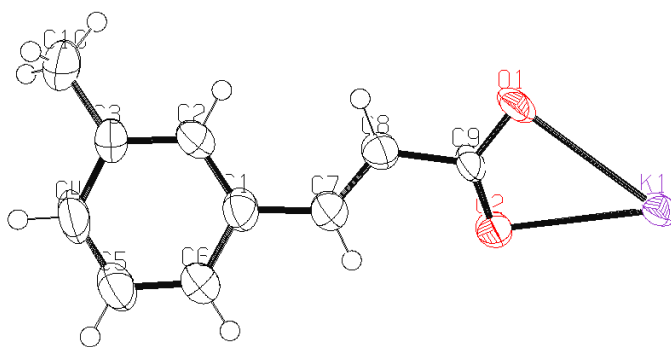
Figure C.4. *The asymmetric unit in the K$^+$ salt of 3-MeCA*
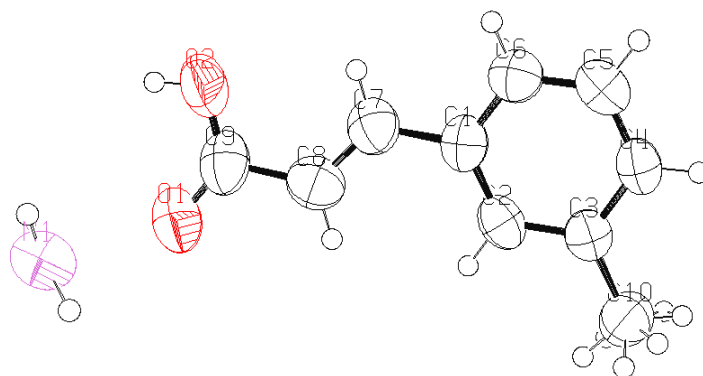
Figure C.5. *The asymmetric unit in the NH$_4^+$ salt of 3-MeCA, showing the disorder.*
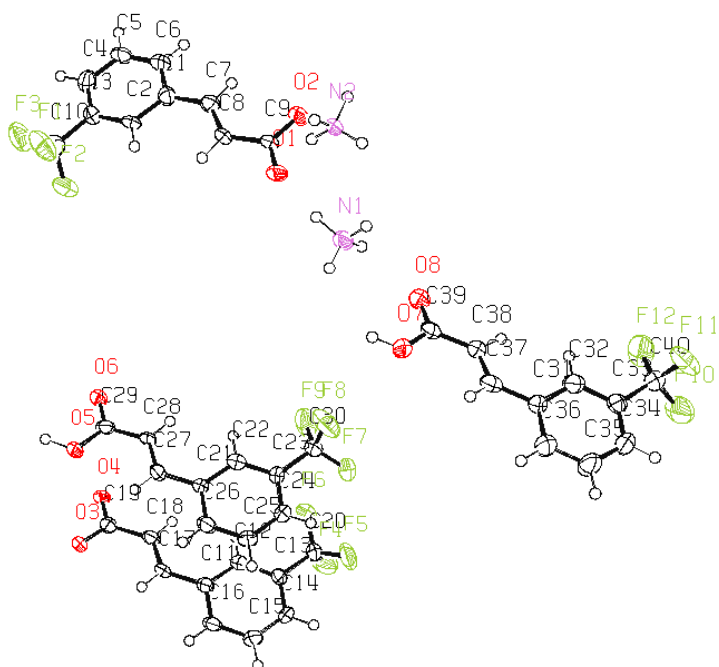
Figure C.6. *The asymmetric unit in the NH$_4^+$ salt of 3-CF$_3$CA, showing the disorder.*
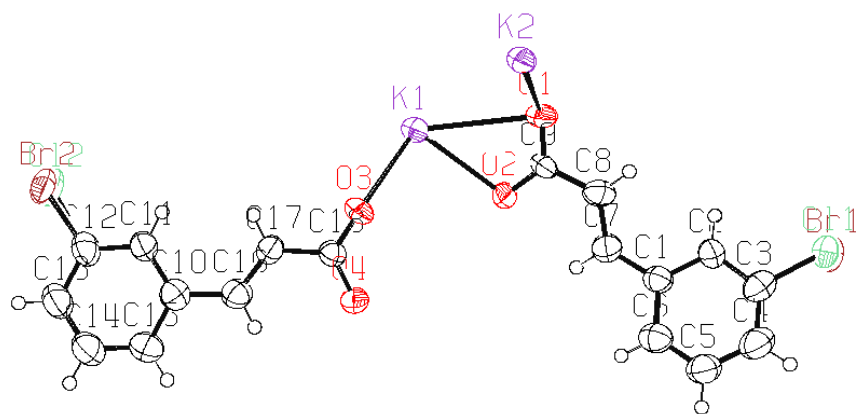
Figure C.7. *The asymmetric unit in K-(3-ClCate/3-BrCate) solid solution.*
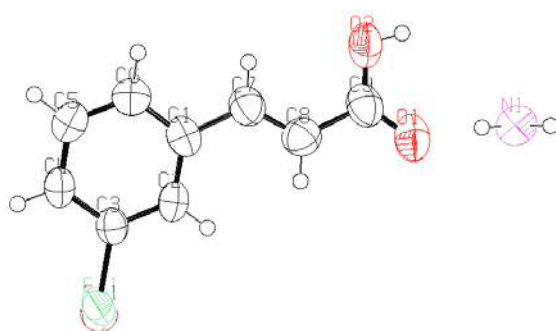
Figure C.8. *The asymmetric unit in NH₄-(3-BrCate/3-ClCate)/(3-BrCA/3-ClCA) solid solution.*
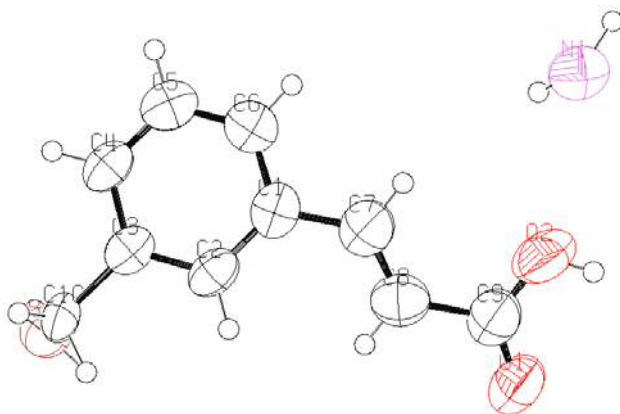
Figure C.9. *The asymmetric unit in NH₄-(3-BrCate/3-MeCate)/(3-BrCA/3-MeCA) solid solution.*
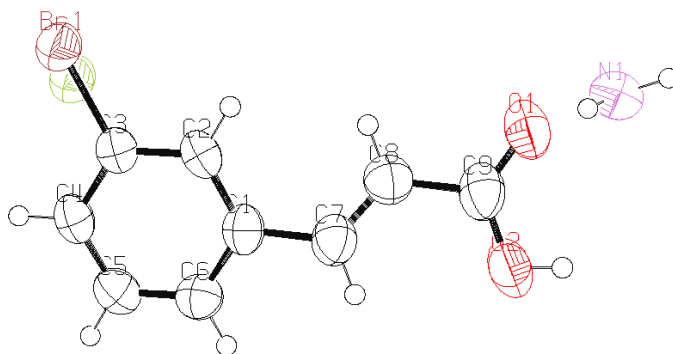
Figure C.10. *The asymmetric unit in NH$_4$-(3-BrCate/3-FCate)/(3-BrCA/3-FCA) solid solution.*
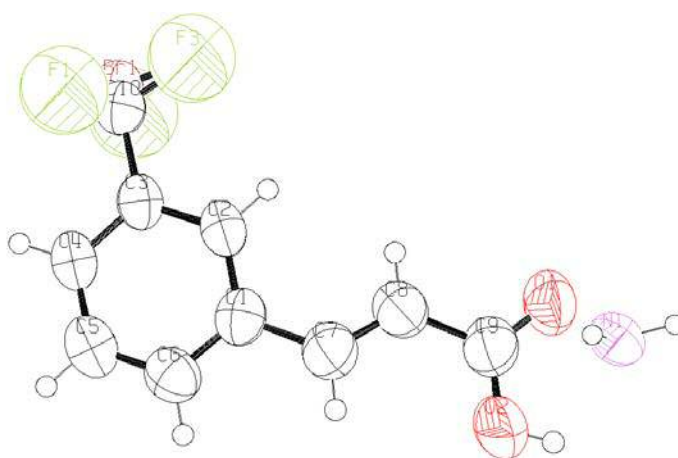
Figure C.11. *The asymmetric unit in NH$_4$-(3-BrCate/3-CF$_3$Cate)/(3-BrCA/3-CF$_3$CA) solid solution.*

Appendix D: Ellipsoid presentation of asymmetric unit of some truxinic acids
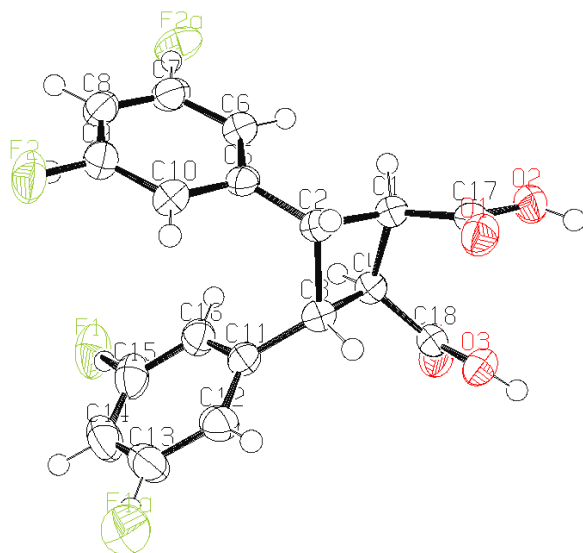
Figure D.1. *The asymmetric unit in the crystal structure of 3,3`difluoro-β-truxinic acid.*
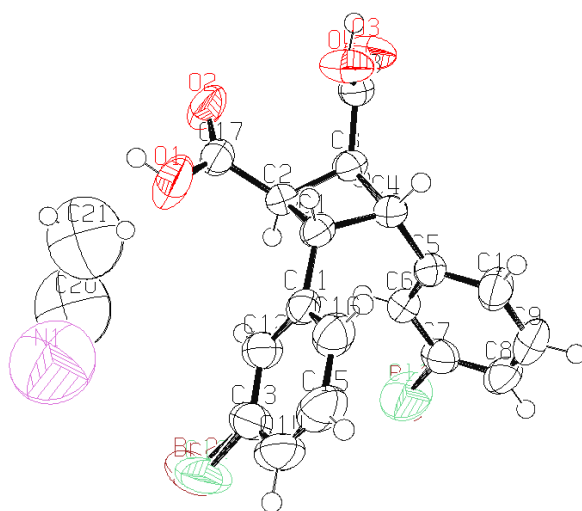
Figure D.2. *The asymmetric unit in the crystal structure of β-3-(Cl/Br)CA-D.*

Appendix E: Work Published during this PhD

Manal A. Khoj, Colan E. Hughes, Kenneth D. M. Harris, and Benson M. Kariuki, Polymorphism in a *trans*-Cinnamic Acid Derivative Exhibiting Two Distinct β-type Phases: Structural Properties, [2 + 2] Photodimerization Reactions, and Polymorphic Phase Transition Behavior, *Cryst. Growth Des.*, 2013, *13* (9), 4110–4117.

Manal A. Khoj, Colan E. Hughes, Kenneth D. M. Harris, and Benson M. Kariuki, Structural Diversity of Solid Solutions Formed between 3-Chloro-trans-cinnamic acid and 3-Bromo-trans-cinnamic Acid; Cryst. Growth Des., Article ASAP, Publication Date (Web): January 18, 2017.